INSTITUT POLYTECHNIQUE DE PARIS

NNT : 2021IPPAX131

Thèse de doctorat

ÉCOLE POLYTECHNIQUE

IP PARIS

Second Harmonic Generation from silicon surfaces functionalized with DNA nucleobases: an ab initio description

Thèse de doctorat de l'Institut Polytechnique de Paris
préparée à École Polytechnique

École doctorale n°626 École doctorale de l'Institut Polytechnique de Paris (EDIPP)
Spécialité de doctorat : Physique

Thèse présentée et soutenue à Palaiseau, le 13/12/2021, par

STEFANO MAZZEI

Composition du Jury :

Henri-Jean Drouhin Professeur, LSI, École Polytechnique (UMR 7642)	Président
Daniele Varsano Chargé de recherche, CNR Institute of nanoscience	Rapporteur
Valerio Olevano Directeur de recherche, Institut Néel (UPR 2940)	Rapporteur
Eleonora Luppi Maîtresse de conférences, LCT, UPMC	Examinateur
Christine Giorgetti CRHC, LSI, École Polytechnique (UMR 7642)	Directrice de thèse
Giancarlo Cappellini Professeur, Università di Cagliari	Examinateur

Contents

Acknolewdgements

Hereafter, I would like to thank all the people which helped and supported me during last three years.

First of all, I wish to thank my supervisor Christine Giorgetti, for having guided me during these three years with infinite patience and energy. She helped and encouraged me every time I needed (included, but not limited to, my awful misadventures with french bureaucracy). I will never forget our five-hours-long scientific discussions, our night time thesis rehearsals, and our intensive debugging sessions. This thesis owes its existence to Christine: working with her has been a honour and a privilege, and I am afraid to not be able to express how much I will miss her.

I wish also to thank all the members of the theoretical spectroscopy group, for all the support that they gave to me. Thanks to Valérie Véniard, Lucia Reining, and Matteo Gatti, for having been always available to listen and critically discuss the results of my work, and for their precious suggestions. Thanks to Francesco Sottile which, with remarkable patience and pedagogical vocation, has always been there to answer my (sometimes naives) questions. I am also grateful to Andrea, for having been always up for a coffee, for suggesting me great movies, and for unveiling me the secrets of Linux. Thanks also to all the non permanent members of the group: I will miss all of you a lot.

I would also to thank all the colleagues of the Laboratoire des Solides Irradiés. Une mention d'honneur va à Michèle Raynaud, la directrice, et à Élodie Dubois et Marylène Raclot, pour la patience dont elles ont toujours fait preuve en m'aidant dans les formalités administratives.

I wish also to thank my referees, Valerio Olevano and Daniele Varsano, for having accepted to revise the manuscript, and I would like to express my gratitude to Christoph Friedrich, Stefan Rost, Andrea Ferretti and Alberto Guandalini for the precious discussions that we had together.

Finally, I wish to thank all my friends. Thanks to Maria, Domenico, Alberto e Cecco: even if we are far, you are always in my heart. Thanks to Bea which accompanied me during a long part of this journey. Thanks to Benjamin, Sarah, Antoine, Gaetan, Jon and to all the *colocs* for having made so great these three years in Paris. Thanks to Léa, which makes every day special.

Infine, grazie a mia madre e a mio padre. Questo traguardo lo devo sopratutto a loro.

Chapter 1

Introduction

1.1 Biofunctionalised surfaces

The chemistry of living systems exhibits an extremely rich phenomenology. At every moment, inside each living system, even the simplest, a huge number of reactions happen, resulting in the simultaneous synthesis of complex macromolecules. Genetic engineering techniques allow nowadays to insert specific genic sequences inside of target cells, allowing to exploit in vitro farmed bacteria as microscopic factories for the production of drug and proteins of commercial interest (see e.g. [1]). At the same times, during last 70 years, the microelectronics industry has made giant strides in the miniaturisation of electronic components. Nowadays, the transistors inside mass-produced microprocessors have reached the size of ~ 5 nm (see e.g. [2],[3]), and a great effort is made in order to go beyond this limit, experimenting novel materials and manufacturing techniques (see e.g. [4] and [5] for a review of 2D-materials based transistors). The possibility to integrate the chemistry of living systems inside microelectronic components open the way to a wide range of exciting applications, from the possibility to design miniaturised bio-sensors (with possible applications to DNA and RNA sequencing[1] (see e.g. Ref.s [6] and [7], see also Fig. (1.1)) Also, integration of biomolecules with well-known semiconductors technology, could allow to manufacture devices with novel properties. For exemple DNA has been proposed as base for design of new-generation memories [8]. DNA, as it is well known, is a molecule which encodes in itself all the information necessary to make a perfect copy of a given living being. Nucleic-acid-based memories, may in principle exhibit unreached retention time, information density, and low energy consumption properties (for a comparison with memories manufactured with current technology, see Tab. (1.1)) By the way, in order to achieve the ambitious goal of integrating microelectronics technology with biochem-

[1] In the moment this thesis is being written, the second year of COVID-19 pandemic is coming at the end and words like "RT-PCR", "antigenes", and "antibodies", are now part of the every-day-life vocabulary. The need for developing novel effective and cost-contained methods for detection of specific genetic sequences is just self-explanatory

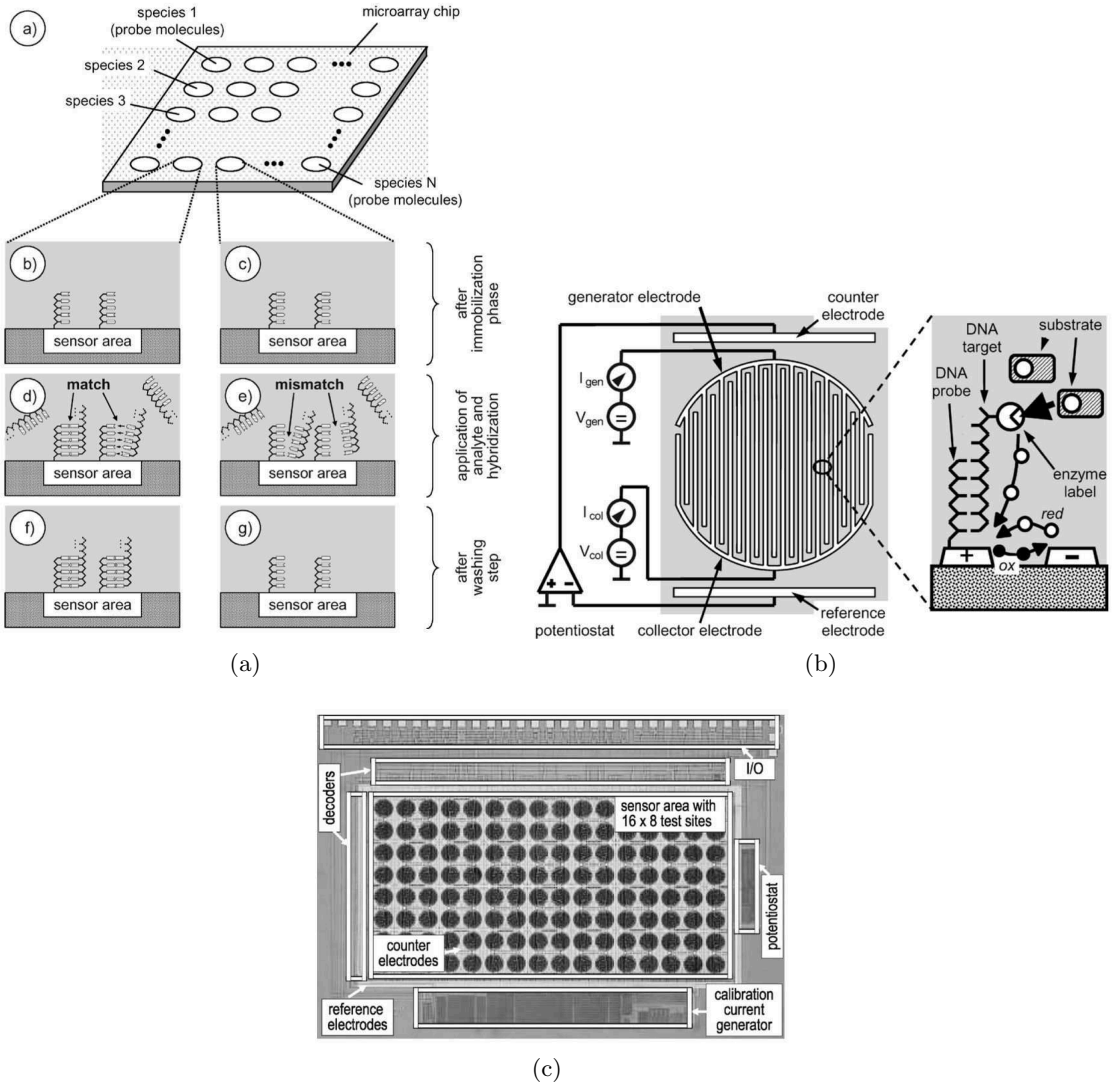

Figure 1.1: Working principle of a DNA-array sensor (reproduced from Ref. [7]). This technology allows the manufacturing of devices with capability to detect in a given sample the presence of specific genic sequences. As shown in (a), on the surface of the sensor, a single-strained filament of DNA (called probe) is adsorbed. After that, the sensor is exposed to the sample to analyse. If the sample contain the genic sequence compatible with the probe filament, the two filaments will hybridise (left column of panel (a)), otherwise, after the washing step, the sensor will just contain the unhybridised probe filament (right column of panel (a)). In this specific design, the analyte is labelled with the alkaline-phosphatase enzyme (see panel (b)). After the hybridisation and washing phase, a layer of para-aminophenylphosphate is applied on the sensor surface. This induces a redox reaction in correspondence of the sites where the labelled analyte hybridised with the probe, generating a current flow into the electrodes, and allowing the detection of the hybridisation sites. In panel (c), a microphotograph of the sensor manufactured by Schienle et. al in Ref. [7] is reported (the picture covers a area of $6.4 \times 4\text{mm}^2$)

Nucleic Acid memories: comparison with current technologies

Metrics	Hard disk	Flash memory	DRAM	cellular DNA
Read/Write latency	$3 \div 5$ ms per bit	100 μs/bit	< 10 ns/bit	< 100 μs/bit
Retention	> 10 years	~ 10 years	~ 64 ms	> 100 years
ON power	0.04 W/GB	$0.01 \div 0.04$ W/GB	0.4 W/GB	$< 10^{-10}$ W/GB
Volumetric density	10^{13} bit cm^{-3}	10^{16} bit cm^{-3}	10^{13} bit cm^{-3}	10^{19} bit cm^{-3}

Table 1.1: Theoretical limits of DNA-based memories compared with characteristic quantities of memories based on current technologies (adapted from Ref. [8]) . As we can see, nucleic acid memories may in principle outperform current ones on retention time, energy consumption, and information density.

istry, a deep understanding of the adsorption of biomolecules on semiconductors surfaces is mandatory. This thesis aim to study, by mean of *ab initio* methods, how the optical response of silicon surfaces is influenced by the adsorption of small molecules of biological interests, taking nucleobasis (a particular class of biomolecules formed by the fondamental constituents of DNA) as case study. The study of the optical response of this kind of systems is an interesting and useful subject: in no matter which manufacturing process of functionalised surfaces, one needs for reliable techniques to characterise the adhesion of the molecules on the substrate. Optical spectroscopy technique constitute a very well suited tool for this task, because they allow one to perform such investigation in real time and in a non-destructive way (also, they are generally cheaper compared to other surface characterisation techniques). A special focus in the present work will be devoted to the study of the second-order optical response, due to its unique surface sensitivity.

1.2 Second Harmonic Generation (SHG)

Optical properties of a material, depend on the way its electrons react to an external electromagnetic field. When the material is perturbed, the charge carriers rearrange, giving arise to induced charge and current densities, which can be represented via the polarisation field $\mathbf{P}$. If the applied perturbation is not too intense, then the relationship between $\mathbf{P}$ and

the electric field **E** (including the external *and* the induced field) will be linear:

$$\mathbf{P} = \overset{\leftrightarrow}{\chi}^{(1)} \mathbf{E} \tag{1.1}$$

The quantity $\overset{\leftrightarrow}{\chi}^{(1)}$ is a rank 2 tensor, and it takes the name of *first order susceptibility*. The relation (1.1) implies that if the external field is monochromatic of frequency ω, so the polarisation **P** (and as a consequence also the emitted field) will be. By the way, the more the external perturbation is intense, the more deviations from law (1.1) will be observed. In order to describe these deviations, we can expand **P** as a Taylor series of the electric field **E**:

$$\mathbf{P} = \overset{\leftrightarrow}{\chi}^{(1)} \mathbf{E} + \overset{\leftrightarrow}{\chi}^{(2)} \mathbf{EE} + \overset{\leftrightarrow}{\chi}^{(3)} \mathbf{EEE} + \dots \tag{1.2}$$

The terms evidenced in (1.2) constitute the nonlinear part of **P**, in the following called $\mathbf{P}^{NL}$. The need for coherent and intense light sources in order to access the nonlinear regime, made almost impossible to explore these properties before the invention of lasers, which happened in the 50's. After that, the nonlinear optics knew a rapid development: in 1961 the Second Harmonic Generation was discovered by Franken [9], and six years later, experimental evidence of Third Harmonic Generation [10] and of Electric Field Induced Second Harmonic generation (EFISH) [11] were reported. Under usual experimental conditions, when the perturbation is not too intense, the nonlinear term of the Polarisation has magnitude much lower than the linear contribution, and the expansion (1.2) converges quite quickly. Analogously, the third order term will be much smaller than the second order one, and so on. This property is no more satisfied in the case of perturbations which have the form of very strong, ultra-short, laser pulses. In that case phenomena of Higher Harmonic Generation take place, and many harmonics of comparable intensity can be created [12]. This kind of phenomena is way beyond the scope of the present work, and in the following we will always assume that the condition of weak enough perturbation is always satisfied. In this thesis, we will limit ourself to the study of non-linear phenomena of second order. The quantity which describes the second order response of a given material to an electric field **E**, as we have shown in Eq. (1.2) is the *second order susceptibility* $\overset{\leftrightarrow}{\chi}^{(2)}$:

$$\mathbf{P}^{(2)} = \overset{\leftrightarrow}{\chi}^{(2)} \mathbf{EE} \tag{1.3}$$

The second order susceptibility $\overset{\leftrightarrow}{\chi}^{(2)}$ is a three index tensor of rank 3, containing in principle 27 indipendent component. The k-th cartesian component of $\mathbf{P}^{(2)}$ can be written as:

$$P_k^{(2)} = \sum_{i,j} \chi_{kij}^{(2)} E_i E_j \tag{1.4}$$

Because of the interchangeability of the index referring to the electric field, we have that $\chi_{kij}^{(2)} = \chi_{kji}^{(2)}$, reducing to 18 the number of independent component of the tensor. The

number of non-zero or independent component can be further reduced exploiting the symmetries of the material (see e.g. Ref. [13]). At this purpose, we will limit for the moment to show a very important symmetry property: if the material is invariant under inversion (i.e. it has central symmetry), then the second order susceptibility is identically zero $\overset{\leftrightarrow}{\chi}^{(2)} = 0$. Indeed, for materials invariant under inversion of the cartesian axis, we will have:

$$\hat{\mathcal{I}}\mathbf{P}^{(2)} = \overset{\leftrightarrow}{\chi}^{(2)} (\hat{\mathcal{I}}\mathbf{E})(\hat{\mathcal{I}}\mathbf{E}) \tag{1.5}$$

where $\hat{\mathcal{I}}$ represent the inversion operator:

$$\begin{aligned} \hat{\mathcal{I}}\mathbf{P}^{(2)} &= -\mathbf{P}^{(2)} \\ \hat{\mathcal{I}}\mathbf{E} &= -\mathbf{E} \end{aligned} \tag{1.6}$$

Substituting the quantities (1.6) in Eq. (1.5), we have:

$$\begin{aligned} \hat{\mathcal{I}}\mathbf{P}^{(2)} &= \\ &= -\mathbf{P}^{(2)} \\ &= \overset{\leftrightarrow}{\chi}^{(2)} (\hat{\mathcal{I}}\mathbf{E})(\hat{\mathcal{I}}\mathbf{E}) \\ &= \overset{\leftrightarrow}{\chi}^{(2)} (-\mathbf{E})(-\mathbf{E}) \\ &= \mathbf{P}^{(2)} \end{aligned} \tag{1.7}$$

implying $\mathbf{P}^{(2)} = -\mathbf{P}^{(2)}$, which is satisfied only for $\mathbf{P}^{(2)} = 0$. As we will see later, this property plays an important role in making the second harmonic generation a well adapted tool to study surfaces. The second order susceptibility contains in itself all the necessary information to describe a wide range of nonlinear phenomena (briefly resumed in Tab. (1.2)) In the present work, we will limit to the study of the second harmonic generation. In this process, two photon at frequency ω are absorbed, and one photon having frequency 2ω is emitted (see Fig. (1.2)) The main application of the SHG, as it is easy to imagine, is the frequency conversion. Using a non-linear crystal, and a pump laser as primary source, it is possible to obtain coherent light in a range of frequency where no lasers are currently available, making a matter of extreme interest the quest for more and more effective non-linear materials (see e.g. Ref [14]). Due to its unique sensitivity to the symmetry of the material, moreover, Second Harmonic Generation has been intensively studied for imaging of biological tissues [15][16] and for the characterisation of microstructures [17] (see Fig. (1.3)) Finally, another important application of the SHG is the characterisation of surfaces and interfaces, which also relies on the symmetry sensitivity of the $\overset{\leftrightarrow}{\chi}^{(2)}$ tensor.

1.2.1 Surface Second Harmonic Generation (SSHG)

As we explained in the previous section, the second order susceptibility $\overset{\leftrightarrow}{\chi}^{(2)}$ is equal to zero for materials having central symmetry. On the other side, the inversion symmetry is

Second order phenomena

Second Harmonic Generation	$\chi(-2\omega, \omega, \omega)$
Optical rectification	$\chi(0, -\omega, \omega)$
Sum frequency	$\chi(-(\omega_1 + \omega_2), \omega_1, \omega_2)$
Frequency difference	$\chi(-(\omega_2 - \omega_1), -\omega_1, \omega_2)$

Table 1.2: Some second order optical phenomena. In addition to Second Harmonic Generation, we report the Sum frequency (in which two photon of different frequency ω_1 and ω_2 are absorbed and one photon of frequency $\omega_1 + \omega_2$ is emitted), the Frequency difference (in which one photon of frequency ω_2 is absorbed, and two photons are emitted, one having frequency ω_1 and the other one having frequency $\omega_2 - \omega_1$), and the optical rectification (in which one photon of frequency ω is absorbed, one photon of frequency ω is emitted, and a static field is created in the material. Notice that in this table we used the convention which describes with positive frequencies the absorbed photons, and with negative frequencies the emitted ones. However, this convention is not used in this thesis.

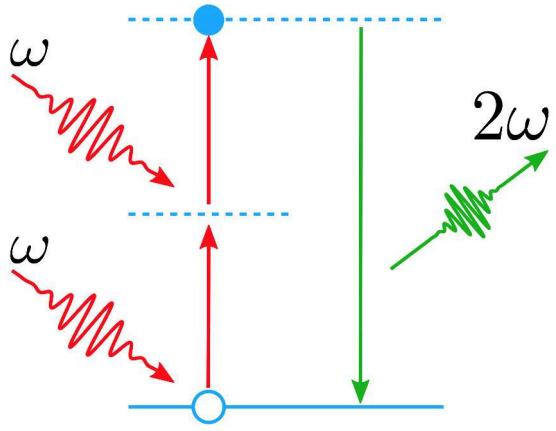

Figure 1.2: Schematic sketch of second harmonic generation. Two photons of frequency ω are absorbed by the material, promoting an electron in an an unoccupied state. The system then decays to the ground state with the emission of a photon of energy 2ω.

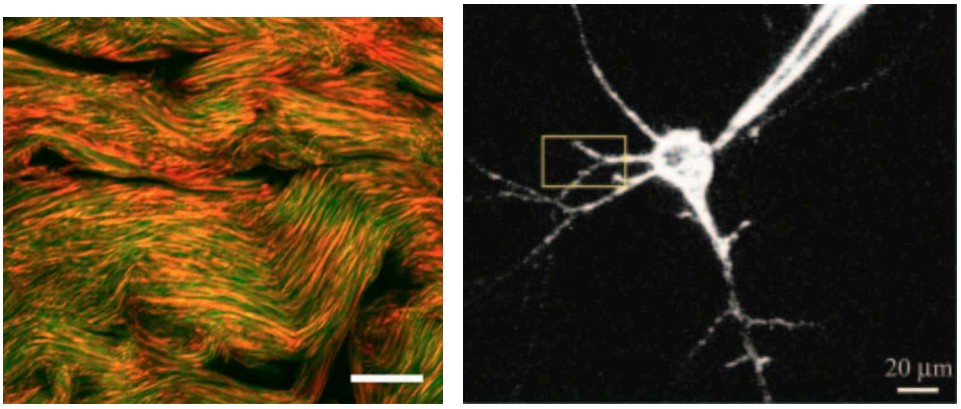

(a) (b)

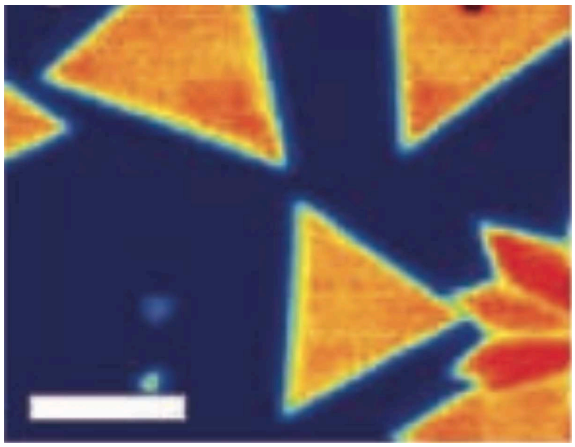

(c)

Figure 1.3: Selection of the possible applications of SHG as imaging technique. In panel (a), a SHG image of the collagen fibres contained in a rat foot flexor tendon cryosection is reported (reproduced from Ref. [15]). Collagen is formed by two type of fibers, one of which is centrosymmetric, corresponding to the bright filaments in panel (a), and the other not, corresponding to the darker filaments. In panel (b) (reproduced from Ref. [16], a SHG image of a neuron is shown. In panel (c) (reproduced from Ref. [17]), a SHG imaging technique has been used in order to characterise the shape of MoS_2 flakes over a SiO_2 substrate. MoS_2 is a non centro-symmetric material, and therefore it can generate a second harmonic signal (orange regions). SiO_2, on the other side, has inversion symmetry, and therefore it cannot produce any second order response (blue part), resulting in a high-contrast picture of the MoS_2 structures. The scale bar is set to 20 μm in all the three pictures

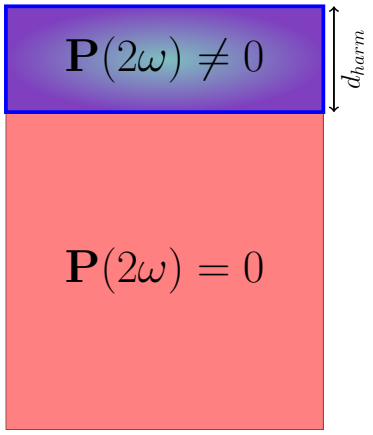

Figure 1.4: Schematic sketch of the second order response of a surface of centro-symmetric material undergoing an external perturbation of frequency ω. The polarisation density $\mathbf{P}(2\omega)$ is confined in a thin surface layer of thickness d_{harm} (we will come back on this parameter in Chapter 8), while in the inner region of the material we recover the bulk response $\mathbf{P}(2\omega) = 0$

an exact symmetry of the system just if we consider a perfect crystal, which is infinitely extended an translationally invariant in all directions. This is clearly no more the case for a finite crystal, which has finite extension and presents surfaces. Let's consider for exemple the case of Silicon, one of the materials studied in the present work. As it is well known, Silicon exhibits inversion symmetry, and therefore, an infinitely extended Silicon crystal undergoing to an external perturbation will have second order response equal to zero. On the other side, if the crystal is cut and a surface is created, the inversion symmetry is broken, and a thin layer of harmonically active material is created nearby the cut (see Fig. (1.4)). All the second order response come from this layer: if we go deep inside into the material, the electronic wave-functions will become more and more bulk-like and the symmetry of the infinite crystal will be recovered, resulting in a zero second order response from the inner region of the material.

1.3 Conclusion and summary of the thesis

In this chapter we tried to give an overview of the motivations which justify a research to better understand optical properties of functionalised surfaces. We also briefly illustrated how materials react to an external electromagnetic field, with a special focus on non-linear response. We then discussed more in detail why SHG is a good quantity to measure in order to investigate surface properties of material presenting inversion summetry, like the silicon (functionalised) surfaces which are the systems studied in this work. In this section,

we present the structure of the present thesis: in Chapter 2 I briefly introduce the Density Functional Theory and the Time-Dependent Density Functional Theory, which constitute the theoretical framework in which our calculations have been performed. In Chapter 3 I present in detail the surfaces which have been object of the present thesis, illustrating their atomic reconstruction and adsorption configuration. In Chapter 4, I present the so-called vacuum problem. This problem affect macroscopic response functions calculated within the supercell formalism, and it typically manifests when local field effects are included in the calculation. Treated in detail for the first time by Tancogne-Dejean et al. in 2015, this problem has been solved with the introduction of the Selected-G method (see Ref.s [18], [19], [20]). In the same chapter, I will present the result of the first SHG calculation for the surface of silicon functionalised with Thymine with the inclusion of Local Field Effects, and I will briefly describe the main features of these spectra. As it will be seen, Local Field Effects strongly suppress the response of the silicon surface upon thymine adsorption: understanding the origin of this effect will be the aim of Chapter 5. In this chapter, in order to better understand the effect of functionalisation , I isolate the system from its replicas, in order to eliminate any spurious interaction coming from the adoption of the supercell formalism. In a first moment I will derive the main features of the response of an isolated slab, using a simple Lorentz model. Then, I will present the calculations of the optical quantities of interest performed within the mixed-space approach, which allows to obtain the response of the isolated system in a fully *ab initio* way. Chapter 7 will be then devoted to analyse in detail the link between the calculated quantities and the quantities which are actually experimentally measured in a spectroscopy experiment (i.e. reflectance, transmittance and adsorbance). The most important result of this Chapter (and one of the most important of the present thesis) is that the ambiguity affecting the calculation of the macroscopic optical response functions (which has been described in Chapter 4), actually does not affect the quantities which are experimentally measured, adding a further block to the understanding of the so-called vacuum problem, and ideally closing the circle opened by Tancogne-Dejean in his thesis [20]. In Chapter 8 I present the result of the SHG calculations from functionalised silicon surfaces, and I will try to estimate the sensitivity of this spectroscopic technique to the adsorbed specimen and to the adsorption configuration.

Chapter 2

DFT and TD-DFT: an introduction

In this chapter we want to give a brief description of the many-body problem and of *ab initio* methods which have been used during this work. This chapter is articulated in three parts: we start with describing the many-electrons hamiltonian and explaining difficulties coming from the two-body interaction between particles. In the second part, we will expose the foundation of the Density Functional Theory (DFT), which, by mean of the Kohn-Sham equations, is an efficient -and in principle exact- instrument to inquire the ground state properties of many electrons systems, and we will continue with its time-dependent extension. We will summarise the quantity used to calculate the first and second order response functions, and how they are modified to get surface properties.

2.1 The full many electron hamiltonian

Systems like molecules, clusters, or solids, are basically aggregated of nuclei and electrons interacting via Coulomb potential. This kind of system can be therefore described by an Hamiltonian of the following form:

$$\hat{H} = \sum_{i}^{N_e} \frac{p_i^2}{2m_e} + \sum_{I}^{N_I} \frac{p_I^2}{2M_I} + \sum_{i}^{N_e} \hat{V}_{ne}(\mathbf{r}_i) + \hat{V}_{ee} + \hat{V}_{nn} \tag{2.1}$$

where $\hat{V}_{ee}$ is the electron-electron interaction term:

$$\hat{V}_{ee} = \frac{1}{2} \sum_{i \neq j} \frac{e^2}{|\mathbf{r}_i - \mathbf{r}_j|} \tag{2.2}$$

and

$$\hat{V}_{ne}(\mathbf{r}) = -\sum_I \frac{Z_I e^2}{|\mathbf{r} - \mathbf{R}_I|} \tag{2.3}$$

is the potential given by nuclei. In principle, to solve the Schroedinger equation associated with this hamiltonian, we should account for nuclear degree of freedom as well as the electronic ones. Ionic and electronic degrees of freedom, in fact, are coupled via the electron-nuclei interaction term, giving arise sometimes to important effects: in molecule, for example, electronic transitions could allow conformational changing, and in crystals, collective oscillations of the lattice, could allow transitions otherwise forbidden. Nevertheless, treating on the same footing electronic and nuclear degrees of freedom would make unapproachable the problem. Considering that the ion masses are much bigger than the electronic mass, we can adopt the following approximation, known as *Born-Oppenheimer* approximation: we will consider the ions as fixed in their equilibrium positions. The wavefunction will contain therefore only the electronic degrees of freedom. Moreover, being fixed the nuclear coordinates, we remove the nucleus-nucleus interaction term from the hamiltonian, since in this approximation just act as an additive constant. The problem to solve is now an eigenvalues problem of this kind:

$$H_e \Psi(\mathbf{x}_1, \ldots, \mathbf{x}_N) = E_i \Psi(\mathbf{x}_1, \ldots, \mathbf{x}_N) \tag{2.4}$$

where H_e has the following form:

$$H_e = \sum_i \frac{p_i^2}{2m_i} + \sum_i \hat{V}_{ne}(\mathbf{r}_i) + \frac{1}{2}\sum_{i \neq j} \frac{e^2}{|\mathbf{r}_i - \mathbf{r}_j|} \tag{2.5}$$

The problem of electronic correlation

Due to the presence of two-body interaction term (2.2), the Schroedinger equation (2.4) is extremely difficult to approach. The simplest way to search an approximate solution is to exploit the well known variational theorem of quantum mechanics:

Theorem 1 (Variational theorem)**.** *Let H be an hamiltonian, and let Ψ_0 and E_0 be respectively the ground state wavefunction and the ground state energy of this hamiltonian (we assume for sake of simplicity that the ground state is not degenerate). For each trial wavefunction $\tilde{\Psi}$,*

$$\langle \tilde{\Psi} | H | \tilde{\Psi} \rangle \geq \langle \Psi_0 | H | \Psi_0 \rangle = E_0 \tag{2.6}$$

In the relation above, the equality holds if, and only if, $\tilde{\Psi} = \Psi_0$

The way to proceed now, is to choose a certain functional form for the trial wavefunction, depending on some parameters, and then finding the parameters who minimise the expectation value $\langle\tilde{\Psi}|H|\tilde{\Psi}\rangle$. The simplest functional form we can choose for the trial wavefunction is an antisymmetrised [1] product of N single particle spin-orbital functions:

$$\tilde{\Psi} = \frac{1}{\sqrt{N!}}\det\{\psi_1, \ldots, \psi_N\} \tag{2.7}$$

where the spin-orbital ψ_i

$$\psi_i(\mathbf{r_i}, \sigma(i)) = \varphi_i(\mathbf{r_i})\chi(i) \tag{2.8}$$

is simply the product of a spatial wavefunction and a spin wavefunction. At this point, one could minimise the expectation value of the hamiltonian on the wavefunction (2.7), and finding a set of one-particle equation for the spin orbitals.
This approach the Hartree-Fock method [21]. It is well known that it fails to reproduce correlation effects. To illustrate this point, let's consider now a very simple model of interacting system: the Helium atom. This system is formed by two electrons subject to a central potential given by a point charge of charge $2e$.

$$V_{ne} = -\frac{2e^2}{|\mathbf{r_1}|} - \frac{2e^2}{|\mathbf{r_2}|} \tag{2.9}$$

and interacting between them via a potential:

$$V_{ee} = \frac{e^2}{|\mathbf{r_1} - \mathbf{r_2}|} \tag{2.10}$$

In the Hartree-Fock approximation, the ground state wavefunction will have the form of (2.7):

$$\tilde{\Psi} = \frac{1}{\sqrt{2}}\varphi_{1s}(\mathbf{r}_1)\varphi_{1s}(\mathbf{r}_2)\big[\alpha(1)\beta(2) - \beta(1)\alpha(2)\big] \tag{2.11}$$

where $\alpha(i)$ and $\beta(i)$ stands respectively for spin up and down. Let's consider now the square modulus of this wavefunction:

$$|\tilde{\Psi}|^2 = |\varphi_{1s}(\mathbf{r}_1)|^2|\varphi_{1s}(\mathbf{r}_2)|^2 \tag{2.12}$$

The physical meaning of $|\tilde{\Psi}|^2 d\mathbf{r}_1 d\mathbf{r}_2$ is the probability to find one electron in the volume $d\mathbf{r}_1$ centred in $\mathbf{r}_1$, *and* one electron in the volume $d\mathbf{r}_2$ centred in $\mathbf{r}_2$. Therefore, the expression (2.12), states that the probability to find *both* the electron in the point $\mathbf{r}$ is given by:

$$|\tilde{\Psi}|^2 d\mathbf{r}_1 d\mathbf{r}_2 = |\varphi_{1s}(\mathbf{r})|^2|\varphi_{1s}(\mathbf{r})|^2 d\mathbf{r}_1 d\mathbf{r}_2 \tag{2.13}$$

[1] The determinantal form has been required in order to assure the antisymmetry of the wavefunction under exchange of coordinates of different particles, i.e. the Pauli exclusion principle

This is the point which makes wavefunctions of kind (2.7) intrinsically not adapted to describe the wavefunction of an interacting electron system. Due to the repulsive coulombian divergence the probability to find one electron in $\mathbf{r}_1$ *and* one electron in $\mathbf{r}_2$, should goes to zero as $\mathbf{r}_1$ approaches to $\mathbf{r}_2$, forming the so called *correlation hole*. Fixing the position of one particle, I'm also modifying the position *of all other ones*: this explains why we refer to interacting particles system saying that "they are correlated", in opposition to "independent particle systems", where the position of one particle is not related to the position of other ones, and that are *exactly* described by wavefunction like the (2.7). The correlation hole, therefore, is the cause of complicated dependence of wavefunctions on the electronic coordinates; moreover, the absence of the correlation hole in wavefunctions of the form (2.7), leads to an overestimation of coulombian interaction energy (since this wavefunction allows electron to get closer than they actually could). This excess of energy, is called *correlation energy*.

2.2 Density Functional Theory

The Hohenberg-Kohn's theorems

As we saw in the previous section, what makes the many-electrons problem so difficult to approach, is the presence of coulombian interelectronic interaction. This term induces a complicated dependence of the wavefunction on the electronic coordinates $\mathbf{r_i}$, and makes extremely hard to directly solve the Schrödinger equation. Moreover, methods to directly solve the Schrödinger equations, like full-CI (see [21] for instance), which are largely used in quantum chemistry, are simply not applicable in solids, due to their disadvantageous computational scaling. The Density Functional Theory (DFT), in a way, allow us to bypass the problem to solve the Schroedinger equation to find the ground states wavefunction. DFT relies on the osservation that *it's not strictly necessary to find the ground state wavefunction, in order to find the ground state energy of an interacting electrons system.* This important result, is contained in [22]:

Theorem 2 (First Hohenberg-Kohn's theorem)**.** *Let $n(\mathbf{r})$ be the ground state density of an electron system subject to an external potential $v_{ext}(\mathbf{r})$. Then, the potential inducing that density is unique.*

If it's true, as stated by this theorem, that fixed the one-particle density, it's also fixed the external potential that induces that density, then the one-particle density also univocally determines the whole hamiltonian and, as a consequence the ground state wave function Ψ_0. In other words, we can say that the external potential (and the hamiltonian, and the ground state wavefunction) are functional of the ground state density $n(\mathbf{r})$. We

will write:

$$n(\mathbf{r}) \longrightarrow v_{ext}[n] \tag{2.14}$$
$$n(\mathbf{r}) \longrightarrow H[n] \tag{2.15}$$
$$n(\mathbf{r}) \longrightarrow \Psi_0[n] \tag{2.16}$$
$$\tag{2.17}$$

Since the ground state wavefunction is a functional of density, also the expectation value of an operator on the ground state will be a density functional:

$$\begin{aligned} n(\mathbf{r}) &\longrightarrow T[n] = \langle \Psi_0[n] | \hat{T} | \Psi_0[n] \rangle \\ n(\mathbf{r}) &\longrightarrow E_{ee}[n] = \langle \Psi_0[n] | \hat{V}_{ee} | \Psi_0[n] \rangle \end{aligned}$$

we can therefore express the ground state energy as a density functional:

$$E_v[n] = T[n] + E_{ee}[n] + \int d\mathbf{r} v_{ext}(\mathbf{r}) n(\mathbf{r}) \tag{2.18}$$

The result expressed in eq. (2.18) is astonishing. As we've seen in the previous section, the electronic interaction energy is a quantity which depends on the probability to find two electron at a certain distances the one from the other. For this reason, it can be easily expressed as function of the two-particle density. Nevertheless, the first Hohenberg-Kohn theorem, assure us that it can be also express as funtion of the one body density. This means that, in some non trivial way, *all the information about electronic correlation is encoded inside the one particle density*, an object intrinsecally simpler than the complicated N-body wavefunction. This simplification is only apparent: the way the correlation is encoded in $n(\mathbf{r})$ -i.e. the functional form of $V_{ee}[n]$ - is not known, and we have to develop approximation for it.
The following theorem [22] is the variational principle of the theory:

Theorem 3 (Second Hohenberg-Kohn's theorem)**.** *Let $v(\mathbf{r})$ be the external potential acting on a N electrons system, let $n_0(\mathbf{r})$ be the ground state one-particle density of this system, and let $E_v[n]$ be the functional* (2.18)*. For each $\tilde{n}(\mathbf{r})$ such that:*

$$\begin{aligned} \tilde{n}(\mathbf{r}) &\geq 0 \quad \forall\ \mathbf{r} \\ \int \tilde{n}(\mathbf{r}) d\mathbf{r} &= \quad N \end{aligned}$$

then:

$$E_v[n_0] \leq E_v[\tilde{n}]$$

2.2.1 Kohn-Sham equations

The Hohenberg-Kohn's theorems represent a milestone from a theoretical point of view, since they rigorously justify that the ground state one particle density can be chosen as fundamental variable of the many body problem. Nevertheless, from a practical point of view, they are a pretty poor instrument: even if we had the exact form of the functional $E_v[n]$, they don't suggest any way to efficiently calculate $n(\mathbf{r})$. What made the DFT a useful tool for real calculation, have been the Kohn-Sham equations[23].

The Kohn-Sham method is based on the following consideration: the formulation of the first Hohenberg-Kohn theorem, doesn't require as hypothesis that electrons are interacting. The theorem could be in principle applied to any system of fermions, regardless they're interacting or not. Therefore, the first Hohenberg-Kohn's theorem tell us that, for each density $n(\mathbf{r})$, it exists one, and only one external potential $v_{ext}(\mathbf{r})$, such that a system of interacting electron subject to $v_{ext}(\mathbf{r})$ reproduces the ground state density $n(\mathbf{r})$. But it also guarantee that, for the same $n(\mathbf{r})$, it exists one and only one external potential $v_s(\mathbf{r})$, such that a fictitious system of non-interacting electrons subjected to this potential, reproduces exactly $n(\mathbf{r})$.
In a system of non-interacting electrons, the wavefunction will be *exactly* given by:[2]

$$\Psi_s = \frac{1}{\sqrt{N!}}\det\{\psi_1, \ldots, \psi_N\} \tag{2.19}$$

where the ψ_i are the N eigenstates of lowest energy of the one particle hamiltonian:

$$h_s = \left[-\frac{1}{2}\nabla^2 + v_s(\mathbf{r}) \right] \tag{2.20}$$

The kinetic Energy of this system will be exactly given by:

$$T_s[n] = \sum_i^N \langle\psi_i| -\frac{1}{2}\nabla^2|\psi_i\rangle \tag{2.21}$$

and the ground state density will be given by:

$$n(\mathbf{r}) = \sum_i^N |\psi_i(\mathbf{r})|^2 \tag{2.22}$$

Now, let's consider again the functional (2.18). It can be written as:

$$\begin{aligned} E_v[n] =& T_s[n] + \int v_{ext}(\mathbf{r})n(\mathbf{r})d\mathbf{r} + J[n] + T[n] - T_s[n] - J[n] + E_{ee}[n] \\ =& T_s[n] + \int v_{ext}(\mathbf{r})n(\mathbf{r})d\mathbf{r} + J[n] + E_{xc}[n] \end{aligned} \tag{2.23}$$

[2] In previous sections, we have explicitly written electronic masses and charges in the equations. From now on, we will adopt the Hartree atomic units, in which $\hbar = e = m_e = 1$

where we have introduced $J[n]$, the Hartree's interaction energy:

$$J[n] = \frac{1}{2}\int \frac{n(\mathbf{r}')n(\mathbf{r}'')}{|\mathbf{r}' - \mathbf{r}''|} d\mathbf{r}' d\mathbf{r}'' \tag{2.24}$$

and the so called exchange-correlation functional:

$$E_{xc}[n] = T[n] - T_s[n] + E_{ee}[n] - J[n] \tag{2.25}$$

This functional is made of two terms: the first is the difference between the kinetic energy of the interacting system and the kinetic energy of non-interacting one (typically a small difference). The second term, is the difference between the interelectronic interaction energy, and $J[n]$, which is the interaction energy of a classical density of charge distribution $n(\mathbf{r})$. This last difference, therefore, will contain the non-classical part of the coulombian interaction, which means, the correlation effects.
We're now able to express the functional (2.18) as function sum of $E_{xc}[n]$, which is an unknown functional, and quantities like $T_s[n]$, $J[n]$, and $\int v_{ext}(\mathbf{r})n(\mathbf{r})d\mathbf{r}$, which we can express as functions of orbitals of non-interacting system. Variating respect to the orbitals ψ_i, we obtain the following important result: the one-particle ground state density of a system of interacting electrons, subject to an external potential $v_{ext}(\mathbf{r})$, can be reproduced by a fictitious system of non-interacting electrons subject to the effective potential:

$$v_s[n] = v_{ext}(\mathbf{r}) + v_H[n](\mathbf{r}) + v_{xc}[n](\mathbf{r}) \tag{2.26}$$

where $v_{xc}[n]$ is:

$$v_{xc}(\mathbf{r}) = \frac{\delta E_{xc}[n]}{\delta n(\mathbf{r})} \tag{2.27}$$

and is called *exchange-correlation potential*, and

$$\begin{aligned} v_H[n](\mathbf{r}) &= \frac{\delta J[n]}{\delta n(\mathbf{r})} \\ &= \int d\mathbf{r}' \frac{n(\mathbf{r}')}{|\mathbf{r} - \mathbf{r}'|} \end{aligned} \tag{2.28}$$

is called Hartree's potential.
To find the ground state one-particle density, we will need, as a consequence, solve the following one particle equations:

$$\left[-\frac{1}{2}\nabla^2 + v_s[n](\mathbf{r}) \right] \psi_i(\mathbf{r}) = \varepsilon_i \psi_i(\mathbf{r}) \tag{2.29}$$

which are the celebrated *Kohn-Sham equations*.
This result is truly remarkable: the Kohn-Sham equations allow us to find the ground state energy of the true N-electron system -in principle in an exact way - just solving N

one-particle equation with a rigorously local potential, instead to solve the complicated full many-body Schroedinger equation. In particular, the system described by the hamiltonian (2.5) can be viewed as an N electrons system subject to an external potential $v_{ext}(\mathbf{r}) = V_{ne}(\mathbf{r})$. The complication is now to find a reasonable approximation of the exchange correlation potential, which is unknown. In the next section we will briefly describe the idea of the popular Local Density Approximation (LDA), which has been the approximation of v_{xc} used throughout the thesis work.
Before to conclude, a last remark has to be done. In this section, we have seen that it is possible to calculate, in principle in an exact way, the ground state energy and the ground state density of a many electrons system, by mean of the Kohn-Sham equations. These two are the only physically meaningful quantities we can get via the Kohn-Sham approach: no physical meaning, on the contrary, can be related to the eigenvalues ε_i and the orbitals ψ_i, which are quantities living only in the fictitious non-interacting Kohn-Sham system. The eigenvalues of the non-occupied Kohn-Sham orbitals, in particular, should not be interpreted as the excitation energies of the true many electron system. Regardless of the goodness of the exchange correlation potential v_{xc}, in fact, the DFT underestimate systematically the energy separation between HOMO and LUMO. Therefore, in solids, bandgap values predicted by DFT are typically significantly lower of real values. Anyway, the dispersion of bands is often quite accurate; for this reason, and also for its reasonable computational cost, the DFT is widely used for band structure calculations, as first estimate, or as starting point for more sophisticated approaches.

Local Density Approximation (LDA)

The Local Density Approximation is the simplest approximation to the exchange-correlation functional. In this family of functionals, the exchange correlation functional is approximated by:

$$E_{xc}^{(LDA)}[n] = \int \varepsilon_{xc}(n(\mathbf{r}))n(\mathbf{r})d\mathbf{r} \tag{2.30}$$

where $\varepsilon_{xc}(\mathbf{r})$ is the exchange correlation energy (per number of electrons) of an homogenous electron gas of density $n(\mathbf{r})$. In other words, in this approximation we assume that the contribution of the exchange correlation energy given by the $n(\mathbf{r})d\mathbf{r}$ electrons which are around $\mathbf{r}$, is the same of an homogenous electron gas with the same density. Given a certain value of n (which is obviously constant in the case of an homogenous electron gas), the exchange correlation energy can be calculated almost exactly via Montecarlo techniques. Values of $\varepsilon_{xc}^{(HEG)}[n]$ for several values of n, can be then fitted in order to obtain analytic expressions. The functional we used during this work is reported in [24],and reproduces Ceperley-Alder Montecarlo calculation. As it's easy to imagine, the goodness of this approximation depends on the degree of homogeneousness of the system. Due to this reason, the great success of LDA in solids, where often the wavefunctions are delocalised

2.2.2 Solving the Kohn-Sham equation in periodic systems

The Density Functional Theory, is a tool that, in principle, allow us to approach every kind of many electron system. Ground state properties of atoms and molecules, as well as solids (regardless to their periodicity), can be enquired by mean of the Kohn-Sham equations. Anyway, since in this work only crystal structures have been studied, we will limit our discussion to the methods to solve the Kohn-Sham equations in periodic systems.

A crystalline solid is made of an array of repeated units. The smallest one is called *primitive cell*. If the primitive cell of the crystal contains only one atom, we'll say that the lattice is a *simple lattice*. In this case, the position of each atom of the crystal, can be expressed as the sum of integer multiples of three vectors, called *primitive vectors*:

$$\mathbf{t}_n = n_1\mathbf{t}_1 + n_2\mathbf{t}_2 + n_3\mathbf{t}_3 \tag{2.31}$$

In the case there are, let's say, N_{at} atoms for unit cell, we will say that the lattice is a *composite lattice*. In this case, in addition to the primitive vectors $\mathbf{t}_i$, to describe the position of every atom of the crystal, we need N_{at} vectors $\mathbf{d}_\nu$, called *basis vectors*. Now: it's reasonable to assume that, if ions are distributed periodically in the space, also the one particle density will have the same periodicity:

$$n(\mathbf{r} + \mathbf{t}_n) = n(\mathbf{r}) \tag{2.32}$$

Then the effective Kohn-Sham potential will be periodic as well:

$$v_s[n](\mathbf{r} + \mathbf{t}_n) = v_s[n](\mathbf{r}) \tag{2.33}$$

Let's introduce now, together the direct lattice, the so called *reciprocal lattice*. This lattice is defined as the sum of integer multiples of the following three vectors, called reciprocal primitive vectors:

$$\begin{aligned} \mathbf{g}_1 &= \frac{2\pi}{\Omega}\mathbf{t}_2 \times \mathbf{t}_3 \\ \mathbf{g}_2 &= \frac{2\pi}{\Omega}\mathbf{t}_3 \times \mathbf{t}_1 \\ \mathbf{g}_3 &= \frac{2\pi}{\Omega}\mathbf{t}_1 \times \mathbf{t}_2 \end{aligned} \tag{2.34}$$

with Ω:

$$\Omega = \mathbf{t}_1 \cdot (\mathbf{t}_2 \times \mathbf{t}_3) \tag{2.35}$$

the volume of the primitive cell. It is possible to proof that, if a certain function is periodic with the same periodicity of the direct lattice, then it can be expressed as a Fourier sum of plane waves having wave vectors equal to the reciprocal lattice vectors:

$$f(\mathbf{r} + \mathbf{t}_n) = f(\mathbf{r}) \Longrightarrow f(\mathbf{r}) = \sum_n f_n e^{i\mathbf{g}_n \mathbf{r}} \tag{2.36}$$

In a crystal, as a consequence, the Kohn-Sham potential could be expressed as:

$$v_s[n](\mathbf{r}) = \sum_j v_j e^{i\mathbf{g}_j \mathbf{r}} \tag{2.37}$$

We now observe that, if I let the Kohn-Sham potential act on a plane wave $e^{i\mathbf{qr}}$, I obtain:

$$v_s[n](\mathbf{r}) e^{i\mathbf{qr}} = \sum_j v_j e^{i(\mathbf{g}_j + \mathbf{q})\mathbf{r}} \tag{2.38}$$

if now we project this quantity on another plane wave $e^{i\mathbf{kr}}$, it's easy to show that we obtain:

$$\langle e^{i\mathbf{kr}} | v_s[n](\mathbf{r}) e^{i\mathbf{qr}} \rangle = \sum_j v_j \delta(\mathbf{k} - \mathbf{q} - \mathbf{g}_j) \tag{2.39}$$

It's evident that $e^{i\mathbf{kr}}$ and $v_s[n](\mathbf{r}) e^{i\mathbf{qr}}$ will be orthogonal if, and only if

$$\mathbf{k} - \mathbf{q} \neq \mathbf{g}_j \ \forall \ \mathbf{g}_j \tag{2.40}$$

In other words, the two functions will be orthogonal only if $\mathbf{k}$ cannot be obtained summing to $\mathbf{q}$ a reciprocal lattice vector.
Let's introduce the concept of first Brillouin zone. The first Brillouin zone can be operatively defined as the locus of points of reciprocal space, who are closer to the origin than to any else vector of reciprocal lattice. Evidently, the points of first Brillouin zone, automatically satisfy the property (2.40). The observation that two plane waves having as wave vectors two different points of the first Brillouin zone, are mapped by the periodical potential $v_s[n](\mathbf{r})$ in orthogonal functions, can be formalised in the following

Theorem 4 (Bloch theorem)**.** *The wavefunctions of a single particle hamiltonian with periodic potential have the following form:*

$$\psi(\mathbf{k}, \mathbf{r}) = e^{i\mathbf{kr}} u(\mathbf{k}, \mathbf{r}) \tag{2.41}$$

where $\mathbf{k}$ *is a vector in the first Brillouin zone, and* $u(\mathbf{k}, \mathbf{r})$ *is a function with periodicity of lattice*

The Bloch theorem can be also reformulated in the following useful form:

Theorem 5. *In the basis set of plane waves* $\{e^{i(\mathbf{k}+\mathbf{g}_j)\mathbf{r}}\}_{\mathbf{k},\mathbf{g}_j}$ *(where* $\mathbf{k}$ *are vectors in the first Brillouin zone, and* $\mathbf{g}_j$ *are the vectors of reciprocal lattice), the matrix representation of a one-particle hamiltonian with periodic potential, is block diagonal:*

$$H = \begin{bmatrix} H_{\mathbf{k_2}} & & 0 & \\ & H_{\mathbf{k_2}} & & \\ & & \ddots & \\ 0 & & & \ddots \end{bmatrix} \tag{2.42}$$

each block $H_{\mathbf{k_j}}$ *corresponds to a point in the first Brillouin zone, and it's the matrix representation of the hamiltonian on the subspace:*

$$W_{\mathbf{k_j}} = span\{e^{i(\mathbf{k_j}+\mathbf{g_1})\mathbf{r}}, e^{i(\mathbf{k_j}+\mathbf{g_2})\mathbf{r}}, \dots\}$$

Plane waves expansion and pseudopotentials

The Bloch theorem implicitly suggest that the most natural basis set to represent the Kohn-Sham hamiltonian is the set of plane waves $\{e^{i(\mathbf{k}+\mathbf{G}_n)\mathbf{r}}\}_{\mathbf{G}_n}$. The use of such a basis set presents anyway a serious drawback. The lowest energy crystal states (the so called *core states*), in fact, result to be extremely localised in real space. An accurate description of these states would require therefore plane waves of very large wave vectors, and consequently basis set so large to make unfeasible the diagonalisation of the single particle hamiltonian. In order to overcome this difficulty (known as "the variational collapse problem"), a possible solution is given by the pseudopotentials methods. The basic idea behind this approach is very simple: the core electrons, which due to their localisation are the source of the variational collapse problem, do not mix with valence states, and practically do not feel the influence of other atoms of the crystal. As a consequence, we can substitute the true crystal potential which some sort of effective potential incorporating the effect of core electrons, and then solve the secular problem for just the valence and conduction states. Such effective potential, as one can easily argue, is called pseudopotential. During this work, Troullier-Martins pseudopotentials [25] have been used. We will not give here a detailed discussion about the different kind of pseudopotentials. We will just say that the ones we used belong to a larger class, the so called *norm conserving pseudopotentials*. Pseudopotentials of this kind are design in order to make the pseudo-wavefunction reproduce as accurately as possible the true crystal wavefunction outside the core radius.The price to pay to obtain this result is the nonlocality of the pseudopotential, which, in general, acts differently on the different components of angular momentum. Compared to the huge basis sets which would be necessary for an all-electron calculation, this is anyway a minor

disadvantage, and the ability to correctly calculate the crystal wavefunctions outside the core region allows us to get the conduction and the valence energies in an efficient and accurate way.

2.3 Excited states beyond DFT: the TD-DFT

As we have seen in previous part, the DFT is a theory which allows one to obtain, in principle in an exact way, the ground state energy of a many electron system under the effect of an external static potential. Here we will introduce an extension of DFT, the Time Dependent-Density Functional Theory (TD-DFT). This development of DFT allows to obtain the response of a many electron system under the effect of a time dependent potential, and it will be our starting point for the calculation of optical absorption spectra.

2.3.1 Existence theorems

The starting point is the time dependent Schroedinger equation, in the Born-Oppenheimer approximation, where the external potential (given by the nuclei-electrons potential plus an external scalar potential) varies with time:

$$i\frac{\partial}{\partial t}|\Psi(t)\rangle = \hat{H}|\Psi\rangle \tag{2.43}$$

The hamiltonian is defined as:

$$\hat{H} = \hat{T} + \hat{V}_{ee} + \hat{V}_{ext}(t) \tag{2.44}$$

where:

$$\hat{V}_{ee} = \frac{1}{2}\sum_{i\neq j}\frac{1}{|\mathbf{r_i} - \mathbf{r_j}|} \tag{2.45}$$

and

$$V_{ext}(t) = \int d\mathbf{r} v_{ext}(\mathbf{r}, t) n(\mathbf{r}, t) \tag{2.46}$$

Runge and Gross demonstrated that it's possible find a one-to-one connection between the time dependent electronic density $n(\mathbf{r}, t)$ and the external potential $V_{ext}(\mathbf{r}, t)$. This result is contained in the following theorem [26]:

Theorem 6 (Runge-Gross theorem)**.** *Two densities $n(\mathbf{r}, t)$ and $n'(\mathbf{r}, t)$, evolving from a common initial state $|\Psi_0\rangle$ under the influence of two Taylor expandable potential $v(\mathbf{r}, t)$ and $v'(\mathbf{r}, t)$, are different if and only if v_{ext} and v'_{ext} differ for more than a time dependent constant $c(t)$*

As a consequence, the Hamiltonian is univocally determined, unless an irrelevant additive constant, from the one-particle time dependent density $n(\mathbf{r},t)$. This means that also the temporal evolved of the states $|\psi_0\rangle$ (the time dependent wavefunction $|\psi(\mathbf{r},t)\rangle$), is univocally determined from $n(\mathbf{r},t)$. In other words, the evolved wavefunction is a functional of the time dependent density:

$$\Psi[n(\mathbf{r},t)] \longrightarrow \Psi(\mathbf{r},t) \tag{2.47}$$

For this reason, the expectation values of observables on the temporal evolved of the initial states are functionals of $n(\mathbf{r},t)$ too:

$$\hat{O}[n(\mathbf{r},t)] = \langle\Psi[n(\mathbf{r},t)]|\hat{O}|\Psi[n(\mathbf{r},t)]\rangle \tag{2.48}$$

Therefore, every quantity necessary to calculate optical properties of materials (like transitions amplitudes, or excited states energies) can be derived from $n(\mathbf{r},t)$. The role of the Runge-Gross theorem is analogous to the role of first Hohenberg-Kohn theorem of the static DFT: it gives us a formal justification to use $n(\mathbf{r},t)$ as fundamental variable of the theory, since it proofs that the total hamiltonian is univocally determined by $n(\mathbf{r},t)$, but it doesn't give us any suggestion about how $n(\mathbf{r},t)$ can be calculated. An hint arrives from the [27]:

Theorem 7 (Van Leeuwen's theorem)**.** *Let $n(\mathbf{r},t)$ be the time-dependent density of a system of electrons interacting via a two-particle potential $W(\mathbf{r_1},\mathbf{r_2})$, and evolving from an initial state $|\Psi_0\rangle$ under the influence of a scalar external potential $v_{ext}(\mathbf{r},t)$. For each two-particle potential $W'(\mathbf{r_1},\mathbf{r_2})$, there are a state $|\Phi_o\rangle$ and a scalar external potential $v'_{ext}(\mathbf{r},t)$, such that the one-electron time-dependent density of a system of electrons interacting via W', evolving from the state $|\Phi_0\rangle$ under the effect of v'_{ext}, is exactly $n(\mathbf{r},t)$*

The formulation of Van-Leeuwen's theorem is extremely general, and it holds for every kind of interaction $W'(\mathbf{r_1},\mathbf{r_2})$. In particular, it guarantees that for every system of electrons interacting via the two-body coulombian potential , and subjected to the effect of an external potential $v_{ext}(\mathbf{r},t)$, it exists a non-interacting electron system ($W'=0$) which, under the effect of an appropriate effective potential $v_s(\mathbf{r},t)$, reproduces exactly the same density $n(\mathbf{r},t)$ of the interacting system.

2.3.2 Kohn-Sham time dependent equations

Let's consider the case in which the external time dependent potential is zero for $t<t_0$, and it's turned on at the time t_0. This is not such a big limitation: in fact, it corresponds to the experimental situation, where the perturbation is turned on at a finite time t_0. For $t<t_0$ the external potential will not depend on time, and the electronic density will be static:

$$n(\mathbf{r},t) = n_0(\mathbf{r}) \qquad\qquad \text{for } t<t_0$$

As we know from DFT, the effective potential who will reproduce this static density in a non-interacting electron system, is given by:

$$v_s[n](\mathbf{r}) = v_0(\mathbf{r}) + \int d\mathbf{r}' \frac{n(\mathbf{r}')}{|\mathbf{r} - \mathbf{r}'|} + v_{xc}[n](\mathbf{r}) \tag{2.49}$$

At the time t_0, the perturbation is turned on, and as a consequence also the effective potential who acts of the electrons in the non-interacting system will start to depend on time. In analogy with the effective potential of static DFT, we separate the electron-electron interaction in a classical Hartree's term, and in another term including the effects of quantum nature:

$$v_s[n](\mathbf{r}, t) = v_{ext}(\mathbf{r}, t) + \int d\mathbf{r}' \frac{n(\mathbf{r}', t)}{|\mathbf{r}' - \mathbf{r}|} + v_{xc}(\mathbf{r}, t) \tag{2.50}$$

Time dependent orbitals in the non interacting system are obtained solving the following time-dependent Schroedinger equations, the so called time-dependent Kohn-Sham equations:

$$i\frac{\partial}{\partial t}\varphi_i^{(KS)}(\mathbf{r}, t) = \left[-\frac{\nabla^2}{2} + v_s[n](\mathbf{r}, t) \right] \varphi_i^{(KS)}(\mathbf{r}, t) \tag{2.51}$$

with initial conditions:

$$\varphi_i^{(KS)}(\mathbf{r}, t)\Big|_{t=t_0} = \varphi_i^{(KS)}(\mathbf{r}) \tag{2.52}$$

Once we have found the time-dependent orbitals, the time-dependent density is obtained as:

$$n(\mathbf{r}, t) = \sum_i \left|\varphi_i^{(KS)}(\mathbf{r}, t)\right|^2 \tag{2.53}$$

In principle, in order to find the time dependent orbitals, we should (and we could) solve (2.51). Anyway, in the great majority of cases we are interested to study, the difference between time-evolved of single-particle orbitals and unperturbed orbitals is very small. For this reason, it's more practical to adopt a perturbative approach. Before showing how perturbation theory can be applied to the TD-DFT in order to obtain the time-dependent density, let's recall some general results.

2.4 Response theory and Dyson equation(s) of TD-DFT

2.4.1 Perturbation theory

Let's consider a system described from the following Hamiltonian:

$$\hat{H} = \hat{H}_0 + \hat{H}_{int}(t) \tag{2.54}$$

where $\hat{H}_0$ is the hamiltonian of the unperturbed system, with known eigenstate $\{\Psi_i\}_i$ and eigenvalues $\{E_i\}_i$, and $\hat{H}_{int}(t)$ is a time dependent perturbation. Under the effect of the perturbation, the wavefunction of the system (which we assume to be in the state Ψ_0 at time $t = t_0$)will depend on time. Since the set of eigenstates of unperturbed hamiltonian is a complete set, we can expand the time evolved of Ψ_0 as sum of eigenstates of unperturbed hamiltonian:

$$|\Psi(t)\rangle = \sum_j e^{-iE_j t} c_j(t) |\Psi_j\rangle \tag{2.55}$$

As well known from perturbation theory, if the perturbation is weak, we can perturbatively expand the coefficient of the last expansion: at the zero order, we obtain:

$$c_i^{(0)} = \begin{cases} 1 \text{ for } i = 0 \\ 0 \text{ for } i \neq 0 \end{cases} \tag{2.56}$$

and at first order in perturbation theory we have:

$$c_j^{(1)}(t) = -i \int_{t_0}^{t} dt' e^{i\omega_{j0}t'} \langle \Psi_j | \hat{H}_{int}(t') | \Psi_0 \rangle \tag{2.57}$$

where we introduced:

$$\omega_{mn} = E_m - E_n \tag{2.58}$$

Density response

Let's suppose we want calculate the time evolution of one particle density. The one particle density is an observable, and its time evolution can be calculated evaluating the expectation value of the one particle density operator $\hat{n}(\mathbf{r})$ on the time evolved wavefunction $|\Psi(t)\rangle$:

$$n(\mathbf{r}, t) = \langle \Psi(t) | \hat{n}(\mathbf{r}) | \Psi(t) \rangle \tag{2.59}$$

If we substitute with its perturbative expansion

$$|\Psi(t)\rangle = e^{-iE_0 t} |\Psi_0\rangle + \sum_j e^{-iE_j t} (c_j^{(1)}(t) + c_j^{(2)}(t) + \dots) |\Psi_j\rangle$$

it's immediate to find that:

$$\begin{aligned} n(\mathbf{r}, t) = \langle \Psi_0 | \hat{n}(\mathbf{r}) | \Psi_0 \rangle & \\ + \sum_l e^{iE_0 t} e^{-iE_l t} \langle \Psi_0 | \hat{n} | \Psi_l \rangle c_l^{(1)}(t) & \\ + \sum_l e^{-iE_0 t} e^{iE_l t} \langle \Psi_l | \hat{n} | \Psi_0 \rangle c_l^{*(1)}(t) & \\ + \mathcal{O}(2) & \end{aligned} \tag{2.60}$$

We see that, by mean of perturbative expansion of the wavefunction, also the time evolution of one particle density can be perturbatively expanded: the first term of the expression above is the order zero of this expansion, and it's the density of the initial state (in this case, the ground state). The second and the third term of the expression, are the variation of density at first order. After some simple algebraic manipulation, the first order variation of density can be recasted in this more explicit form:

$$\delta n^{(1)}(\mathbf{r},t) = i\sum_{k\neq 0}\frac{\langle\Psi_0|\hat{n}(\mathbf{r})|\Psi_k\rangle\langle\Psi_k|\hat{H}_{int}(\mathbf{r},t)|\Psi_0\rangle}{\omega-\omega_{k0}+i\eta} \tag{2.61}$$

Let's now assume that the interaction hamiltonian has the following form:

$$H_{int}(\mathbf{r},t) = \sum_i v(\mathbf{r_i})e^{-i\omega t} \tag{2.62}$$

The first order variation of density can be rewritten as:

$$\delta n(\mathbf{r},t) = \int d\mathbf{r}'\sum_k \frac{\langle\Psi_0|\hat{n}(\mathbf{r})|\Psi_k\rangle\langle\Psi_k|\hat{n}(\mathbf{r}')|\Psi_0\rangle}{\omega-\omega_{k0}+i\eta}v(\mathbf{r}')e^{-i\omega t} \tag{2.63}$$

The quantity

$$\chi(\mathbf{r},\mathbf{r}',\omega) = \sum_k \frac{\langle\Psi_0|\hat{n}(\mathbf{r})|\Psi_k\rangle\langle\Psi_k|\hat{n}(\mathbf{r}')|\Psi_0\rangle}{\omega-\omega_{k0}+i\eta} \tag{2.64}$$

is the so called *polarizability* (also called *density-density response function*). We see that, with the definition of the polarizability, the first order variation of density can be rewritten in the more compact form

$$\delta n(\mathbf{r},\omega) = \int d\mathbf{r}'\chi(\mathbf{r},\mathbf{r}',\omega)v_{ext}(\mathbf{r}',\omega) \tag{2.65}$$

The physical meaning of the polarizability is therefore the following: $\chi(\mathbf{r},\mathbf{r}',\omega)$ is the contribution to the variation of density in the point $\mathbf{r}$, given by the δ-like potential centered in the point $\mathbf{r}'$. Integrating on $\mathbf{r}'$ (which means, summing the contribution by the potential in every point of space), we obtain the density variation in the point $\mathbf{r}$, at first order in perturbation theory.
We notice that to obtain the expression of $\chi(\mathbf{r},\mathbf{r}',\omega)$, we didn't make any approximation (except assuming to be in regime of linear response). Therefore, our expression for the linear susceptibility, is an exact result: if I had the wavefunctions of ground and excited states of the system, I could use the (2.64) to evaluate $\chi(\mathbf{r},\mathbf{r}',\omega)$, and using it to derive optical quantities of interest. Unfortunately, this is not the case: even if the (2.64) is exact, having the unperturbed states $\{\Psi_i\}_i$ of the system would require to solve the time-independent many electrons problem, which we're not able to do.

Independent particle polarizability

As we saw before, we are not able to directly calculate the susceptibility of the interacting electrons system, because of our ignorance of the wavefunctions. On the other side, we are able to calculate both eigenfunctions and eigenvalues of the non-interacting Kohn-Sham system: we can therefore use the (2.64) in order to derive the susceptibility of the Kohn-Sham system.The ground state of Kohn-Sham system will be given by the N $\psi_i(\mathbf{r},t)$ spin-orbitals of lowest energy. Such orbitals, which in the ground state have occupation number equal to 1, are called *real orbitals*, while higher energies orbitals, which in the ground states have occupation number equal to 0, are called *virtual orbitals*. The excited states of the Kohn-Sham system are built adding the to the real orbitals $|\varphi_n\rangle$ a certain number of virtual orbital $|\varphi_\nu\rangle$. The susceptibility of a non-interacting Kohn-Sham system can therefore written as:

$$\chi_s(\mathbf{r},\mathbf{r}',\omega)=\sum_n^{real}\sum_\nu^{virt.}\frac{\varphi_n^*(\mathbf{r})\varphi_\nu(\mathbf{r})\varphi_\nu^*(\mathbf{r}')\varphi_n(\mathbf{r}')}{\omega-\omega_{\nu n}+i\eta} \tag{2.66}$$

which can be rewritten in the following more readable form:

$$\chi_s(\mathbf{r},\mathbf{r}',\omega)=\sum_i\sum_j(f_i-f_j)\frac{\varphi_i^*(\mathbf{r})\varphi_j(\mathbf{r})\varphi_j^*(\mathbf{r}')\varphi_i(\mathbf{r}')}{\omega-\omega_{ji}+i\eta} \tag{2.67}$$

where f_i and f_j are the Fermi occupation numbers of φ_i and φ_j orbitals.
In analogous way we can obtain the second order density response function. Retaining the terms of second order in Eq. (2.60), we obtain second order contribution to the density. This term will be quadratic in the external perturbation:

$$\delta n^{(2)}(\mathbf{r},t)=\int d\mathbf{r_1}d\mathbf{r_2}\chi^{(2)}_{\rho\rho\rho}(\mathbf{r},\mathbf{r}_1,\mathbf{r}_2,2\omega,\omega,\omega)v^{ext}(\mathbf{r}_1,\omega)v^{ext}(\mathbf{r}_2,\omega) \tag{2.68}$$

where $\chi^{(2)}_{\rho\rho\rho}$ is the second order density response function. The second order response function of the independent particle system will be given by:

$$\begin{aligned}\chi^{0,(2)}_{\rho\rho\rho}(\mathbf{r},\mathbf{r}_1,\mathbf{r}_2,2\omega,\omega,\omega)=&\\ &=\sum_{n,n',n''}\frac{\varphi_n^*(\mathbf{r})\varphi_{n'}(\mathbf{r})}{E_n-E_{n'}+2\omega+2i\eta}\times\\ &\times\Bigg[(f_n-f_{n''})\frac{\varphi_{n'}^*(\mathbf{r}_1)\varphi_{n''}(\mathbf{r}_1)\varphi_{n''}^*(\mathbf{r}_2)\varphi_n(\mathbf{r}_2)}{E_n-E_{n''}+\omega+i\eta}\\ &+(f_n-f_{n''})\frac{\varphi_{n'}^*(\mathbf{r}_2)\varphi_{n''}(\mathbf{r}_2)\varphi_{n''}^*(\mathbf{r}_1)\varphi_n(\mathbf{r}_1)}{E_n-E_{n''}+\omega+i\eta}\\ &+(f_{n'}-f_{n''})\frac{\varphi_{n'}^*(\mathbf{r}_2)\varphi_{n''}(\mathbf{r}_2)\varphi_{n''}^*(\mathbf{r_1})\varphi_n(\mathbf{r}_1)}{E_{n''}-E_{n'}+\omega+i\eta}\\ &+(f_{n'}-f_{n''})\frac{\varphi_{n'}^*(\mathbf{r}_1)\varphi_{n''}(\mathbf{r}_1)\varphi_{n''}^*(\mathbf{r}_2)\varphi_n(\mathbf{r}_2)}{E_{n''}-E_{n'}+\omega+i\eta}\Bigg]\end{aligned} \tag{2.69}$$

2.4.2 Dyson equation of TD-DFT

The Van Leeuwen theorems assure us that the time-dependent density $n(\mathbf{r},t)$ of a system of interacting electrons subjects to an external potential $v(\mathbf{r},t)$, can be reproduced by a fictitious non-interacting electron system moving inside a proper effective potential. The time dependent single particle potential who has to act on the non-interacting electrons is given by:

$$v_s[n](\mathbf{r},t) = v(\mathbf{r},t) + \int d\mathbf{r}' \frac{n(\mathbf{r}',t)}{|\mathbf{r}'-\mathbf{r}|} + v_{xc}[n](\mathbf{r},t) \tag{2.70}$$

As we saw in the previous section, the time dependent density can be expanded around the ground state density:

$$n(\mathbf{r},t) = n_0(\mathbf{r}) + \delta n^{(1)}(\mathbf{r},t) + \dots$$

The Kohn-Sham effective potential is a functional of density: since we are assuming that the density variation is small, we can expand it around the ground state density $n_0(\mathbf{r})$, dropping all term of order higher than first order:

$$\begin{aligned} v_s[n](\mathbf{r},t) \approx & v(r,t) + \int d\mathbf{r}' \frac{n_0(\mathbf{r}') + \delta n^{(1)}(\mathbf{r}',t)}{|\mathbf{r}-\mathbf{r}'|} + v_{xc}[n_0](\mathbf{r}) + v_{1,xc}[\delta n^{(1)}](\mathbf{r},t) \\ = & v_s[n_0](\mathbf{r}) + v_{1,s}[\delta n^{(1)}](\mathbf{r},t) \end{aligned} \tag{2.71}$$

where:

$$v_{1,s}[\delta n^{(1)}](\mathbf{r},t) = v_1(\mathbf{r},t) + \int d\mathbf{r}' \frac{\delta n^{(1)}(\mathbf{r},t)}{|\mathbf{r}-\mathbf{r}'|} + \int d\mathbf{r}' \frac{\delta v_{xc}[n](\mathbf{r},t)}{\delta n^{(1)}(\mathbf{r}',t)}\bigg|_{n_0} \delta n^{(1)}(\mathbf{r}',t) \tag{2.72}$$

The quantity:

$$f_{xc}(\mathbf{r},\mathbf{r}',t,t') = \frac{\delta v_{xc}[n](\mathbf{r},t)}{\delta n(\mathbf{r}',t)}\bigg|_{n_0} \tag{2.73}$$

is the so called *exchange-correlation kernel*. On the other hand, also the density is a functional of potential, and it can therefore expanded around the "zero order potential", which means, the static Kohn-Sham potential $v_s[n_0](\mathbf{r})$. The first order response of density, will be given by:

$$\delta n^{(1)}(\mathbf{r},t) = \int d\mathbf{r}' \chi_s(\mathbf{r},\mathbf{r}',t) v_{1,s}(r',t') \tag{2.74}$$

This allows me to make the following identification:

$$\int d\mathbf{r}' \chi(\mathbf{r},\mathbf{r}',\omega) v_{ext}(\mathbf{r}',\omega) = \int d\mathbf{r}' \chi_s(\mathbf{r},\mathbf{r}',t) v_{1,s}(r',t') \tag{2.75}$$

By this equality, we obtain the following relation between the polarizability of an interacting electron system and the independent particle susceptibility:

$$\chi(\mathbf{r},\mathbf{r}',\omega) = \\ = \chi_s(\mathbf{r},\mathbf{r}',\omega) + \int d\mathbf{r}''\chi_s(\mathbf{r},\mathbf{r}'',\omega)\times \\ \times \int d\mathbf{r}'''\left[\frac{1}{|\mathbf{r}''-\mathbf{r}'''|}+f_{xc}(\mathbf{r}'',\mathbf{r}''',\omega)\right]\chi(\mathbf{r}''',\mathbf{r}',\omega) \tag{2.76}$$

This equation is the so called Dyson equation of TD-DFT.
After some algebra, one finally gets the Dyson equation at second order:

$$\int d\mathbf{r}_4 \left[\delta(\mathbf{r}_1-\mathbf{r}_4) - \int d\mathbf{r}_5 \chi^{0(1)}_{\rho\rho}(\mathbf{r}_1,\mathbf{r}_5,\omega)\ f_{uxc}(\mathbf{r}_5,\mathbf{r}_4,\omega)\right]\ \chi^{(2)}_{\rho\rho\rho}(\mathbf{r}_4,\mathbf{r}_2,\mathbf{r}_3,2\omega,\omega,\omega)$$
$$= \int d\mathbf{r}_5\ d\mathbf{r}_7\ \chi^{0(2)}_{\rho\rho\rho}(\mathbf{r}_1,\mathbf{r}_5,\mathbf{r}_7,2\omega,\omega,\omega)$$
$$\left[\delta(\mathbf{r}_5,\mathbf{r}_2) + \int d\mathbf{r}_4\ f_{uxc}(\mathbf{r}_5,\mathbf{r}_4)\ \chi^{(1)}_{\rho\rho}(\mathbf{r}_4,\mathbf{r}_2,\omega)\right] \times \left[\delta(\mathbf{r}_7,\mathbf{r}_3) + \int d\mathbf{r}_6\ f_{uxc}(\mathbf{r}_7,\mathbf{r}_6,\omega)\ \chi^{(1)}_{\rho\rho}(\mathbf{r}_6,\mathbf{r}_3,\omega)\right]$$
$$+ \int d\mathbf{r}_4\ d\mathbf{r}_5\ d\mathbf{r}_6\ \chi^{0(1)}_{\rho\rho}(\mathbf{r}_1,\mathbf{r}_4)\ g_{xc}(\mathbf{r}_4,\mathbf{r}_5,\mathbf{r}_6,\omega,\omega)\ \chi^{(1)}_{\rho\rho}(\mathbf{r}_5,\mathbf{r}_2)\ \chi^{(1)}_{\rho\rho}(\mathbf{r}_6,\mathbf{r}_3)$$

where with f_{uxc} we denoted:

$$f_{uxc}(\mathbf{r},\mathbf{r}',\omega) = \frac{1}{|\mathbf{r}-\mathbf{r}'|} + f_{xc}(\mathbf{r},\mathbf{r}',\omega) \tag{2.77}$$

and where we have defined:

$$g_{xc}(\mathbf{r},\mathbf{r}',\mathbf{r}'',t,t') = \left.\frac{\delta^2 v_{xc}[n](\mathbf{r},t)}{\delta n(\mathbf{r}',t)\delta n(\mathbf{r}'',t)}\right|_{n_0} \tag{2.78}$$

as the second order exchange-correlation kernel. The Dyson equation can be easily solved by mean of a matrix inversion. We obtain that the response function of the interacting system is given by:

$$\chi = \left(1-\chi_s(f_H+f_{xc})\right)^{-1}\chi_s \tag{2.79}$$

This is a truly remarkable result: it allows us - in principle in an exact way - to find the response function of the true interacting many electron system, starting from the much easier response function of non-interacting Kohn-Sham system. The fundamental ingredient of this equation is the exchange correlation kernel f_{xc}. Inside the xc-kernel are incorporated both the effects of hole-electron interaction - which are responsible for the

arise of excitons- and the opening of the bandgap effects.
Unfortunately, exactly as in the case of static DFT, the exact f_{xc} is not known, and we've forced to develop some approximation for it. Building approximation for the f_{xc} kernel is a not trivial problem, and it's still matter of research. In the following, we will limit to mention the RPA approximation, which has been used throughout this work.

Random Phase Approximation (RPA)

The simplest approximation to attempt to solve the Dyson equation is to impose $f_{xc} = 0$ and $g_{xc} = 0$. Within this approximation, the first order Dyson equation becomes (we temporarily suppress the dependence in $\mathbf{r}$ and ω in order to make the expressions more readable):

$$\chi_{\rho\rho} = \left(1 - \chi^0_{\rho\rho} f_H\right)^{-1} \chi^0_{\rho\rho} \tag{2.80}$$

while the solution of the second order one will be:

$$\chi^{(2)}_{\rho\rho\rho} = (1 - \chi^{0,1} v)\chi^{0,2}_{\rho\rho\rho}(1 + v\chi_{\rho\rho})(1 + v\chi_{\rho\rho}) \tag{2.81}$$

This easy approximation is the first step on the way going from the independent particle susceptibility χ_s to the real interacting system susceptibiility χ. In this approximation, the variation of density, is not given just by the transition of Kohn-Sham electrons under the effect of external perturbing field $H_{int}(\mathbf{r}, t)$. It will be given, insted, by the transition of electron between Kohn-Sham states under the effect of the external perturbing field $H_{int}(\mathbf{r}, t)$, **plus** the Hartree potential, representing the classical coulombian potential given by the variation of density $\delta n^{(1)}(\mathbf{r}, t)$. This is the most elementary way to go beyond mimic inside the non-interacting electrons, the complicated two-body coulombian interaction. This approximation leave outsides all non-classical effects due to correlations, like for example the excitonic effects

2.5 From response functions to optical properties

The TDDFT, as we already have seen, is a theory who allows us to calculate (in principle, in an exact way) the one electron time dependent density induced by an external scalar perturbation. This density can be expressed as a perturbative expansion of the external potential, and the exact response functions, order by order, can be derived from the response function of the noninteracting Kohn Sham system by mean of the Dyson equation. Now we want to deal with the following problems: once we obtained the response functions of the system, how can we connect them with the macroscopic optical quantities of the system, kind of the dielectric function?

2.5.1 Dielectric function from TD-DFT

Before to explain how we can use TDDFT to inquire the optical properties of materials, a special remark has to be done. The radiation beam used in spectroscopy experiments are, as it's well known from the classical electrodynamics, transverse waves (which means that electric field of the perturbation will be orthogonal to the propagation direction). The TDDFT, on the other hand, allows one to find the time-dependent density of a many electron system under the action of a scalar time-dependent potential. For this reason, in principle, TD-DFT allow us to study just the longitudinal response of the system, described by the longitudinal dielectric function $\varepsilon^{LL}(\mathbf{q},\omega)$. This problem can be bypassed by mean of the following consideration: the frequencies of the perturbations we are going to study, are in a range from 0 to about 10 eV. This means wavelength of about 10^2 nm, about three orders of magnitude bigger of the characteristic length of our systems, the lattice constant: $\lambda/a_{cell} \sim 10^3 \gg 1$. For perturbation of such big wavelength, it is no more meaningful distinguish between longitudinal and transverse perturbations: in both case, each atom of the lattice will just "feel" an oscillating uniform electric field. For this reason, in the limit $\mathbf{q} \to 0$, the response of a material to an electromagnetic perturbation can be studied by mean of the longitudinal dielectric function. Having said that, let's see how it can be calculated.

We start with recalling the physical meaning of the longitudinal dielectric function. As we already have seen in the previous section, the charge carriers inside the system displace under the effect of the electric field, determining in this way induced density of current and density of charge $\mathbf{J}_{ind}$ and ρ_{ind}. From this displacement of charge, an induced electric field $\mathbf{E}_{ind}$ arises. Therefore, the potential "felt" by an external test charge inside the material will not be equal to the external potential v_{ext}: it will be given by the sum of external potential plus the potential induced by charge displacement.
In other words, in homogenous medium approximation (induced density of charge has the same wave vector of perturbing field), and linear response (induced density of charge oscillates at the same frequency of external perturbation), the total potential will be:

$$\begin{aligned} v_{tot}(\mathbf{r},\omega) &= v_{ext}(\mathbf{r},\omega) + \int d\mathbf{r}' \frac{\rho_{ind}(\mathbf{r},\omega)}{|\mathbf{r}-\mathbf{r}'|} \\ &= v_{ext}(\mathbf{r},\omega) + \int d\mathbf{r}' \frac{1}{|\mathbf{r}-\mathbf{r}'|} \int d\mathbf{r}'' \chi_{\rho\rho}(\mathbf{r}',\mathbf{r}'',\omega) v_{ext}(\mathbf{r}'',\omega) \end{aligned} \tag{2.82}$$

or, in reciprocal space:

$$\begin{aligned} v_{tot}(\mathbf{q},\omega) &= v_{ext}(\mathbf{q},\omega) + v(\mathbf{q})\chi_{\rho\rho}(\mathbf{q},\omega) v_{ext}(\mathbf{q},\omega) \\ &= \big[1 + v(\mathbf{q})\chi_{\rho\rho}(\mathbf{q},\omega)\big] v_{ext}(\mathbf{q},\omega) \end{aligned} \tag{2.83}$$

The factor between square bracket in the last equation, is the so called inverse dielectric function:

$$\varepsilon^{-1}(\mathbf{q},\omega) = 1 + v(\mathbf{q})\chi_{\rho\rho}(\mathbf{q},\omega) \tag{2.84}$$

From this expression is now clear the physical meaning of inverse dielectric function: it is the screening factor containing information about how much the external potential is screened by induced polarization.
Introducing the inverse dielectric function, we made two important assumptions: the assumption of homogenous material, and the assumption of linear response. We will not be concerned here by the non-linear response. In the next section, we will rather try to go beyond the linear response assumption.

Local field effects

It's evident that no real material is homogenous: every real system contains discontinuities on the atomic length, due to the discrete nature of his microscopic constituents. This is evident if we look for a moment at the expression of induced density in term of response function:

$$\delta\rho^{(1)}(\mathbf{q}+\mathbf{G},\omega) = \sum_{\mathbf{G}'} \chi_{\rho\rho}(\mathbf{q}+\mathbf{G},\mathbf{q}+\mathbf{G}',\omega) v_{ext}(\mathbf{q}+\mathbf{G}',\omega)$$

Even if (as usually happens) the external potential contains only the macroscopic Fourier component of wave vector $\mathbf{q}$ (which means, in the notation of the expression above, the $(\mathbf{q}+\mathbf{G}')_{\mathbf{G}'=\mathbf{0}}$ component), the induced density of charge at frequency ω will contain many others Fourier components of higher wave vector. In other words, the induced density of charge, will be not simply an oscillation of wave vector $\mathbf{q}$: it will be more like an oscillation of $2\pi/|\mathbf{q}|$ wavelength (the $(\mathbf{q}+\mathbf{0})$ term), modulated in amplidude by several oscillation term of atomic scale (the $(\mathbf{q}+\mathbf{G})$s terms). Therefore, the quantity we obtain from response theory, will be the microscopic inverse dielectric matrix:

$$\varepsilon^{-1}_{\mathbf{G}\mathbf{G}'}(\mathbf{q},\omega) = \delta_{\mathbf{G}\mathbf{G}'} + v_{\mathbf{G}}\chi_{\mathbf{G}\mathbf{G}'}(\mathbf{q},\omega) \tag{2.85}$$

The problem we now want to address is how to pass from this quantity (which is, as we have just seen, intrinsically microscopic) to the macroscopic dielectric function. From the expression above, it follows that also the total potential will contain microscopic oscillations term:

$$v_{tot}(\mathbf{q}+\mathbf{G},\omega) = \sum_{\mathbf{G}'} \varepsilon^{-1}_{\mathbf{G}\mathbf{G}'}(\mathbf{q},\omega) v_{ext}(\mathbf{q}+\mathbf{G},\omega) \tag{2.86}$$

The difference between the total potential and his macroscopic average are the so called local field effects. Let's find the macroscopic average of microscopic total potential following the average procedure of Ehrenreich [28]. The total potential can be written as sum of plane

waves:

$$\begin{aligned} v_{tot}(\mathbf{r},\omega) &= \sum_{\mathbf{G}} v_{tot}(\mathbf{q}+\mathbf{G},\omega)e^{i(\mathbf{q}+\mathbf{G})\mathbf{r}} \\ &= e^{i\mathbf{q}\mathbf{r}} \sum_{\mathbf{G}} v_{tot}(\mathbf{q}+\mathbf{G},\omega)e^{i\mathbf{G}\mathbf{r}} \end{aligned}$$

Let's suppose now to perform an average of the total potential inside the space occupied by the unit cell in position $\mathbf{R}$:

$$\begin{aligned} \langle v_{tot}(\mathbf{r},\omega)\rangle_{\mathbf{R}} &= \frac{1}{\Omega}\sum_{\mathbf{G}} \int_{\mathbf{R}} d\mathbf{r} v_{tot}(\mathbf{q}+\mathbf{G},\omega)e^{i\mathbf{G}\mathbf{r}}e^{i\mathbf{q}\mathbf{r}} \\ &= \frac{e^{i\mathbf{q}\mathbf{R}}}{\Omega} v_{tot}(\mathbf{q},\omega) \end{aligned} \tag{2.87}$$

where the term $e^{i\mathbf{q}\mathbf{r}}$ has been extracted out of the integral, since $1/q \gg a_{cell}$, and where we exploited the definition of Dirac δ-function. Moreover, we notice that, being the external potential macroscopic, the macroscopic average of total potential will be:

$$v_{tot,M}(\mathbf{q},\omega) = \varepsilon^{-1}_{\mathbf{00}}(\mathbf{q},\omega) v_{ext}(\mathbf{q},\omega) \tag{2.88}$$

Therefore, the macroscopic dielectric function, will be:

$$\varepsilon_M(\mathbf{q},\omega) = \frac{1}{\varepsilon^{-1}_{\mathbf{00}}(\mathbf{q},\omega)} \tag{2.89}$$

2.5.2 Second order susceptibility from TD-DFT

In 2.4.2, we have shown how the second order response function of a system of interacting electrons can be obtained, via the second order Dyson equation Eq. (2.77). In the present section, we will present a procedure to link second order macroscopic susceptibility with second order response function of density. Such a procedure has been introduced for the first time by Luppi et al. [29], and Hübener et al. [30][31], which extended to the second order the linear formalism developed by Del Sole in Ref. [32]. The first step of this procedure consists to define a perturbing field

$$\mathbf{E}^P = \mathbf{E} - \mathbf{E}^{i,L} \tag{2.90}$$

where $\mathbf{E}$ is the total electric field, and $\mathbf{E}^{i,L}$ is the longitudinal part of the induced field. Then, two quasi-polarisabilities $\tilde{\alpha}$ linking the first and second order polarisations with the perturbing field are introduced:

$$\mathbf{P}^{(1)}_{\mathbf{G}}(\mathbf{q},\omega) = \sum_{\mathbf{G}_1} [\overset{\leftrightarrow}{\tilde{\alpha}}^{(1)}(\mathbf{q}_1,\omega)]_{\mathbf{G}\mathbf{G}_1} \mathbf{E}^P_{\mathbf{G}_1}(\mathbf{q},\omega) \tag{2.91}$$

$$\begin{aligned}\mathbf{P}^{(2)}_{\mathbf{G}}(\mathbf{q},\omega) = \sum_{\mathbf{q_1}\mathbf{q_2}}^{BZ}\sum_{\mathbf{G_1}\mathbf{G_2}}\int d\omega_1 d\omega_2 \delta_{\mathbf{q},\mathbf{q_1}+\mathbf{q_2}}\delta(\omega-\omega_1-\omega_2)\times \\ \times[\overset{\leftrightarrow}{\tilde{\alpha}}^{(2)}(\mathbf{q},\mathbf{q}_1,\mathbf{q}_2,\omega_1,\omega_2)]_{\mathbf{G}\mathbf{G}_1\mathbf{G}_2}\mathbf{E}^P_{\mathbf{G}_1}(\mathbf{q}_1,\omega_1)\mathbf{E}^P_{\mathbf{G}_2}(\mathbf{q}_2,\omega_2)\end{aligned} \tag{2.92}$$

where $\mathbf{q}$,$\mathbf{q}_1$,$\mathbf{q}_2$ are vectors in the first brillouin zone while $\mathbf{G}$,$\mathbf{G}_1$,$\mathbf{G}_2$ label reciprocal lattice vectors. With a bit of algebra, we can express both the macroscopic dielectric function and the second order susceptibility as function of quasi-polarisability:

$$\overset{\leftrightarrow}{\varepsilon}_M(\mathbf{q}_1,\omega) = \overset{\leftrightarrow}{\mathbb{1}} + 4\pi[\overset{\leftrightarrow}{\tilde{\alpha}}^{(1)}(\mathbf{q}_1,\omega)]_{\mathbf{00}}\left[\overset{\leftrightarrow}{\mathbb{1}} + 4\pi\frac{\mathbf{q}}{q}\frac{\mathbf{q}}{q}\frac{[\overset{\leftrightarrow}{\tilde{\alpha}}^{(1)}(\mathbf{q}_1,\omega)]_{\mathbf{00}}}{1-4\pi[\tilde{\alpha}^{(1),LL}(\mathbf{q}_1,\omega)]_{\mathbf{00}}}\right] \tag{2.93}$$

$$\begin{aligned}\overset{\leftrightarrow}{\chi}^{(2)}_M(\mathbf{q},\mathbf{q}_1,\mathbf{q}_2,\omega_1,\omega_2) = &\left[\overset{\leftrightarrow}{\mathbb{1}} + 4\pi\frac{[\overset{\leftrightarrow}{\tilde{\alpha}}^{(1)}(\mathbf{q},\omega)]_{\mathbf{00}}}{1-4\pi[\tilde{\alpha}^{(1),LL}(\mathbf{q},\omega)]_{\mathbf{00}}}\frac{\mathbf{q}}{q}\frac{\mathbf{q}}{q}\right][\overset{\leftrightarrow}{\tilde{\alpha}}^{(2)}(\mathbf{q},\mathbf{q}_1,\mathbf{q}_2,\omega_1,\omega_2)]_{\mathbf{000}} \\ &\times\left[\overset{\leftrightarrow}{\mathbb{1}} + 4\pi\frac{\mathbf{q_1}}{q_1}\frac{\mathbf{q_1}}{q_1}\frac{[\overset{\leftrightarrow}{\tilde{\alpha}}^{(1)}(\mathbf{q}_1,\omega)]_{\mathbf{00}}}{1-4\pi[\tilde{\alpha}^{(1),LL}(\mathbf{q}_1,\omega)]_{\mathbf{00}}}\right] \\ &\times\left[\overset{\leftrightarrow}{\mathbb{1}} + 4\pi\frac{\mathbf{q_2}}{q_2}\frac{\mathbf{q_2}}{q_2}\frac{[\overset{\leftrightarrow}{\tilde{\alpha}}^{(1)}(\mathbf{q}_2,\omega)]_{\mathbf{00}}}{1-4\pi[\tilde{\alpha}^{(1),LL}(\mathbf{q}_2,\omega)]_{\mathbf{00}}}\right]\end{aligned} \tag{2.94}$$

Taking the longitudinal longitudinal contraction of the latter equation, we finally obtain:

$$\chi^{LLL}_M(\mathbf{q},\mathbf{q}_1,\mathbf{q}_2,\omega_1,\omega_2) = \varepsilon^{LL}_M(\mathbf{q},\omega)[\chi^{(2)}_{\rho\rho\rho}(\mathbf{q},\mathbf{q}_1,\mathbf{q}_2,\omega_1,\omega_2)]_{\mathbf{000}}\varepsilon^{LL}_M(\mathbf{q}_1,\omega_1)\varepsilon^{LL}_M(\mathbf{q}_2,\omega_2) \tag{2.95}$$

The link between the components of χ_M and its longitudinal part is not trivial. In the following we give the relations for some of these components:

$$\chi^{(2)}_{M,iii} = \chi^{(2),LLL}_M(2\mathbf{q},\mathbf{q},\mathbf{q}) \tag{2.96}$$

$$2\chi^{(2)}_{M,iij} = \chi^{(2),LLL}_M(q\hat{\mathbf{i}}+q\hat{\mathbf{j}},q\hat{\mathbf{i}},q\hat{\mathbf{j}}) + \chi^{(2),LLL}_M(-q\hat{\mathbf{i}}+q\hat{\mathbf{j}},-q\hat{\mathbf{i}},q\hat{\mathbf{j}}) \tag{2.97}$$

$$\frac{1}{2}\left(\chi^{(2)}_{M,iij}+\chi^{(2)}_{M,ijj}+(1+\sqrt{2})(\chi^{(2)}_{M,jji}+\chi^{(2)}_{M,jjj})\right) = \chi^{(2),LLL}_M(q\hat{\mathbf{i}}+q\hat{\mathbf{j}},q\hat{\mathbf{i}},q\hat{\mathbf{j}}) \tag{2.98}$$

2.5.3 Second order surface susceptibility

2.5.3.1 Independent particles surface susceptibility

Second order susceptibility is written (in velocity gauge and independent particle approximation) as [33]:

$$\chi^{(2)}_{0,\alpha\beta\gamma} = \\ = \frac{i}{2\Omega\omega^3}\sum_{n,n',n''}\sum_{\mathbf{k}}^{BZ}\frac{\langle n\mathbf{k}|p^\alpha|n'\mathbf{k}\rangle\Big(\langle n'\mathbf{k}|p^\beta|n''\mathbf{k}\rangle\langle n''\mathbf{k}|p^\gamma|n\mathbf{k}\rangle + \langle n'\mathbf{k}|p^\gamma|n''\mathbf{k}\rangle\langle n''\mathbf{k}|p^\beta|n\mathbf{k}\rangle\Big)}{E_{n\mathbf{k}} - E_{n'\mathbf{k}} + 2\omega + 2i\eta} \\ \times\left[\frac{f_{nn''}}{E_{n\mathbf{k}} - E_{n''\mathbf{k}} + \omega + i\eta} + \frac{f_{n'n''}}{E_{n''\mathbf{k}} - E_{n'\mathbf{k}} + \omega + i\eta}\right] \tag{2.99}$$

where the three greek letters stand for the cartesian indexes, n,n',n'' are indexes of bands, and f_{ij} is the difference between Fermi occupation numbers of band i and j. When one wants to calculate the second harmonic generation of a surface, a special care must be done to the symmetry of the studied system. As we have seen in chapter one, in materials having inversion symmetry, the macroscopic second order susceptibility is identically equal to zero. This may not seem a concern, since an ideal surface, being a semi-infinite system, is clearly not invariant under inversion. However, due to the impossibility to treat a truly semi-infinite object, through this thesis we sill adopt the supercell approach, which consists in modelling the surface with an array of periodically repeated slabs. This approach, which has the advantage to allowing to exploit the computational effectiveness of plane-waves codes, presents on the other hand several drawbacks when we come to the calculation of optical properties. Many of these difficulties will be examined in detail during next chapters; in this section, we focus on an issue which is specifically related to the calculation of second order polarisability. When we model a surface with a slab, an artificial centro-symmetry is introduced in the system, and the signals produced by the two faces of the slab interfere destructively. As a consequence, a straightforward application of Eq. (2.99), would lead to an identically zero second harmonic signal. In order to overcome this problem, one needs to find the way to isolate the contribution of a single interface. The technique to accomplish this goal has been presented for the first time by L. Reining et al. [34], which replaced, in the expression for SHG probability, the matrix element of momentum with matrix element of a modified momentum operator:

$$\mathcal{P} = \frac{\mathbf{p}C(z) + C(z)\mathbf{p}}{2} \tag{2.100}$$

Here $C(z)$ stands for a cut function which is equal to 1 on one surface and equal to zero on the other one. Performing the substitution of the matrix elements, we obtain the surface

second order independent particle susceptibility:

$$\chi^{(2)}_{0,\alpha\beta\gamma} = \\ = \frac{i}{2\Omega\omega^3} \sum_{n,n',n''} \sum_{\mathbf{k}}^{BZ} \frac{\langle n\mathbf{k}|\mathcal{P}^\alpha|n'\mathbf{k}\rangle \Big(\langle n'\mathbf{k}|p^\beta|n''\mathbf{k}\rangle\langle n''\mathbf{k}|p^\gamma|n\mathbf{k}\rangle + \langle n'\mathbf{k}|p^\gamma|n''\mathbf{k}\rangle\langle n''\mathbf{k}|p^\beta|n\mathbf{k}\rangle \Big)}{E_{n\mathbf{k}} - E_{n'\mathbf{k}} + 2\omega + 2i\eta} \\ \times \left[\frac{f_{nn''}}{E_{n\mathbf{k}} - E_{n''\mathbf{k}} + \omega + i\eta} + \frac{f_{n'n''}}{E_{n''\mathbf{k}} - E_{n'\mathbf{k}} + \omega + i\eta} \right] \tag{2.101}$$

2.5.3.2 Second order surface susceptibility with Local Field Effects

The formalism previously illustrated, which allows to calculate the second order susceptibility with local field effects, has been extended to the case of surfaces by Tancogne-Dejean [19][20]. The first step consists in introducing two auxiliary response functions called $\bar{\chi}^{(1)}$ and $\bar{\chi}^{(2)}$, where only the short range of the Coulomb potential appears. For this, one separate the Coulomb interaction in a macroscopic and a microscopic part: $v = v_{\mathbf{0}} + \bar{v}$. It comes:

$$V^{tot(1)} = V^{ext(1)} + v_{\mathbf{0}}\ \rho^{(1)}_{ind} + \bar{v}\ \rho^{(1)}_{ind} = V^{mac(1)} + \bar{v}\ \rho^{(1)}_{ind} \tag{2.102}$$

$$V^{tot(2)} = v_{\mathbf{0}}\ \rho^{(2)}_{ind} + \bar{v}\ \rho^{(2)}_{ind} = V^{mac(2)} + \bar{v}\ \rho^{(2)}_{ind} \tag{2.103}$$

where we have defined:

$$V^{mac(1)} = V^{ext(1)} + v_{\mathbf{0}}\ \rho^{(1)}_{ind} \tag{2.104}$$

$$V^{mac(2)} = v_{\mathbf{0}}\ \rho^{(2)}_{ind} \tag{2.105}$$

Proceding as in the previous part, it now comes two coupled Dyson equations:

$$\chi^{(1)}_{\rho\rho} = \bar{\chi}^{(1)}_{\rho\rho} + \bar{\chi}^{(1)}_{\rho\rho}\ v_{\mathbf{0}}\ \chi^{(1)}_{\rho\rho} \tag{2.106}$$

$$\bar{\chi}^{(1)}_{\rho\rho} = \chi^{0(1)}_{\rho\rho} + \chi^{0(1)}_{\rho\rho}\ \bar{v}\ \bar{\chi}^{(1)}_{\rho\rho} \tag{2.107}$$

and

$$\chi^{(2)}_{\rho\rho\rho} = \bar{\chi}^{(2)}_{\rho\rho\rho} \left[1 + v_{\mathbf{0}}\ \chi^{(1)}_{\rho\rho}\right] \left[1 + v_{\mathbf{0}}\ \chi^{(1)}_{\rho\rho}\right] + \bar{\chi}^{(1)}_{\rho\rho}\ v_{\mathbf{0}}\ \chi^{(2)}_{\rho\rho\rho} \tag{2.108}$$

$$\bar{\chi}^{(2)}_{\rho\rho\rho} = \chi^{0(2)}_{\rho\rho\rho} \left[1 + \bar{v}\ \bar{\chi}^{(1)}_{\rho\rho}\right] \left[1 + \bar{v}\ \bar{\chi}^{(1)}_{\rho\rho}\right] + \chi^{0(1)}_{\rho\rho}\ \bar{v}\ \bar{\chi}^{(2)}_{\rho\rho\rho} \tag{2.109}$$

By definition, one has:

$$\bar{\chi}^{S}_{\mathbf{00}} = \tfrac{1}{L_z} \textstyle\sum_{\mathbf{G}_z} C(-\mathbf{G}_z)\ \bar{\chi}_{\mathbf{G}_z 0} \tag{2.110}$$

and:

$$\bar{\chi}^{(2)S}_{\mathbf{000}} = \frac{1}{L_z}\sum_{\mathbf{G}_z} C(-\mathbf{G}_z)\ \bar{\chi}_{\mathbf{G}_z\mathbf{00}} \tag{2.111}$$

where $C(-\mathbf{G}_z)$ is the Fourier transform of the cut function introduced in Eq. (2.100). Finally, one can obtain the surface second order susceptibility as:

$$\chi^{(2)S,LLL}_{M}(\mathbf{q},\mathbf{q}_1,\mathbf{q}_2;\omega,\omega_1,\omega_2) = \frac{-i}{2|\mathbf{q}||\mathbf{q}_1||\mathbf{q}_2|}\ \bar{\chi}^{(2)S}_{\mathbf{000}}(\mathbf{q},\mathbf{q}_1,\mathbf{q}_2;\omega,\omega_1,\omega_2) \tag{2.112}$$

Chapter 3

Bare and functionalised Silicon (001) surfaces

3.1 Bare Si(001) surface

In this section, we want to discuss of the properties of silicon (001) surface, which is the one chosen in this thesis. In general, when a crystal is cut, the atoms located in the most external layers do not stand in their equilibrium bulk positions, but tend to displace in order to create a configuration which minimise the total energy of the system. Because of the cut, the most external ions experience an abrupt change in the atomic forces acting on them, and therefore start to move, giving arise to a surface reconstruction. These surface reconstructions can have quite an important effect on the electronic properties of the crystal. When silicon is cut in the (001) direction, the atoms constituting the most external layer tend to get closer the one to the other, resulting in formation of surface dimers accommodated in adjacent rows [35]. It is nowadays a commonly accepted fact that these dimers are not symmetric (i.e. they are not parallel to the surface), but slightly buckled. As shown for the first time by Chadi [36], by mean of tight-binding calculations, a reconstruction with symmetric dimers would result in the formation of metallic surface states, in disagreement with experimental observation. On the other side, if one allows dimer to relax breaking the symmetry, it is found that the surface with buckled dimers is lower in energy of ~ 0.1 eV per primitive cell compared to the symmetric dimers reconstruction, and the surface states recover their semiconductor character. The same findings were then obtained by Rohlfing et al. [37], which confirmed the metallic behaviour of the symmetric dimers reconstruction by mean of GW calculations. At temperature close to 0K, the most favorable reconstruction is the c(4x2) [38] (see Fig. (3.1)). As we have already mentioned, the dimers forming on the top of the Si(001) surfaces are organised in parallel rows, which extend in the crystallographic direction $(1\bar{1}0)$ (the y-axis in Fig. (3.1)). In the reconstruction c4x2, consecutive dimers in the same row are buckled in

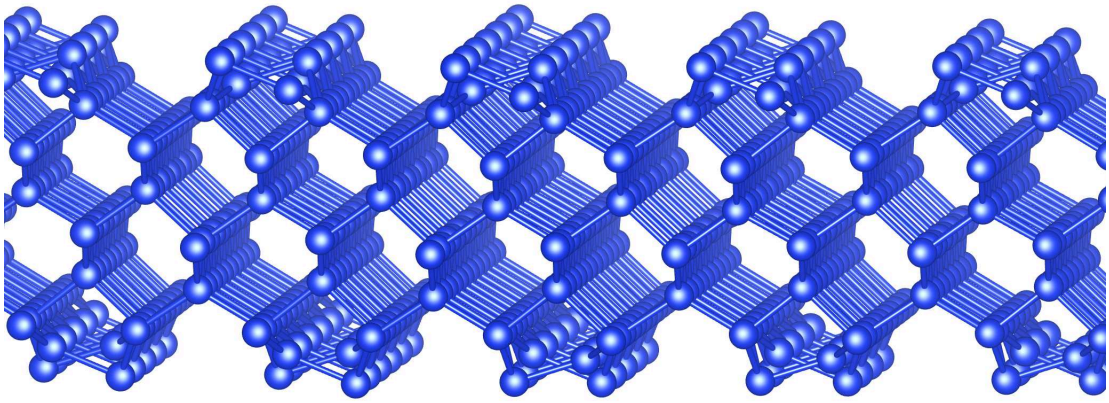

Figure 3.1: Silicon (001) surface with c4x2 reconstruction. Adjacent dimers in the same row have opposite buckling orientation.

opposite directions. Moreover, the buckling orientation, also change when displacing from a dimer row to the immediately adjacent one. At around 200 K, as reported in Ref. [39], the most favorable reconstruction become the p(2x1) (see Fig. (3.2)). In this reconstruction, all the dimers are buckled in the same direction. Since it is the most stable structure at room temperature, and since it has already been extensively studied from the point of view of Second Harmonic Generation [20], we have chosen it as model for the bare silicon surface.

3.2 Silicon(001) surfaces functionalised with nucleobases

In the present section, I will present the main characteristics of the silicon surfaces undergoing the adsorption of small organic molecules. In particular, in the present work, we will focus on the study of the interaction between nucleobasis and the silicon surfaces. The DNA, as it is well known, is a polymer formed by several monomers, called nucleotides (see Fig. (3.3)). Each of these monomers is formed by a phosphate group, a pentose sugar , and a nucleobase (adenine, thymine, cytosine, guanine for the DNA, while in the case of RNA thymine is substituted with uracil, see Fig. (3.4)). As demonstrated in the '50s by Watson and Crick [40], two filaments of DNA can hybridise, forming a characteristic double helix structure, which is kept together by the hydrogen bond between the nucleobasis of the two filament. The nucleobasis have the important properties to selectively bind with just their complementary base: the adenine with the thymine (with the uracil in the case of RNA), and the guanine with the cytosine. This means that, given a single filament of the two

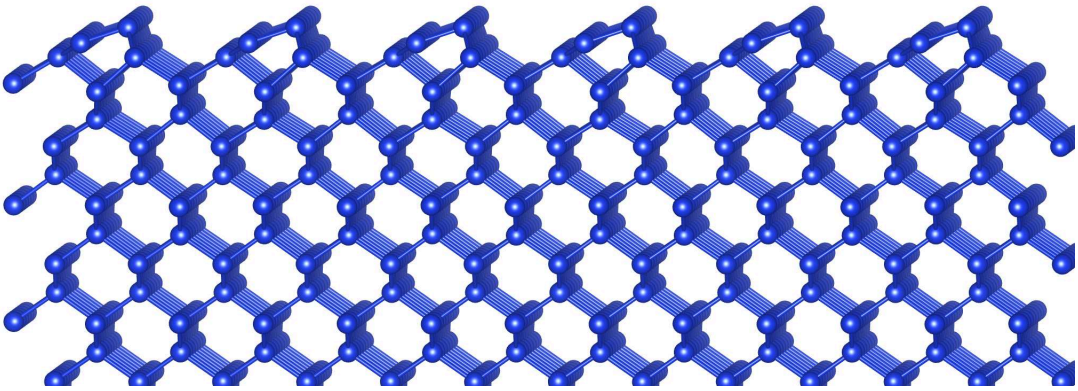

Figure 3.2: Silicon (001) surface with p2x1 reconstruction. All dimers have the same buckling orientation.

which composes the double helix, it contains all the information necessary to reconstruct the total molecule. This exceptional property is at the basis of the replication mechanism of DNA, which allows to obtain two perfectly identical copies of the genetic pool of each individual. In this thesis we will limit ourselves to the study of absorption of pyrimidines. The absorption of pyrimidines over silicon surfaces has been extensively studied with both experimental [41] and theoretical [42],[43],[44],[45],[46],[47] approaches. In 2002 Lopez et al. Ref. [41] managed for the first time to create a sub-monolayer coverage of uracil on the Si(001) surface, letting evaporate in controlled way uracil in a Ultra-High-Vacuum (UHV) chamber. Images taken with Atomic Force Microscope (see Fig. (3.5)) proof that the uracil sub-monolayer exhibit a short range order, with the molecules presenting an adsorption pattern along the silicon dimers row. Lopez and coworkers also characterise their sample using High-Resolution Electron Energy Loss (HREEL). Analysing the low energy part of the spectrum (which carries information about the vibrational mode of the system), they identified spectral lines which are attributable to the presence of Si-H and Si-O stretching modes, suggesting that the adsorption mechanism may feature the dissociation of at least one hydrogen atom from the uracil molecule and the formation of at least one oxygen-silicon bond. The experimental findings of Lopez stimulating further theoretical works on the adsorption of nucleobases on the Si(001) surface. In 2003, Seino et al. [42] calculated the total energy for several adsorption configuration of Uracil on Si(001), finding that the most convenient are the ones where the two oxygen atoms bridge two silicon atoms on adjacent dimers lines[1] (see Fig. (3.6)). In particular Seino and coworkers individuate two

[1]Actually, in Ref. [42], the authors found that the adsorption configurations in which the C=O bond of Uracil is dissociated and oxygen atoms insert in between silicon dimers is even lower in energy than the

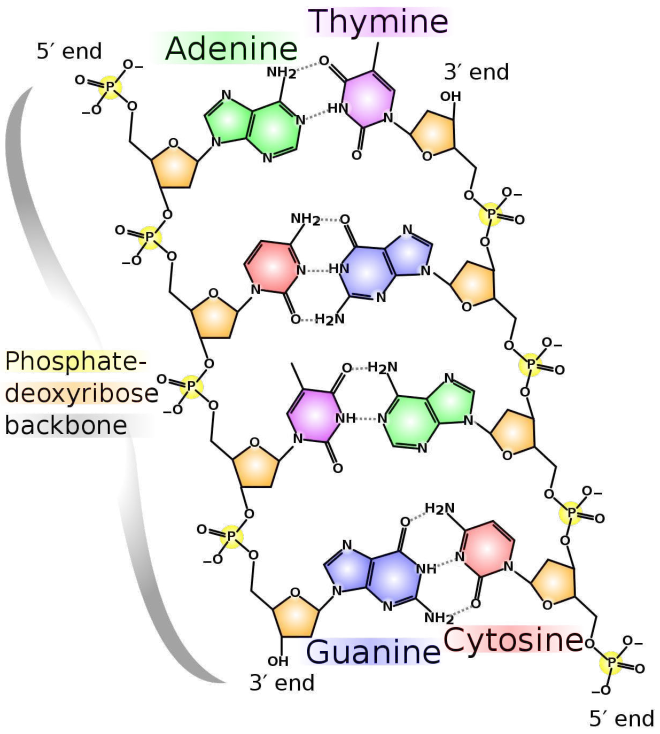

Figure 3.3: Schematic representation of the structure of the DNA molecule. Double helix structure of DNA is formed by two filaments, each of them composed by several monomers called nucleotides. Each of these nucleotides is formed by a phosphate group (yellow), a pentose sugar (orange), and one nucleobase (pink, violet, blue and green). Image released by Mad Price Ball under licence CC BY-SA 3.0

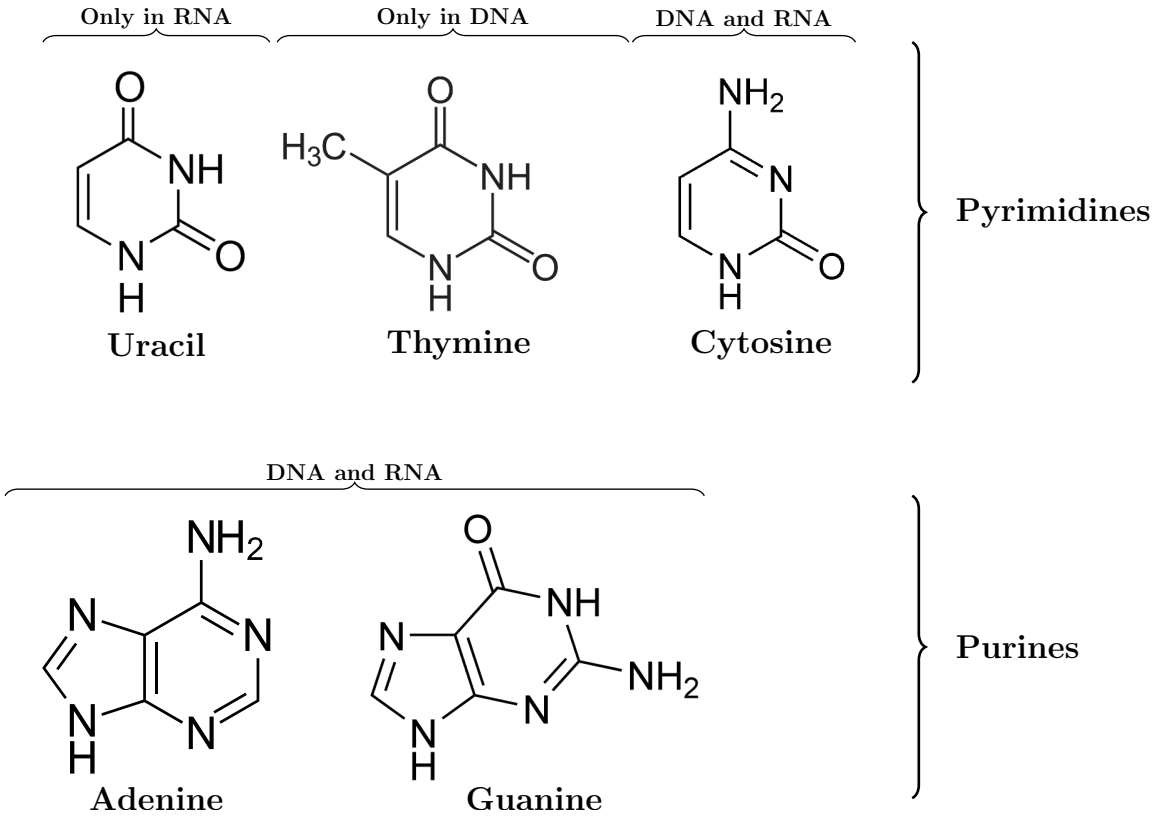

Figure 3.4: Schematic classification of nucleobases. Nucleobases are fondamental constituents of nucleic acids, and are divided between Purines and Pyrimidines. Pyrimidines are the Uracil (which is present just in RNA), Thymine (which is present just in DNA) and Cytosine (which is present in both DNA and RNA), while the Purines are Adenine and Guanine, both present in DNA and RNA. Each pyrimidine couples with only one of the purines: Uracil and Thymine selectively bond just with Adenine, while Cytosine bonds only with Guanine. This complementarity principles between nucleobases make possible the duplication mechnism of DNA double helix.

adsorption configurations, one called dative (see Fig. (3.6b)), in which just one of the N-H bond is dissociated, and the other one, of around $\sim$ 0.9 eV lower in total energy, called covalent, where both the N-H bonds of the Uracil molecule are dissociated and the dangling bonds at the silicon surface are completely saturated (see Fig. (3.6c)). Moreover they found that, compared to the 4x1 configuration (in which molecules are all adsorbed with the same orientation), a 4x2 reconstruction (in which adjacent molecules at the surface are flipped of 180 degrees) is energetically more convenient. In [43], same authors performed band structure calculations for both the 4x1 and 4x2 covalent and dative adsorption. They found that, when the reconstruction is constrained to be 4x1, the dative configuration gives rise to a metallic band structures, while the covalent one results in a band gap of $\sim$ 1 eV. On the other side, they reported that when one allows molecules to adsorb with a 4x2 reconstruction, the configuration in which molecules are flipped of 180 degrees open a small band gap even in the dative structure. After the first studies of Seino and coworkers, other theoretical works on the adsorption of nucleobases on silicon surfaces followed. In particular, we cite the works of Molteni et al. [45],[46], which studied the adsorption of Thymine ,Uracil, and 5-Fluorouracil on the Si(001) surfaces and calculated linear optical response at the independent particles level of the theory, and the work of Kyung [47], which confirmed the possibility of dimer-bridge adsorption also for Cytosine.
To conclude this section, we spend some words about the reconstructions that we used to model the functionalises surfaces. The code that we use in order to calculate the second order optical response (2light) only allows us to perform calculation on semiconducting systems, limiting our choice to both the 4x1 and 4x2 covalent adsorption configurations and the 4x2 dative one. At the same time, due to the high computational cost of second harmonic calculation, we cannot afford to describe a system having 4x2 reconstruction, because it would require to double the number of atoms per unit cell, leading to unfeasible SHG calculations. Because of this reasons, in order to describe the silicon surfaces functionalised with nucleobases, we chose the covalent 4x1 reconstruction. During this thesis, four of these surfaces have been studied, each of them functionalised with a different purine: in Fig. (3.7) we report their unit cells.

dimer bridge reconstruction. However, as pointed out by the authors, the total energy alone is not enough to establish the adsorption configuration: in particular, Seino et al. found that the insertion of oxygen atoms in the silicon dimers would require to overcome the relatively high energy barrier of $\sim$ 1.2 eV, and in addition to that Lopez and coworkers did not find any indication of structures attributable to Si-C modes in the HREEL spectra. For these reason, in this thesis we will limit ourselves to the study of the dimer-bridge configuration

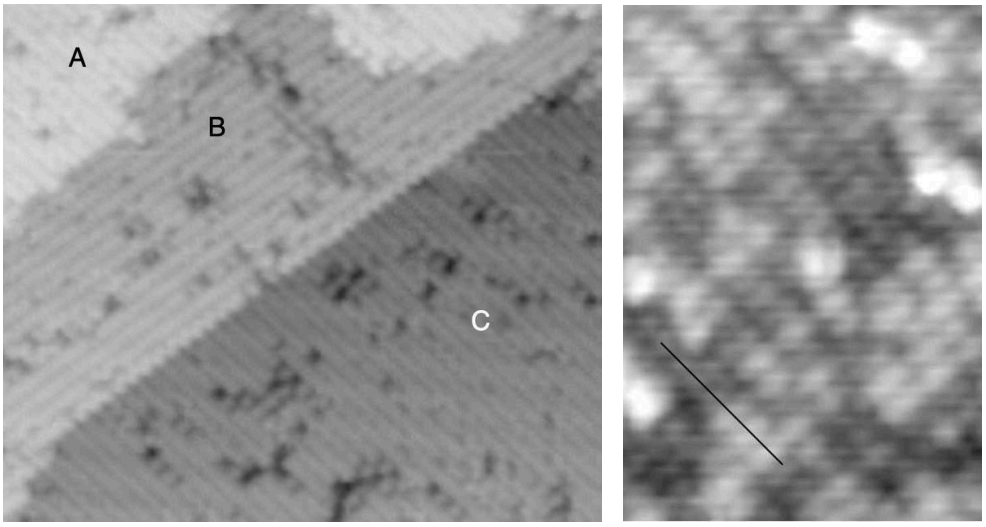

(a) (b)

Figure 3.5: Atomic force microscopy images of sub-monolayer adsorption of Uracil on Si(001) (reproduced from Ref. [41]) are reported. In panel (a), the picture corresponds to an area of 35x30 nm . The three regions A,B,C identify three silicon terraces, and brighter spots correspond to adsorbed molecules. As we can clearly see from this image, molecules tend to order themselves in lines, following the dimers row at the silicon surface. In panel (b), an area of 5x7 nm is reproduced. The black lines correspond to a dimer row formed by seven dimers, with four uncovered dimers (corresponding to the darker spots) and three adsorbed molecules (corresponding to the three brighter spots).

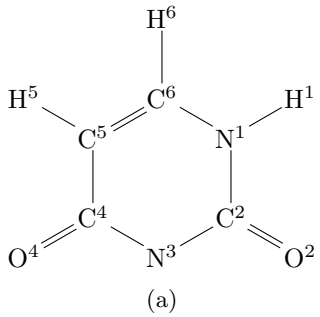

(a)

Dative configuration **Covalent configuration**

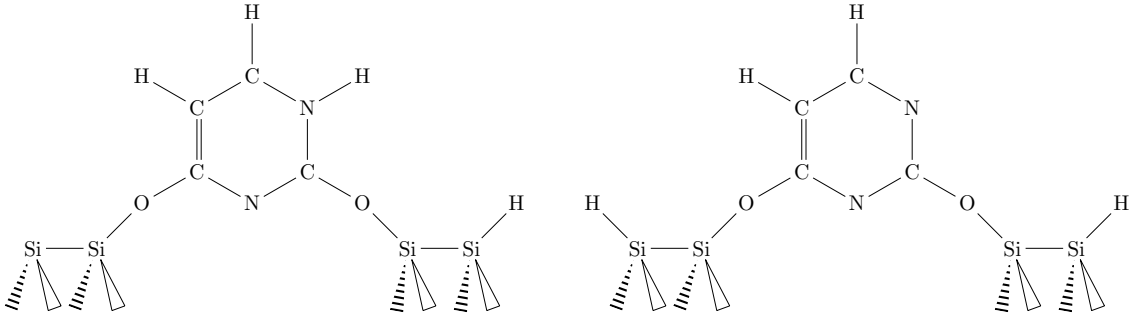

(b) (c)

Figure 3.6: In this figure we report in panel (a) the structural formula of the Uracil molecule, while in panel (b) and (c) we report a sketch of the dimer bridge adsorption configuration. In panel (b) is reported the configuration which, according the lexicon of Ref. [42] and [43], is called partially dative configuration. In this case, just the hydrogen atom on the 3-N is dissociated, and one dangling bond per unit cell remain at silicon surface. In panel (3.6c), the covalent adsorption configuration is shown: here all the N-H bonds are dissociated, and all dangling bonds at silicon surface can be saturated.

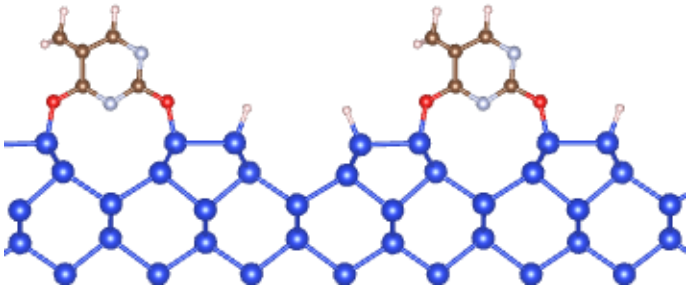

(a) Silicon+Thymine

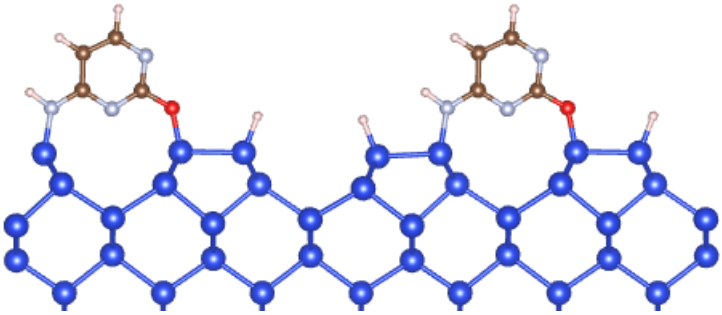

(b) Silicon+Cytosine

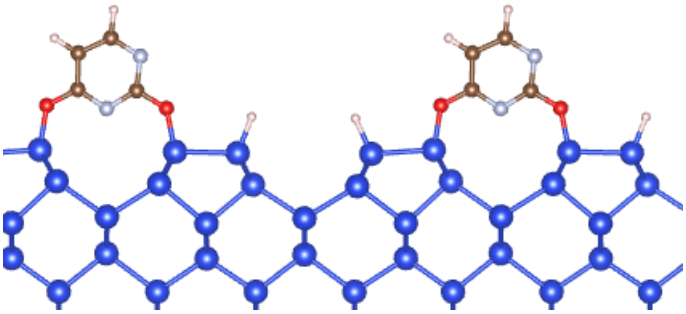

(c) Silicon+Uracil

Figure 3.7: Surfaces studied in this thesis

Chapter 4

Vacuum problem and first results

The vacuum problem has been approached in detail for the first time by Nicolas Tancogne-Dejean in its PhD thesis [20], and the Selected-G method [18] has been developed in this previous work to cure this spurious effect. Nevertheless, how I will explain during the present chapter, the behaviour of spectra of functionalised surfaces lead me to further investigate the presence of vacuum. This brought me to investigate the definition of the thickness of the slab to enlight the differences between the properties of a 2D object and a surface (a semi-infinite object). For these reasons it is useful to summarise here the fundamentals of vacuum problem.

4.1 The vacuum problem

What we will call "The vacuum problem" is a problematic which affects the calculation of optical response functions within the supercell formalism, and that therefore concerns us very closely, since, as we have explained, the functionalised surfaces that we want to study are modelled as slab in a supercell. Let's start to expose a practical example: we consider bare silicon slab (2x1 reconstruction, 16 atomic layer of thickness, see Fig. (4.1)), and we want to get its dielectric function.

The slab will be contained inside a supercell, which will contain a certain amount of vacuum, in order to isolate the slab from its replicas. When one wants to obtain the dielectric function of a crystal, one has to proceed in the following way: first of all, solving the Dyson equation of TD-DFT:

$$\chi_{\mathbf{GG'}} = \chi^0_{\mathbf{GG'}} + \sum_{\mathbf{G_1},\mathbf{G_2}} \chi^0_{\mathbf{GG_1}} v_{\mathbf{G_1G_2}} \chi_{\mathbf{G_2G'}} \tag{4.1}$$

we obtain the interacting-particle density response function of the system (the $\chi_{\mathbf{GG'}}(\mathbf{q},\omega)$).

Then, using this quantity, one can obtain the microscopic inverse dielectric function:

$$\varepsilon^{-1}_{\mathbf{G}\mathbf{G}'}(\mathbf{q},\omega) = \delta_{\mathbf{G}\mathbf{G}'} + \sum_{\mathbf{G_1}} v_{\mathbf{G}\mathbf{G_1}}(\mathbf{q})\chi_{\mathbf{G_1}\mathbf{G}'}(\mathbf{q},\omega) \tag{4.2}$$

And finally, the macroscopic dielectric function is obtained as (in the optical limit):

$$\varepsilon_M(\mathbf{q},\omega) = \frac{1}{\varepsilon^{-1}_{\mathbf{00}}(\mathbf{q},\omega)} \tag{4.3}$$

Following this procedure, which also allow us to include local field effects, we calculated the macroscopic dielectric function for the slab reported in Fig. (4.1) (introduced in a supercell of size ~ 80 Bohr. The result of this calculation is reported in Fig. (4.2). In the figure, we reported in red the in-plane component, and in black, the out-of-plane component of the dielectric function of the slab, while in blue we report the dielectric function of bulk silicon. As we can see, the in-plane component of the slab's spectrum present a peak at 4 eV, in the same position of the bulk spectrum, but with an amplitude smaller of a factor ~ 2. The out-of-plane component of the spectrum is more problematic: this component (black line in Fig. (4.2)), is not only quenched, but also displaced at higher energy (~ 12 eV).

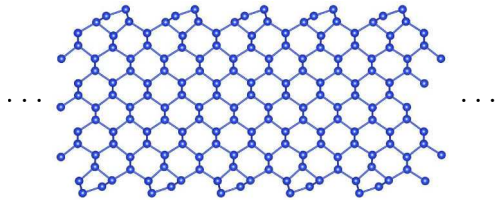

Figure 4.1: Silicon slab made of 16 atomic layers (corresponding to ~ 40 Bohr of thickness), used in the calculation to model the bare silicon surface. Both the faces are p(2x1) reconstructed.

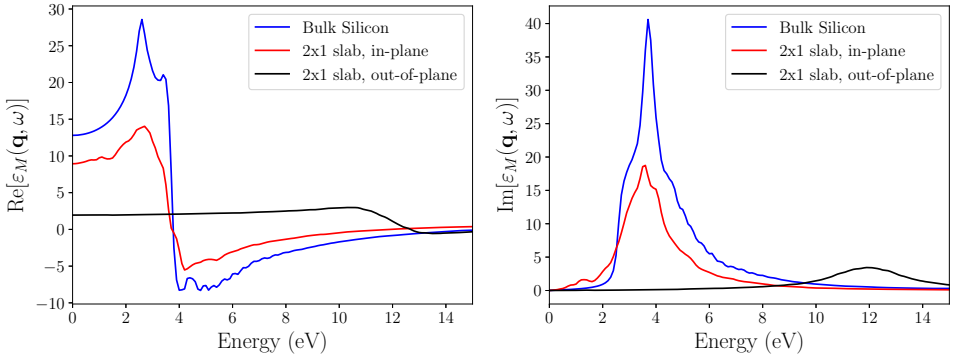

Figure 4.2: Dielectric function of bulk silicon compared with the dielectric function of a p(2x1) silicon slab calculated within the standard supercell formalism, with local field effects. The in-plane component is reported in red, the out-of-plane in black.

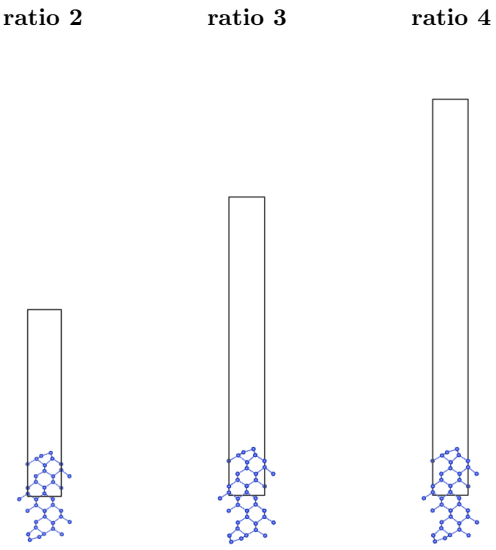

Figure 4.3: Supercells used to study the effect of vacuum on the calculation of the optical properties. The parameter `ratio` refers to the ratio $L_{supercell}/L_{mat}$, where $L_{supercell}$ is the vertical length of the supercell, and L_{mat} is the thickness of the slab.

In Fig. (4.4), we present the spectra of the same silicon slab, calculated in supercells containing different amount of vacuum (see Fig. (4.3)). With "ratio 2" we label the calculation performed in a supercell with the ratio $L_{mat}/L_{supercell} = 2$. This means that in this supercell it will be $L_{mat} = L_{vacuum} \sim 40$ Bohr, corresponding to the system already shown in Fig. (4.1). Analogously, "ratio 3" and "ratio 4" label the supercells where $L_{mat}/L_{supercell} = 3$ and $L_{mat}/L_{supercell} = 4$ respectively. As we can see in Fig. (4.4), when the vacuum in the supercell increases, the in-plane component of the dielectric function is more and more quenched. The out-of-plane component of the spectrum, instead, when vacuum is augmented is not only more suppressed, but also shifts at higher and higher energies. Actually the spectrum converges to the plasmon of bulk silicon (which is at ~ 17 eV), as it will be explained in the following. Nevertheless it cannot be the absorption spectrum of the silicon surface.

As pointed out by Tancogne-Dejean et al. [18], the behaviour of the slab's dielectric function shown in Fig.s (4.2) and (4.4), is due to an effective medium theory with vacuum. The dielectric functions reported in Fig. (4.4), should be considered not as the slab dielectric function, but as the dielectric functions of effective media, each of them containing a different vacuum/matter proportion.

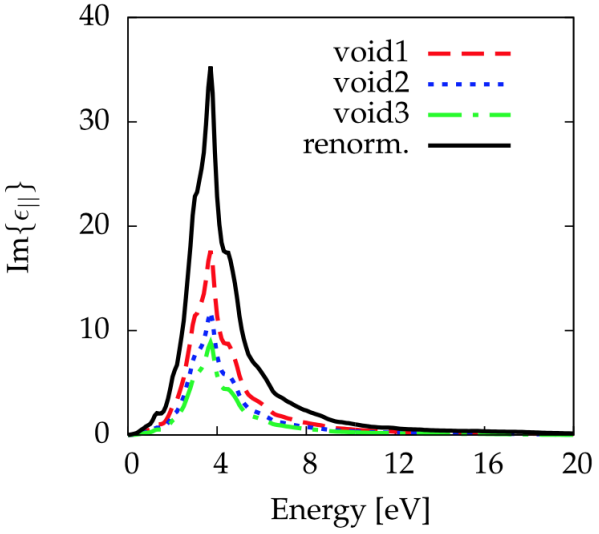

(a)

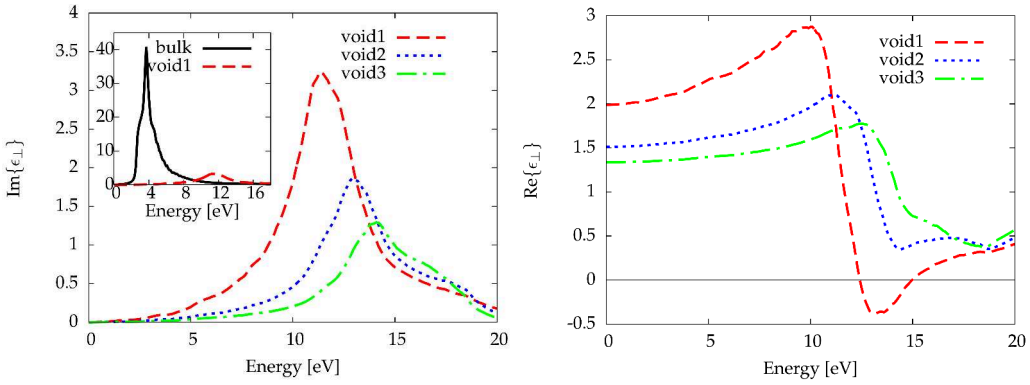

(b)

Figure 4.4: Panel (a) (reproduced from [20]): effect of vacuum on the in-plane component of the dielectric function. Panel (b)(reproduced from Ref. [18]): effect of vacuum on the out-of-plane component of the dielectric function (void1, void2, void3 correspond respectively to `ratio 1`, `ratio 2` and `ratio 3` of Fig. (4.3))

In order to show this, we calculate the dielectric function of an effective medium formed by vacuum and Silicon in variable proportion. The dielectric function of the system will be given by:

$$\varepsilon_{||}^{eff} = f_{Si}\varepsilon_{Si} + f_{vac}\varepsilon_{vac} \tag{4.4a}$$

$$\frac{1}{\varepsilon_{\perp}^{eff}} = \frac{f_{Si}}{\varepsilon_{Si}} + \frac{f_{vac}}{\varepsilon_{vac}} \tag{4.4b}$$

where f_{Si} and f_{vac} stand for the volumic fraction of respectively Silicon and vacuum. Making the substitution $\varepsilon_{vac} = 1$ in Eq. (4.4b), and $f_{vac} = 1 - f_{Si}$, we obtain:

$$\varepsilon_{\perp}^{eff} = \frac{1}{1 - f_{Si} + \frac{f_{Si}}{\varepsilon_{Si}}} \tag{4.5}$$

In the high diluition limit (corresponding to a supercell with much more vacuum than matter, i.e. $f_{Si} \ll 1$), we have:

$$\varepsilon_{\perp}^{eff} \approx 1 + \frac{f_{Si}}{\varepsilon_{Si}} \tag{4.6}$$

which explains why the effective medium theory with vacuum converges to the plasmon, as the vacuum in the supercell is increased. Using Eq.s (4.4) we calculate the dielectric functions of effective media containing respectively 50% of Silicon and 50% of vacuum, 33.33% of Silicon and 66.66% of vacuum, and 25% of Silicon and 75% of vacuum, corresponding respectively to the three supercell reported in Fig. (4.3). Results are reported in Fig. (4.5). In this figure, we compare the spectra obtained from effective medium theory with variable relative concentrations of vacuum and matter. These results show that when vacuum concentration is increased in formulas (4.4), the in-plane component of the resulting dielectric function is scaled. Concerning the out-of-plane component of the effective medium spectrum, it displaces towards the plasma frequency. This allow us to explain the behaviour of the spectra presented in Fig. (4.4): when we calculate the dielectric function using Eq. (4.3), strictly speaking, we are calculating the ratio between the external field and the total field *averaged on the whole supercell*. Therefore, the dielectric function obtained with this procedure, should be not considered as the dielectric function of the slab: this is the dielectric function of an effective medium containing the slab plus a certain amount of vacuum, and the properties of this effective medium of course will depends on the relative concentrations of its two constituents. In the following section, I will present the "Selected-G" method, developed by Tancogne-Dejean et al. [18].

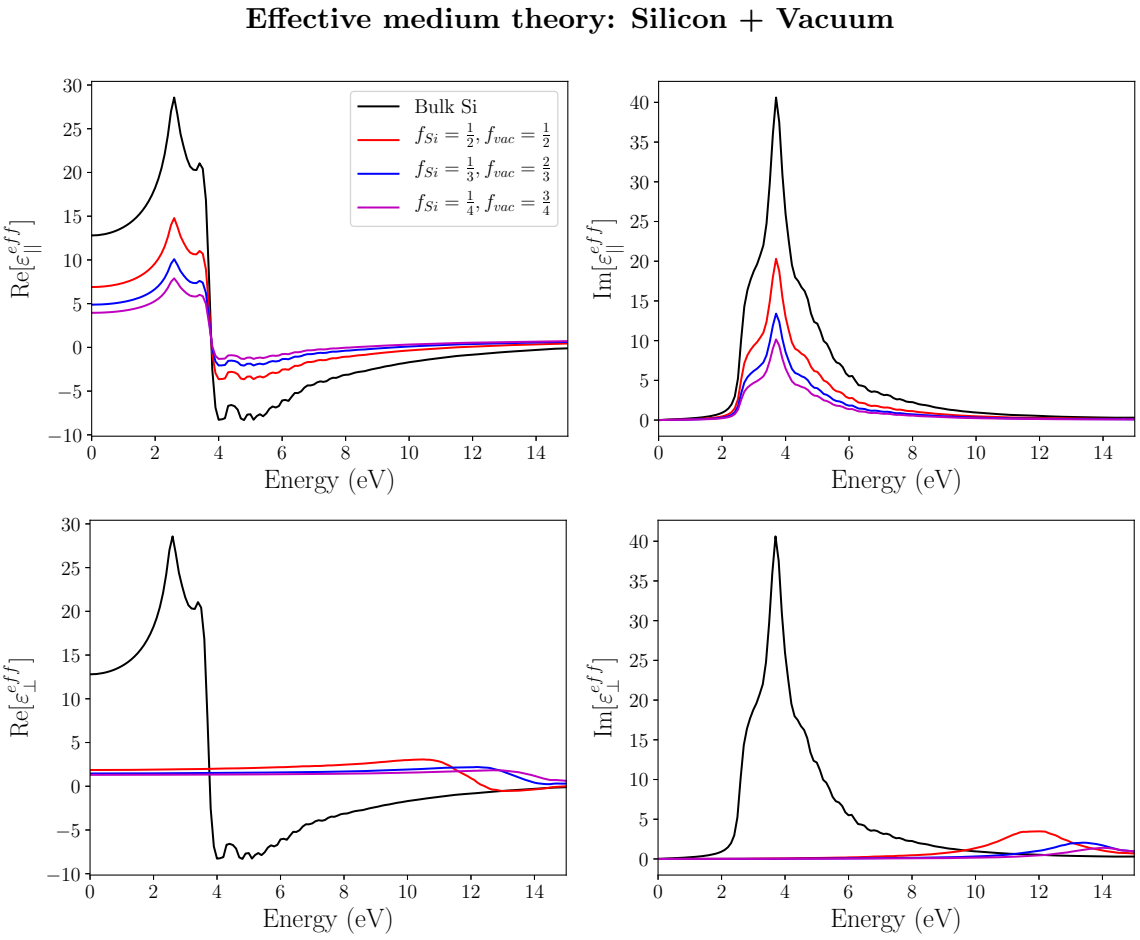

Figure 4.5: Effect of mixing the dielectric function of silicon with vacuum. As model dielectric function of silicon, we used the dielectric function of bulk silicon (here represented by the black line). The dielectric function of effective media containing respectively 50%, 66%, and 75% of vacuum correspond respectively to the red, the blue, and the magenta lines. Top panels show the effect of vacuum on the in-plane component of the dielectric function, which results just in a scaling of the spectra. On the other hand, augmentation of vacuum has a much more dramatic effect on the out-of-plane component (shown in the bottom panels), changing abruptly both amplitude and shape of the spectrum.

4.2 The selected-G method

In order to eliminate the spurious vacuum effect, the selected-G method has been developed [18]. This method consists in retain in the calculation of the response function $\chi_{\mathbf{GG'}}$ just those $\mathbf{G}$-vectors corresponding to oscillations of period L_{mat}. In other words, one has to keep just those $\tilde{\mathbf{G}}$ such to satisfy the following condition:

$$\tilde{G}_z = \frac{2\pi}{L_{mat}} m \quad , \quad m \in \mathbb{Z} \tag{4.7}$$

(see Fig. (4.6))

After having evaluated the $\chi^0_{\tilde{\mathbf{G}}\tilde{\mathbf{G}}'}$ on the set of $\tilde{\mathbf{G}}$ vectors, one has to solve the Dyson equation:

$$\tilde{\chi}_{\tilde{\mathbf{G}}\tilde{\mathbf{G}}'} = \chi^0_{\tilde{\mathbf{G}}\tilde{\mathbf{G}}'} + \sum_{\tilde{\mathbf{G}}_1,\tilde{\mathbf{G}}_2} \chi^0_{\tilde{\mathbf{G}}\tilde{\mathbf{G}}_1} v_{\tilde{\mathbf{G}}_1\tilde{\mathbf{G}}_2} \tilde{\chi}_{\tilde{\mathbf{G}}_2\tilde{\mathbf{G}}'} \tag{4.8}$$

with:

$$v_{\tilde{\mathbf{G}}_1\tilde{\mathbf{G}}_2} = \delta_{\tilde{\mathbf{G}}_1\tilde{\mathbf{G}}_2} \frac{4\pi}{|\mathbf{q} + \tilde{\mathbf{G}}_1|^2} \tag{4.9}$$

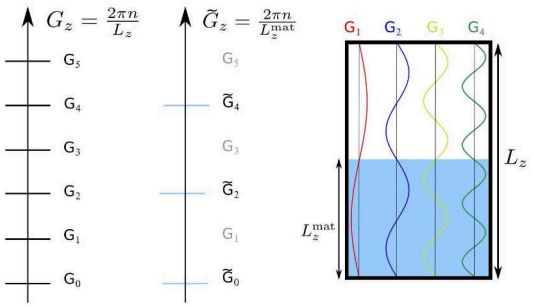

Figure 4.6: Selected-G method consist in just retaining the $\mathbf{G}$-vectors having the same periodicity of the slab.

The response function $\chi_{\mathbf{GG'}}$ obtained solving Eq. (4.1), and the response function $\tilde{\chi}_{\tilde{\mathbf{G}}\tilde{\mathbf{G}}'}$ obtained solving Eq. (4.8), differs in a fundamental aspect. The first one describes the density response of an array of slabs infinitely repeated in the z direction, spaced out by a layer of vacuum of thickness L_{vac}. The latter describes instead the response of an analogous array of infinitely repeated slab, where the vacuum layers have been suppressed (see Fig. (4.7)). The system described by the function $\tilde{\chi}_{\tilde{\mathbf{G}}\tilde{\mathbf{G}}'}$, therefore, does not contain vacuum. The dielectric function can be calculated as

$$\tilde{\varepsilon}^{-1}_{\tilde{\mathbf{G}}\tilde{\mathbf{G}}'} = \delta_{\tilde{\mathbf{G}}\tilde{\mathbf{G}}'} + \sum_{\tilde{\mathbf{G}}_1} v_{\tilde{\mathbf{G}}\tilde{\mathbf{G}}_1} \tilde{\chi}_{\tilde{\mathbf{G}}_1\tilde{\mathbf{G}}'} \tag{4.10}$$

$$\varepsilon_M = \frac{1}{\tilde{\varepsilon}^{-1}_{\mathbf{00}}} \tag{4.11}$$

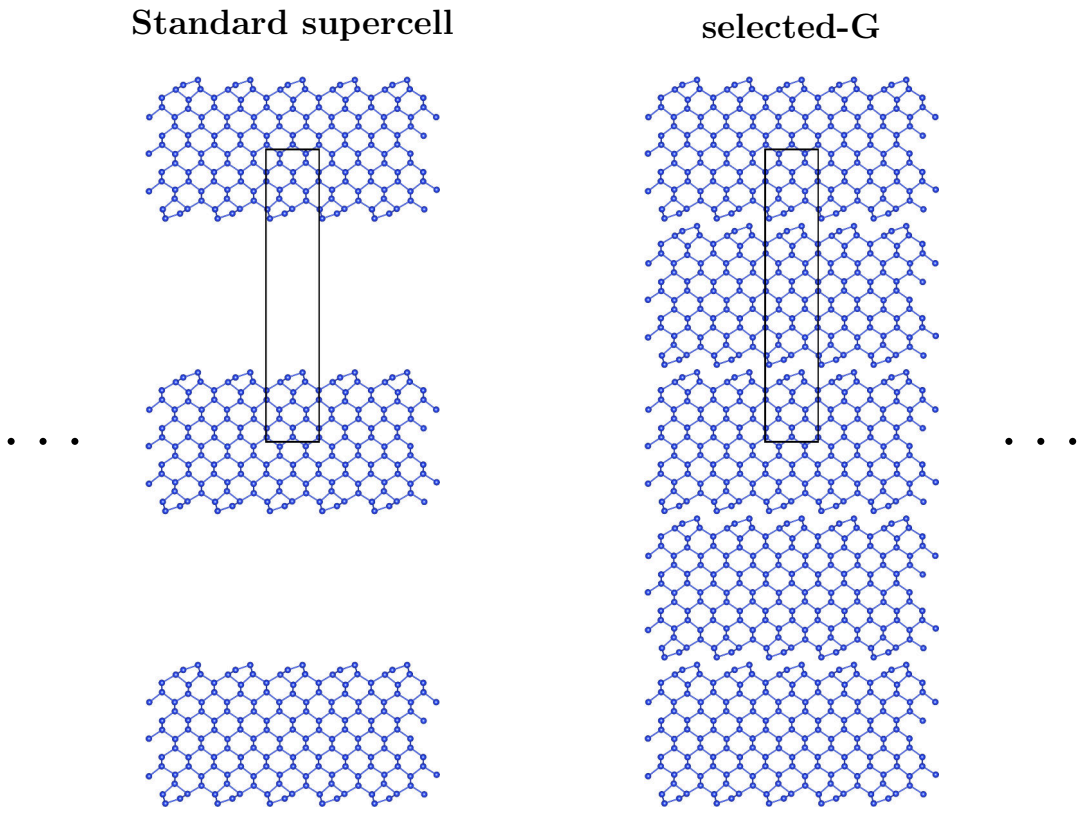

Figure 4.7: Selected-G method replaces the original supercell with a new one, having half of the periodicity of the original system. Vacuum between replicas is filled with a copy of the slab, and therefore the vacuum problem is eliminated.

In Fig. (4.8) the application of the selected-G method to the calculation of the dielectric function of the bare silicon surface is shown. As we can see in the figure, the spurious effect of vacuum is eliminated, and the peak of the out-of-plane component is pushed back at $\sim$ 4 eV.

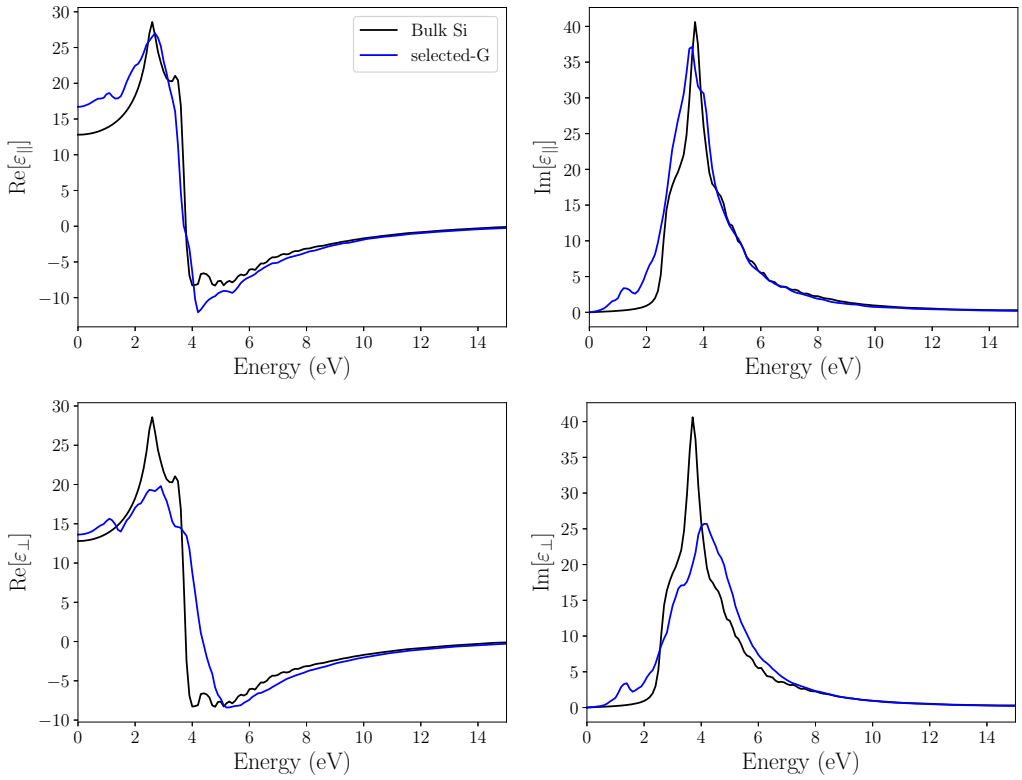

Figure 4.8: Dielectric function of the silicon slab calculated within the selected-G approach (blue lines) compared with the bulk silicon spectrum (black lines). The selected-G method eliminates the effect of vacuum from the calculation: the in-plane component is now correctly rescaled, and the out-of-plane component is pushed-back at $\sim$ 4 eV.

4.3 Silicon(001)+Thymine: Optical response

In this section I present the calculation that I have performed on the silicon slab functionalised with Thymine. This system (shown in Fig. (4.9)) is composed by 8 atomic plane of silicon, and it has a reconstruction 4x1 (see Chapter 3 and Fig. (3.7)). $L_{supercell}$ is the length of the supercell in the out-of-plane direction, and it has been chosen as $L_{supercell} = 2L_{mat}$ in order to apply the selected-G method. L_{mat} is the thickness of the slab, and here it has been defined as the distance between the top-most hydrogen atom and the bottom most one, resulting in $L_{mat} \sim 38.2$ Bohr. L_{vac} is the size of vacuum, and it is defined as $L_{vac} = L_{supercell} - L_{mat}$.

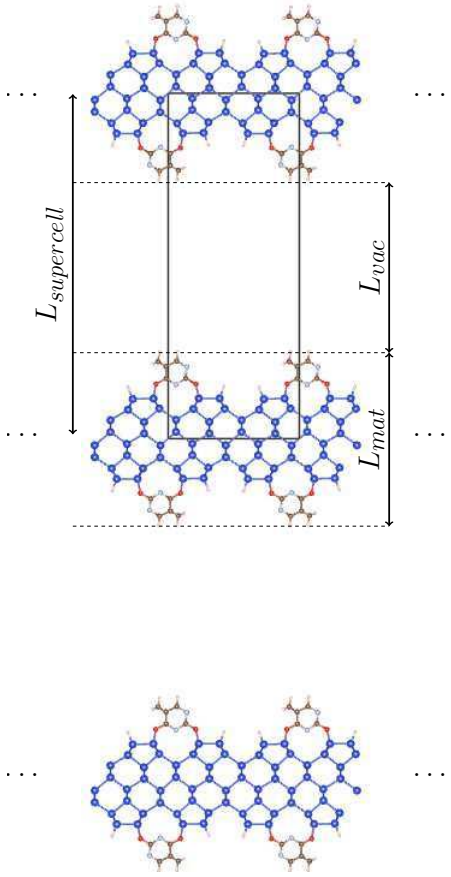

Figure 4.9: Supercell used to model the Si(001)+Thymine surface. $L_{supercell}$ labels the length of the supercell in the out-of-plane direction. L_{mat} labels the thickness of the slab, and here it has been defined as the distance between the top-most hydrogen atom and the bottom most one, resulting in $L_{mat} \sim 38.2$ Bohr. L_{vac} is the size of vacuum, and it is defined as $L_{vac} = L_{supercell} - L_{mat}$.

The spectra which I will present in this section, have been all calculated within the selected-G formalism. As we have explained in section 4.2, the selected-G method consists basically in retaining inside the evaluation of χ just those $\tilde{\mathbf{G}}$ vectors having periodicity L_{mat} in the out-of-plane direction. In order to apply this method, we have firstly to choose the value of L_{mat}, and then to choose the length of the supercell in the out-of-plane direction (the parameter $L_{supercell}$) such that it is an integer multiple of L_{mat}. In the calculations that I will present in this section, I have chosen as L_{mat} value the distance between the top-most atom of the top thymine molecule, and the bottom-most atom of the bottom thymine molecule, resulting in $L_{mat} \approx 39$ Bohr (see Fig. (4.9)).

4.3.1 Si(001)+Thymine: linear response

In this section, I present the calculation of the dielectric function that I have performed for the silicon slab functionalised with Thymine within the selected-G formalism. In Fig. (4.10)

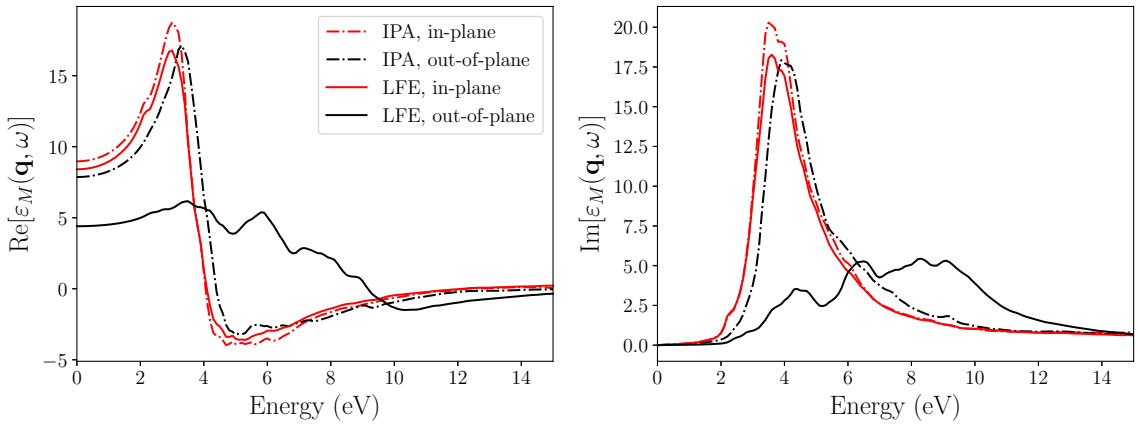

Figure 4.10: Dielectric function of the Si(001)+Thymine slab. In-plane component (in red), out-of-plane component (in black), dashed and solid lines stand respectively for IPA and LFE spectra. The inclusion of local field effects have been performed via the selected-G approach

I report as dashed lines the spectra calculated in Independent Particle Approximation (IPA), while the solid lines represent the spectra with Local Field Effects (LFE). As we can see from the solid lines in Fig. (4.10), the local field effects have quite a reduced influence on the in-plane component of the dielectric function (represented in red),in agreement with the fact that electronic density is quite homogeneous in the in-plane direction. On the contrary, the effect is much more important on the out-of-plane component (represented in black). Local field effects are expected to be stronger for the out-of-plane component, due to the abrupt change in electron density perpendicular to the surface. Nevertheless, if we compare to results obtained for the bare silicon surface (see Fig. (4.8)), the effect appears extremely large: the spectrum is almost totally quenched around 4 eV, and spreads over a range of energy up to 14 eV.

4.3.2 Si(001)+Thymine: second order response

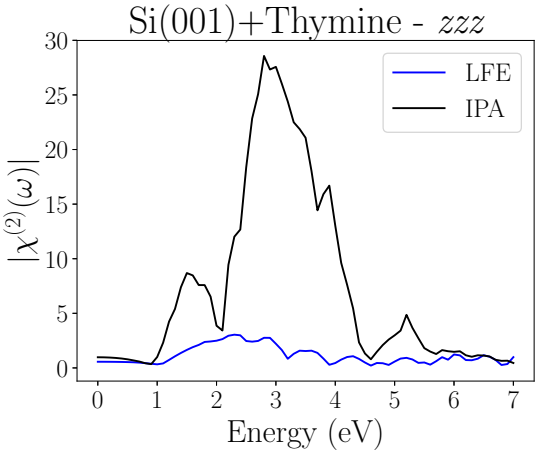

Figure 4.11: In this figure, we report the calculation of the zzz component of the $\chi^{(2)}$ tensor, with and without local field effects (represented respectively by the blue and the black lines). Inclusion of local field effects has been performed within the selected-G formalism. Despite of that, when local field effects are added, the spectrum results to be almost completely suppressed.

In this section I present the calculations that I have performed on the second order response of the silicon slab functionalised with Thymine. In Fig. (4.11) I report the zzz component of the second order susceptibility tensor. The black line corresponds to the calculation performed in the Independent Particle Approximation, the blue line to the inclusion of local field effects. As we can see, the zzz component of the spectrum is dramatically quenched once local field effects are added. So, to recap: when local field effects are included, the out-of-plane component of the functionalised slab's spectra - both at first and second order - appears to be dramatically quenched, contrarily to what happens in the case of the bare silicon surface. What is the origin of this stunning feature ? Is it a real physical effect associated with functionalisation, or this suppression is just another spurious effect related to the presence of vacuum inside the supercell, as it has been illustrated before (Sec. 4.1)?.
Indeed, the selected-G method, which has been developed in order to get rid of the vacuum introduced between replicas, requires to define in some way the thickness of the slab (see Section 4.2). For the case of the bare silicon surface, which is roughly uniform, it has been naturally defined as the distance between the top most and bottom most atomic layers. But in the case of the functionalised surface, the thickness is not uniform anymore, and this task is less trivial: in the point where the adsorbed molecule is present, the slab is thicker, while in the point where no molecule is present the slab is thinner. Is the vacuum between

lines of molecules at the origin of the quenching ? Should it be considered as spurious vacuum? In other words: should the thickness of the adsorbed overlayer be included in the definition of L_{mat}? Next section will be devoted to answer these questions.

4.4 Intermolecular vacuum

In order to establish if the intermolecular vacuum is responsible for the quenching of the spectra reported in Fig.s (4.10) and (4.11), we have studied two new systems: the silicon slab completely covered with Thymine (Fig. (4.13)), and the silicon stepped surface (Fig. (4.15)).

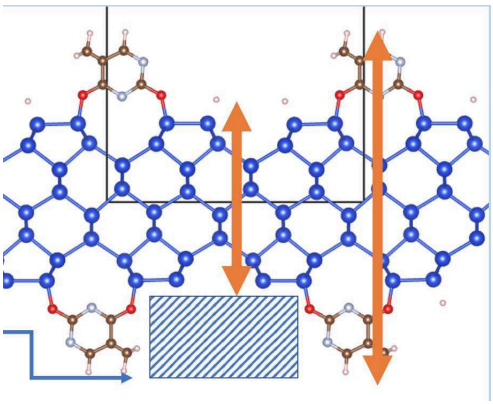

Figure 4.12: Illustration of intermolecular vacuum

4.4.1 Completely covered surface

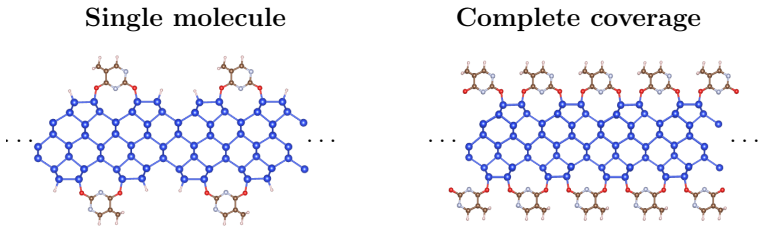

Figure 4.13: In order to question if the suppression of the spectra is due to the intermolecular vacuum, we investigate the completely covered surface. If the quenching come from the space between molecules, spectra of the completely covered slab should not be affected by that.

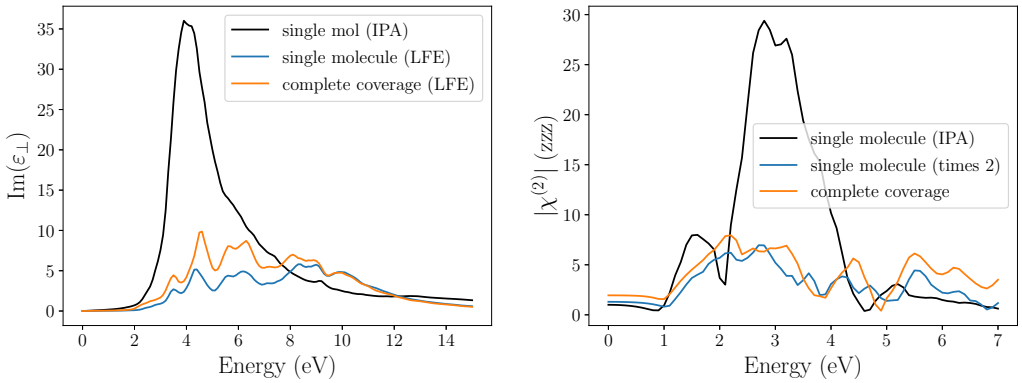

Figure 4.14: Out-of-plane component of the dielectric function (panel (a)) and $\chi^{(2)}_{zzz}$ (panel (b)) of single molecule (blue lines) and the completely covered surface (orange).

This new system (that we report in Fig. (4.13)), is obtained from the slab reported in Fig. (4.9) adding an additional molecule in between two contiguous adsorbate rows. This new system, even if it does not represent the most favourable adsorption configuration, does not contain vacuum between molecules anymore. In Fig. (4.14) we show the calculation of the out-of-plane component of the dielectric function and of the zzz component of the second order susceptibility of the completely covered surface, and we compare it with the spectra of the previously studied slab (which contains just a single molecule per unit cell on each side). As we can see in figure, in both cases the out-of-plane component of the spectra results to be greatly quenched. This proofs that the suppression of optical response observed in Fig.s (4.10) and (4.11) cannot be attributed to the spacing between molecules.

4.4.2 Si(001) stepped surface

In order to corroborate this finding, we studied another system which presents non uniform thickness: the silicon stepped surface (see Fig. (4.15)). As the surfaces functionalised with nucleobases, also this system contains vacuum between one step and the other ones, so, if vacuum between molecules is at the origin of the suppression of the spectrum, the same effect should be expected for the stepped surface. The out-of-plane component of the spectrum of the stepped surface, with the inclusion of local field effects, is reported in Fig. (4.16) (black line). As we can see, the main peak of the spectrum is still located at around $\sim$ 4 eV, exactly as it happens for the bare surface (blue line), and the effect of vacuum between steps results just in a scaling of the spectrum. The study of the stepped surface confirms that the quenching and blueshift observed in the spectra of the functionalised surface is not due to vacuum between molecules: understanding the origin of this effect will be one of the main goals of next chapter.

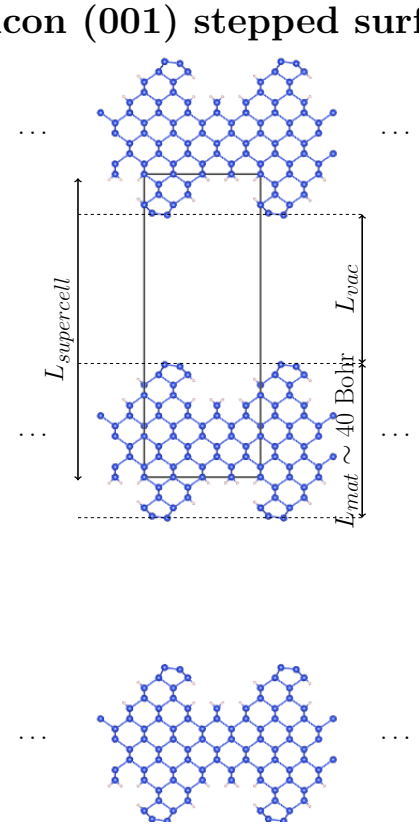

Figure 4.15: Unit cell used to model the silicon (001) stepped surface. Dangling bonds have been passivated with hydrogen atoms.

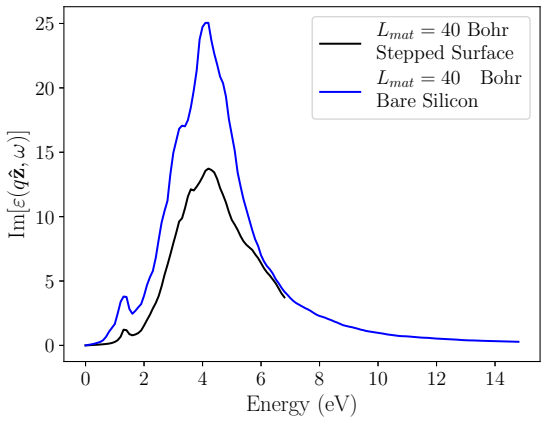

Figure 4.16: Comparison of dielectric functions of the stepped surface (in black) and of the bare silicon surface (in blue).

4.5 Conclusions

Through this chapter we illustrated the so called vacuum problem. When calculations of optical properties are performed within the standard supercell formalism, the inclusion of local field effects produces an important effect on the dielectric function, resulting in a rescaling of the spectrum in the in-plane direction, and in a strong quenching and blue-shift for the out-of-plane component. As we have shown, this does not reflect a physical property of the studied system, but it is just a spurious effect coming from the presence of vacuum inside the cell: the more the size of the supercell (and the amount of empty space in it) is increased, the more this effect become important. Subsequently, we have shown how this behaviour can be cured using the selected-G technique [18], and showing an application of this method to the bare silicon surface. Finally, we presented the first calculations that we have performed on the silicon surfaces functionalised with Thymine, and we have shown how, despite having applied the selected-G technique, the out-of-plane component of these spectra still exhibit an important quenching. In order to clarify if this effect could be attributed to the presence of vacuum between adsorbed molecules, we also performed a study of the fully covered surface and the bare silicon surface, which allowed us to exclude the role of intermolecular vacuum in the suppression of the spectra. In parallel to these calculations done within the reciprocal space formalism, in order to clarify the optical response of the functionalised surfaces I developed a mixed space approach, in which the direction perpendicular to the slab is treated in real space, and the parallel one in reciprocal space. This formalism enabled me to study a truly isolated thin slab, and it gave me also the opportunity to further question the definition of L_{mat}, as well as the role of the interaction between replicas.

Chapter 5

Response of a (thin) isolated slab: the mixed space approach

As we have seen in the previous chapter, the spectra of the out-of-plane dielectric function as well as the zzz component of the second order susceptibility, are strongly quenched compared to the bare silicon surfaces. This feature remains also in the case of full covered surface, excluding the role of vacuum in between lines of molecules. In order to understand the influence of the adsorbed molecules on the Si(001) surface, I decided to study this system in the real space. Working in reciprocal space as we usually do, we are forced to adopt the supercell formalism, and therefore we are obliged to model the system of interest (i.e. the surface) with an array of periodically repeated slabs. Approaching the problem in the real space domain, allows us to describe an object which is really isolated (i.e. we are sure that we have eliminated the spurious interaction between replicas). Moreover, a calculation in the real space, allows us to obtain all the physical quantities of interest (the density variation, the induced electric field, etc...) expressed as function of the position. This should permit a layer-by-layer analysis of the system, leading to a better understanding of the contribution of the adsorbed layer. Since the system used to model the surface is limited to a quite thin object (due to the computational constraints), the mixed space framework will also allow us to inquire the difference between the optical and electronic properties of 2D and 3D objects.

5.1 Mixed space approach

The goal of this section is to show how it's possible to obtain the response function of an isolated slab. This can be done using the so called mixed space approach [18]. In this approach, the in-plane directions -where the system is actually infinite and periodic - are treated in the reciprocal space, while the out-of-plane direction (here taken along z) - where the system is finite and the periodicity is broken - is treated in the real space. In

practice, switching from the reciprocal space description to the mixed space one, consists just in change of the basis set. In the reciprocal space representation, the basis set in which we expand the physical quantities of interest is the plane waves basis set:

$$\mathcal{B}_{pw} = \left\{ \frac{e^{i(\mathbf{q}+\mathbf{G})\mathbf{r}}}{\sqrt{V}} \right\}_{\substack{\mathbf{q}\in BZ \\ \mathbf{G}\in RL}} \tag{5.1}$$

while in the mixed space representation, the basis set will be:

$$\mathcal{B}_m = \left\{ \frac{e^{i(\mathbf{q}_{||}+\mathbf{G}_{||})\mathbf{r}_{||}}}{\sqrt{S}} \delta(z-z_0) \right\}_{\substack{\mathbf{q}_{||}\in 2dBZ \\ \mathbf{G}_{||}\in 2dRL \\ z_0\in\mathbb{R}}} \tag{5.2}$$

In the reciprocal space representation, a given function $f(\mathbf{r})$ will be expressed as $f_{\mathbf{G}}(\mathbf{q})$, where:

$$f(\mathbf{r}) = \sum_{\mathbf{G}} \int_{BZ} d\mathbf{q} f_{\mathbf{G}}(\mathbf{q}) \frac{e^{i(\mathbf{q}+\mathbf{G})\mathbf{r}}}{\sqrt{V}} \tag{5.3}$$

while in the mixed space, it will represented as $f_{\mathbf{G}_{||}}(\mathbf{q}_{||}, z)$,where:

$$f(\mathbf{r}) = \sum_{\mathbf{G}_{||}} \int_{2dBZ} d\mathbf{q}_{||} \int dz' f_{\mathbf{G}_{||}}(\mathbf{q}_{||}, z') \frac{e^{i(\mathbf{q}_{||}+\mathbf{G}_{||})\mathbf{r}_{||}}}{\sqrt{S}} \delta(z-z') \tag{5.4}$$

If we know the plane waves representation of the function $f(\mathbf{r})$, we can obtain the mixed space representation via a Fourier transform in the variable z:

$$f_{\mathbf{G}_{||}}(\mathbf{q}_{||}, z) = \sum_{G_z} \frac{1}{\sqrt{L_z}} \int dq_z f_{\mathbf{G}}(\mathbf{q}) e^{i(q_z+G_z)z} \tag{5.5}$$

In an analogous way, if I have an operator $\mathcal{O}_{\mathbf{G}\mathbf{G}'}(\mathbf{q})$(for example a response function) expressed in the base of plane waves, I can obtain its mixed space representation in the following way:

$$\mathcal{O}_{\mathbf{G}_{||}\mathbf{G}_{||}'}(\mathbf{q}_{||}, z, z') = \frac{1}{L_z} \sum_{\mathbf{G},\mathbf{G}'} e^{-i(G_z+q_z)z} \mathcal{O}_{\mathbf{G}\mathbf{G}'}(\mathbf{q}) e^{i(q_z+G'_z)z'} \tag{5.6}$$

The starting point of our calculation is the Kohn-Sham independent particle response function, which is obtained in reciprocal space via DP-CODE[48]. The independent particle response function is then obtained in the mixed space representation via a Fourier transform:

$$\begin{aligned} \chi^0_{\mathbf{G}\mathbf{G}'}(\mathbf{q},\omega) &\longrightarrow \chi^0_{\mathbf{G}_{||}\mathbf{G}_{||}'}(\mathbf{q}_{||}, z, z', \omega) \\ \chi^0_{\mathbf{G}_{||}\mathbf{G}_{||}'}(\mathbf{q}_{||}, z, z', \omega) &= \frac{1}{L_z} \sum_{\mathbf{G},\mathbf{G}'} e^{-i(G_z+q_z)z} \chi^0_{\mathbf{G}\mathbf{G}'}(\mathbf{q},\omega) e^{i(q_z+G'_z)z'} \end{aligned} \tag{5.7}$$

The Dyson equation of TD-DFT (in RPA), which in reciprocal space reads:

$$\chi_{\mathbf{G}\mathbf{G}'}(\mathbf{q},\omega) = \chi^0_{\mathbf{G}\mathbf{G}'}(\mathbf{q},\omega) + \sum_{\mathbf{G_1}\mathbf{G_2}} \chi^0_{\mathbf{G}\mathbf{G_1}}(\mathbf{q},\omega) v^{coul}_{\mathbf{G_1}\mathbf{G_2}}(\mathbf{q}) \chi_{\mathbf{G_1}\mathbf{G_2}}(\mathbf{q},\omega) \tag{5.8}$$

in the mixed space becomes:

$$\begin{aligned} \chi_{\mathbf{G}_{||}\mathbf{G}'_{||}}(\mathbf{q}_{||},z,z',\omega) &= \chi^0_{\mathbf{G}_{||}\mathbf{G}'_{||}}(\mathbf{q}_{||},z,z',\omega) + \\ + \sum_{\mathbf{G_{1||}}\mathbf{G_{2||}}} \int_{-\infty}^{\infty} dz_1 \int_{-\infty}^{\infty} dz_2 \chi^0_{\mathbf{G}_{||}\mathbf{G_{1||}}}(\mathbf{q}_{||},z,z_1,\omega) v^{coul}_{\mathbf{G_{1||}}\mathbf{G_{2||}}}(\mathbf{q}_{||},z_1,z_2) \chi_{\mathbf{G_{2||}}\mathbf{G}'_{||}}(\mathbf{q}_{||},z_2,z',\omega) \end{aligned} \tag{5.9}$$

We want to stress out that Eq. (5.8) and Eq. (5.9) are strictly equivalent. As we stated in the beginning of this section, switching from the plane waves representation to the mixed space one, constitutes just a change of the basis set. Eq. (5.8) and Eq. (5.9), therefore, contain exactly the same physics, which is the physics of a system infinite and periodic in all directions. As we can see in Eq. (5.9), the integration in z_1 and z_2 is performed from $-\infty$ to $+\infty$, meaning that the Hartree potential felt by the electrons will be not just the potential induced by the isolated slab, but the potential induced by all the replicas. In order to get the response of the isolated slab, we have to eliminate in some way the potential induced by the replicas. This can be achieved applying a cut-off in the z direction to the Coulomb potential operator:

$$\begin{aligned} v^{coul}(\mathbf{q}_{||},z,z') \longrightarrow & \tilde{v}^{coul}(\mathbf{q}_{||},z,z') = \\ & = \Theta(z'+\frac{L}{2})\Theta(-z'+\frac{L}{2}) v^{coul}(\mathbf{q}_{||},z,z') \Theta(z+\frac{L}{2})\Theta(-z+\frac{L}{2}) \end{aligned} \tag{5.10}$$

The cut Coulomb operator $\tilde{v}^{coul}(\mathbf{q}_{||},z,z')$, acting on a periodic distribution of charge, does not produce the potential induced by the whole distribution, but just the potential induced by the charges inside the region $z \in [-L/2, L/2]$. If the distribution of charge is the density variation induced by an external perturbation in an array of slab infinitely repeated in the z direction, in other words, the operator $\tilde{v}^{coul}(\mathbf{q}_{||},z,z')$ will produce the potential induced by just one isolated slab. Substituting (5.10) in Eq. (5.9), we obtain therefore the Dyson equation for the response function of an isolated slab:

$$\begin{aligned} \chi_{\mathbf{G}_{||}\mathbf{G}'_{||}}(\mathbf{q}_{||},z,z',\omega) &= \chi^0_{\mathbf{G}_{||}\mathbf{G}'_{||}}(\mathbf{q}_{||},z,z',\omega) + \\ + \sum_{\mathbf{G_{1||}}\mathbf{G_{2||}}} \int_{-L/2}^{L/2} dz_1 \int_{-L/2}^{L/2} dz_2 \chi^0_{\mathbf{G}_{||}\mathbf{G_{1||}}}(\mathbf{q}_{||},z,z_1,\omega) v^{coul}_{\mathbf{G_{1||}}\mathbf{G_{2||}}}(\mathbf{q}_{||},z_1,z_2) \chi_{\mathbf{G_{2||}}\mathbf{G}'_{||}}(\mathbf{q}_{||},z_2,z',\omega) \end{aligned} \tag{5.11}$$

5.1.1 Mixed-space representation of the Coulomb potential operator

The coulomb potential operator v is defined as the Green function of the Poisson equation:

$$\nabla^2\phi(\mathbf{r}) = -4\pi\rho(\mathbf{r}) \tag{5.12}$$

In other words, $v(\mathbf{r},\mathbf{r}')$, must be that operator which acting on a density of charge distribution, produces the induced potential associated with that charge distribution. In the mixed space representation, the Coulomb potential operator will be given by:

$$v^{coul}_{\mathbf{G}_{||}\mathbf{G}'_{||}}(\mathbf{q}_{||},z,z') = \delta_{\mathbf{G}_{||}\mathbf{G}'_{||}}\frac{2\pi}{|\mathbf{q}_{||}+\mathbf{G}_{||}|}e^{-|\mathbf{q}_{||}+\mathbf{G}_{||}|\cdot|z-z'|} \tag{5.13}$$

This expression has the following physical meaning: it's the electrostatic potential induced by a planar charge distribution modulated in the in-plane direction by an oscillation of wavevector $\mathbf{q}_{||}+\mathbf{G}_{||}$. This expression by the way has a problem: it's divergent for $\mathbf{q}_{||}+\mathbf{G}_{||}=0$. In our calculation, we would like to describe the response of the system to an external perturbation having no long wavelength component in the in-plane direction (i.e. an external perturbation having the electric field along z). In order to find the expression of v^{coul} for $\mathbf{q}_{||}=0$ we propose the following argument. $v^{coul}_{\mathbf{G}_{||}\mathbf{G}'_{||}}(\mathbf{q}_{||}=0)$ must be that potential associated to a distribution of planar charge modulated by a wavevector $\mathbf{G}_{||}$. The case $\mathbf{G}_{||}=0$ corresponds to the potential induced by an infinite charged plane. It's well known that an infinite positively (negatively) charged plane induces an electric field constant and uniform diverging from (converging to) the plane. Therefore the Coulomb potential operator in the mixed space representation will be given, for $\mathbf{q}_{||}=\mathbf{0}$, by:

$$v^{coul}_{\mathbf{G}_{||}\mathbf{G}'_{||}}(\mathbf{q}_{||}=0,z,z') = \delta_{\mathbf{G}_{||}\mathbf{G}'_{||}} \times \begin{cases} -2\pi|z-z'| & \text{for} \quad \mathbf{G}_{||}=0 \\ \\ \dfrac{2\pi}{|\mathbf{G}_{||}|}e^{-|\mathbf{G}_{||}|\cdot|z-z'|} & \text{for} \quad \mathbf{G}_{||}\neq 0 \end{cases} \tag{5.14}$$

5.2 Numerical implementation

The independent particle response function of the system has been evaluated in the reciprocal space via DP-CODE [48]. After that, a Discrete Fourier Transform has been performed in order to evaluate the mixed space representation of the χ^0 on a discretised spacial domain:

$$\chi^0_{\mathbf{G}_{||}\mathbf{G}_{||}'}(\mathbf{q}_{||},z_i,z_j,\omega) = \frac{1}{L_z}\sum_{\mathbf{G},\mathbf{G}'} e^{-i(G_z+q_z)z_i}\chi^0_{\mathbf{G}\mathbf{G}'}(\mathbf{q},\omega)e^{i(q_z+G'_z)z_j} \tag{5.15}$$

In order to simplify the problem (and since local field effects are expected to be smaller in the in-plane direction, see e.g. [49]), in all the calculations we have performed the $\chi^0_{\mathbf{G}\mathbf{G}'}$

matrix has been evaluated over a set of `npwmat` G-vectors of the form:

$$\mathbf{G} = (0, 0, G_z) \tag{5.16}$$

For this reason, from now on we will omit to write $\mathbf{G}_{||}$ in our notations. The real space grid on which we evaluated the χ^0 consists in `npwmat` points uniformly distributed in the interval $z \in [-L_{supercell}/2, L_{supercell}/2]$:

$$z_i \in \left\{ -\frac{L_{supercell}}{2}, -\frac{L_{supercell}}{2} + \Delta_z, \ldots, \frac{L_{supercell}}{2} \right\} \quad \text{with} \quad \Delta_z = \frac{L_{supercell}}{\texttt{npwmat}} \tag{5.17}$$

The Dyson equation for an isolated slab, in its discretised form (and in the approximation (5.16)), will be[1]:

$$\begin{aligned} \chi(\mathbf{q}_{||}, z_i, z_j) = \chi^0(\mathbf{q}_{||}, z_i, z_j) + \\ + \sum_{l,m} \chi^0(\mathbf{q}_{||}, z_i, z_l) v^{coul}(\mathbf{q}_{||}, z_l, z_m) \chi(\mathbf{q}_{||}, z_m, z_j) \Delta_z^2 \end{aligned} \tag{5.18}$$

The solution of this matrix equation will be given by:

$$\chi(\mathbf{q}_{||}, z_i, z_j) = \frac{1}{\Delta_z} \sum_l [\mathbb{A}^{-1}]_{il} \chi^0(\mathbf{q}_{||}, z_l, z_j) \tag{5.19}$$

where $\mathbb{A}$ is the matrix defined by:

$$\mathbb{A}_{ij} = \frac{\delta_{ij}}{\Delta_z} - \sum_l \chi^0(\mathbf{q}_{||}, z_i, z_l) v^{coul}(\mathbf{q}_{||}, z_l, z_j) \Delta_z \tag{5.20}$$

5.3 In-plane response

In this section we present the calculation that I have performed within the mixed space approach for a slab undergoing an external perturbation parallel to the plane. In order to test my mixed-space approach, I firstly applied it on the bare silicon slab (see Fig. (5.1)). The slab we used has been a 2x1 silicon slab formed of 16 atomic layers. After having relaxed atomic positions and having obtained the asymmetric dimer reconstruction, we carried out the calculation of the Kohn-Sham wavefunctions, which has been performed with ABINIT code [50], using the PBE approximation [51] for the exchange correlation part of the potential. Following the procedure outlined in the previous section, I have first computed the independent particle response function in the reciprocal space, using DP-CODE (parameters of the calculation are reported in Tab. (5.1)). This calculation has been performed for $\mathbf{q} = q\hat{\mathbf{x}}$, which is equivalent to set the direction of the perturbing

[1] we omit here the frequency ω to simplify the notation

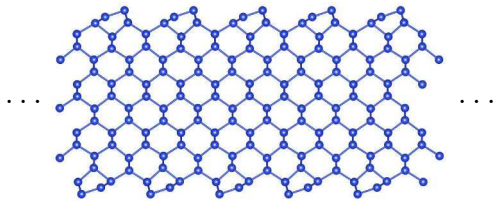

Figure 5.1: In this picture we report the silicon slab that we used, in the calculation presented in this chapter, to model the bare silicon surface. This slab is made of 16 atomic layers (corresponding to $\sim$ 40 Bohr of thickness), and both the faces are p(2x1) reconstructed.

Parameters of the calculation of χ^0 for the bare silicon slab:

$N_{\mathbf{kpt}}$	$N_{\mathbf{G}}$	N_{pw}	N_{bands}
128	165	18997	400

Table 5.1: Parameters used for the calculations of the response function of the bare silicon surface.

electric field parallel to the plane. Moreover, this calculation has been performed in the optical limit, i.e. for $\mathbf{q} \to \mathbf{0}$. In practice, this limit is achieved by choosing a value of $|\mathbf{q}|$ much smaller than the typical dimension of the Brillouin zone. In this particular calculation, $|\mathbf{q}| = 10^{-5}\text{Bohr}^{-1}$. According Eq. (5.15), I have then calculated the mixed space representation of the independent particle response function (see Fig. (5.2)). As we can see, the $\chi^0(z, z')$ presents structures in the (z,z') region corresponding to the matter, and is zero in the rest of the box.

Then, I solved Eq. (5.18) (with the potential defined in Eq. (5.13)) in order to find the interacting response function of the isolated slab. At this point, I want to use this quantity in order to extract the macroscopic dielectric function. When the same problem is treated in the case of a infinite and periodic material, the standard procedure is to calculate the inverse dielectric function:

$$\varepsilon_{\mathbf{GG'}} = \delta_{\mathbf{GG'}} + \sum_{\mathbf{G_1}} v_{\mathbf{GG_1}} \chi_{\mathbf{GG_1}} \tag{5.21}$$

and then obtain the macroscopic dielectric function as:

$$\varepsilon_M = \frac{1}{\varepsilon^{-1}_{\mathbf{00}}} = \frac{v^{ext}_{\mathbf{0}}}{v^{tot}_{\mathbf{0}}} \tag{5.22}$$

In analogy with Eq.s (5.21) and (5.22), I first evaluated the microscopic inverse dielectric

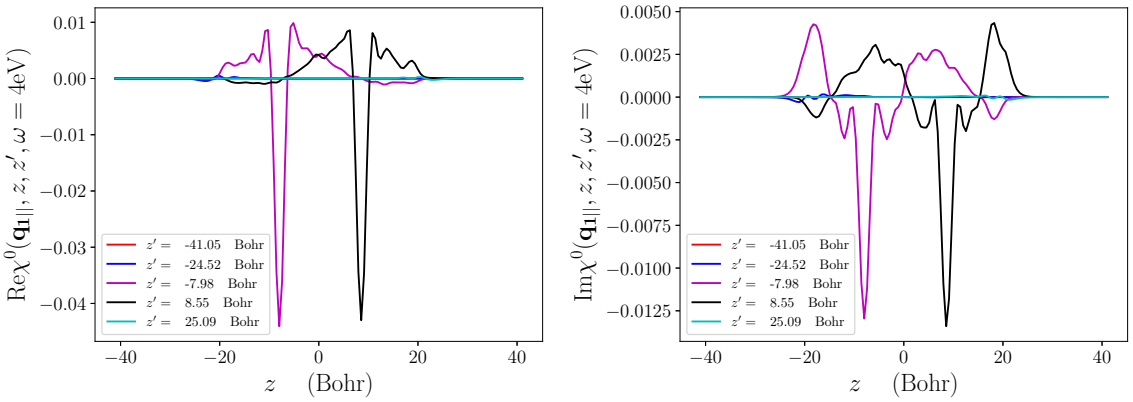

Figure 5.2: Independent particle response function of the bare silicon slab in the mixed space representation: real part is reported to the left, imaginary part to the right. Horizontal axis corresponds to the z variable. The different curves correspond to different values of z'.

function:

$$\varepsilon^{-1}(\mathbf{q}_{||}, z_i, z_j; \omega) = \frac{\delta_{ij}}{\Delta_z} + \sum_l v^{coul}(z_i, z_l)\chi(\mathbf{q}_{||}, z_l, z_j; \omega)\Delta_z \tag{5.23}$$

and then we performed a Fourier transform, in order to extract its macroscopic average:

$$\langle \varepsilon^{-1} \rangle(\mathbf{q}, \omega) = \sum_{ij} e^{-iq_z z_i} \varepsilon^{-1}(\mathbf{q}_{||}, z_i, z_j; \omega) e^{iq_z z_j} \Delta_z^2 \tag{5.24}$$

Finally, we evaluated the quantity:

$$\frac{1}{\langle \varepsilon^{-1} \rangle}(\mathbf{q}, \omega) \tag{5.25}$$

The result of this calculation is shown in Fig. (5.3) The quantity calculated according eq. (5.25) has a peak at around 4 eV (more or less where the absorption peak of bulk silicon is located), but, compared to the dielectric function of bulk silicon is suppressed of about four order of magnitude. As we can see, the real part of the function is ≈ 1, while the imaginary part is almost zero.

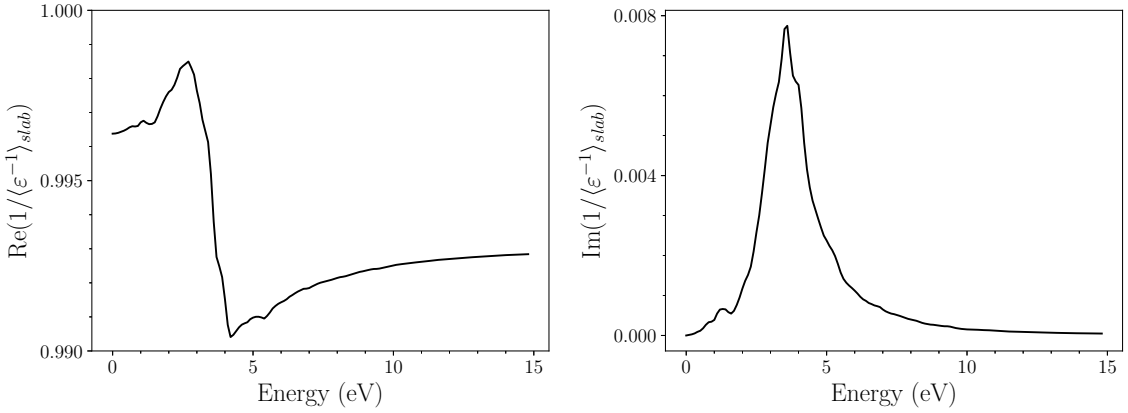

Figure 5.3: In-plane dielectric function of the bare silicon slab calculated according Eq.s (5.24) and (5.25), a procedure which consists basically in evaluating the ratio between the averages of the external and induced potential.

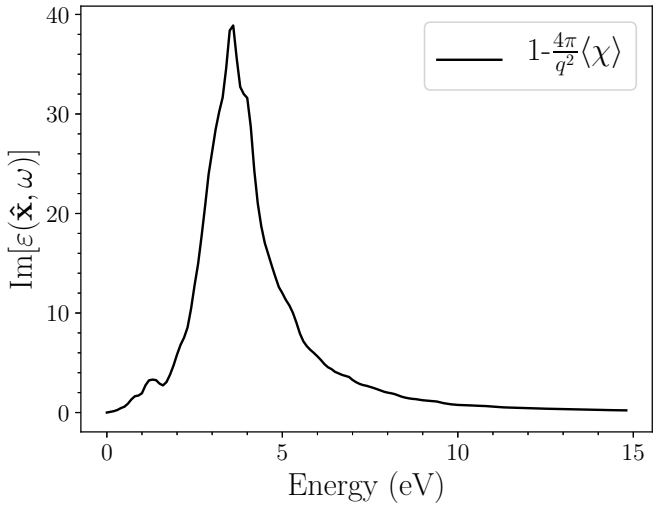

Figure 5.4: In-plane dielectric function calculated with Eq. (5.26) and Eq. (5.27).

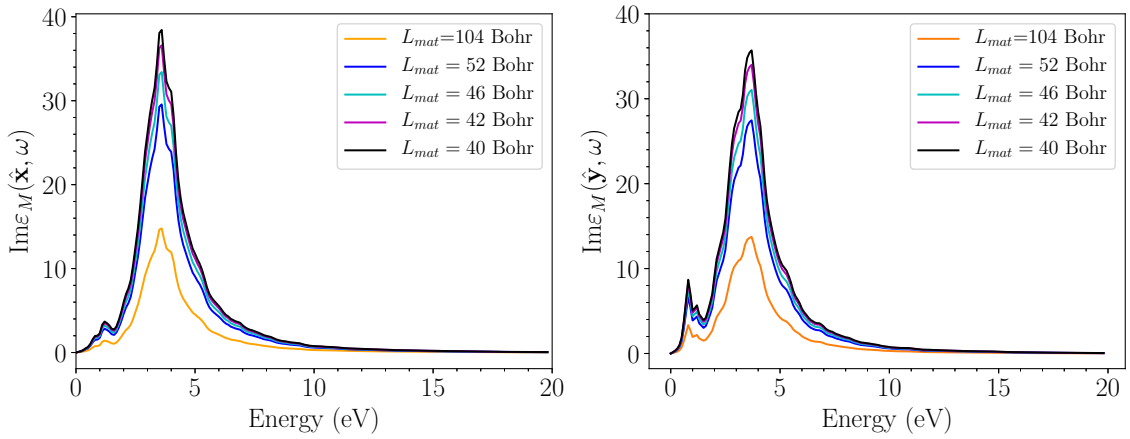

(a) (b)

Figure 5.5: Calculation of the in-plane components of the dielectric function for several integration domains for $\langle\chi\rangle$ (see Eq. (5.26) and (5.27). Panel (a): xx component (orthogonal to the dimer lines). Panel (b): yy component (parallel to the dimer lines)

.

In next chapter, using the Lorentz model, we will explain the physical meaning of this behaviour, and we will demonstrate that the in-plane dielectric function is:

$$\varepsilon_{M,||} = 1 - \frac{4\pi}{|\mathbf{q}|^2}\langle\chi\rangle \tag{5.26}$$

where:

$$\langle\chi\rangle = \frac{1}{L_{mat}}\int_{-L_{supercell}/2}^{L_{supercell}/2} dz \int_{-L_{supercell}/2}^{L_{supercell}/2} dz' \chi(\mathbf{q}_{||}, z, z') \tag{5.27}$$

The spectrum calculated with Eq. (5.26) and Eq. (5.27) is reported in Fig. (5.4). The peak is located at 4 eV, as we expect for the absorption of silicon. Here the response function χ has been averaged over a region of size $L_{mat} = 40$ Bohr, corresponding to the distance between the top-most and the bottom-most atomic plane of the slab. From comparison with Fig. (5.3), we see that the correct amplitude is recovered. In Fig. (5.5), I report several calculation of the in-plane component of the dielectric function, each of them performed averaging the χ over a space region of different length. As we can see in the figure, it results from these mixed space calculations that the interacting response function has one peak at $\omega_0 = 4eV$ for the in-plane component. If I increase the size of the interval $[-L_{mat}/2, L_{mat}/2]$, pushing the integration extrema out of the slab, the absorption peak decreases its amplitude. This is due to the fact that the $\chi(z, z')$ goes rapidly to zero out of the region occupied by atoms (see Fig. (5.6)). Therefore, extending the size of the integration interval outside the atoms, will not change the result of the integral in Eq.

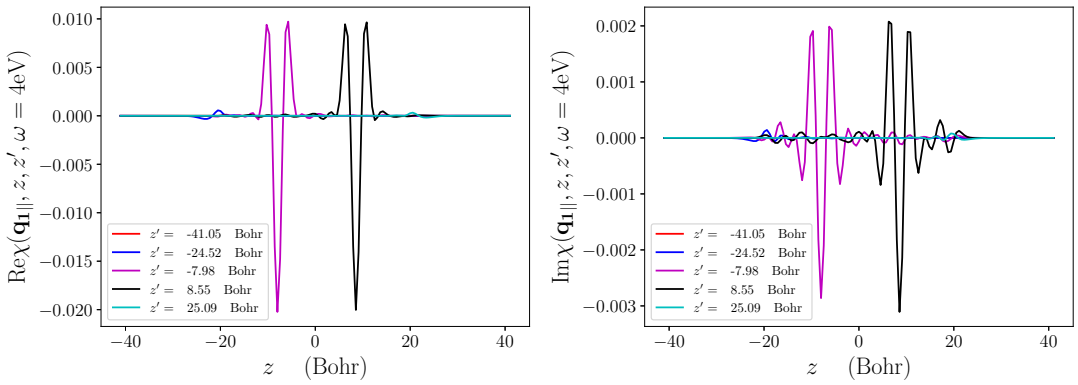

(a)

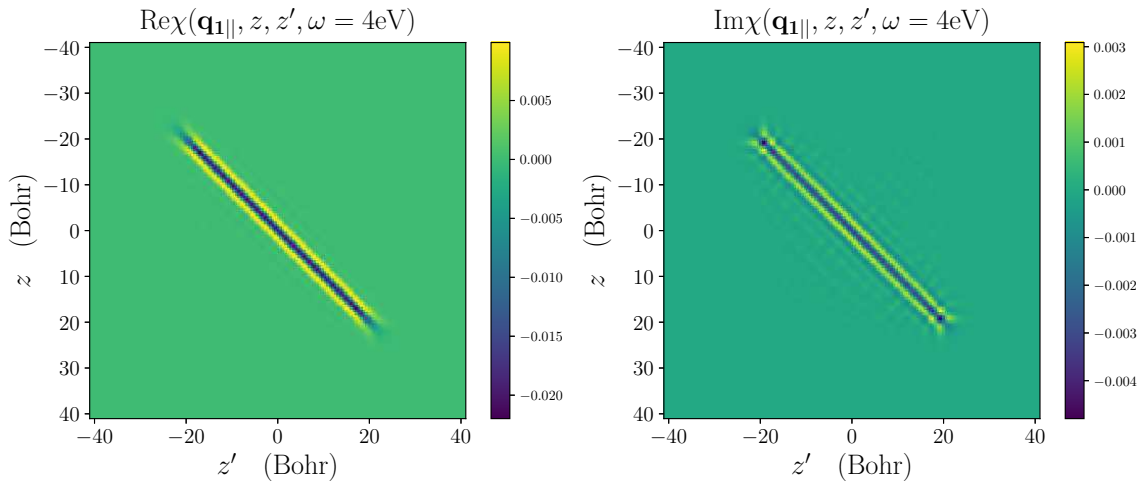

(b)

Figure 5.6: Panel (a): interacting response function $\chi(z, z')$ evaluated as function of z for fixed values of z'. Panel (b): heat map of the $\chi(z, z')$.

(5.27), but will reduce anyway the value of $\langle\chi\rangle$ because of the prefactor $\frac{1}{L_{mat}}$. As I will explain more in detail in the remaining part of this chapter, there is not an evident way to establish the space-region where one should perform the average. However, this may not seem a big problem: after all, the spectra shown in Fig. (5.5) just differ for a scale factor.

5.4 Mixed space: out-of-plane response

In this section I calculate, within the mixed space approach, the response of an isolated slab undergoing an external perturbation orthogonal to its surface. The independent particle response function has been calculated via DP-CODE, in the optical limit ($\mathbf{q} = 10^{-5}\text{Bohr}^{-1}$, with $\mathbf{q} = q\hat{\mathbf{z}}$). Then I proceeded to the calculation of the interacting response function, which has been obtained solving the Discretised Dyson equation (5.18). In Fig. (5.7) we report the macroscopic average of the response function of density, calculated within the mixed space approach for a bare silicon slab:

$$\langle \chi \rangle = \frac{1}{L_{supercell}} \int dz dz' e^{-iq_z z} \chi(z, z') e^{iq_z z'} \tag{5.28}$$

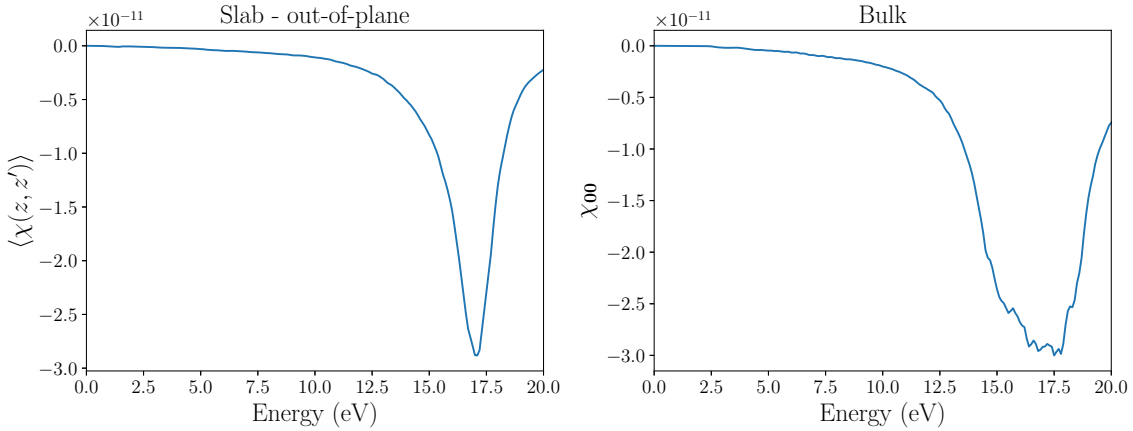

(a) (b)

Figure 5.7: Panel (a): macroscopic average of density response function of the slab, for an out-of-plane perturbation. Panel (b): macroscopic average of density response function of bulk silicon.

As we can see in this figure, the peak of the density response function is located at ~ 17 eV, exactly as it happens for the bulk silicon. This leads us to calculate the dielectric function using a similar procedure as for the bulk:

$$\varepsilon_{M,\perp} = \frac{\langle E_\perp^{ext} \rangle}{\langle E_\perp^{ext} \rangle + \langle E_\perp^{ind} \rangle} = \frac{1}{1 + \frac{\langle E_\perp^{ind} \rangle}{\langle E_\perp^{ext} \rangle}} \tag{5.29}$$

where $\langle E_\perp^{ext} \rangle$ and $\langle E_\perp^{ind} \rangle$ are respectively the macroscopic averages of the external and the induced electric field. The induced field can be derived from the interacting response

function in the following way. Let's suppose that the slab is perturbed by an external field directed orthogonally to the surface, of infinite wavelength, oscillating in time at frequency ω:

$$v^{ext}(z,t) = v^{ext}(z,\omega)e^{i\omega t} \tag{5.30}$$

with:

$$v^{ext}(z,\omega) = z \tag{5.31a}$$

$$E_{\perp}^{ext}(z,\omega) = -\frac{\partial}{\partial z}v^{ext}(z,\omega) = -1 \tag{5.31b}$$

The response function of density allow us to obtain the density variation induced by such an external field:

$$\delta\rho(z,\omega) = \int dz'\chi(z,z',\omega)v^{ext}(z',\omega) \tag{5.32}$$

In Fig. (5.8), I show the profile of the density variation, calculated for the bare silicon slab. As we can see, when a slab is undergoing an external perturbation orthogonal to the surface, the electrons moves in the direction of the external field, determining a charge accumulation of opposite sign on the two surfaces. The density variation is reported in Fig. (5.8). Once we have calculated the density variation, we can use this quantity in order to obtain the induced potential:

$$v^{ind}(z,\omega) = \int dz' v^{coul}(z,z')\delta\rho(z',\omega) \tag{5.33}$$

And, as a consequence, the induced field:

$$E_{\perp}^{ind}(z,\omega) = -\frac{\partial}{\partial z}v^{ind}(z,\omega) \tag{5.34}$$

I report the calculation of the induced field for the bare silicon slab in Fig. (5.9). As we can see the induced field is roughly uniform and constant inside the slab, while is identically zero outside. At this point we have all the ingredient to evaluate the expression (5.29)

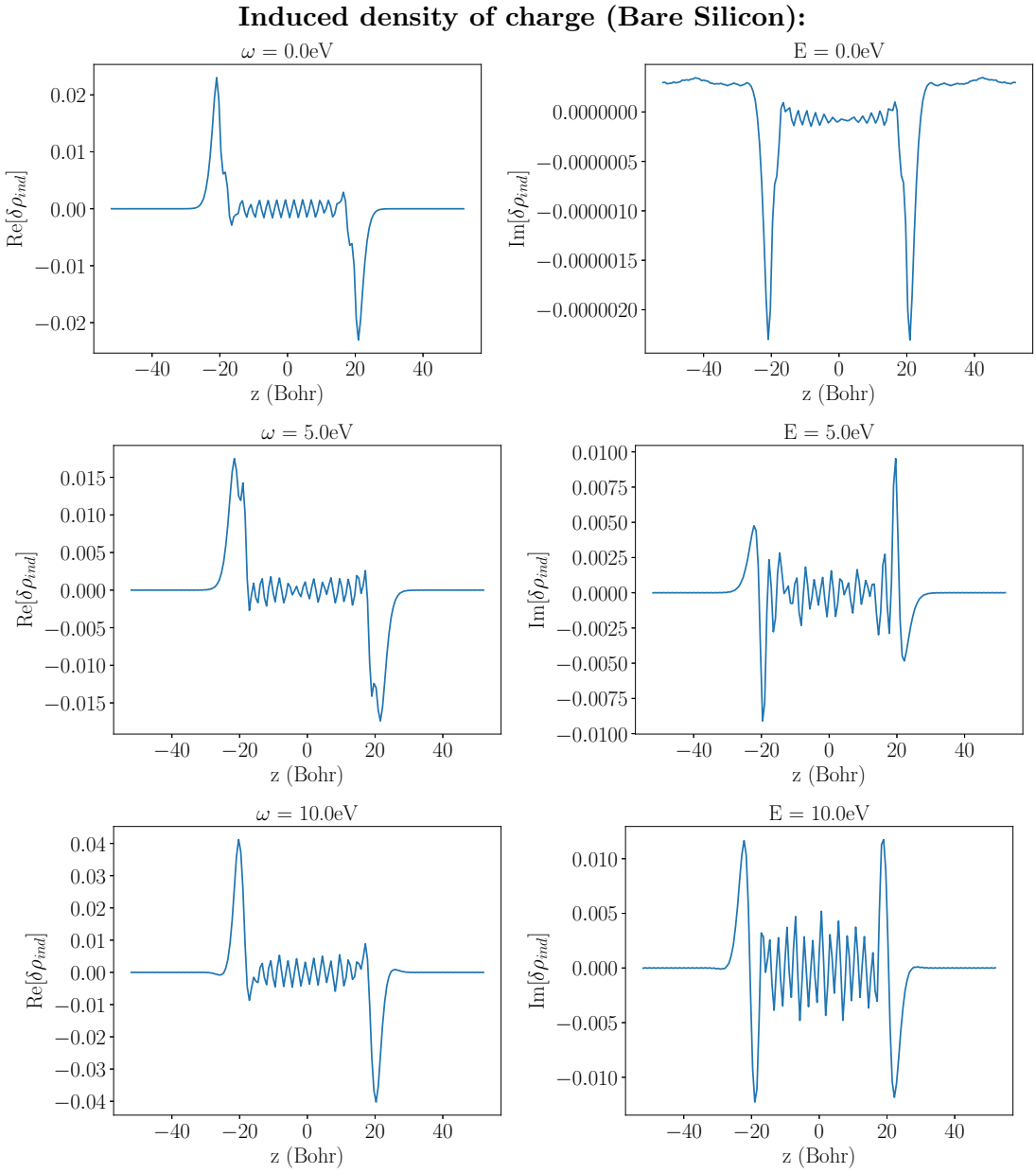

Figure 5.8: Calculation of the variation of density induced in the bare silicon slab by an out-of-plane perturbation of infinite wave-length. Left: real part, right: imaginary part, for different frequencies. First line: static perturbation ($\omega = 0$ eV), second line $\omega = 5$ eV, third line $\omega = 10$ eV

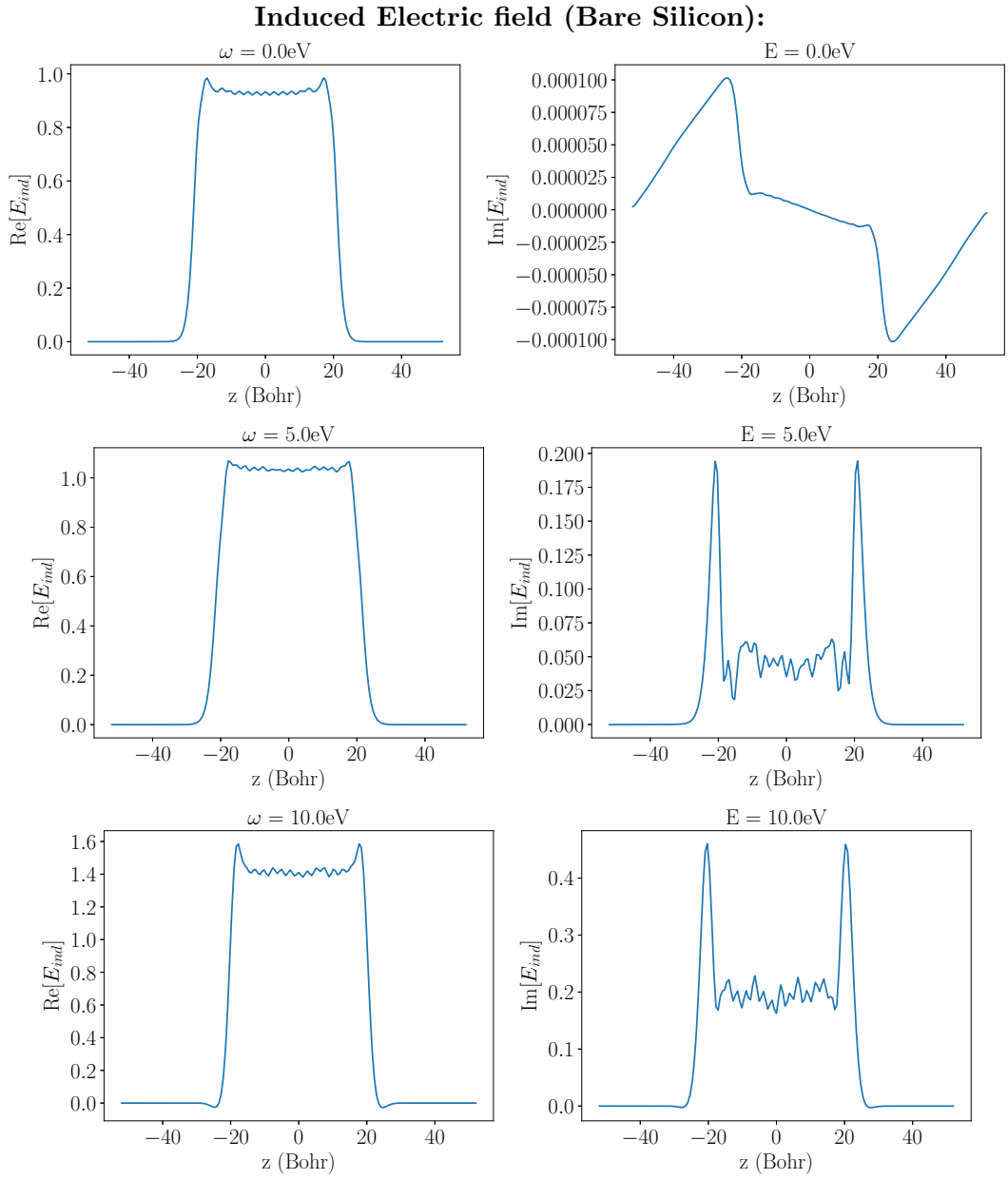

Figure 5.9: Calculation of the electric field induced in a bare silicon slab by a long-wavelength out-of-plane perturbation. Left: real part, right: imaginary part, for different frequencies. First line: static perturbation ($\omega = 0$ eV), second line $\omega = 5$ eV, third line $\omega = 10$ eV

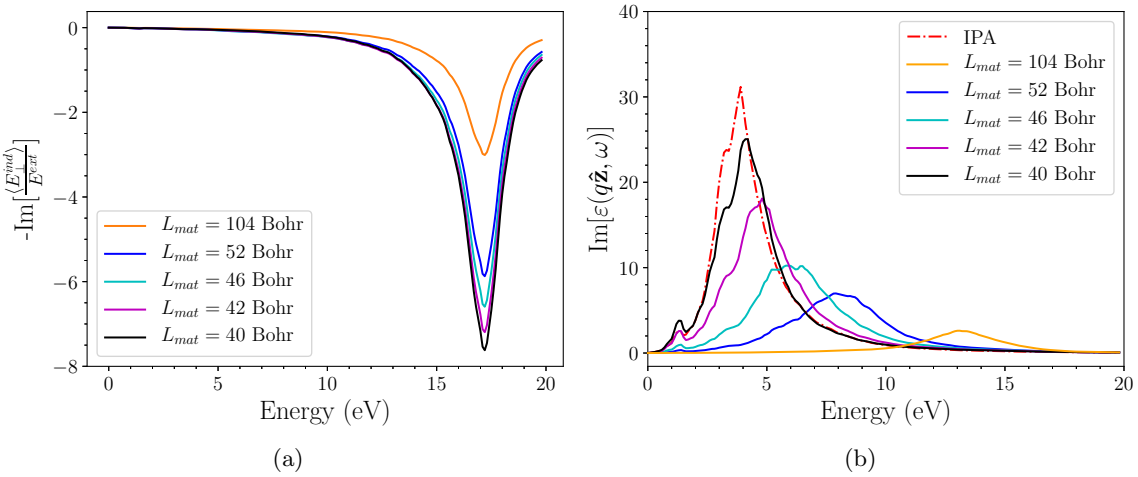

Figure 5.10: Panel (a): average of $E_{\perp}^{ind}$. Panel (b): Calculation of the out-of-plane component of the dielectric function for several integration domains for $E_{\perp}^{ind}$ (see Eq. (5.36)).

5.4.1 The out-of-plane component of ε_M and the L_{mat} problem

In the previous section I have presented the calculation of the induced electric field inside a slab perturbed by an external field orthogonal to the surface. In order to evaluate expression (5.29), and to obtain the dielectric function, we need to calculate the macroscopic average of the external and the induced field. The first quantity is easy to average: the external field is purely macroscopic, and therefore its macroscopic average will be simply a constant:

$$\langle E_{\perp}^{ext} \rangle = -1 \tag{5.35}$$

The second quantity, instead, requires a bit more effort to be worked out. The induced field, in fact, as it's possible to see in Fig. (5.9), it's not uniform in space. In order to obtain its macroscopic average, therefore, one needs to integrate it on a given space region and divide by the size of the integration range:

$$\langle E_{\perp}^{ind} \rangle = \frac{1}{L_{mat}} \int_{-L_{mat}/2}^{L_{mat}/2} dz' E_{\perp}^{ind}(z', \omega) \tag{5.36}$$

As we can see in Eq. (5.36), in order to accomplish the average operation, the interval where the integration is performed has to be established.

If we represent first the denominator of Eq. (5.29) $1 + \frac{\langle E^{ind} \rangle}{\langle E^{ext} \rangle} = 1 + v\chi$ we get that spectra are all located at the frequency of the bulk plasmon (see Fig. (5.10a)), scaled by $L_{mat}/L_{supercell}$, as it results from the EMT with vacuum for $1/\varepsilon_{\perp}$. It results from these mixed space calculations that the interacting response function has one peak at

$\omega_{pl} \sim 17$ eV for the out-of-plane component. In Fig. (5.10b), I report several calculations of the dielectric functions, each of them corresponding to a different choice of the integration interval used to average the induced field. As we can see in Fig. (5.10b), when we take as integration interval the whole supercell (corresponding to taking $L_{mat} = 104$ Bohr, represented in Figure as the orange curve), we obtain the same result already obtained via the standard supercell approach (see Fig.(5.11)), which corresponds to an effective medium theory with vacuum.

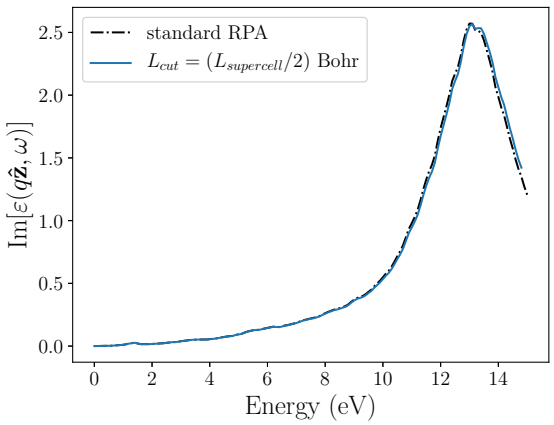

Figure 5.11: Imaginary part of the out-of-plane component of the dielectric function of the bare silicon slab. Violet line: mixed space calculation performed averaging the induced field over the whole simulation box (corresponding to the orange line of Fig. (5.10b)). Black dashed line: standard RPA calculation.

As the size of the integration interval is reduced (see Fig. (5.10b)), the absorption peak increases its amplitude and displaces at lower energies. We see that when we take $L_{mat} = 40$ Bohr, corresponding to choose the integration extremes as the atomic positions of the top most and bottom most layer (represented in Fig. (5.10b) as the black curve) the absorption peak is situated at 4 eV , just like in the bulk silicon spectrum.
Nevertheless, if we can be sure that it is meaningless to integrate up to 104 Bohr, since it is obvious that we are including vacuum, the problem appears to be critical in the region between 52 and 40 Bohr (Fig. (5.10b)). The question which naturally arises is: how to chose the right interval where to integrate the induced field? Quite a natural choice could seem to take the region where

$$\delta\rho(z, \omega) \neq 0 \tag{5.37}$$

Unfortunately one find that the region where the induced density is different than zero (and the induced field as well) is quite larger than the region defined by the coordinates of surface atomic layers (see Fig.s (5.8) and (5.9)). A similar finding has been reported in literature for jellium [52],[53], for graphene [54], and for PbPdO2 [55].More specifically,

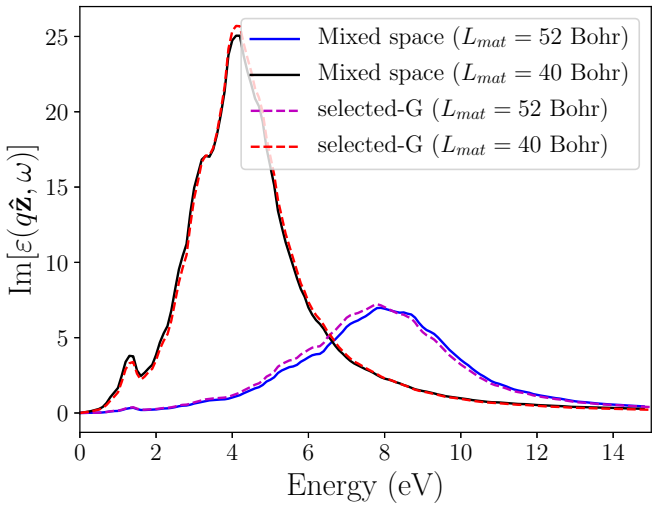

Figure 5.12: In this figure we report the out-of-plane component of the dielectric function calculated within the mixed-space approach (solid lines), and we compare it with the selected-G result (dashed lines). As we can see, if the same value of L_{mat} is chosen, the same result is obtained.

one finds that the density variation is non-zero on a region of around 52 Bohr, while the region defined by the atomic coordinates of surface layers is large around $\sim$ 40 Bohr. When we choose to average the induced field in the region corresponding to a thickness $L_{mat} \sim 52$ Bohr, represented in Fig. (5.10b) as the blue curve, we see that the peak is located at ~ 8 eV. This is what we call "the L_{mat} problem": there is not a clear way to define the slab thickness, and this uncertainty affects in a dramatic way the calculation of the dielectric function, making in practice ambiguous the calculation of the absorption spectrum. We want to underline that this ambiguity is not due to the specific formalism in which the spectrum is calculated, in this case via the mixed space approach, but it is truly intrinsic to the nature of the system. As we have explained in Chapter 4, when we perform a calculation in the selected-G formalism, we implicitly define the thickness of the matter. Until this moment, each time we performed a selected-G calculation, it seemed a natural choice to chose as value of L_{mat} the distance between the most external atomic planes. But if we observe the plot of the density variation along z reported in Fig. (5.8), such a choice is much less evident, since that, as we have discussed, the density variation and the induced field extend over a significantly larger region. In Fig. (5.12), I report a calculation of the dielectric function of the bare silicon slab performed with the selected-G method using $L_{mat} = 52$ Bohr and $L_{mat} = 52$ Bohr (respectively magenta and red dashed lines), and I compare it with the calculation performed within the mixed space approach using the same value of L_{mat} (respectively blue and black solid lines). As we can see, the two

spectra, calculated with two different procedures, overlay almost perfectly, sign that the ambiguity in the definition of L_{mat} is intrinsic in the nature of a slab, and it is not due to the specific way the calculation is carried out. The calculations reported in Fig.(5.12), in other words, show that the mixed space and the selected-G approaches produce the same result, provided that the calculations are performed under the same conditions (i.e. the same choice of L_{mat}), corroborating the validity of the mixed space approach developed in this Chapter.

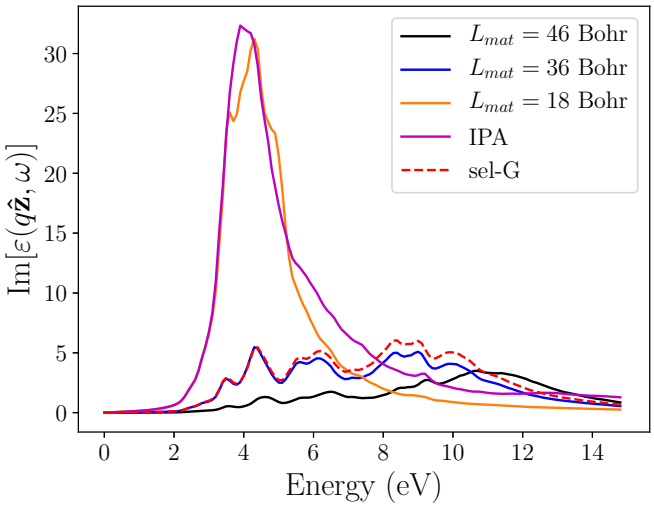

Figure 5.13: In this figure, we report a calculation of the dielectric function of the Si(001)+Thymine slab. Each of these calculations has been performed averaging the induced field over a space region of different size.

In Fig. (5.13) I report the absorption spectra of the silicon slab functionalised with Thymine, each of them performed averaging the induced field over a different region of space. Also in the case of the functionalised slab, as we can see in Fig.s (5.15) and (5.16), the region where the induced density and the induced field go zero and the region delimited by the most external atomic planes have significantly different largeness, being the first one large ~ 46 Bohr and the second one ~ 36 Bohr. In Fig. (5.13), the dielectric function obtained averaging the field on the first region is shown as the black curve, while the spectrum calculated averaging on the second region is shown as the blu curve. In Fig. (5.13) we also report as the red dashed line the calculation of the dielectric function that we have performed within the selected-G formalism (with $L_{mat} \sim 36$ Bohr. As we can see in figure, the blue and the red dashed lines overlay almost perfectly. This is very interesting: in fact, as we have discussed in the chapter 4, the selected-G method allows one to eliminate the spurious effect of vacuum, but does not remove the ficticious periodicity of the system in the z direction. A selected-G calculation, therefore, may a priori still include an interaction between the slab and its replicas. The mixed space approach, instead, as we have explained, make possible to cut this unwanted interaction, allowing one to get the response of a truly isolated slab. One of the reasons that pushed us to develop the mixed space approach, as we have explained in the beginning of the present chapter, was to understand if the suppression of the out-of-plane component of the spectrum observed for the functionalised slab could be attributed to some kind of spurious interaction between the slab and its replicas. The almost perfect agreement between the selected-G and the mixed space calculation allow us to exclude this hypothesis. Actually, one key to understand this effect is given by Fig. (5.9): the induced field is zero outside the matter, and no interaction between replicas should occur for an external excitation orthogonal to the slab. This will be also clarified in the next chapter. Moreover, in Fig. (5.13), we notice another interesting fact. If the dielectric function is calculated averaging the induced field just in the region delimited by the silicon atoms (see the blue dashed lines in Fig.s (5.15) and (5.16)), corresponding to

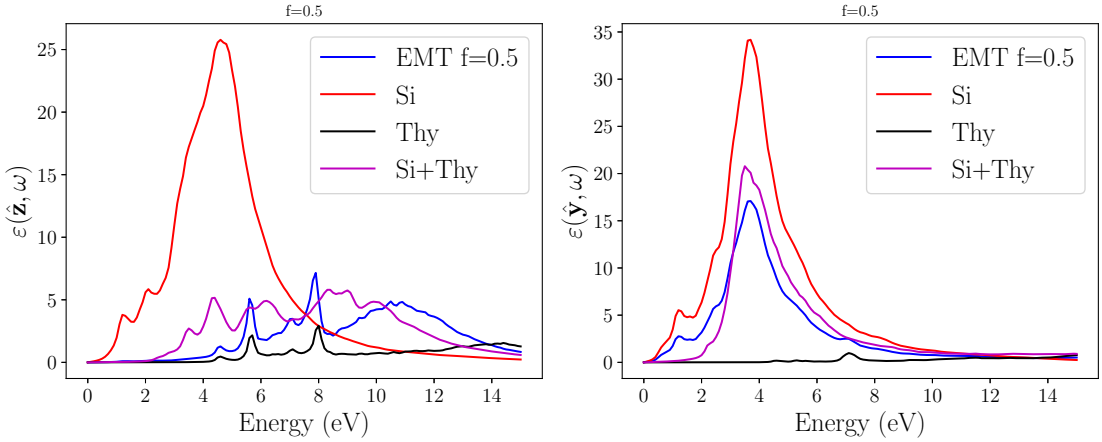

Figure 5.14: Effective medium theory between silicon and thymine (50% each)(blue line). Panel (a): out-of-plane component, panel (b): in-plane component (parallel to molecule rows).

a thickness of ~ 18 Bohr, so the absorption peak is located at ~ 4 eV (see the orange curve in Fig. (5.13)), just as in the case of the bare slab. The spectrum of the functionalised slab appears to be suppressed compared to the spectrum of the bare one. Actually it can be seen as a sort of effective medium theory between the adsorbed layer and the silicon substrate (as it can be shown in Fig. (5.14)). Since the spectrum of free molecules (black line) has small amplitude compared to the spectrum of bare silicon (red line), and peaks located at higher energies, so the macroscopic dielectric function of the functionalised slab (magenta line) - being an average between the spectrum of the silicon and the spectrum of molecules - will be strongly reduced in amplitude and spread over a much larger range of energies compared to the bare silicon.

Induced density of charge (Silicon+Thymine):

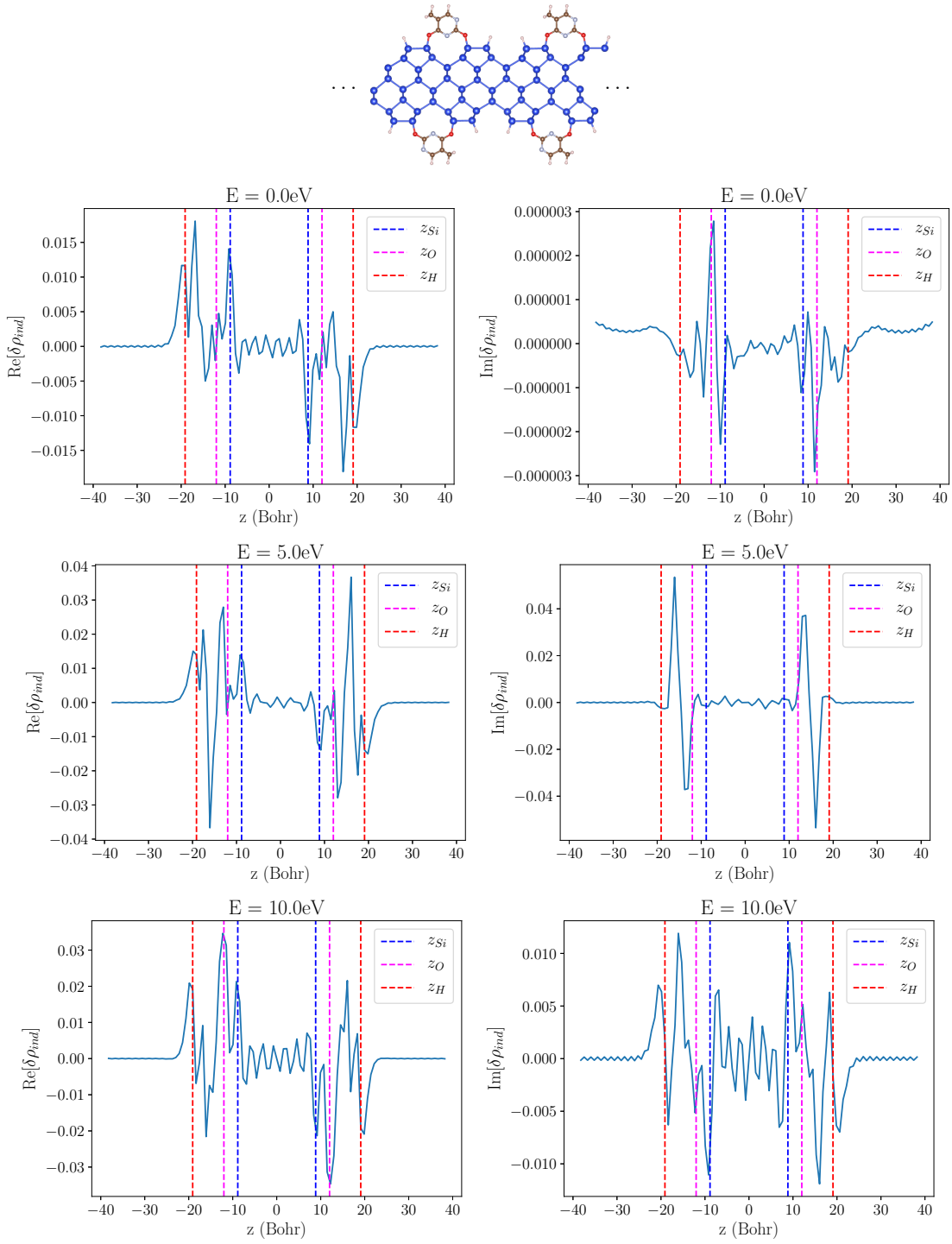

Figure 5.15: Density variation induced in the Si(001)+Thymine slab by an out-of-plane perturbation of infinite wave-length.

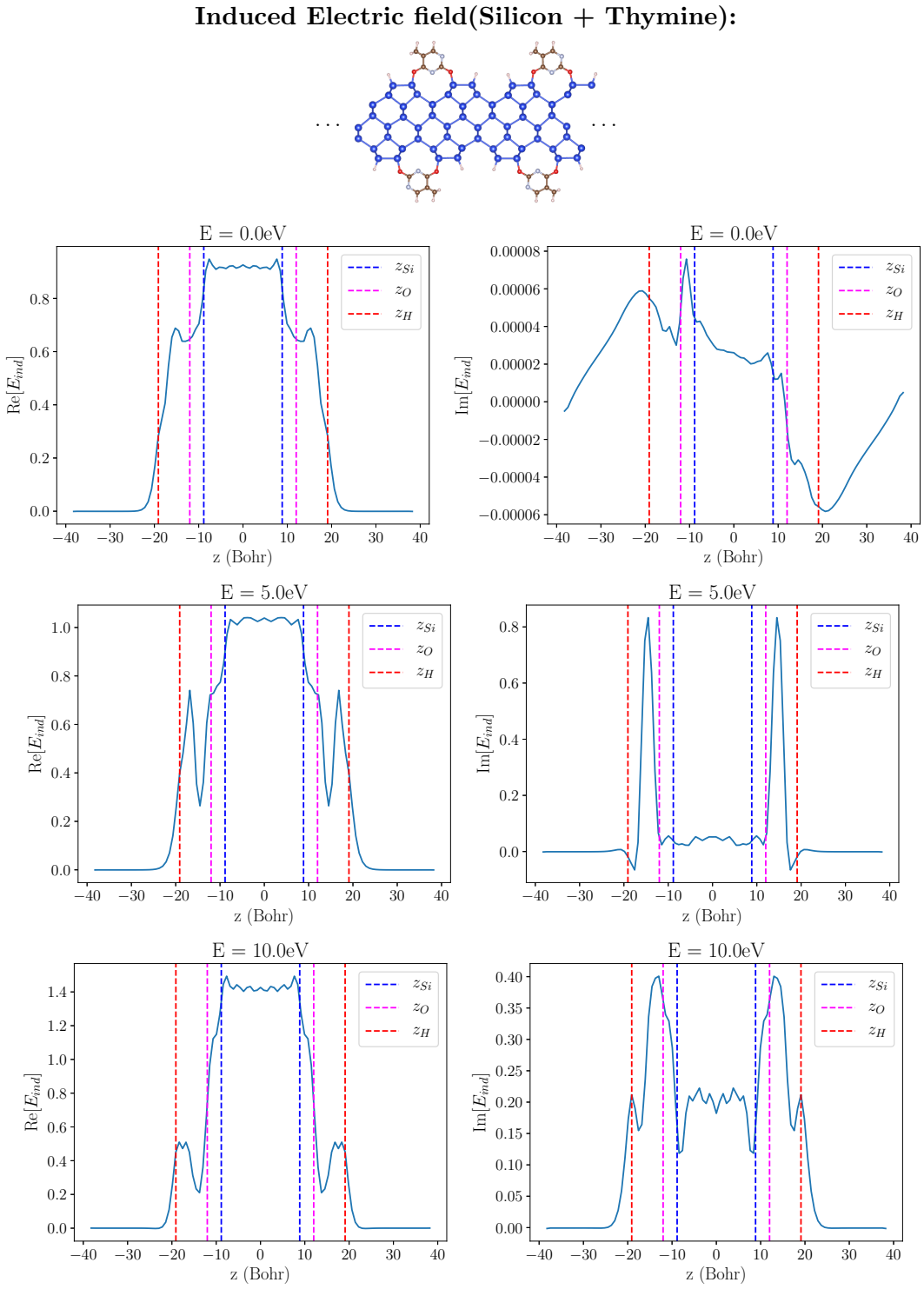

Figure 5.16: Electric field induced in the Si(001)+Thymine slab by an out-of-plane perturbation of infinite wave-length.

5.5 Conclusion

During this chapter, I developed a mixed space formalism, which allowed us to calculate, in a fully *ab initio* way, the response of an isolated slab. From the response function of density of the slab, we then obtained the absorption spectra for the isolated bare silicon slab and the functionalised slab. In particular, we have found that the out-of-plane component of the absorption spectrum calculated via the mixed space approach, is in perfect agreement with the selected-G calculation. This result allowed us to exclude that the quenching in the absorption spectrum of the functionalised slab is an effect due to the fictitious interaction between the replicas of the slab. It also demonstrates that there is no interaction for a perturbation orthogonal to the slab. As we explained, the quenching of the spectrum is due to the fact, that when one calculates the macroscopic dielectric function of a slab with an adsorbed overlayer, the result of the macroscopic average operation is similar to an effective medium theory between the substrate and the adsorbate. With reference to the system we are focussed on, since the Thymine spectrum has peaks much higher in energy and much less intense than silicon, it is normal that the dielectric function will have properties in the middle between the two systems. By the way, even if we can accept that the dielectric function of a functionalised slab is quenched because of the average between the properties of the adsorbed layer and the substrate (and this is specially true for the slab that we have studied, where the thickness of the substrate and the thickness of the adsorbed layer are almost equivalent) a new problem arises: how to define the thickness of the slab? Even slight differences in the choice of the L_{mat} parameter lead to significant differences in the macroscopic dielectric function. If the mechanism is similar to the one described in Chapter 4 (effective medium theory with vacuum), here the problem refers to the thickness of the matter (should it be defined at the extension of atomic positions or to the distance where the response functions go to zero?). To cure the ambiguity that affect the definition of L_{mat} and of the dielectric function will be the second main task of next two chapters.

Chapter 6

Response of a (thin) isolated slab: the Lorentz model

In the previous chapter, we calculated the response of an isolated slab to an external longitudinal perturbation using the mixed space approach. In the present chapter I will approach the same problem within a simple Lorentz oscillators model. In this model, the electrons inside the material will be depicted as classical oscillators, bond to the nuclei by an elastic force of frequency ω_0. When the material is perturbed by an exernal electric field, the electrons start to oscillate around their equilibrium positions, giving rise to an induced electric field. The equation of motions for the electrons, within such model, can be exactly solved (or, in some cases, they become solvable at the price of just some meaningful approximation), allowing us to extract the quantities which characterise the response of the material, and to give a more significant interpretation to the result of the *ab initio* calculations presented in Chapter 5. The chapter is organised in the following way: in section 1, I will start with deriving the response properties of a bulk material. Even if this result is already well known, it will be useful to present the derivation in order to make comparison with the 2D case. In section 2 I will derive the response of a slab to a longitudinal perturbation directed in the in-plane direction, while in section 3 I will study the case of out-of-plane perturbation. Finally, I will present the conclusion in section 4.

6.1 Response of the infinite system

Let's suppose to have a material, infinitely extended in the space, which is constituted of n_e oscillators per unit of volume. Each of these oscillators will have electric charge e, mass m_e, and frequency ω_0. We want to study the response of such a system to an external longitudinal perturbation of the form:

$$\mathbf{E}^{ext}(\mathbf{r},t) = \mathbf{E}_0^{ext} e^{i\mathbf{q}\cdot\mathbf{r}-i\omega t} \tag{6.1}$$

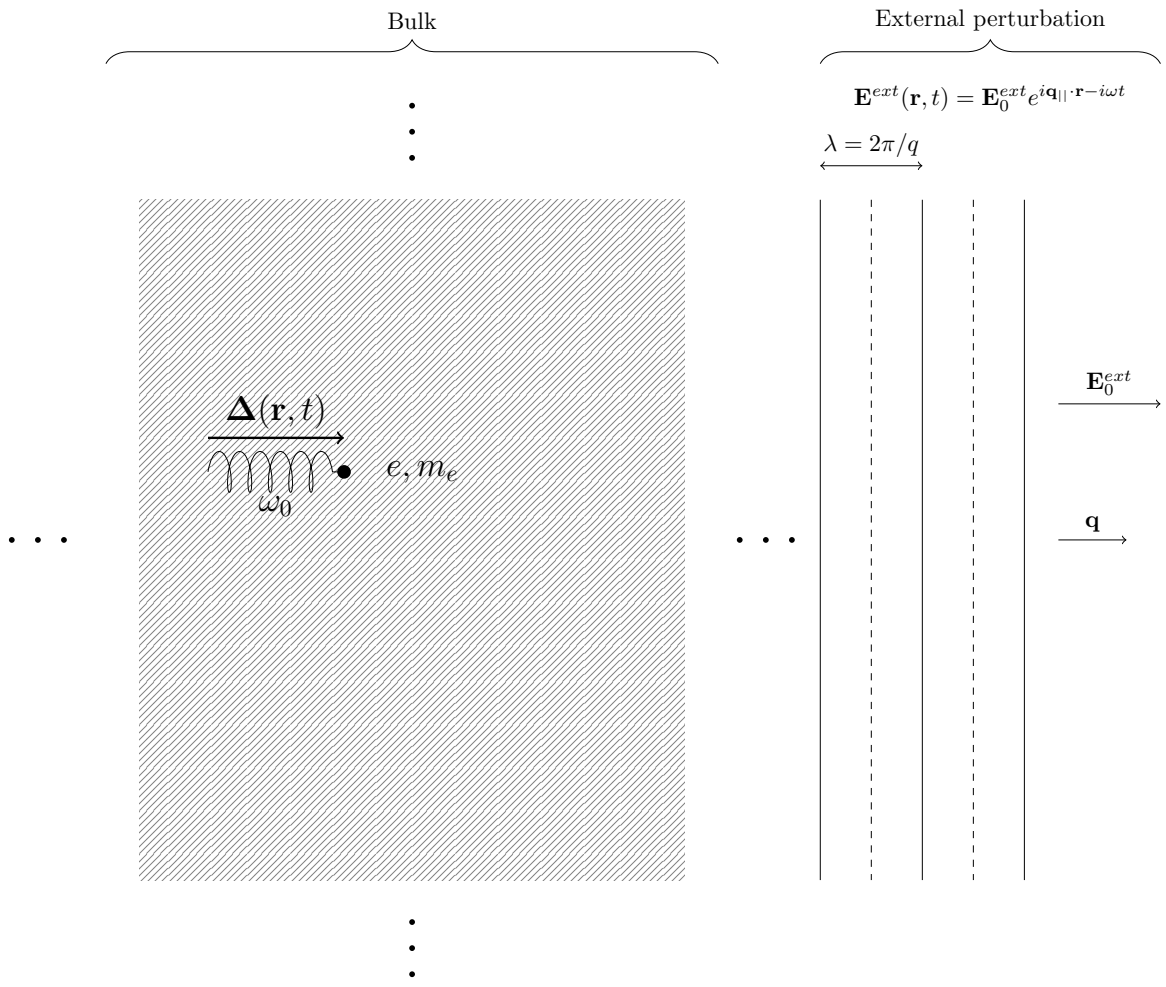

Figure 6.1: Sketch of the Lorentz model to study the response of an infinite system of interacting electrons to an external longitudinal perturbation of wave-vector $\mathbf{q}$ and frequency ω. Electrons are depicted as classical oscillators having each of them characteristic frequency ω_0, mass m_e, and charge e.

with $\mathbf{E}_0^{ext}||\mathbf{q}$ (as shown in Fig. (6.1)). The displacement of oscillators from their equilibrium position will be described via the vector field $\mathbf{\Delta}(\mathbf{r},t)$, which gives the displacement from the equilibrium position of the oscillator located in $\mathbf{r}$ at time t. Each oscillator, will feel an harmonic force $-m_e\omega_0^2\Delta$, a dampening force $-(m_e/\tau)\dot{\Delta}$, and the electrostatic force given by the external perturbation $e\mathbf{E}^{ext}$. Moreover, since the oscillator are charged, when moving they will produce an induced electric field $\mathbf{E}^{ind}$. The oscillator will feel this induced field as well, and therefore the equation of motion of the oscillators could be written:

$$m_e\ddot{\mathbf{\Delta}}(\mathbf{r},t) = -m_e\omega_0^2\mathbf{\Delta}(\mathbf{r},t) - \frac{m_e}{\tau}\dot{\mathbf{\Delta}}(\mathbf{r},t) + e\mathbf{E}^{ext}(\mathbf{r},t) + e\mathbf{E}^{ind}(\mathbf{r},t) \tag{6.2}$$

to solve this equation, we need to establish a relation between the induced field $\mathbf{E}^{ind}$ and the vector field $\mathbf{\Delta}(\mathbf{r},t)$. In order to do that, we remark that the density of polarization $\mathbf{P}(\mathbf{r},t)$ inside the material can be easily expressed as function of $\mathbf{\Delta}(\mathbf{r},t)$. Each oscillator in the material, indeed, can be seen as an oscillating dipole:

$$\mathbf{d}(\mathbf{r},t) = e\mathbf{\Delta}(\mathbf{r},t) \tag{6.3}$$

The density of polarization inside the material could be therefore expressed as:

$$\mathbf{P}(\mathbf{r},t) = n_e e\mathbf{\Delta}(\mathbf{r},t) \tag{6.4}$$

Moreover, we know that the induced density of charge can be extracted from the following relationship:

$$\nabla\cdot\mathbf{P}(\mathbf{r},t) = -\rho^{ind}(\mathbf{r},t) \tag{6.5}$$

Combining the latter equality with the Maxwell-Gauss equation

$$\nabla\cdot\mathbf{E}^{ind}(\mathbf{r},t) = 4\pi\rho^{ind}(\mathbf{r},t) \tag{6.6}$$

we got:

$$\nabla\cdot\mathbf{E}^{ind}(\mathbf{r},t) = (-)4\pi\nabla\cdot\mathbf{P}(\mathbf{r},t) \tag{6.7}$$

and therefore:

$$\mathbf{E}^{ind}(\mathbf{r},t) = (-)4\pi\mathbf{P}(\mathbf{r},t) = (-)4\pi n_e e\mathbf{\Delta}(\mathbf{r},t) \tag{6.8}$$

We finally expressed the induced electric field as a function of the displacement of oscillators from their equilibrium position, and the motion equation of the system could be rewritten as:

$$m_e\ddot{\mathbf{\Delta}}(\mathbf{r},t) = -m_e\omega_0^2\mathbf{\Delta}(\mathbf{r},t) - \frac{m_e}{\tau}\dot{\mathbf{\Delta}}(\mathbf{r},t) + e\mathbf{E}^{ext}(\mathbf{r},t) - m_e\omega_{pl}^2\mathbf{\Delta}(\mathbf{r},t) \tag{6.9}$$

where we used $\omega_{pl}^2 = (4\pi n_e e^2/m_e)$. In order to find a solution of the motion equation, let's make a guess on the functional form of $\Delta(\mathbf{r},t)$:

$$\mathbf{\Delta}(\mathbf{r},t) = \mathbf{\Delta_0}e^{i\mathbf{q}\cdot\mathbf{r}-i\omega t} \tag{6.10}$$

We find that the expression in Eq. (6.10) is a solution of Eq. (6.9) if, and only if:

$$\mathbf{\Delta}_0 = \frac{e}{m_e}\frac{1}{-\omega^2+\omega_0^2-i\frac{\omega}{\tau}+\omega_{pl}^2}\mathbf{E}_0^{ext} \tag{6.11}$$

This relation, which express the displacement of oscillators as a function of the external electric field, is strictly linked to the response function of density, which gives the density variation as a function of the external potential. Expressing the induced density as a function of $\mathbf{\Delta}(\mathbf{r},t)$, and using Eq. (6.11), we obtain:

$$\rho^{ind}(\mathbf{r},t) = (-)i|\mathbf{q}|n_e\frac{e^2}{m_e}\frac{1}{-\omega^2+\omega_0^2-i\frac{\omega}{\tau}+\omega_{pl}^2}\mathbf{E}^{ext}(\mathbf{r},t) \tag{6.12}$$

and expressing the external field $\mathbf{E}^{ext}(\mathbf{r},t)$ as a function of the external potential ($\mathbf{E}^{ext}(\mathbf{r},t) = -\nabla\phi^{ext}(\mathbf{r},t)$) we have:

$$\rho^{ind}(\mathbf{r},t) = \frac{|\mathbf{q}|^2}{4\pi}\frac{\omega_{pl}^2}{\omega^2-\omega_0^2+i\frac{\omega}{\tau}-\omega_{pl}^2}\phi^{ext}(\mathbf{r},t) \tag{6.13}$$

leading therefore to:

$$\chi_{\rho\rho} = \frac{|\mathbf{q}|^2}{4\pi}\frac{\omega_{pl}^2}{\omega^2-\omega_0^2+i\frac{\omega}{\tau}-\omega_{pl}^2} \tag{6.14}$$

As we can see this function (reported in Fig. (6.2a)) presents a peak at $\approx \sqrt{\omega_0^2+\omega_{pl}^2}$: this resonance correspond to a collective excitation of the system, called plasmon.
As a consequence, we will obtain that the solution of the motion equation is given by:

$$\mathbf{\Delta}(\mathbf{r},t) = \frac{e}{m_e}\frac{1}{-\omega^2+\omega_0^2-i\frac{\omega}{\tau}+\omega_{pl}^2}\mathbf{E}^{ext}(\mathbf{r},t) \tag{6.15}$$

Recasting this solution as a function of the total field, we obtain:

$$\mathbf{\Delta}(\mathbf{r},t) = \frac{e}{m_e}\frac{1}{-\omega^2+\omega_0^2-i\frac{\omega}{\tau}}\mathbf{E}^{tot}(\mathbf{r},t) \tag{6.16}$$

which allows us to express the density of current as :

$$\begin{aligned}\mathbf{J}(\mathbf{r},t) &= \frac{e}{m_e}\frac{-ien_e\omega}{-\omega^2+\omega_0^2-i\frac{\omega}{\tau}}\mathbf{E}^{tot}(\mathbf{r},t)\\ &= \frac{1}{4\pi}\frac{i\omega\omega_{pl}^2}{\omega^2-\omega_0^2+i\frac{\omega}{\tau}}\mathbf{E}^{tot}(\mathbf{r},t)\end{aligned} \tag{6.17}$$

So we can extract the following expression for the conductivity:

$$\sigma(\omega) = \frac{1}{4\pi}\frac{i\omega\omega_{pl}^2}{\omega^2-\omega_0^2+i\frac{\omega}{\tau}} \tag{6.18}$$

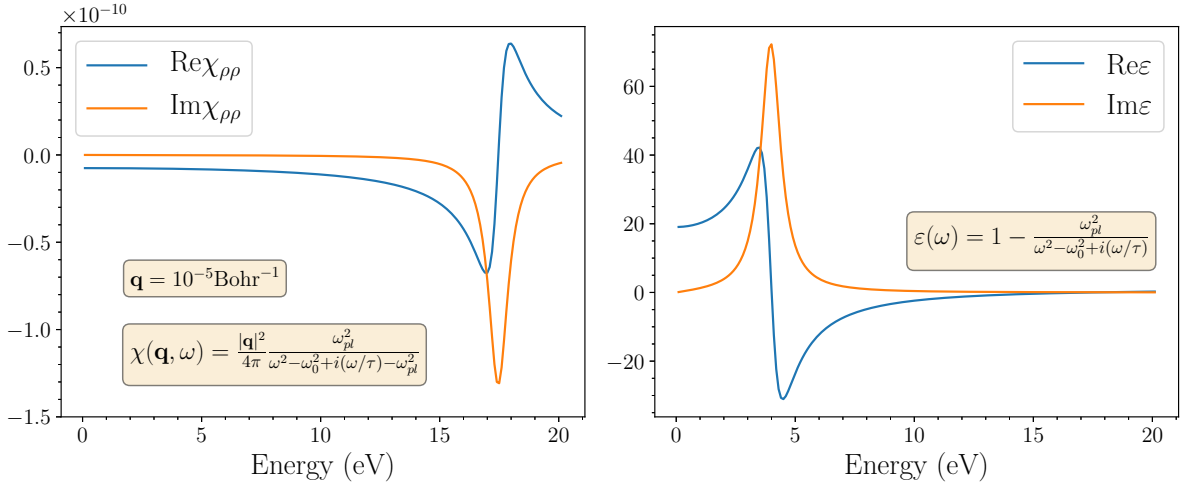

(a) (b)

Figure 6.2: Response of the infinite system to an external perturbation. In panel (a) the response function of the density is shown. In panel (b), the dielectric function is reported. Here we have chosen as parameters $\omega_0 = 4$ eV , $\omega_{pl} = 17$ eV, $\tau = 10$ eV^{-1}. The perturbation wavevector has been set to $\mathbf{q} = 10^{-5}$Bohr^{-1}, corresponding to the perturbation wavelength which we adopted in our *ab initio* calculations.

from the conductivity, it is trivial to extract the dielectric function, via the well known expression $\varepsilon(\omega) = 1 + \frac{4\pi i\sigma(\omega)}{\omega}$:

$$\varepsilon(\omega) = 1 - \frac{\omega_{pl}^2}{\omega^2 - \omega_0^2 + i\frac{\omega}{\tau}} \tag{6.19}$$

As we can see, we recover the well known Drude-Lorentz dielectric function, which is resonant at ω_0, and verify the plasmon condition at ω_{pl}. This function is plotted in Fig. (6.2b).

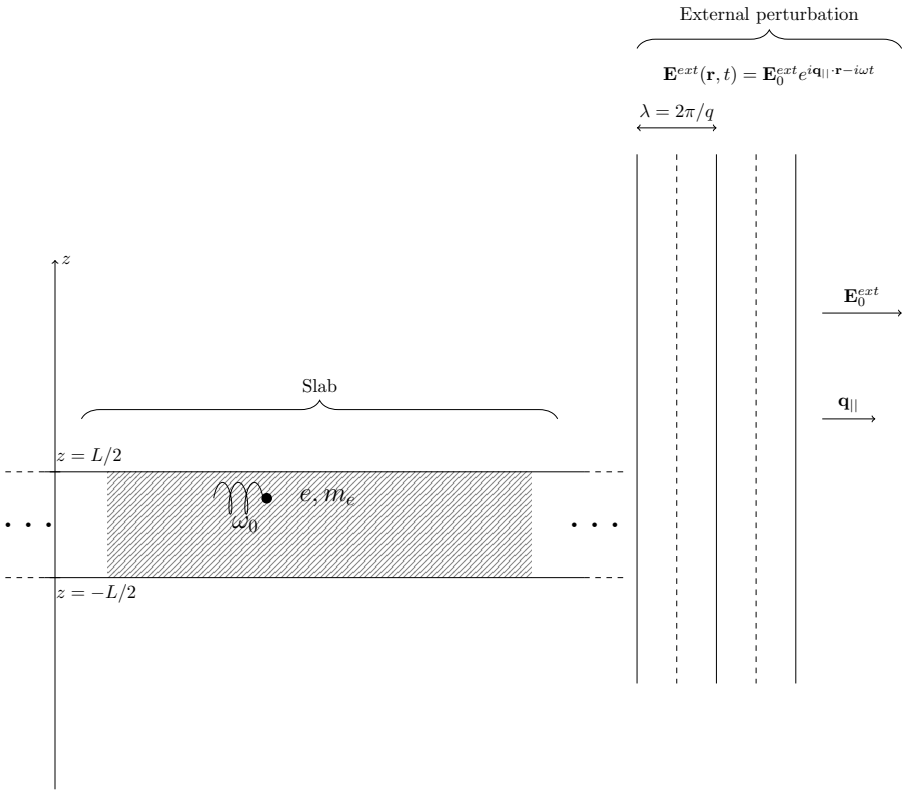

Figure 6.3: Sketch of a slab undergoing an external longitudinal perturbation of wave-vector $\mathbf{q}$ and frequency ω, with the electric field parallel to the surface of the slab (i.e. in-plane perturbation).

6.2 Response of the slab - in-plane perturbation

Let's now consider the system sketched in Fig. (6.3), which is always made of n_e oscillators per unit of volume, but, instead to be infinite in all directions, it has been cut in form of slab of thickness L with the interfacial planes lay in correspondence of the planes $z = \pm\frac{L}{2}$. We want to calculate the response of this system to an external, longitudinal perturbation of the form:

$$\mathbf{E}^{ext} = \mathbf{E}_0 e^{i\mathbf{q}_{||}\cdot\mathbf{r} - i\omega t} \tag{6.20}$$

with $\mathbf{q}_{||} \propto \hat{\mathbf{x}}$ (see Fig. (6.3)).
Also in this case, the displacement of oscillators from their equilibrium position can be described via a vector field $\mathbf{\Delta}(\mathbf{r},t)$, and the equation of motion of our system will be written as:

$$m_e \ddot{\mathbf{\Delta}}(\mathbf{r},t) = -m_e\omega_0^2 \mathbf{\Delta}(\mathbf{r},t) - \frac{m_e}{\tau}\dot{\mathbf{\Delta}}(\mathbf{r},t) + e\mathbf{E}^{ext}(\mathbf{r},t) + e\mathbf{E}^{ind}(\mathbf{r},t) \tag{6.21}$$

Again, we have to find a relationship between the induced electric field $\mathbf{E}^{ind}(\mathbf{r},t)$ and the displacement of the oscillators $\mathbf{\Delta}(\mathbf{r},t)$. The polarisation density will be given by:

$$\mathbf{P}(\mathbf{r},t) = n_e e \mathbf{\Delta}(\mathbf{r},t) \tag{6.22}$$

and the induced density will be defined as:

$$\rho^{ind}(\mathbf{r},t) = -\nabla \cdot \mathbf{P}(\mathbf{r},t) \tag{6.23}$$

The induced electrostatic potential can be deduced from the induced density of charge

$$\phi^{ind}(\mathbf{r},t) = \int d\mathbf{r}' v_{coul}(\mathbf{r},\mathbf{r}')\rho^{ind}(\mathbf{r}',t) \tag{6.24}$$

and from the induced electrostatic potential we can deduce the induced electric field:

$$\mathbf{E}^{ind}(\mathbf{r},t) = -\nabla\phi^{ind}(\mathbf{r},t) \tag{6.25}$$

In order to make some progress, we have to do some assumption on the form of the displacement field $\mathbf{\Delta}$. In order to evaluate the form of the induced field, we still do the guess that the displacement of oscillators is proportional to the external field and confined in the slab. We will verify a posteriori that it is also a solution of the equation of motion. Let's assume that $\mathbf{\Delta}(\mathbf{r},t)$ has the following form:

$$\mathbf{\Delta}(\mathbf{r},t) = \Theta(z+\frac{L}{2})\Theta(-z+\frac{L}{2})\mathbf{\Delta}_0 e^{i\mathbf{q}_{||}\cdot\mathbf{r}-i\omega t} \tag{6.26}$$

with $\mathbf{\Delta}_0 || \mathbf{q}_{||}$. As a consequence, we can write the polarization as:

$$\mathbf{P}(\mathbf{r},t) = en_e\Theta(z+\frac{L}{2})\Theta(-z+\frac{L}{2})\mathbf{\Delta}_0 e^{i\mathbf{q}_{||}\cdot\mathbf{r}-i\omega t} \tag{6.27}$$

and the induced density of charge as:

$$\begin{aligned}\rho^{ind}(\mathbf{r},t) &= -\nabla\cdot\mathbf{P}(\mathbf{r},t) \\ &= -iq_{||}en_e\Theta(z+\frac{L}{2})\Theta(-z+\frac{L}{2})\mathbf{\Delta}_0 e^{i\mathbf{q}_{||}\cdot\mathbf{r}-i\omega t}\end{aligned} \tag{6.28}$$

After tedious algebra (see App B) we find the following expression for the induced potential:

$$\phi^{ind}(\mathbf{r},t) = \frac{2\pi}{|q_{||}|}(-)ien_e q_{||}\Delta_0 e^{iq_{||}r_{||}-i\omega t}\times$$

$$\times \begin{cases} \dfrac{2}{|q_{||}|}e^{-|q_{||}|z}\sinh(|q_{||}|L/2) & \text{for} \quad z > L/2 \\ \dfrac{1}{|q_{||}|}\left[2 - 2e^{-|q_{||}|\frac{L}{2}}\cosh(|q_{||}|z)\right] & \text{for} -L/2 < z < L/2 \\ \dfrac{2}{|q_{||}|}e^{|q_{||}|z}\sinh(|q_{||}|L/2) & \text{for} \quad z < -L/2 \end{cases} \tag{6.29}$$

For sake of clarity, we define the function $F(z)$ (see Fig. (6.4)):

$$F(z) = \begin{cases} e^{-|q_{||}|z}\sinh(|q_{||}|L/2) & \text{for} \quad z > L/2 \\ \left[1 - e^{-|q_{||}|\frac{L}{2}}\cosh(|q_{||}|z)\right] & \text{for} -L/2 < z < L/2 \\ e^{|q_{||}|z}\sinh(|q_{||}|L/2) & \text{for} \quad z < -L/2 \end{cases} \tag{6.30}$$

so that the induced potential can be easily rewritten as:

$$\phi^{ind} = \frac{4\pi}{|q_{||}|^2}(-)ien_e q_{||}F(z)\Delta_0 e^{iq_{||}r_{||}-i\omega t} \tag{6.31}$$

The in-plane component of the induced electric field, therefore, will be given by:

$$\begin{aligned} E_x^{ind}(\mathbf{r},t) &= -\frac{\partial}{\partial x}\phi^{ind}(\mathbf{r},t) \\ &= (-)4\pi en_e\Delta_0 e^{iq_{||}r_{||}-i\omega t}\times \end{aligned}$$

$$\times \begin{cases} e^{-|q_{||}|z}\sinh(|q_{||}|L/2) & \text{for} \quad z > L/2 \\ \left[1 - e^{-|q_{||}|\frac{L}{2}}\cosh(|q_{||}|z)\right] & \text{for} -L/2 < z < L/2 \\ e^{|q_{||}|z}\sinh(|q_{||}|L/2) & \text{for} \quad z < -L/2 \end{cases} \tag{6.32}$$

and the component of the induced electric field orthogonal to the surface:

$$\begin{aligned} E_z^{ind}(\mathbf{r},t) &= -\frac{\partial}{\partial z}\phi^{ind}(\mathbf{r},t) \\ &= (-)^2\frac{1}{|q_{||}|}4\pi i n_e e\left(\frac{\partial}{\partial z}F(z)\right)\Delta_0 e^{iq_{||}r_{||}-i\omega t} \\ &= (-)^2 4\pi i n_e e\Delta_0 e^{iq_{||}r_{||}-i\omega t}\times \\ &\times\begin{cases} -e^{-|q_{||}|z}\sinh(|q_{||}|L/2) & \text{for} \quad z > L/2 \\ -e^{-|q_{||}|\frac{L}{2}}\sinh(|q_{||}|z) & \text{for} -L/2 < z < L/2 \\ e^{|q_{||}|z}\sinh(|q_{||}|L/2) & \text{for} \quad z < -L/2 \end{cases} \end{aligned} \tag{6.33}$$

6.2.1 Induced electric field: differences between bulk and slab

Let's now try to understand the differences between the induced electric field arising from the perturbation of the slab and the one generated from the perturbation of the bulk. We recall that the expression of the induced electric field induced inside of a bulk material is given by:

$$\mathbf{E}^{ind}(\mathbf{r},t) = (-)4\pi n_e e\boldsymbol{\Delta}_0 e^{i\mathbf{q}\cdot\mathbf{r}-i\omega t} \qquad \text{(Bulk)} \tag{6.34}$$

which shows that for a bulk subjected to a longitudinal perturbation of wave vector $\mathbf{q}$, the induced electric field is entirely directed along $\mathbf{q}$: on the contrary, in a slab, even subject to a longitudinal perturbation parallel to the surface, the presence of the interfaces leads to an induced electric field orthogonal to the surface.
Let's now try to understand something more on the differences between the *intensity* of the induced electric field in the case of a slab and in the case of the bulk. Let's put ourselves in the middle of the slab (i.e. in the plane $z = 0$), and let's see how strong is the x component of the induced electric field:

$$E_x^{ind}(\mathbf{r},t)\Big|_{z=0} = (-)4\pi n_e e\Delta_0 e^{i\mathbf{q}_{||}\cdot\mathbf{r}-i\omega t}\times\left(1-e^{-|q_{||}|\frac{L}{2}}\right) \qquad \text{(Slab)} \tag{6.35}$$

It is particularly interesting to study the behaviour of the latter expression in two limits:

1. $|q_{||}|\frac{L}{2} \gg 1$ (i.e. , the limit where **the thickness of the slab is much greater than the perturbation wave length**). In this limit, we have $\left(1-e^{-|q_{||}|\frac{L}{2}}\right) \longrightarrow 1$, and therefore we have that the induced electric field of the slab is given by:

$$E_x^{ind}(\mathbf{r},t)\Big|_{z=0} \xrightarrow{|q_{||}|\frac{L}{2}\gg 1} (-)4\pi n_e e\Delta_0 e^{i\mathbf{q}_{||}\cdot\mathbf{r}-i\omega t} \tag{6.36}$$

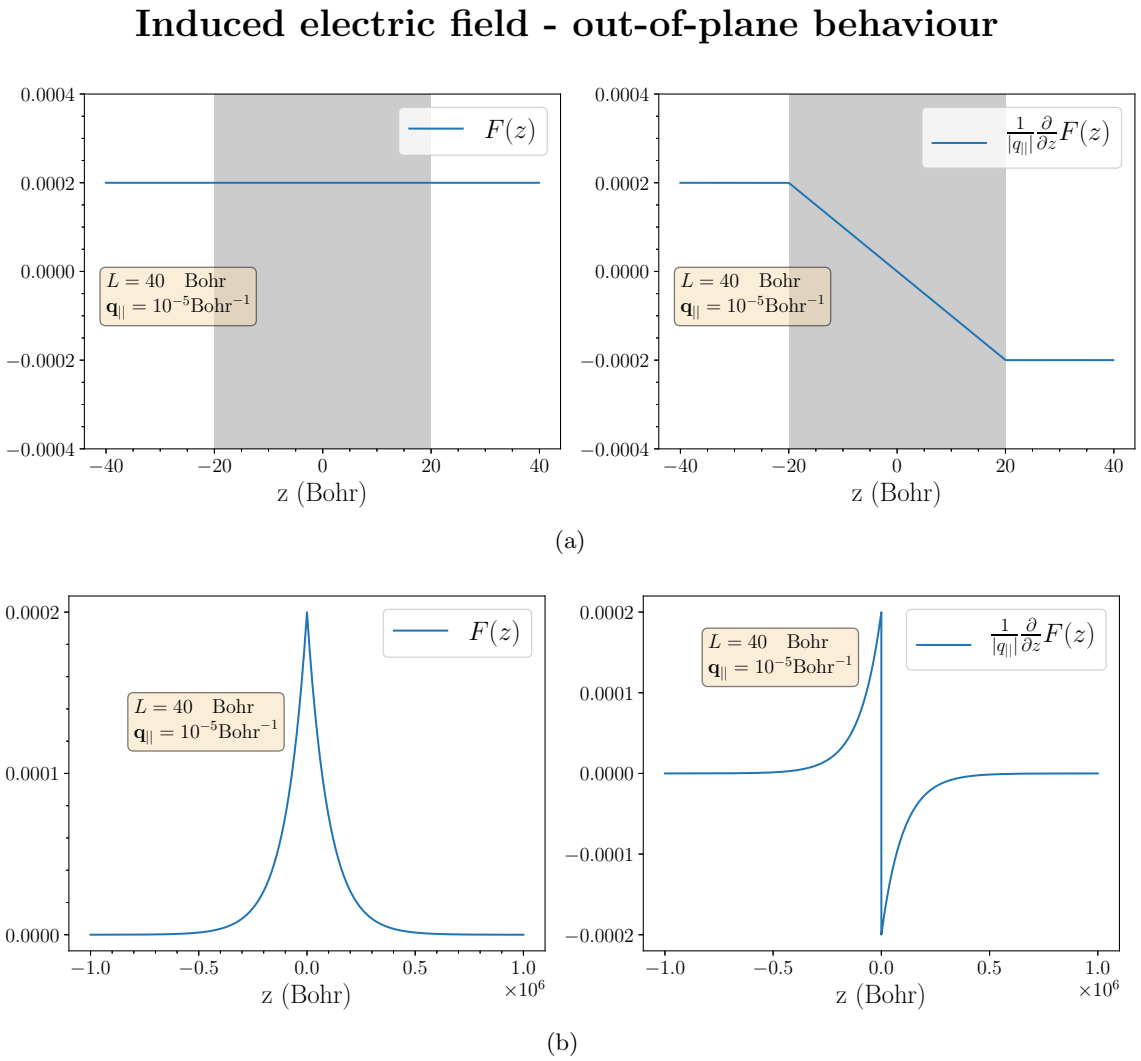

Figure 6.4: Sketch of the function $F(z)$ (Eq. (6.30)) and of its derivative along z, which, as shown in Eq.s (6.32) and (6.33), determines the behaviour of the field $\mathbf{E}^{ind}$ in the out-of-plane direction.Panel (a): in proximity of the slab, denoted as the gray region. Panel (b): the long range behaviour.

So, in the limit where the thickness of the slab is much greater of the perturbation wave length, the induced electric field far from the surfaces (i.e., in the middle of the slab) becomes equal to the bulk value (Eq. (6.34)) .

2. $|q_{||}|\frac{L}{2} \ll 1$ (i.e. the limit where **the wave length of the perturbation is much greater than the thickness of the slab**[1]). In this limit we have that $\left(1 - e^{-|q_{||}|\frac{L}{2}}\right) \approx |q_{||}|\frac{L}{2}$. So, in this limit, the induced electric field in the middle of the slab becomes:

$$E_x^{ind}(\mathbf{r},t)\Big|_{z=0} \xrightarrow{|q_{||}|\frac{L}{2}\ll 1} (-)4\pi n_e e q_{||}\frac{L}{2}\Delta_0 e^{i\mathbf{q}_{||}\cdot\mathbf{r}-i\omega t} \tag{6.37}$$

Therefore, in the case where the thickness of the slab is much lesser than the perturbation wave length, the electric field induced inside the slab is, respect to the case of the bulk, smaller of a factor $|q_{||}|(L/2)$

We remark that in the limit of very thin slab, the induced electric field result to be much smaller than the field induced in the infinite material by the same perturbation. This is due to the long-range and non-local nature of the Coulomb interaction. The electric field induced in no matter which point $\mathbf{r}$ inside the slab depends not only on the charge density in $\mathbf{r}$, but also on the charge in the rest of the space. More specifically, a slab can be seen as a bulk from which two parallel half spaces have been cutted away. If the slab is very thin compared to the perturbation wavelength, so even most of charges contributing to the coulomb potential inside the slab have been cut away, leading therefore to a dramatic reduction of the induced field. Moreover, in the very thin slab limit, one can also see that:

$$E_z^{ind} \to -i4\pi n_e e|\mathbf{q}_{||}|z\Delta_0 e^{iq_{||}x-i\omega t} \tag{6.38}$$

which implies that

$$E_z^{ind}, E_x^{ind} \sim |q_{||}|L/2 \ll |\mathbf{E}^{ext}| \tag{6.39}$$

Eq. (6.39), together with $\mathbf{E}^{ext}||\mathbf{q}$ (longitudinal perturbation), justifies the guess $\mathbf{\Delta}(\mathbf{r},t)||\mathbf{q}$.

6.2.2 Solution of the equation of motion in the limit $|q_{||}|\frac{L}{2} \ll 1$

In the following, we will focus on the limit $|q_{||}|\frac{L}{2} \ll 1$, corresponding to the case of a slab much thinner than the perturbation wave-length. All the *ab initio* calculations of the optical response that we have done have been performed in the optical limit, and therefore they always verify this condition. Using the expression that we have found for the induced

[1] notice that this is the limit in which we performed all our *ab initio* calculation, since we have slab of thickness ~ 40 Bohr and perturbation with $q_{||} \sim 10^{-5}\text{Bohr}^{-1}$

electric field we can solve the equation of motion, and to express the displacement of oscillators as a function of the external electric field:

$$\mathbf{\Delta}_0 = \frac{e}{m_e} \frac{1}{-\omega^2 + \omega_0^2 - i\frac{\omega}{\tau} + \omega_{pl}^2 |q_{||}| \frac{L}{2}} \mathbf{E}_0^{ext} \tag{6.40}$$

From this relation we can extract the response function of density:

$$\chi_{\rho\rho} = \frac{|\mathbf{q}|^2}{4\pi} \frac{\omega_{pl}^2}{\omega^2 - \omega_0^2 + i\frac{\omega}{\tau} - |q_{||}| \frac{L}{2} \omega_{pl}^2} \tag{6.41}$$

It presents a significative difference compared to Eq. (6.14). Contrarily to its bulk analogous the maximum of this quantity is located at:

$$\sqrt{\omega_0^2 + |q_{||}| \frac{L}{2} \omega_{pl}^2} \approx \omega_0$$

(see Fig. (6.5)). As we have already discussed, the point of maximum of this quantity represents the frequency at which the electron oscillates in absence of external perturbation, or, in other words, the frequency of the plasma oscillations of the system. In a thin slab, it is at ω_0, and no more at $\sqrt{\omega_0^2 + \omega_{pl}^2}$ as in the bulk. This is exactly the results that we have found in the mixed space approach (Eq. (5.27) and Fig.(5.5)). The reason of this difference is to be found in the suppression of the induced field in the limit of thin slab. It's well known that plasma oscillations are a collective phenomenon which consists in the motions of electrons inside the field generated by their displacement. In the case of a very thin slab, as we have seen, the field induced by the in-plane displacement of electrons is extremely weak, and therefore they act like free oscillators (i.e. they oscillate at frequency ω_0). This quantity is closely associated to the EELS spectrum. The derivation of the work done by the slab over an external electrons' beam is reported in Appendix B. One can notice that this finding is in agreement with EELS spectra of few-layers graphene [56] where the plasmon is pushed toward low energy when the thickness is decreased.

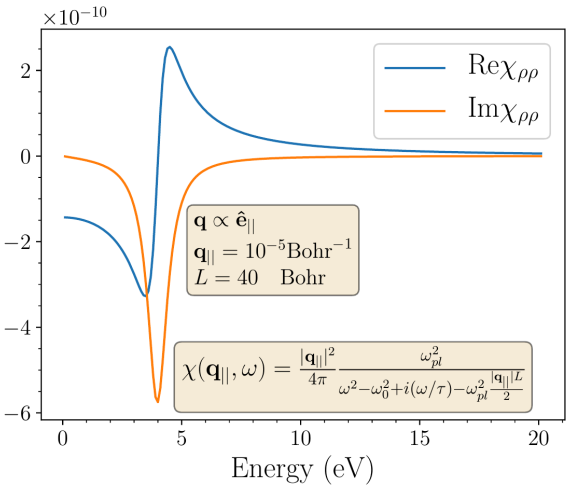

Figure 6.5: Density response of the slab (for the case of an in-plane pertrubation of great wave-length). Contrarily to what happens in a bulk (see Fig. (6.2)), the response function is peaked at ω_0: in the case of thin slab ($|\mathbf{q}_{||}|L \ll 1$)the induced field becomes negligible, and electrons act like independent oscillators.

We can then express the electronic displacement as a function of the total electric field:

$$\mathbf{\Delta}(\mathbf{r},t) = \frac{e}{m_e}\frac{\Theta(z+\frac{L}{2})\Theta(-z+\frac{L}{2})}{-\omega^2+\omega_0^2-i\frac{\omega}{\tau}}\mathbf{E}(\mathbf{r},t) \tag{6.42}$$

and use this relation in order to find an expression for the conductivity of the slab $\sigma(\omega)$ as:

$$\sigma(\omega) = \frac{1}{4\pi}\frac{i\omega\omega_{pl}^2}{\omega^2-\omega_0^2+i\frac{\omega}{\tau}} \tag{6.43}$$

and for the dielectric function:

$$\varepsilon(\omega) = 1 - \frac{\omega_{pl}^2}{\omega^2-\omega_0^2+i\frac{\omega}{\tau}} \approx 1 - \frac{4\pi}{q^2}\chi_{\rho\rho} \tag{6.44}$$

This result is indeed remarkable. Despite the density response function corresponding to the thin slab (Fig. (6.5)) is radically different from the bulk one (Fig. (6.2a)), both the systems has the same dielectric function. This result also validates the calculation of absorption spectrum with Eq. (5.26) within the mixed space approach.

6.2.3 Some considerations on the in-plane component of the dielectric function

In the previous section, we derived the in-plane component of the dielectric function of a thin slab constituted by charged classical oscillators. We solved in a first moment the equation of motions of the oscillators, finding a relation between the displacement of the oscillators and the external perturbation. This relation (which allowed us to extract the density response function of the system, see Fig. (6.5)) has been then employed to obtain a relation between the displacement of electrons and the total electric field, giving us access to the conductivity, and therefore to the dielectric function of the system. Despite the significant differences in the induced field and the response function, the dielectric function of slab and bulk turned out to be the same. However, this is not the procedure that we usually follow in our *ab initio* calculations. When we calculate optical properties from TD-DFT, the fundamental quantity we access to is the response function of density, which is obtained solving the Dyson equation (2.76). Once we have the interacting response function $\chi_{\mathbf{GG'}}$, the microscopic inverse dielectric function can be calculated:

$$\varepsilon^{-1}_{\mathbf{GG'}} = \delta_{\mathbf{GG'}} + \sum_{\mathbf{G_1}} v^{coul}_{\mathbf{GG_1}}\chi_{\mathbf{G_1G'}} \tag{6.45}$$

and finally, we get the macroscopic dielectric function as:

$$\varepsilon_M = \frac{1}{\varepsilon^{-1}_{\mathbf{00}}} \tag{6.46}$$

From the definition of inverse dielectric function (6.45), it is easy to see that the latter equation is equivalent to the ratio between cell-averaged external and total potential:

$$\varepsilon_M = \frac{1}{\varepsilon^{-1}_{\mathbf{00}}} = \frac{v^{ext}_{\mathbf{0}}}{v^{tot}_{\mathbf{0}}} \tag{6.47}$$

This equation is written in reciprocal space, and therefore refers to systems which are intrinsically periodic. This is clearly not the case for the slab of oscillators that we are studying in this chapter: our system is finite and isolated in the out-of-plane direction, and in this context, definition of cell-averaged quantities makes no sense. By the way, having calculated the field induced in the slab by an external perturbation, we may try to calculate the dielectric function in analogy with Eq. (6.47), replacing the cell averaged quantities with the fields averaged *over the slab*[2]:

$$\varepsilon_M = \frac{\langle E^{ext}_{||}\rangle_{slab}}{\langle E^{ext}_{||}\rangle_{slab} + \langle E^{ind}_{||}\rangle_{slab}} \tag{6.49}$$

which in the limit $\mathbf{q}_{||}L/2 \ll 1$ reduces to:

$$\frac{\langle E^{ext}_{||}\rangle_{slab}}{\langle E^{ext}_{||}\rangle_{slab} + \langle E^{ind}_{||}\rangle_{slab}} \approx 1 - \frac{|\mathbf{q}_{||}|L}{2}\frac{\omega^2_{pl}}{\omega^2 - \omega^2_0 + i\frac{\omega}{\tau}} \tag{6.50}$$

The result of this calculation is shown in Fig. (6.6). As we can see in the figure, the dielectric function calculated according formula (6.49) has real part ≈ 1 and imaginary part ≈ 0, coherently with spectra that we have calculated with Eq. (5.25) within our mixed space approach (compare Fig. (6.6) with Fig. (5.3)). The study performed within the Lorentz model allows us to identify the origin of this behaviour: this is a consequence of the strong reduction of the induced field occurring in the limit of thin slab $\mathbf{q}_{||}L/2 \ll 1$. We stress out that, since the induced field has been averaged *over the slab*, this result cannot be interpreted as an effective medium theory with vacuum, but it's a real physical effect due to the suppression of induced field in the case of very thin film. The situation is quite confusing: the dielectric function calculated passing by the the conductivity (see Eq.s (6.43) and (6.44)) and the one calculated by mean of formula (6.49) are radically different. However, this ambiguity has been already pointed out by several authors in literature. In Ref. [57], Hüser and coworkers, calculated the static dielectric function of a MoS_2 sheet following a procedure very similar to the one reported in Eq.(6.49). Using a truncated Coulombian interaction (see e.g. Ref. [58]), they calculated the potential induced by an

[2]here $\langle\cdot\rangle_{slab}$ stand for:

$$\langle f(z)\rangle_{slab} = \frac{1}{L}\int_{L/2}^{L/2} f(z)dz \tag{6.48}$$

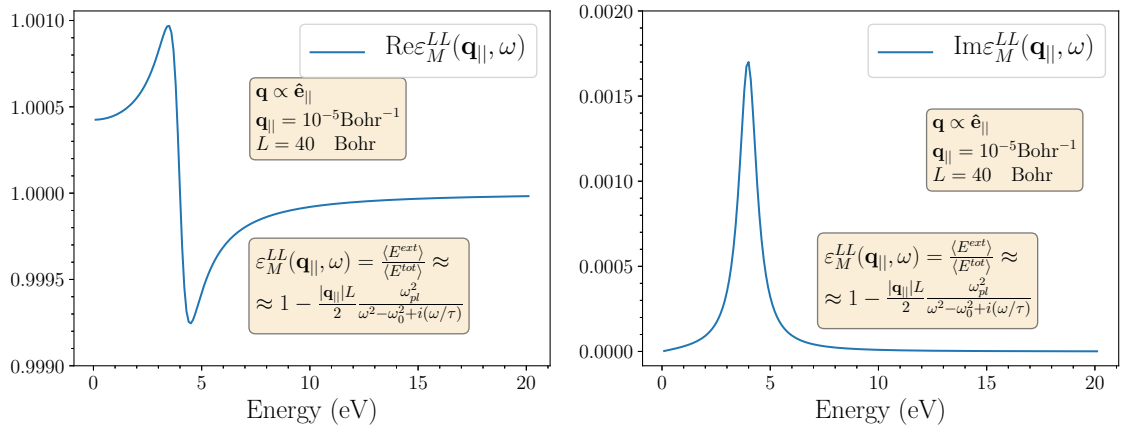

Figure 6.6: Longitudinal-longitudinal part of the dielectric function, calculated as the ratio between the external and the total field (in the limit $|\mathbf{q}_{||}|L \ll 1$, see Eq. (6.50)). As we can see, real part is ≈ 1 while imaginary part is ≈ 0.

isolated sheet, and then they obtained the static dielectric function of the 2D system as:

$$\varepsilon_M^{2D}(\mathbf{q}) = \frac{\langle V^{ext}(\mathbf{q})\rangle_d}{\langle V^{tot}(\mathbf{q})\rangle_d} \tag{6.51}$$

(where $\langle\cdot\rangle_d$ stands for the average over a region of thickness d). Following this procedure, authors of Ref. [57] reported that in the long-wavelength limit $\varepsilon_M^{2D}(\mathbf{q} \to 0) \approx 1$, in agreement with the result that we have shown in Fig. (6.6). We want to underline that this result has a truly physical meaning: the quantity calculated according (6.49) (or equivalently according Eq. (6.51)) reflects an actual phenomenon occurring in very thin films, which is the reduction of the screening. As we have seen, when the thickness of the system is much smaller than the perturbation wavelength, the induced field is strongly reduced, and the total electric field inside the slab approaches the external field. This is the reason because of the dielectric function calculated according approaches such as the one reported in Ref. [57] has been successfully applied to model the screening in GW calculations on 2D materials (see Ref.s [59],[60]). However, even if the quantity defined by Eq. (6.51) succeeds in describing the screening of the material, there is quite a wide agreement in literature that should not be looked at when describing optical properties. As pointed out by several authors [61][62], the quantity which should be link to the absorption is not the 2D-dielectric function but the 2D-polarisability:

$$\alpha_{2D} \propto \frac{4\pi}{|\mathbf{q}|^2}\chi \tag{6.52}$$

and if we define (as done by Molina-Sanchez et al. in Ref. [62]) the dielectric function as:

$$\varepsilon^{Molina} = 1 + \frac{4\pi}{d}\alpha_{2D} \tag{6.53}$$

we obtain:

$$\begin{aligned} \varepsilon^{Molina} &= 1 + \frac{4\pi}{d}\alpha_{2D} \\ &= 1 - \frac{4\pi\omega_{pl}^2}{\omega^2 - \omega_0^2 + i(\omega/\tau)} \end{aligned} \tag{6.54}$$

which is exactly the same result that we obtained deriving the dielectric function from conductivity. However, even if most of the authors agree that formula (6.52) is the one that should be used to describe absorption of an isolated 2d sheet (such as the thin slabs that we are studying), Eq. (6.47) is routinely used when calculating optical properties of bulk systems, and it seems to us that a clear explanation of the link between the two formulas is still lacking. The last part of the present section will be devoted to elucidate this point. The macroscopic dielectric function is formally defined as the quantity which relates the electric displacement $\mathbf{D}$ with the electric field $\mathbf{E}$:

$$\mathbf{D} = \overleftrightarrow{\varepsilon}_M \, \mathbf{E} \tag{6.55}$$

where the electric displacement $\mathbf{D}$ is defined by the constitutive relation:

$$\mathbf{D} = \mathbf{E} + 4\pi\mathbf{P} \tag{6.56}$$

In the beginning of this chapter, within the Lorentz oscillator model, we have seen that, when an infinite material undergoes to a longitudinal external perturbation, the induced electric field ans the polarisation of the system are linked by the following relation (see Eq. (6.8)):

$$\mathbf{E}^{ind} = -4\pi\mathbf{P} \tag{6.57}$$

From the latter equation and the constitutive relationship (6.56), it follows that:

$$\mathbf{D} = \mathbf{E}^{ext} \tag{6.58}$$

Putting Eq. (6.58) in (6.55), we immediately obtain:

$$\varepsilon_M = \frac{E^{ext}}{E^{ext} + E^{ind}} \tag{6.59}$$

In this chapter, we also calculated the response of a thin slab to an external longitudinal perturbation in the in-plane direction, and we derived the induced electric field and polarisation density. From a quick comparison between Eq.s (6.32) and (6.27), we see that in the case of a slab:

$$-4\pi\mathbf{P} \neq \mathbf{E}^{ind} \tag{6.60}$$

Indeed, one can show that $\mathbf{P}$ is no more purely longitudinal, contrarily to the induced field $\mathbf{E}^{ind}$. This can be seen calculating the curl of the fields $\mathbf{E}^{ind}$ and $\mathbf{P}$, which for a purely longitudinal field must be equal to zero. For the induced field we have:

$$\nabla \times \mathbf{E}^{ind} = \begin{pmatrix} 0 \\ \partial_z E_x^{ind} - \partial_x E_z^{ind} \\ 0 \end{pmatrix} \tag{6.61}$$

with:

$$\begin{aligned} \partial_z E_x^{ind} - \partial_x E_z^{ind} = & (-)4\pi n_e e \Delta_0 e^{iq_{||}r_{||} - i\omega t} \times \\ & \times \begin{cases} -|\mathbf{q}_{||}| e^{-|q_{||}|z} \sinh(|q_{||}|L/2) & \text{for} \quad z > L/2 \\ -|\mathbf{q}_{||}| e^{-|q_{||}|\frac{L}{2}} \sinh(|q_{||}|z) & \text{for} -L/2 < z < L/2 \\ |\mathbf{q}_{||}| e^{|q_{||}|z} \sinh(|q_{||}|L/2) & \text{for} \quad z < -L/2 \end{cases} \\ & - \\ & (-)4\pi n_e e \Delta_0 e^{iq_{||}r_{||} - i\omega t} \times \\ & \times \begin{cases} -|\mathbf{q}_{||}| e^{-|q_{||}|z} \sinh(|q_{||}|L/2) & \text{for} \quad z > L/2 \\ -|\mathbf{q}_{||}| e^{-|q_{||}|\frac{L}{2}} \sinh(|q_{||}|z) & \text{for} -L/2 < z < L/2 \\ |\mathbf{q}_{||}| e^{|q_{||}|z} \sinh(|q_{||}|L/2) & \text{for} \quad z < -L/2 \end{cases} \\ & = 0 \end{aligned} \tag{6.62}$$

For the polarisation (Eq. (6.27)) we have:

$$\begin{aligned} \nabla \times \mathbf{P} &= \begin{pmatrix} 0 \\ \partial_z P_x \\ 0 \end{pmatrix} \\ &= \begin{pmatrix} 0 \\ \partial_z \left[\Theta(z + \frac{L}{2}) \Theta(-z + \frac{L}{2}) \right] e n_e e^{iq_{||}r_{||} - i\omega t} \\ 0 \end{pmatrix} \\ &= \begin{pmatrix} 0 \\ \left[\delta(z + \frac{L}{2}) - \delta(-z + \frac{L}{2}) \right] e n_e e^{iq_{||}r_{||} - i\omega t} \\ 0 \end{pmatrix} \\ &\neq 0 \end{aligned} \tag{6.63}$$

Since the polarisation contains a transverse part, while the induced electric field is purely longitudinal (and so it is, by construction, also the external one), we will have:

$$\mathbf{D}_L + \mathbf{D}_T = \mathbf{E}_L^{ext} + \mathbf{E}_L^{ind} + 4\pi \mathbf{P}_L + 4\pi \mathbf{P}_T \tag{6.64}$$

$$\begin{aligned}\mathbf{D}_L &= \mathbf{E}_L^{ext} + \mathbf{E}_L^{ind} + 4\pi\mathbf{P}_L \\ \mathbf{D}_T &= 4\pi\mathbf{P}_T\end{aligned} \tag{6.65}$$

Therefore, it is clear that:

$$\mathbf{D} \neq \mathbf{E}^{ext} \tag{6.66}$$

The fact that a purely longitudinal perturbation induces also a transverse polarisation may be source of perplexity. However, it has been already reported in literature by Del Sole et al. [32] that for infinite materials having cubic symmetry, a longitudinal perturbation always produce a purely longitudinal response, but this is no more the case when the case of non-cubic symmetry is considered, or when surfaces are to take in account (as it can be seen from Eq. (6.63)). However, the constitutive equation (6.55) is still valid, and (assuming the diagonality of the tensor) the in-plane component may be obtained as:

$$\varepsilon_{M,||} = \frac{\langle E_{||}^{ext}\rangle_{slab} + \langle E_{||}^{ind}\rangle_{slab} + 4\pi\langle P_{||}\rangle_{slab}}{\langle E_{||}^{ext}\rangle_{slab} + \langle E_{||}^{ind}\rangle_{slab}} \tag{6.67}$$

Previously in this chapter we calculated the induced field in a slab in both the thin and thick film limits: let's study the behaviour of Eq. (6.67) in these two cases. In the limit of very thick slab (see Eq. (6.36)), the induced field approaches the bulk result, so that condition (6.57) is recovered, and equation (6.67) becomes:

$$\begin{aligned}\varepsilon_{M,||} \xrightarrow{|q_{||}|\frac{L}{2}\gg 1} &\frac{\langle E_{||}^{ext}\rangle_{slab} + \cancel{\langle E_{||}^{ind}\rangle_{slab}} + \cancel{4\pi\langle P_{||}\rangle_{slab}}}{\langle E_{||}^{ext}\rangle_{slab} + \langle E_{||}^{ind}\rangle_{slab}} \\ &= \frac{\langle E_{||}^{ext}\rangle_{slab}}{\langle E_{||}^{ext}\rangle_{slab} + \langle E_{||}^{ind}\rangle_{slab}}\end{aligned} \tag{6.68}$$

i.e. we re-obtain the expression valid for the infinite material. In the limit of very thin slab, on the other hand, the induced field becomes negligible compared to the external one, and we have:

$$\begin{aligned}\varepsilon_{M,||} \xrightarrow{|q_{||}|\frac{L}{2}\ll 1} &\frac{\langle E_{||}^{ext}\rangle_{slab} + \cancel{\langle E_{||}^{ind}\rangle_{slab}} + 4\pi\langle P_{||}\rangle_{slab}}{\langle E_{||}^{ext}\rangle_{slab} + \cancel{\langle E_{||}^{ind}\rangle_{slab}}} \\ &= 1 + 4\pi\frac{\langle P_{||}\rangle_{slab}}{\langle E_{||}^{ext}\rangle_{slab}}\end{aligned} \tag{6.69}$$

Exploiting the relation between polarisation and induced charge density we can express $P_{||}$ as a function of the external field:

$$\begin{aligned}iq_{||}P_{||} &= -\delta\rho^{ind} \\ &= -\chi\phi^{ext} \\ &= \frac{1}{iq_{||}}\chi E^{ext}\end{aligned} \tag{6.70}$$

so that we obtain:

$$\varepsilon_{M,||} \xrightarrow{|q_{||}|\frac{L}{2}\ll 1} 1 - \frac{4\pi}{q_{||}^2}\langle\chi\rangle \tag{6.71}$$

which is the same of Eq. (6.53).
In conclusion, through this section, we elucidated the differences between the response of the slab and a bulk system to an external longitudinal perturbation. The true relationship for the calculation of the dielectric function is Eq. (6.67). In the case of a bulk, it is equivalent to Eq. (6.49), and one recovers the well known result that for bulk cubic materials, in the optical limit, the longitudinal-longitudinal component of the dielectric function can be used to calculate the transverse-transverse one, leading to absorption. For the slab, the presence of a transverse polarisation implies that one should apply (6.67). Even if it is not trivial to identify the components of the dielectric tensor, in the limit of thin slab Eq. (6.67) reproduces the same expression that most of the authors adopt to describe absorption of 2D systems (and that we have demonstrated in Eq.s (6.67) and (6.71)). We believe that a key role in reproducing such result is played by the inclusion of the transverse part of the polarisation.

6.3 Response of the slab: out-of-plane response

Let's consider the same system as in previous section, but now we try to answer the following question: what is the response of this system to a perturbation orthogonal to the surface? Let's suppose moreover that the external electric field, oscillating in time with frequency ω has infinite wave length (see Fig. (6.7a)):

$$\mathbf{E}^{ext}(\mathbf{r},t) = \mathbf{E}_0^{ext} e^{-i\omega t} \qquad \mathbf{E}_0^{ext} || \hat{\mathbf{z}} \tag{6.72}$$

We remember again that the displacement of the oscillator located in $\mathbf{r}$ is described by the vector field $\mathbf{\Delta}(\mathbf{r},t)$. The equation of motion of the oscillators could be written has:

$$m_e \ddot{\mathbf{\Delta}}(\mathbf{r},t) = -m_e\omega_0^2\mathbf{\Delta}(\mathbf{r},t) - \frac{m_e}{\tau}\dot{\mathbf{\Delta}}(\mathbf{r},t) + e\mathbf{E}^{ext}(\mathbf{r},t) + e\mathbf{E}^{ind}(\mathbf{r},t) \tag{6.73}$$

In order to solve this equation, we need to express the induced electric field as function of $\mathbf{\Delta}(\mathbf{r},t)$. Now, we know that the polarisation of the system can be expressed as a function of $\mathbf{\Delta}(\mathbf{r},t)$:

$$\mathbf{P}(\mathbf{r},t) = n_e e \mathbf{\Delta}(\mathbf{r},t) \tag{6.74}$$

Once we have the polarisation of the system, moreover, we can obtain the induced density:

$$\rho^{ind}(\mathbf{r},t) = -\nabla\cdot\mathbf{P}(\mathbf{r},t) \tag{6.75}$$

I make a guess on the functional form of $\mathbf{\Delta}(\mathbf{r},t)$ (we will verify a posteriori that it is correct):

$$\mathbf{\Delta}(\mathbf{r},t) = \Theta(z+\frac{L}{2})\Theta(-z+\frac{L}{2})\mathbf{\Delta}_0 e^{-i\omega t} \qquad \mathbf{\Delta}_0 || \hat{\mathbf{z}} \tag{6.76}$$

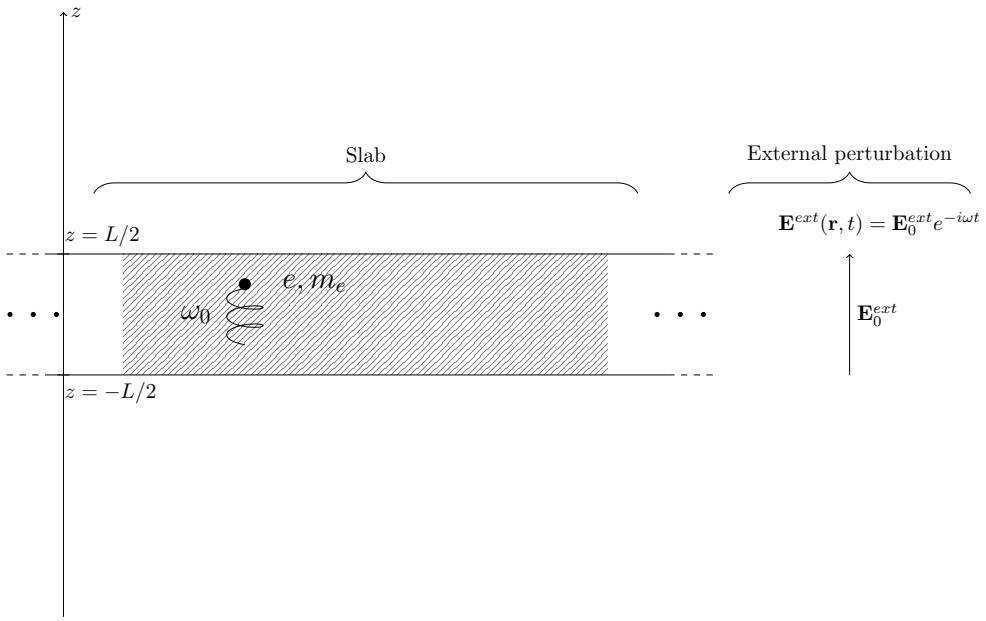

(a)

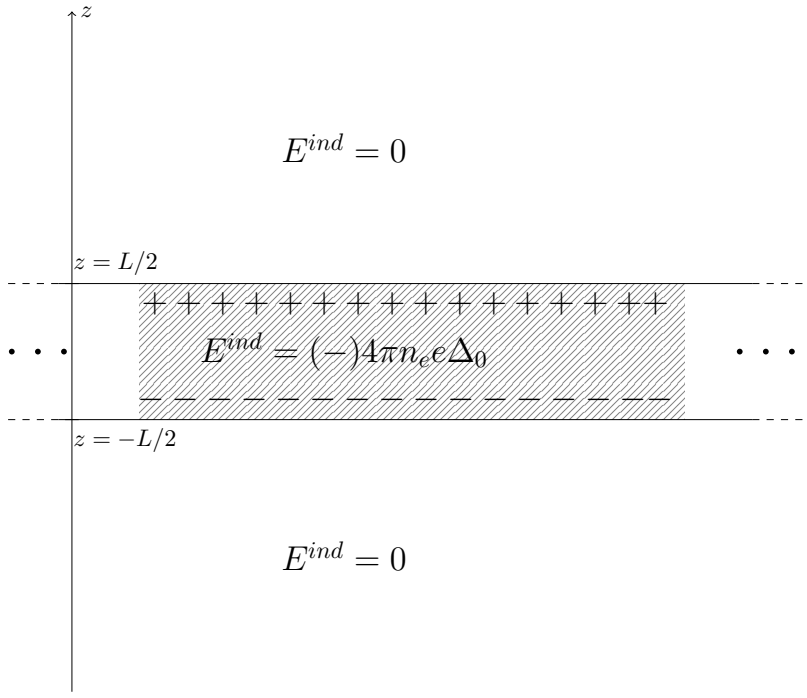

(b)

Figure 6.7: Panel (a): sketch of a slab undergoing an external perturbation of infinite wave-length orthogonal to the surface. Panel (b): the perturbation induces on the two surfaces an accumulation of charge of opposite sign, resulting in an induced electric field uniform and constant inside the slab, and identically zero outside.

where Θ stands for the Heaviside function. In other words, I assume that the displacement of oscillators from their equilibrium position is independent on z in the region occupied by the slab, and zero outside. Such a guess for $\mathbf{\Delta}(\mathbf{r},t)$ implies that polarisation density will be given by:

$$\mathbf{P}(\mathbf{r},t) = n_e e\Theta(z+\frac{L}{2})\Theta(-z+\frac{L}{2})\mathbf{\Delta}_0 e^{-i\omega t} \tag{6.77}$$

Therefore the induced density will be given by:

$$\begin{aligned}\rho^{ind}(\mathbf{r},t) =& -\nabla\cdot\mathbf{P}(\mathbf{r},t)\\ =& -\frac{\partial}{\partial z}P_z\\ =& -n_e e\Delta_0 e^{-i\omega t}\times\\ &\times\left(\Theta(-z+\frac{L}{2})\delta(z+\frac{L}{2})-\Theta(z+\frac{L}{2})\delta(-z+\frac{L}{2})\right)\\ =& -n_e e\Delta_0 e^{-i\omega t}\left(\delta(z+\frac{L}{2})-\delta(-z+\frac{L}{2})\right)\end{aligned} \tag{6.78}$$

We notice that, as it was expected, when we put the slab in an external field of infinite wave length orthogonal to the surface, the density of charge induced in the system is constituted by two planar distribution having opposite sign and located on the faces of the slab (see Fig.(6.7b)). The electric field induced by such a charge distrubution will be given by:

$$\begin{aligned}\mathbf{E}^{ind}(\mathbf{r},t) =&(-)4\pi n_e e\mathbf{\Delta}(\mathbf{r},t)\\ =&(-)4\pi n_e e\Theta(z+\frac{L}{2})\Theta(-z+\frac{L}{2})\mathbf{\Delta}_0 e^{-i\omega t}\end{aligned} \tag{6.79}$$

Contrarily to the case of in-plane perturbation the induced field is no suppressed, and inside the slab it has the same amplitude than in the infinite material (see Eq. (6.8)). Now that we have an expression for the induced electric field as function of $\mathbf{\Delta}(\mathbf{r},t)$, we can rewrite the equation of motion of the oscillators in the following way:

$$m_e\ddot{\mathbf{\Delta}}(\mathbf{r},t) = -m_e\omega_0^2\mathbf{\Delta}(\mathbf{r},t) - \frac{m_e}{\tau}\dot{\mathbf{\Delta}}(\mathbf{r},t) + e\mathbf{E}^{ext}(\mathbf{r},t) - 4\pi n_e e\mathbf{\Delta}(\mathbf{r},t) \tag{6.80}$$

Solving this equation, we find a relation between the displacement of the oscillators and the external field:

$$\mathbf{\Delta}_0 = \frac{e}{m_e}\frac{1}{-\omega^2+\omega_0^2-i\frac{\omega}{\tau}+\omega_{pl}^2}\mathbf{E}_0^{ext} \tag{6.81}$$

We remark that in the case of slab perturbed in the out-of-plane direction (and contrarily to the case of in-plane perturbation), the relation between displacement of oscillators and the external electric field is the same than in bulk (see Eq. (6.11)). This has important consequences on the EELS spectrum (the case of electrons travelling orthogonally to the slab

is described in Appendix (B) ,section (B.2.3)). Let's now try to express the displacement of oscillators as function of the *total electric field*. We need this relationship in order to calculate the conductivity, which is a quantity that we can directly link to the absorption. The external field can be written as:

$$\mathbf{E}^{ext}(\mathbf{r},t) = \begin{cases} \frac{m_e}{e}(-\omega^2 + \omega_0^2 - i\frac{\omega}{\tau} + \omega_{pl}^2)\mathbf{\Delta}(\mathbf{r},t) & \text{for} \quad |z| < \frac{L}{2} \\ \mathbf{E}^{ext}(\mathbf{r},t) & \text{for} \quad |z| \geq \frac{L}{2} \end{cases} \tag{6.82}$$

While the induced electric field can be written as:

$$\mathbf{E}^{ind}(\mathbf{r},t) = \begin{cases} -\frac{m_e}{e}\omega_{pl}^2\mathbf{\Delta}(\mathbf{r},t) & \text{for} \quad |z| < \frac{L}{2} \\ 0 \quad \text{for} \quad |z| \geq \frac{L}{2} \end{cases} \tag{6.83}$$

Therefore, the total electric field will be written as:

$$\mathbf{E}^{tot}(\mathbf{r},t) = \begin{cases} \frac{m_e}{e}(-\omega^2 + \omega_0^2 - i\frac{\omega}{\tau})\mathbf{\Delta}(\mathbf{r},t) & \text{for} \quad |z| < \frac{L}{2} \\ \mathbf{E}^{ext}(\mathbf{r},t) & \text{for} \quad |z| \geq \frac{L}{2} \end{cases} \tag{6.84}$$

As a consequence, the displacement of the electrons will be written:

$$\mathbf{\Delta}(\mathbf{r},t) = \frac{e}{m_e}\Theta(z+\frac{L}{2})\Theta(-z+\frac{L}{2})\frac{1}{-\omega^2+\omega_0^2-i\frac{\omega}{\tau}}\mathbf{E}^{tot}(\mathbf{r},t) \tag{6.85}$$

and the conductivity will be given by:

$$\sigma(\omega) = \frac{1}{4\pi}\Theta(z+\frac{L}{2})\Theta(-z+\frac{L}{2})\frac{i\omega\omega_{pl}^2}{\omega^2-\omega_0^2+i\frac{\omega}{\tau}} \tag{6.86}$$

leading to:

$$\varepsilon(\omega) = 1 - \Theta(z+\frac{L}{2})\Theta(-z+\frac{L}{2})\frac{\omega_{pl}^2}{\omega^2-\omega_0^2+i\frac{\omega}{\tau}} \tag{6.87}$$

Contrarily to the case of in-plane perturbation, both induced electric field and polarisation are purely longitudinal (as it can be easily demonstrated showing that $\nabla \times \mathbf{E}^{ind} = \nabla \times \mathbf{P} = 0$). As a consequence, we have that:

$$\mathbf{E}^{ind} = -4\pi\mathbf{P} \tag{6.88}$$

and therefore:

$$\mathbf{D} = \mathbf{E}^{ext} + \mathbf{E}^{ind} + 4\pi\mathbf{P} \tag{6.89}$$

Contrarily to the case of in-plane perturbation, application of formula (6.49) leads exactly to the same result obtained deriving the dielectric function from conductivity:

$$\begin{aligned} \varepsilon_M &= \frac{\langle E_{||}^{ext}\rangle_{slab}}{\langle E_{||}^{ext}\rangle_{slab} + \langle E_{||}^{ind}\rangle_{slab}} = \frac{1}{1 + \frac{\langle E_{||}^{ind}\rangle_{slab}}{\langle E_{||}^{ind}\rangle_{slab}}} \\ &= 1 - \frac{\omega_{pl}^2}{\omega^2 - \omega_0^2 + i\frac{\omega}{\tau}} \end{aligned} \tag{6.90}$$

This justifies a posteriori the fact that in previous chapter, in section (5.4), we calculated the out-of-plane component of the dielectric function as the ratio between the average of the external and total field.

6.4 Conclusions

We briefly resume in this section the results that we have presented in this chapter. Initially, we explored the differences between the response of a bulk and of a slab to an external longitudinal perturbation. Using a simple oscillators model to describe the electrons dynamics we found that the response of a slab is somewhat halfway between the response of a bulk and the one of a finite system. This is a meaningful result from a physical point of view: a slab is by definition a system which is finite in one direction and infinite in the other two, and therefore it seems reasonable that it has at the same times behaviours typical of finite and infinite systems.

In particular, we found that, when a slab is perturbed in the in-plane direction (provided that the slab is much thinner than the perturbation wave-length), the electric field is much less intense than the field that an identical external perturbation would induce in the bulk system. As a consequence, the system is no more able to sustain collective excitation at the plasma frequency, and the density response function of the system tends to the absorption spectrum, as typically it happens for finite systems.

On the other side, if the slab is perturbed in the out-of-plane direction, the induced field has the same intensity than in the bulk, and as a consequence the slab is able to sustain collective charge oscillation in the direction orthogonal to the surface. Collective plasma excitations are a signature typical of extended systems, and the fact that in a slab they are present or absent according the direction of the perturbation, is the way in which the dual nature of this kind of system reveals.

Nevertheless, it is interesting to note that the behaviour of the bulk object is recovered for the out-of-plane excitation corresponding to the direction where the object is isolated, while the behaviour of the isolated object is found for the in-plane direction where the system is still infinite.

Chapter 7

Optical properties of a thin film: link with the experiment

7.1 The measured quantity

As we have explained in Sec. 5.4.1, the calculation of the macroscopic dielectric function of a slab appears quite ambiguous. The difficulty is in the trickery to define in a clear way what the thickness of the slab is. By mean of the macroscopic average procedure, this uncertainty, impacts quite in a dramatic way the calculation of the out-of-plane macroscopic dielectric function : according the value of L_{mat} chosen, the amplitude and the energy of the absorption peaks may change very abruptly (see Fig. (5.10b)). This is a very problematic result: the dielectric function, is supposed to describe the interaction between light and the electronic system, and it should contains all the informations necessary to describe an optics experiment. But, of course, the result of the experiment cannot depend on the way the macroscopic average is carried out. In this section we will focus on those quantities which are actually measured in an optical spectroscopy experiment, and in which way they are linked with the dielectric function that we have calculated.

In Fig. (7.1), we show a schematic representation of a typical optical spectroscopy experiment. In a reflectance measurement, an incident beam impinges on the surface of the samples. Under the effect of the electric field of the incident wave, the charge carriers inside the material will move, forming induced density of charge and currents. These currents and charges , will act as source terms. As a result, they will appear also a reflected beam (propagating backward respect to the incident one) and a transmitted beams (which is typically suppressed in a characteristic length called *skin depth*). All the information concerning the relation between electric field and the induced source terms (and therefore all the information about the relationship between incident and reflected beam) is contained inside the macroscopic dielectric function. The quantity to be measured in an experiment like the one reproduced in Fig. (7.1) is the complex amplitude of the reflected field. The

ratio between this quantity and the amplitude of the incident field (which is supposed to be known), is called reflection coefficient. Its phase express the phase difference between the incident wave and the reflected wave, while its squared modulus - called *reflectance* - express the fraction of incident photons which are backscattered by the surface. Therefore, the reflection coefficient can be expressed as a function of the dielectric function of the material. In the hypothesises that the two half-spaces are sharply terminated, perfectly homogenous and isotropes, the reflection coefficients can be expressed as:

$$r_{12}^{s} = \frac{\varepsilon_1^{\frac{1}{2}} \cos\theta_i - \sqrt{\varepsilon_2 - \varepsilon_1 \sin^2\theta_i}}{\varepsilon_1^{\frac{1}{2}} \cos\theta_i + \sqrt{\varepsilon_2 - \varepsilon_1 \sin^2\theta_i}} \tag{7.1a}$$

$$r_{12}^{p} = \frac{\varepsilon_2 \cos\theta_i - \varepsilon_1^{\frac{1}{2}} \sqrt{\varepsilon_2 - \varepsilon_1 \sin^2\theta_i}}{\varepsilon_2 \cos\theta_i + \varepsilon_1^{\frac{1}{2}} \sqrt{\varepsilon_2 - \varepsilon_1 \sin^2\theta_i}} \tag{7.1b}$$

and transmission coefficients as:

$$t_{12}^{s} = \frac{2\sqrt{\varepsilon_1}\ cos\theta}{\sqrt{\varepsilon_1}\ cos\theta + \sqrt{\varepsilon_2 - \varepsilon_1 sin^2\theta}} \tag{7.2a}$$

$$t_{12}^{p} = \frac{2\sqrt{\varepsilon_1}\ \sqrt{\varepsilon_2}\ cos\theta}{\varepsilon_2\ cos\theta + \sqrt{\varepsilon_1}\sqrt{\varepsilon_2 - \varepsilon_1 sin^2\theta}} \tag{7.2b}$$

The relationships reported in Eq. (7.1) are the well known Fresnel's formulas. Their derivation (which basically consists in solving the Maxwell equation with the appropriate boundary conditions) can be found in the most of classical electrodynamics textbooks [63],[64]. The overscripts s and p which appears respectively in Eq.s (7.1a) and (7.1b), stand for the light polarisation. The polarisation s corresponds to case where the electric field is orthogonal to the incidence plane (which is the plane defined by the line normal to the surface and by the wave vector of the incident beam): the component of the electric field orthogonal to the surface is by definition equal to zero, at no matter which incidence angle. If the incident beam is p-polarised, the electric field lays in the incidence plane, and for non-normal incidence the electric field of the impinging beam will have a non-zero component orthogonal to the surface. As we remember from previous chapter, the ambiguity in the calculation of the dielectric function, affects mainly the response to a perturbation out-of-plane. Since our main goal is to solve this ambiguity, in the rest of the chapter we will focus mainly on the case of p-polarised light.

The Fresnel Formulas reported in Eq. (7.1), allows one to calculate the reflection coefficients of an infinite half-space of material having a given dielectric function. On the other hand, the systems for which we have calculated the dielectric functions in the previous chapter, are finite in the out-of-plane direction: they are slabs, and not semi-infinite blocks.

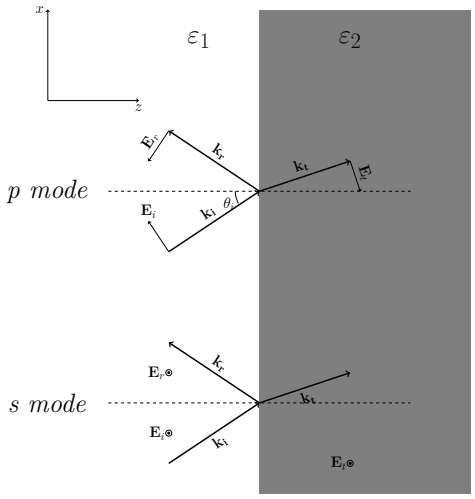

Figure 7.1: Sketch of a typical reflectance experiment: when a light beam impinges on the interface between two semi-infinites materials, part of the beam is reflected, and part of the beam is transmitted. In the upper part of the figure the case of p-polarised radiation (electric field laying in the incidence plane) is shown, while in the lower part the s-polarised case (electric field orthogonal to the incidence plane) is depicted. Reflection amplitudes for both the cases are given in Eq. (7.1)

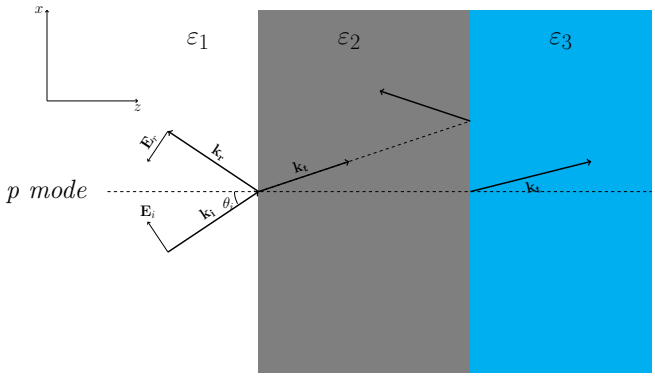

Figure 7.2: Sketch of a reflectance experiment performed over a thin film of dielectric function ε_2, encapsulated between an ambient medium of dielectric function ε_1 and a substrate of dielectric function ε_3. If the film is thin enough, multiple reflections between the two interfaces become possible, and reflection coefficients (7.1) must be replaced by (7.3)

It makes sense to address the problem to find the reflection coefficients of a slab As we can see in Fig. (7.2), in the most general case, we have a slab of thickness d and dielectric function ε_2 encapsulated between two semi-infinite half-spaces having respectively dielectric function ε_1 and ε_3. Respect to the case described in Fig. (7.1) there is an important difference: there are two interfaces. One between the medium 1 and the medium 2, and one other between the medium 2 and medium 3. As a consequence, if the slab thickness is smaller than the characteristic penetration length of the material, multiple reflections between the two interfaces may occur inside the slab, contributing to the reflection coefficient of the thin film and producing a change compared to Eq.s (7.1). The problem to find the reflection coefficients is solved by the so-called Airy's Formulas [65],[66],[64],[67]:

$$r^s_{123} = \frac{r^s_{12} + r^s_{23} e^{2i\beta}}{1 + r^s_{12} r^s_{23} e^{2i\beta}} \tag{7.3a}$$

$$r^p_{123} = \frac{r^p_{12} + r^p_{23} e^{2i\beta}}{1 + r^p_{12} r^p_{23} e^{2i\beta}} \tag{7.3b}$$

while the transmission coefficients are:

$$t^s_{123} = \frac{t^s_{12}\ t^s_{23}\ e^{i\beta}}{1 + r^s_{12}\ r^s_{23}\ e^{2i\beta}} \tag{7.4a}$$

$$t^p_{123} = \frac{t^p_{12}\ t^p_{23}\ e^{i\beta}}{1 + r^p_{12}\ r^p_{23}\ e^{2i\beta}} \tag{7.4b}$$

where r_{12},r_{23},t_{12},t_{23} are the Fresnel's coefficients of the interface 1-2 and 2-3 respectively, and they can be obtained using Eq.s (7.1a) and (7.1b), while the quantity β, appearing in the argument of the exponential is given by:

$$\beta = k_z^{(2)} d = \frac{2\pi}{\lambda_0} d \sqrt{\varepsilon_2 - \varepsilon_1 \sin^2\theta_i} \tag{7.5}$$

where λ_0 is the wavelength of the impinging light in vacuum.

7.1.1 Anisotropic film

In the previous section we reported the expressions of the reflection coefficients of a semi-infinite material (the Fresnel coefficients, see Eq. (7.1)) and the reflection coefficients of a homogeneous film (the Airy's formulas, see Eq. (7.3)). In both cases we made the assumption of isotropic material (i.e. dielectric tensor of the form $\overleftrightarrow{\varepsilon} = \varepsilon\delta_{ij}$). Since we are interested to understand the link between the reflectance and the dielectric functions calculated in previous chapter (Fig.s (5.5) and (5.10b)), where the in-plane and the out-of-plane component are different, we will need to calculate the reflection coefficients of a film of an anisotropic material. In order to get the reflection coefficients of the anisotropic

slab, we exploited the transfer matrix formalism developed by Schubert in Ref. [68]. This method allows one to calculate the coefficients of an arbitrarily big stack of arbitrarily anisotropic films. By the way, in this section, we will limit ourselves to give the expression for the single anisotropic film (which can be obtained as a particular case of the Schubert's formulas, which are reported in Appendix C). Moreover, we will made the assumptions that the anisotropic film is uniaxial, and with optic axis parallel to the cartesian axis:

$$\overleftrightarrow{\varepsilon}(\omega) = \begin{pmatrix} \varepsilon_{||}(\omega) & 0 & 0 \\ 0 & \varepsilon_{||}(\omega) & 0 \\ 0 & 0 & \varepsilon_{\perp}(\omega) \end{pmatrix} \tag{7.6}$$

We also make the assumption that the two halfspaces surrounding the slab are isotropic, having respectively dielectric function ε_1 and ε_2. Under these hypothesis, the reflection coefficients for the slab will be given by:

$$r_{123}^{anis,p} = \frac{r_{12}^{anis,p} + r_{23}^{anis,p} e^{2i\kappa_p}}{1 + r_{12}^{anis,p} r_{23}^{anis,p} e^{2i\kappa_p}} \tag{7.7}$$

where:

$$\kappa_p = k_0 d \frac{\varepsilon_{||}^{\frac{1}{2}}}{\varepsilon_{\perp}^{\frac{1}{2}}} \sqrt{\varepsilon_{\perp} - \varepsilon_1 \sin^2\theta_i} \tag{7.8}$$

and:

$$r_{12}^{anis,p} = \frac{\varepsilon_{||}^{\frac{1}{2}} \varepsilon_{\perp}^{\frac{1}{2}} \cos\theta_i - \varepsilon_1^{\frac{1}{2}} \sqrt{\varepsilon_{\perp} - \varepsilon_1 \sin^2\theta_i}}{\varepsilon_{||}^{\frac{1}{2}} \varepsilon_{\perp}^{\frac{1}{2}} \cos\theta_i + \varepsilon_1^{\frac{1}{2}} \sqrt{\varepsilon_{\perp} - \varepsilon_1 \sin^2\theta_i}} \tag{7.9}$$

$$r_{23}^{anis,p} = \frac{\varepsilon_3 \sqrt{\varepsilon_{\perp} - \varepsilon_1 \sin^2\theta_i} - \varepsilon_{||}^{\frac{1}{2}} \varepsilon_{\perp}^{\frac{1}{2}} \sqrt{\varepsilon_3 - \varepsilon_1 \sin^2\theta_i}}{\varepsilon_3 \sqrt{\varepsilon_{\perp} - \varepsilon_1 \sin^2\theta_i} + \varepsilon_{||}^{\frac{1}{2}} \varepsilon_{\perp}^{\frac{1}{2}} \sqrt{\varepsilon_3 - \varepsilon_1 \sin^2\theta_i}} \tag{7.10}$$

We remark that, if $\varepsilon_{||} = \varepsilon_{\perp} \equiv \varepsilon_2$, we recover the result of Eq. (7.1).

7.2 Bulk reflectance vs Slab reflectance

Which is the difference between the reflectance of a slab and the reflectance of a semi-infinite block of the same material? In order to answer this question, we start with calculating the reflection coefficients (7.1) and (7.3) modelling our material with a Drude-Lorentz dielectric function. Later in this chapter we will calculate the reflectance spectra using as ingredients the dielectric functions obtained via *ab initio* calculation. Our model dielectric function will be given by:

$$\varepsilon(\omega) = 1 - \frac{\omega_{pl}^2}{\omega^2 - \omega_0^2 + i\frac{\omega}{\tau}} \tag{7.11}$$

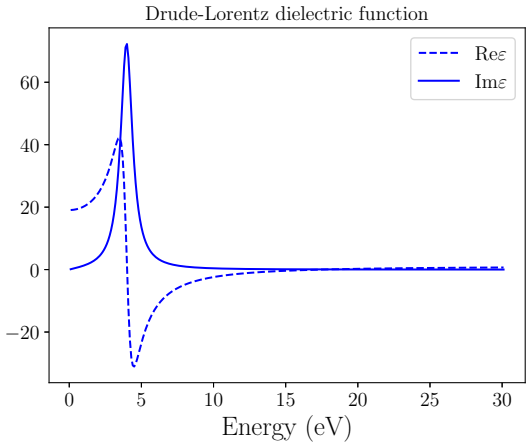

Figure 7.3: The Lorentz dielectric function used to study the reflectance of a thin film. In order to model as accurately as possible the response of silicon, we have chosen as parameters $\omega_0 = 4$ eV, $\omega_{pl} = 17$ eV and $\tau = 10$ eV^{-1}.

In this model, the response of the material depends on the parameters ω_0, ω_{pl}, and τ. The first two parameters are respectively the resonant frequency and the plasma frequency of the system. In order to make our idealised material as similar as possible to silicon (the material the slab described in previous chapters are made of), we have chosen to set:

$$\begin{aligned} \omega_0 &= 4 \quad \text{eV} \\ \omega_{pl} &= 17 \quad \text{eV} \end{aligned} \tag{7.12}$$

while the parameter τ has been set:

$$\tau = 10 \quad \text{eV}^{-1} \tag{7.13}$$

In Fig. (7.3) we report the dielectric function of Eq. (7.11) evaluated for such parameters.

From now on, we will assume that the slab is incapsulated between two semi-infinite spaces of vacuum (i.e. $\varepsilon_1 = \varepsilon_3 = \varepsilon_{vac}$). Under this condition, $r^p_{12} = -r^p_{23} \equiv r$, and the expression for the reflection coefficient of the slab simplifies as:

$$r_{slab} = \frac{r(1 - e^{2i\beta})}{1 - r^2 e^{2i\beta}} \tag{7.14}$$

with r:

$$r = \frac{\varepsilon \cos\theta_i - \varepsilon_{vac}^{\frac{1}{2}} \sqrt{\varepsilon - \varepsilon_{vac} \sin^2\theta_i}}{\varepsilon \cos\theta_i + \varepsilon_{vac}^{\frac{1}{2}} \sqrt{\varepsilon - \varepsilon_{vac} \sin^2\theta_i}} \tag{7.15}$$

and β:

$$\beta = k_0 d \sqrt{\varepsilon - \varepsilon_{vac} \sin^2\theta_i} \tag{7.16}$$

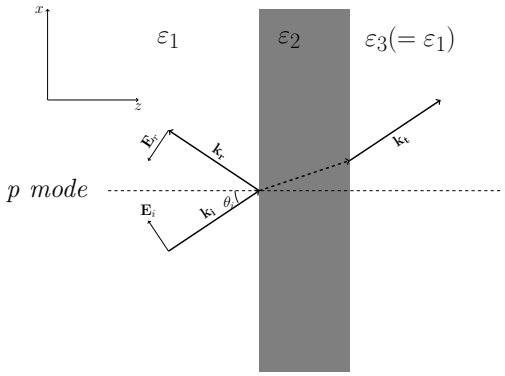

Figure 7.4: Thin film encapsulated between two semi-infinite half-spaces having dielectric constant ε_1

As we have explained in section 7.1, when an electromagnetic wave impinges on the surface of the material, the electric field penetrates in a characteristic length inside the sample, called skin depth. This characteristic length, here labelled as $\delta(\omega)$ is frequency dependent and depends on the dielectric function of the material according the relationship:

$$\delta(\omega) = \frac{\lambda_0}{2\pi \mathrm{Im}(\sqrt{\varepsilon(\omega)})} \tag{7.17}$$

where λ_0 is the wave-length of the impinging light in vacuum. If the slab thickness is of the same order of magnitude (or even smaller) of the skin depth, the wave will penetrate until the back surface of the film. Part of the field will be transmitted through the second interface, and part will be back-scattered, giving rise at multiple reflections which will affect the reflection coefficient of the slab. But if the slab is much thicker than the skin depth (limit $d/\delta \gg 1$), the wave will be suppressed before it can arrive to the second interface. No transmission and no multiple reflections will be possible, and the reflection coefficient of the slab will tend to the reflection coefficient of the semi-infinite material. This can be readily understood via a quick comparison between the expressions (7.1) and (7.3).

7.2.1 Very thick slab limit

We will first compare the reflectance spectra of a semi-infinite block of material and of a very thick slab, both having the dielectric function shown in Fig. (7.3). This calculation is reported in Fig. (7.5a): as we can see, in the limit of very thick slab, the Fresnel formulas (7.1) and the Airy formulas (7.3) produce the same result. Both the curves are characterised by a plateau between the resonant frequency ω_0 and the plasma frequency ω_{pl}. As we can see, in the limit $d \gg \delta$, the exponential $e^{2i\beta}$ tends to zero, and therefore, the expression (7.3) for the reflection coefficient of the film tend to the one valid for the

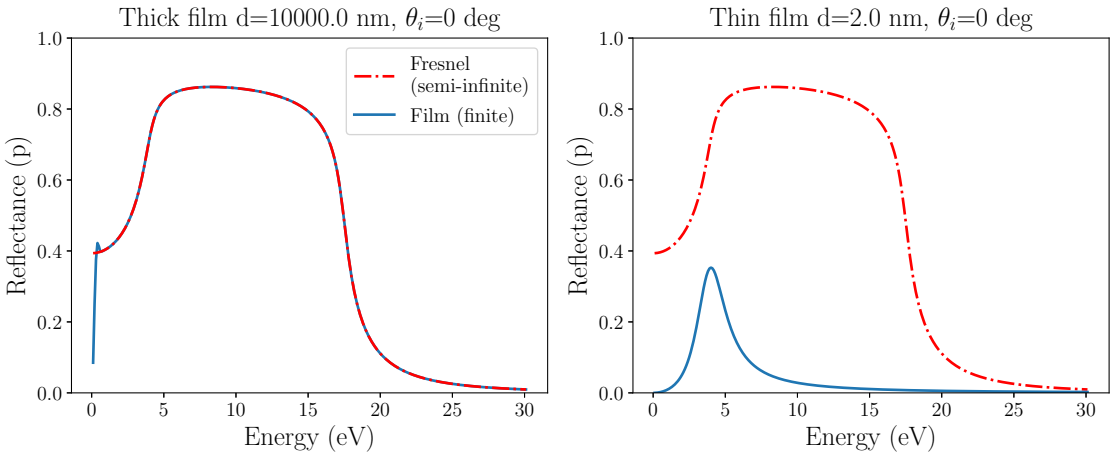

(a) (b)

Figure 7.5: Reflectance at normal incidence of a thick film of thickness $d = 10000$ nm (panel (a)), and of a thin film of thickness $d = 2$ nm (panel (b)), both having the same dielectric function of Eq. (7.11). Compared to the reflectance of the semi-infinite system, which present a plateau between $\omega_0 \sim 4$ eV and $\omega_{pl} \sim 17$, the spectrum of the isolated film contain just one peak located at ω_0.

semi-infinite material:

$$r_{123}^{s/p} \longrightarrow r_{12}^{s/p} \quad \text{for} \quad d \gg \delta \tag{7.18}$$

7.2.2 Very thin slab

In order to study the thin slab limit, we choose to calculate the reflectance of a slab having the dielectric function reported in Fig. (7.3) and thickness $d = 2$ nm. The choice of this value for the thickness is not aleatory : 2 nm is in fact more or less the thickness of the bare silicon slabs studied in the previous chapter. In Fig. (7.5b) we report in blue the reflectance spectrum of this slab, calculated using formula (7.3), while the red dashed line represent the reflectance of the semi infinite material (calculated via the reflection coefficients (7.1)). Both the calculations have been performed at normal incidence (i.e. $\theta_i = 0$). As we can see, the reflectance spectra of the thin film and the one of the semi-infinite material present some remarkable differences. As we can see in Fig. (7.5b), the reflectance spectrum of the thin film is characterised by a single peak located at the resonant frequency ω_0.

In Fig. (7.6) we see that reducing the thickness of the film, the peak of the reflectance spectrum becomes smaller and smaller. This is a very reasonable result from a physical point of view: in the limit of very thin slab, the interaction of the electromagnetic wave with the film will decrease more and more, and in the limit of infinitely thin slab the

incident beam will be completely transmitted (i.e. the reflectance of the system tends to zero).

Let's now go back to our slab of thickness 2 nm. As we already have said, we are interested to study the optical response of the thin film when a component of the electric field orthogonal to the surface is present. In Fig. (7.7) we report (in blue) the reflectance of the slab for several angle of incidence: when the angle of incidence is different from zero, a second peak appears in the spectrum, at the plasma frequency ω_{pl}. Increasing the angle of incidence, the out-of-plane component of the incident electric field increases, and it increases as well the amplitude of the peak at the plasma frequency. On the other hand, when we increase the angle of incidence, the in-plane component of the electric field decreases, and the amplitude of the peak at the resonance frequency ω_0 decreases. In Fig. (7.7) we also report the transmittance T (defined as the square modulus of the amplitude of transmitted field, represented as the orange line), and the absorbance (red line), defined as:

$$A = 1 - R - T \tag{7.19}$$

This quantity represents the number of photons per unit of time which haven't been neither reflected nor transmitted through the slab, and therefore represents the number of incident photons per unit of time which have been absorbed by the slab. As we can see in Fig. (7.7), the absorbance spectra, similarly to the reflectance ones, present two peaks, one at ω_0 and the other one at ω_{pl}. This result may be reason of perplexity. In fact, generally we identify the absorption spectrum of a material with the imaginary part of the dielectric function, and the dielectric function of this slab (see Fig. (7.3)) has only one peak at ω_0. By the way, this is just an apparent contradiction. The dielectric function express an intrinsic property of the material (i.e. its polarisability as function of the total electric field), and it does not depend on the geometry of the sample. The reason because of we are used to identify absorption spectrum and imaginary part of the dielectric function, is that the latter is proportional the power per unit of volume dissipated by the electric field. A peak of the imaginary part of the dielectric function at ω_0, means that the maximum of dissipated power will be when the field oscillates at such frequency, but this does not mean that the absorbance spectrum as it is defined in Eq. (7.19) must have the same shape of the imaginary part of the dielectric function. In the present case, in particular, where the system is constituted by two plane and parallel interfaces, the peak at ω_{pl} can be ascribed to the effect of multiple reflections inside the slab. If the internal reflectivity at ω_{pl} is large enough, the impinging wave, once penetrated inside the slab, will undergo several internal reflections between the two surfaces of the slab, and even if the imaginary part of ε is low at ω_{pl} (i.e. weak absorption), if multiple reflections occur, the optical path of the beam inside the slab will quickly increase, leading to an increase of dissipation. A similar argument (which also allows us to exclude that the peak at ω_{pl} is due to the optical excitation of plasmons) has been used by Economou in Ref. [69]. In this seminal paper, dating from 1969, Economou derived the dispersion relation of surface plasma excitations propagating

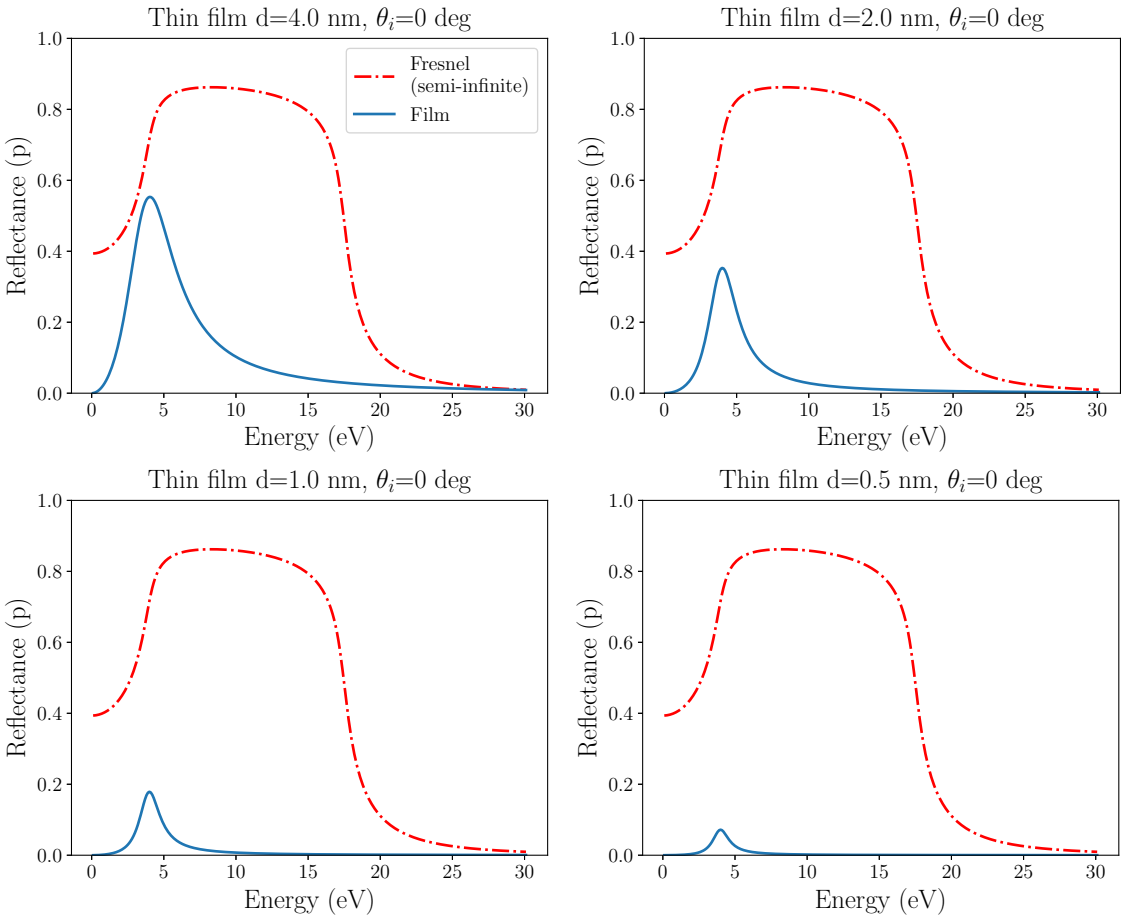

Figure 7.6: Reflectance spectra of a thin film having dielectric function (7.11). All the calculations have been performed at normal incidence ($\theta_i = 0$ degrees), variating each time the thickness of the film: all the spectra feature a peak at $\omega_0 \sim 4$ eV, which increases as the size of the system increases. In order to better illustrate the difference with the semi-infinite system, we also report the Fresnel result (Eq.s (7.1))

in thin metallic films. Using a Drude dielectric function, he found that contrarily to the case of semi-infinite surfaces (where the energy of surface excitations has an upper limit at $\omega_{pl}/\sqrt{2}$), in very thin slabs, they do exist surface charge oscillations which approach the energy of the bulk plasmon ω_{pl}. He also remarked, as we did, that a peak in the reflectance spectrum of the thin film occurs at the bulk plasma frequency, for p polarisation and non normal incidence. However this does not mean, as appearances may suggest, that this peak is due to the excitation of surface (or bulk) plasmons by the impinging light: as shown in Fig. (7.8) (reproduced from Ref. [69]), the dispersion line of surface plasmon never intersect the dispersion line of photon, so that conservation of energy and momentum forbid all processes where just one photon is absorbed and just one plasmon is created (or vice-versa). Because of that, Economou argued that the peak observed at ω_{pl} in the spectrum of the thin film cannot be related to the creation of elementary excitations, but must be ascribed to the total reflection condition which is verified at ω_{pl}. Our results (Fig. (7.7)) show that actually the condition of total reflection is not fulfilled. Indeed the transmittance is larger than reflectance, leading to a substantial absorbance. It is nevertheless clear, by comparing the reflectance resulting from a semi-infinite material (Fig. (7.5a)) that the inclusion of the reflectance on the second interface is at the origin of the appearance of the peak at $\omega = \omega_{pl}$.

In order to better understand the reflectance spectra of the thin film, we studied Eq. (7.14) in the limit $d/\lambda_0 \ll 1$. In this limit, we can expand the exponential $e^{2i\beta}$ as power series of β. In this limit Eq. (7.14) simplifies as:

$$\begin{aligned} r_{slab} &\approx \frac{-2ik_0d[\varepsilon\cos^2\theta_i - 1 + 1/\varepsilon\sin^2\theta_i)]}{4\cos\theta_i - 2ik_0d[\sqrt{\varepsilon}\cos\theta_i - \sqrt{1-1/\varepsilon\sin^2\theta_i}]^2} \\ &= \frac{-2ik_0d[(\varepsilon-1)\cos^2\theta_i + (1/\varepsilon-1)\sin^2\theta_i)]}{4\ \cos\theta_i - 2ik_0d[\sqrt{\varepsilon\cos^2\theta_i} - \sqrt{1-1/\varepsilon\sin^2\theta_i}]^2} \\ &= \frac{-2ik_0d[(\varepsilon-1)\cos^2\theta_i + (1/\varepsilon-1)\sin^2\theta_i)]}{4\cos\theta_i - 2ik_0d[\sqrt{\cos^2\theta_i + (\varepsilon-1)\cos^2\theta_i} - \sqrt{\cos^2\theta_i - (1/\varepsilon-1)\sin^2\theta_i}]^2} \end{aligned} \tag{7.20}$$

which, after some manipulations, becomes:

$$r_{slab} \approx \frac{-2ik_0d[(\varepsilon-1)\cos^2\theta_i + (1/\varepsilon-1)\sin^2\theta_i)]}{4\cos\theta_i - 2ik_0d[(\varepsilon-1)\cos^2\theta_i - (1/\varepsilon-1)\sin^2\theta_i] - 4ik_0d\cos^2\theta_i + 4ik_0d\cos\theta_i\sqrt{\varepsilon-\sin^2\theta_i}]} \tag{7.21}$$

This equation shows clearly the reason why the spectrum contains one peak a ω_0 (resonance of ε) and another one at $\sqrt{\omega_0^2+\omega_{pl}^2}$ (resonance of $1/\varepsilon$). The angular dependence of Fig. (7.7) is also explained by Eq. (7.21).

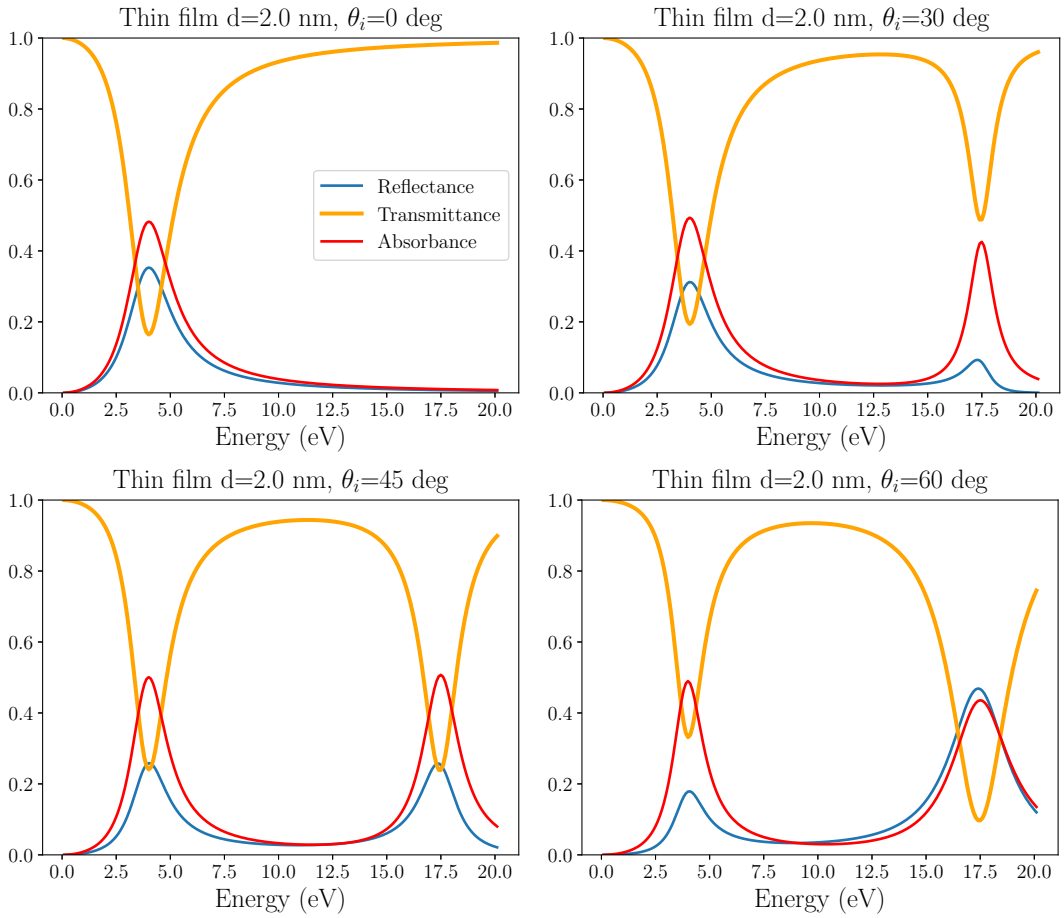

Figure 7.7: Comparison of reflectance, transmittance, and absorbance spectra of a thin film of thickness $d = 2$ nm, for p-polarisation, at several angle of incidence. At normal incidence, the spectra contain a single peak of absorbance and reflectance at $\omega_0 \sim 4$ eV, while it is almost completely transparent in the remaining part of the spectrum. For non-normal incidence, a second structure appears at $\sqrt{\omega_0^2 + \omega_{pl}^2} \sim 17.5$ eV. As the angle of incidence is increased, the reflectance peak at ω_0 decreases, while the peak at ω_{pl} increases its amplitude.

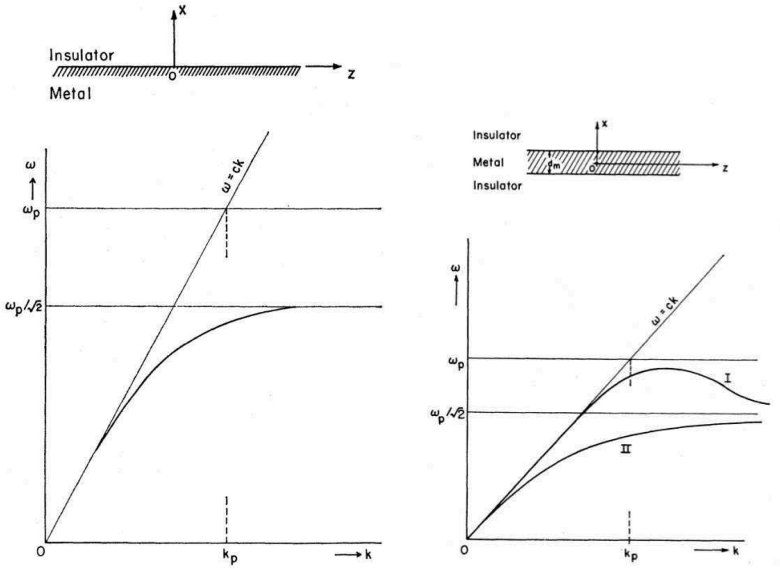

(a) (b)

Figure 7.8: Dispersion relation of surface plasmons (reproduced from Ref. [69]). Panel (a): semi-infinite system. Panel (b): thin metallic film between two dielectric half-spaces.

7.3 Vacuum effect on the reflectance spectrum

As we have seen in Chapter 4, when one performs a calculation of the dielectric function of a slab within the standard supercell approach, the result of the calculation will be an effective dielectric function where the response of the slab is averaged with the response of the vacuum inside the supercell. This has dramatic implications mainly for what concerns the out-of-plane component of the dielectric function: when the vacuum inside the supercell is increased, the peak of the out-of-plane component of the dielectric function is quenched and pushed towards the plasma frequency of the system. In this section , we want to investigate how this spurious effect of vacuum can affect the calculation of reflection coefficients. In order to approach this problem, we start with constructing an effective slab constituted by a layer of matter of thickness d having dielectric function ε of Fig. (7.3), and by a layer of vacuum of equivalent thickness (see Fig. (7.9a)). The effective medium dielectric function of the system vacuum+matter will be :

$$\varepsilon_{||}^{eff} = \frac{d_{vac}\varepsilon_{vac} + d\varepsilon}{d + d_{vac}} \tag{7.22}$$

for the in-plane component, and it will be:

$$\frac{1}{\varepsilon_{\perp}^{eff}} = \frac{1}{(d + d_{vac})}\left(\frac{d}{\varepsilon} + \frac{d_{vac}}{\varepsilon_{vac}}\right) \tag{7.23}$$

for the out-of-plane component. We report this effective dielectric function in Fig. (7.9b), where we compare it with the Drude-Lorentz dielectric function of the "original" slab (which has $d = 2$ nm and dielectric function ε). So in the end we will have an effective slab having effective thickness $d^{eff} = 2d = 4$ nm, and effective dielectric function ε^{eff} We stress out that this effective slab is by construction anisotropic (i.e. $\varepsilon_{||}^{eff} \neq \varepsilon_{\perp}^{eff}$). Using the formalism outlined in Sec. (7.1.1), and making the assumption that the two half-spaces surrounding the slab are occupied by vacuum, we obtain the following expression for the reflection coefficients:

$$r_{slab}^{eff} = r^{eff} \frac{1 - e^{2i\beta^{eff}}}{1 - (r^{eff})^2 e^{2i\beta^{eff}}} \tag{7.24}$$

with r^{eff}:

$$r^{eff} = \frac{(\varepsilon_{\perp}^{eff}\varepsilon_{||}^{eff})^{\frac{1}{2}} \cos\theta_i - \varepsilon_{vac}^{\frac{1}{2}} \sqrt{\varepsilon_{\perp}^{eff} - \varepsilon_{vac} \sin^2\theta_i}}{(\varepsilon_{\perp}^{eff}\varepsilon_{||}^{eff})^{\frac{1}{2}} \cos\theta_i + \varepsilon_{vac}^{\frac{1}{2}} \sqrt{\varepsilon_{\perp}^{eff} - \varepsilon_{vac} \sin^2\theta_i}} \tag{7.25}$$

and β^{eff}:

$$\beta^{eff} = k_0 d^{eff} \left(\frac{\varepsilon_{||}^{eff}}{\varepsilon_{\perp}^{eff}} \right)^{\frac{1}{2}} \sqrt{\varepsilon_{\perp}^{eff} - \varepsilon_{vac} \sin^2\theta_i} \tag{7.26}$$

In Fig. (7.10) we report the calculation of the reflectance of the effective slab, and we compare with the reflectance of the "original" slab (having thickness $d = 2$ nm and dielectric function ε). The result is quite remarkable: as we can see in Fig. (7.10), the reflectance spectra of the effective slab and the original slab overlay almost perfectly. We want to stress out that these two systems are different in all respects: they have different thickness, and as we can see in Fig. (7.9b) they also have a very different dielectric function. This result seems to suggest that the effective medium theory of the slab with vacuum, even if changing quite dramatically the dielectric function, does not affect the reflectance of the system, which is the observable which is actually measured in the experiment. In the next section we will investigate the limit of validity of the latter statement.

7.3.1 Limit of validity of the EMT with vacuum

In the previous section we calculated the reflectance spectrum of an effective system formed by a layer of matter and a layer of vacuum, and we have seen that they are in almost perfect agreement with the reflectance spectrum of the thin film of matter alone. On one side, this seems to suggest that averaging the dielectric function of the slab with vacuum is not that problematic, because even if ε^{eff} and ε are very different , both of them allow to obtain the same reflection coefficient (which is the quantity which is truly measured in an optic experiment). On the other hand, this equivalence between the effective slab mixed with vacuum and the slab alone can be verified only within a certain limit of validity. In order to show that, let's consider the relatively simple case of normal incidence. Let's suppose

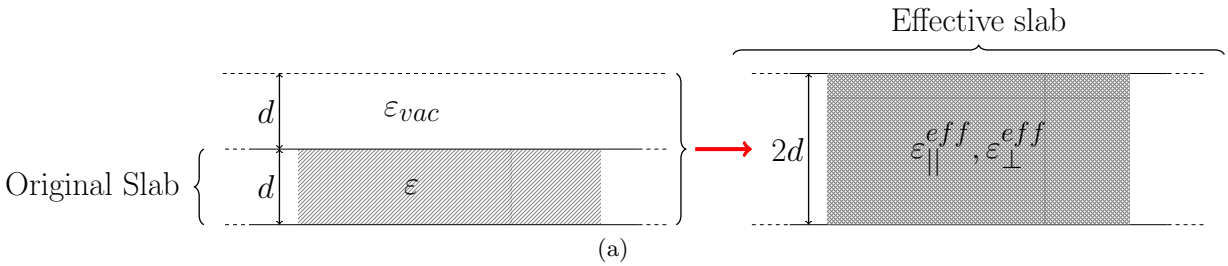

(a)

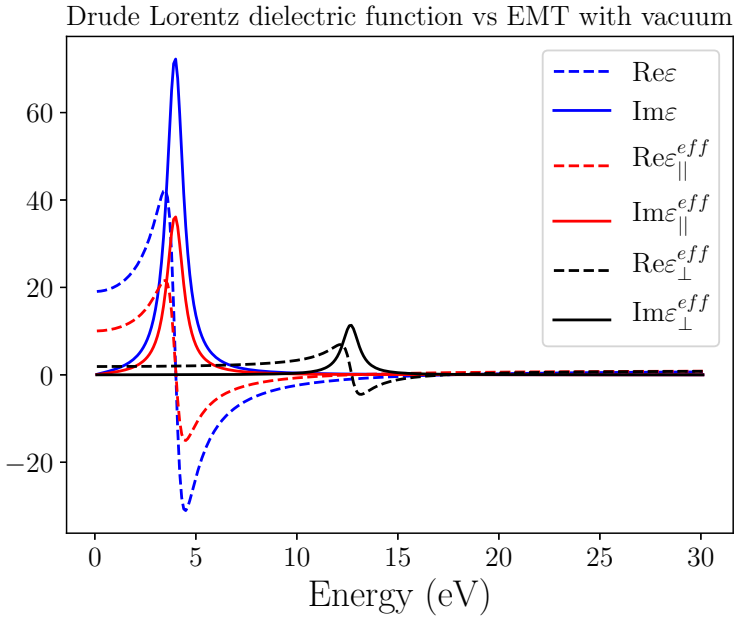

(b)

Figure 7.9: Panel (a): effective slab formed by a layer of matter and a layer of vacuum, both having thickness d. Panel (b): dielectric function of the effective slab (in red and black respectively the in-plane and out-of-plane component). The blue line represent the dielectric function of the "original" (isotropic) film

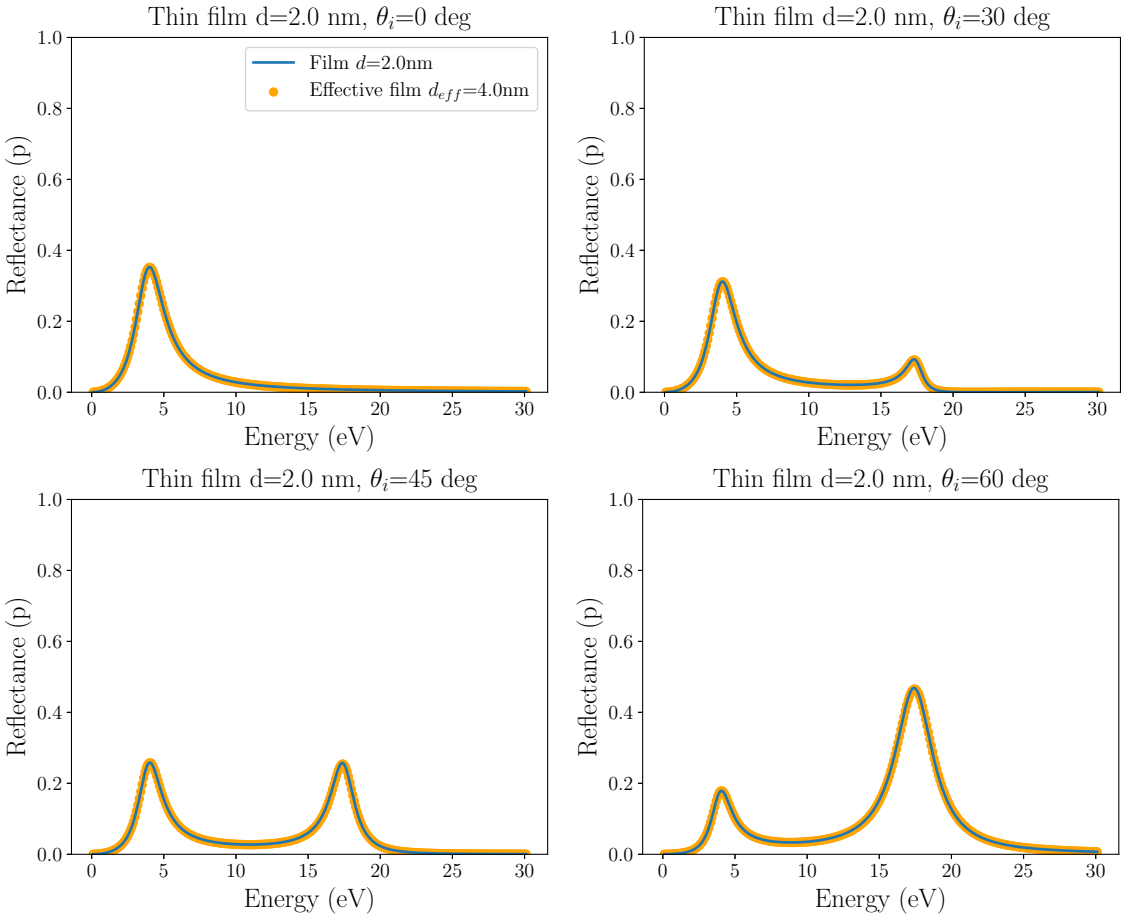

Figure 7.10: Comparison of the reflectance spectrum of a thin film of thickness $d = 2$ nm, and the reflectance spectrum of an effective film consisting of vacuum and matter mixed in equal parts. Despite the differences in the dielectric functions of the two systems (reported in Fig. (7.9b)) the spectra overlap perfectly.

to gradually increase the parameter d, which define the thickness of the slab alone, and also the thickness of the effective slab, via the relationship $d^{eff} = 2d$. We want to compare again the reflectance spectrum of the effective slab mixed with vacuum, having thickness d^{eff} and dielectric function ε^{eff}, with the one of the slab alone, having thickness d and dielectric function ε (see Fig. (7.10)). Since we are in normal incidence, and the only component of the electric field is the one parallel to the surface, the reflection coefficient of the effective slab will be given by:

$$r_{slab}^{eff} = r^{eff} \frac{1 - e^{2i\beta^{eff}}}{1 - (r^{eff})^2 e^{2i\beta^{eff}}} \tag{7.27}$$

with r^{eff}:

$$r^{eff} = \frac{(\varepsilon_{||}^{eff})^{\frac{1}{2}} - \varepsilon_{vac}^{\frac{1}{2}}}{(\varepsilon_{||}^{eff})^{\frac{1}{2}} + \varepsilon_{vac}^{\frac{1}{2}}} \tag{7.28}$$

In the limit of thick slab ($d \gg \delta$), the exponential goes to zero, and the reflection coefficient of the effective slab become simply:

$$r_{slab}^{eff} \longrightarrow r^{eff} \tag{7.29}$$

As we have seen in the previous section, and as we can see in Fig. (7.9), the in-plane component of the dielectric function of the effective system (red lines) verifies the plasmon condition $\mathrm{Re}\varepsilon_{||}^{eff} = \mathrm{Im}\varepsilon_{||}^{eff} = 0$ at lower energies compared to the dielectric function of the slab alone (blue lines). This means that the expression (7.29) (which is nothing but the Fresnel formula (7.1b) evaluated for $\varepsilon_1 = 1$ and $\varepsilon_2 = \varepsilon_{||}^{eff}$) will be characterised by a plateau between ω_0 and ω_{pl}^{eff}, and therefore will be necessarily different from the spectrum of the true slab, which in the limit $d \gg \delta$ is characterised by a plateau between ω_0 and ω_{pl}. In Fig. (7.11), I report the calculation of the reflectance of the effective slab and of the slab alone in the limit $d \gg \delta$. As we can see in the figure, contrarily to what we have observed in Fig. (7.10) for the case of very thin film, the two spectra are remarkably different. This proofs that the effective slab mixed with vacuum produces the same reflection coefficient than the true slab provided that the slab is not too thick. In the limit of thin slab ($d^{eff} = 2d \ll \delta$), it is possible to proof that the reflection coefficients of the effective and the original slab converge to the same limit (see Appendix C).

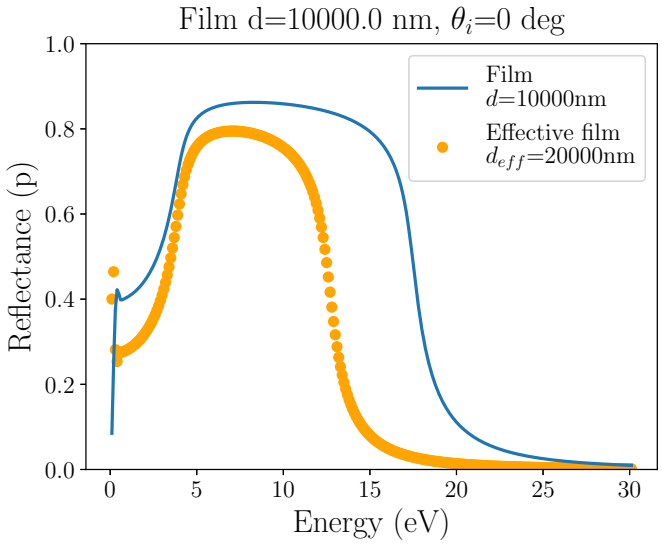

Figure 7.11: Reflectance of the effective and of the original film in the limit of large thickness. Increasing the size of the system, the agreement of the two systems is lost.

7.4 Solution of the L_{mat} problem

At the end of the Chapter 5, we presented what we called the L_{mat} problem. As we have shown in Section 5.4.1, the average procedure which has to be performed in order to obtain the macroscopic dielectric function, requires to define the thickness of the slab. This quantity, by the way, is not defined in a clear way, and, especially in the case of thin slabs (constituted by relatively few atomic layers), this uncertainty impacts quite dramatically the calculation of the absorption spectra, which change abruptly in amplitude and energy range according the chosen value of L_{mat} (see Fig. (5.10b)). This is a problem which is strictly related with the vacuum problem that we have discussed in Chapter 4. As we have seen in section 5.4.1, if we increase enough the value of L_{mat}, we obtain again the effective medium theory with vacuum: in a certain way, the problem to determine the good value of L_{mat} could be reformulated as the problem to establish where the matter finishes and the vacuum starts. On the other hand, in the previous section, we have studied the response of an effective slab constituted by a layer of matter and a layer of vacuum, having an effective dielectric function ε^{eff} and effective thickness d^{eff}, and we have seen that the reflectance of this system (which is the quantity which is actually measured in an optics experiment), in the limit of thin slab, is exactly the same of the layer of matter alone. This suggests the idea that the dielectric functions reported in Fig. (5.10b), may be interpreted as the effective dielectric functions of several effective slabs, each of them having a different effective thickness (i.e. each of them mixed with a different amount of vacuum).

In order to corroborate this hypothesis, I calculated the reflectance spectra of a set of slabs having each of them, as thickness and dielectric function, respectively the value of L_{mat} and $\varepsilon(L_{mat})$ reported in Fig. (5.10b). The result is reported in Fig. (7.12). As we can see in the figure, all the reflectance spectra overlay perfectly, despite they have been calculated using slabs having not only different thicknesses, but also very different dielectric functions. This solve the so-called "L_{mat}-problem" that we presented in the previous chapter, and that we recalled in the beginning of this section. As we explained, there is not a clear way to define the thickness of the system (the parameter L_{mat}) and therefore even the macroscopic dielectric function results affected by this uncertainty, being not a clear choice for the space region where the macroscopic average procedure has to be performed. By the way, the calculation shown in Fig. (7.12) solves our problem: provided that the thickness of the slab is much smaller than the wave-length of the impinging light, one finds that the uncertainty on L_{mat} does not affect neither the reflectance, nor the transmittance spectra, which are the quantity that are measured in a spectroscopy experiment. We want to stress out another time that the *microscopic* quantities of interest (like for example the response function $\chi(\mathbf{r}, \mathbf{r}', \omega)$, or the induced densities and fields reported in Fig.s (5.8) and (5.9)) are unambiguous and well defined. The arbitrariness on the choice of L_{mat} is introduced only at the moment to perform the macroscopic average procedure. This actually comes from the fact that for a 2D object, the macroscopic average has no meaning. Only the integration of the microscopic functions, where the limit of integration can be extended without consequences, is the quantity of interest. It results to be proportional to the thickness without requiring its definition. One remarks that in that case no inversion of the quantities can be done. Nevertheless, to describe a surface, or a semi-infinite object, we are back to the definition of the size of the unit cell.

Performing the macroscopic average procedure with an arbitrary choice of L_{mat} is an operation that in some way consists to replace the true slab (which does not have a well defined thickness, does not have sharply terminated edges, and is inhomogeneous at the microscopic scale) with an ideal slab (which is perfectly homogeneous, has sharply terminated edges, and therefore has a well defined thickness). But, because of the arbitrariness on the choice of L_{mat}, multiple choices are possible for this ideal slab, all of them having different thickness and macroscopic dielectric function, but all of them reproducing the same spectroscopic observables (provided that $L_{mat} \ll \lambda_0$). It is interesting that the same arbitrariness, in some way, also appears on the experimentalist's side. As it is well known, spectroscopic ellipsometry is often exploited in order to measure the thickness and the optical constants of adsorbed films. But when experimentalists do that, or they assume to know the dielectric function (and from reflectance measurements they deduce the thickness of the sample) or they assume to know the thickness of the adsorbed film, and from the reflectance measurement they deduce the dielectric function. Only making further hypothesis on the nature of the sample (i.e. isotropy, non absorbing film, resonance energies etc...) it is possible to extract at the same time optical constants and thickness of the film from the reflectance spectra (see for exemple Hans Arwin in Ref. [70]).

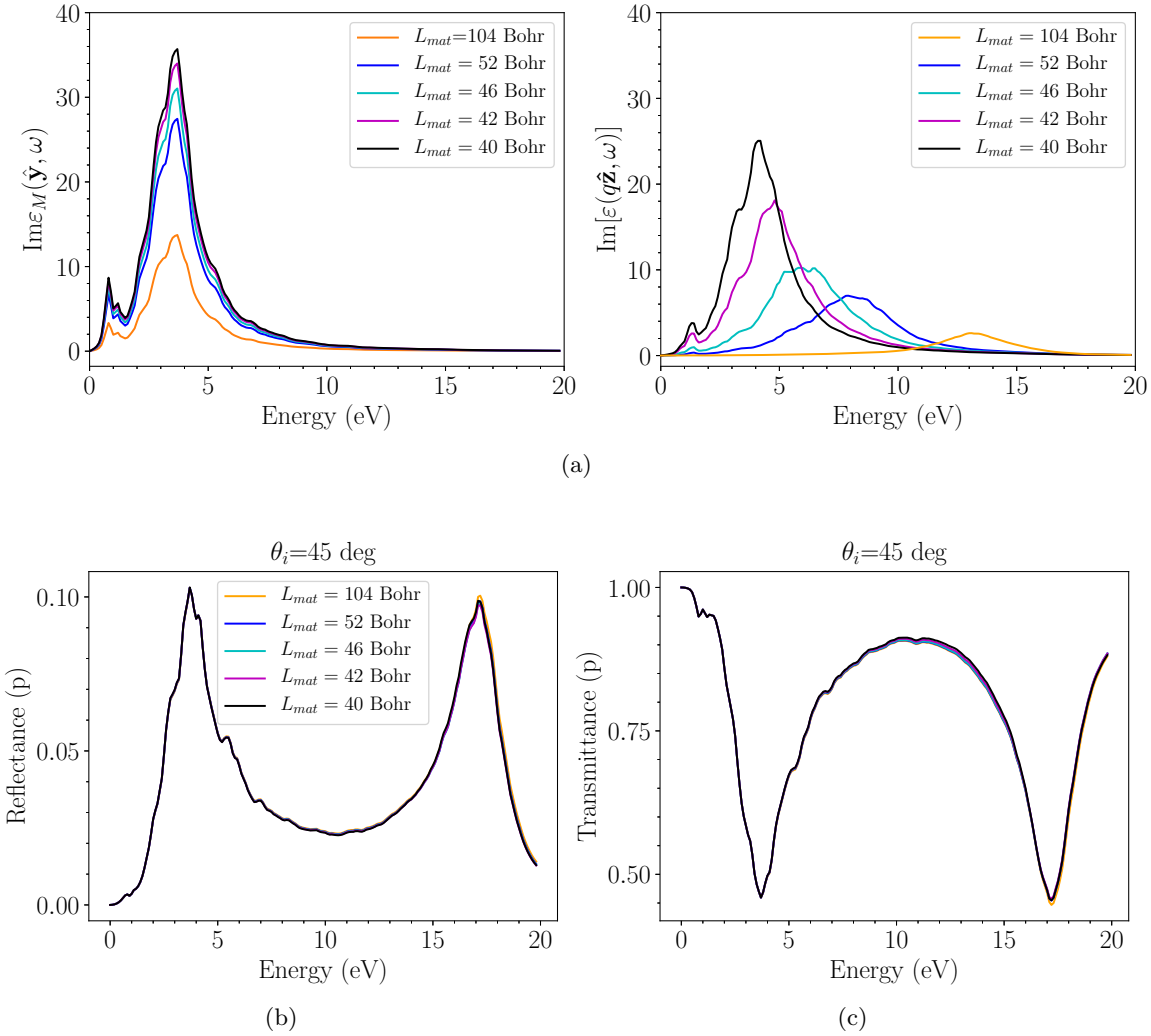

Figure 7.12: In this figure, the calculation of the reflectance spectrum of the silicon slab is reported. In panel (a), I report the dielectric function calculated within the mixed-space approach, performing each time the average procedure over a region of space of different size. All these dielectric functions can be considered as the dielectric functions of effective slab having different thickness L_{mat}, each of them containing a different proportion of vacuum and matter. In panels (b) and (c), I report the respectively reflectance and transmittance spectra calculated for all these effective slabs. All the spectra overlap perfectly.

7.5 Conclusions

Through this chapter the link between the dielectric function -which is the quantity that we calculate in our *ab initio* formalism - and the reflectance spectrum -which is the quantity which is measured in a real spectroscopy experiment - has been done. As we have seen in Chapter 4, when the dielectric function is obtained in the standard supercell approach, the presence of vacuum in the cell severely affects the result, producing a strong quenching and blueshift of the spectrum. On the other hand, when calculations are performed within the mixed space approach - which allows us to eliminate the interaction between replicas - another problem arises: even if this technique allows one to perform the macroscopic average over a space region of arbitrary length, it turns out that there is not a clear way to define the size of the slab. This uncertainty - which through this work we called the "L_{mat} problem" - reflects in a dramatic way on the calculation of the dielectric function (see Fig. (7.12a)). The solution of this problem is the main result of the present chapter: as shown in Fig. (7.12b), even if the macroscopic average operation is ambiguously defined, the reflectance spectra - which are the true observable of the system - are not, and all the macroscopic dielectric functions calculated according different values of L_{mat} produce the same result. This comes from the fact that reflectance and transmittance spectra appear to be a linear combination of $\varepsilon - 1$ and $1/\varepsilon - 1$ (see Eq. (7.21)), which are the quantities that are a scaled in the so-called effective medium theory with vacuum. Fig. (7.12) shows that the scaling factor exactly compensates.

Moreover, these results evidence that the reflectance, transmittance, and absorbance of a 2D object exhibit a peak at ω_0 (associated with the in-plane excitation), and a peak at $\sqrt{\omega_0^2 + \omega_{pl}^2}$ (associated with the out-of-plane excitation). These two features are present in the $\chi_{\rho\rho}$ response functions that we have calculated in the mixed space approach and also in the Lorentz model. These two approaches are based on longitudinal framework. It seems that they also give the correct spectrum for the absorbance spectrum, which should refers to a purely transverse phenomenon. Using $\chi_{\rho\rho}$ to access to absorption spectrum is currently done for 0D objects [71][72][73][74]; here we show that it is also valid for 2D systems. This result is remarkable since it allows to calculate a transverse response from a longitudinal one in extended systems in a geometry completely different to the one used by Ehrenreich [28]. This finding add an important block to the understanding of the response of an isolated object, clarifying which are the relevant quantities to describe the optical properties of a thin film, and ideally closing the circle opened by Tancogne-Dejean during its thesis [20], which approached for the first time the vacuum problem. Next chapter will be devoted to the study of nonlinear optical properties of functionalised slabs.

Chapter 8

Second Harmonic Generation from functionalised surfaces

During previous chapters we have discussed in detail how to calculate the linear response of slabs, because we have seen that defining L_{mat} larger than the extension of atomic positions has the consequence to shift the $\varepsilon_{M\perp}$ off to the silicon absorption resonance. To calculate surface properties we will adopt L_{mat} equal to the extension of atomic positions. This is the solution which allows one to recover the induced electric field of the 3D object, as well as preserving the surface states. It also confirms the choice made in the previous thesis [20]. In this chapter, we present the calculation of the second harmonic spectra for silicon surfaces functionalised with nucleobases. As we have discussed in Chapter 1, inside a centrosymmetric material, the second harmonic generation can take place just in the neighbourhood of the surface, where, because of the cut, the electronic wave-functions loose their symmetry. Contrarily to the case of linear spectroscopies, where the impinging beam penetrates inside the material in a depth comparable to the wave-length of the incoming light, in a surface second harmonic generation (SSHG) experiment the second order signal takes place in a region of just few atomic layer of thickness.

Therefore, the SHG is an extremely well suited tool for the study of surface properties of material having inversion symmetry, and it has been extensively used to characterise adsorbed overlayers on silicon surfaces, both experimentally [75],[76],[77],[78], [79] and theoretically [80][81]. In this thesis, we will investigate how the adsorption of nucleobasis change the second order response of the Si(001) surface. We will concentrate on three aspects. In particular, we want to quantify the sensitivity of the SSHG upon the adsorption of nucleobasis, i.e. we want estimate the accuracy of the SHG to discriminate between the bare and the functionalised surface. The second aspect that we want to quantify, is the chemical selectivity, i.e. the accuracy of the SHG in distinguishing different adsorbed specimens (in our case, between three different nucleobases). Finally, we will also investigate the dependence of the second harmonic signal on the adsorption geometry. As we have

seen in Chapter 1, HREELS measurements performed on Uracil-functionalised surfaces [41] allowed to establish the presence of covalent Si-O bond, but this alone is not enough to completely clarify the adsorption configuration. Due to its unique sensitivity to the geometry of the system, SSHG could be a reliable way to discriminate between different adsorption configurations.

Before to the aforementioned goals, in this chapter we will also study how much surface sensitive is SHG of silicon surfaces (i.e. we will try to evaluate the thickness of the SHG active layer). This result will be obtained via reciprocal and real space calculations.

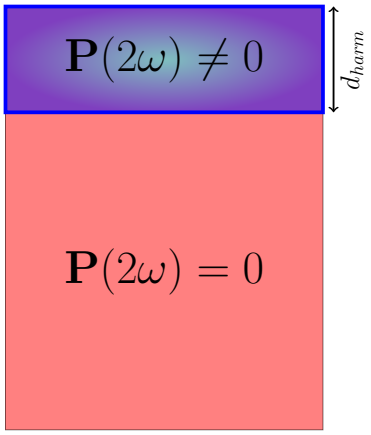

Figure 8.1: Sketch of the second order polarisation induced in a centro-symmetric material.

8.1 Numerical details

In this section, we present the numerical details of the calculations that we have performed on our slabs. For all the studied slabs, the calculation of the Kohn-Sham wave functions has been performed in a self-consistent way via ABINIT code [50]. Core electrons have been modelled via norm conserving Trouillier-Martins pseudopotentials [25], while for the exchange-correlation potential the PBE approximation has been chosen [51]. For all the calculations, an energy cut-off E_{cut} of 20 Hartree has been used for the plane waves basis set. After having obtained the Kohn-Sham wave-functions, the second order susceptibility has been obtained via 2light code [29],[19]. In order to converge the second order susceptivity, we proceeded in the following way: first of all, we calculated the spectra at the independent particle level of the theory, using a relatively small Monkhorst-Pack grid [82] (8 off-symmetry k-points). Then, we gradually increased the values of the parameters `nbands` (which controls the number of bands included in the calculation), `npwwfn` (which controls the number of plane-waves included in the calculation of matrix elements), and `npwmat` (which controls the size of the $\chi_{\mathbf{G_1 G_2 G_3}}$ matrix). Finally, we carefully converged the spectra in the number of k-points, gradually increasing the size of the Monkhorst-Pack grid used for the calculation (the details about this standard convergence procedure can be found in Appendix D).

8.2 Active SHG layer

8.2.1 Independence of the two surfaces

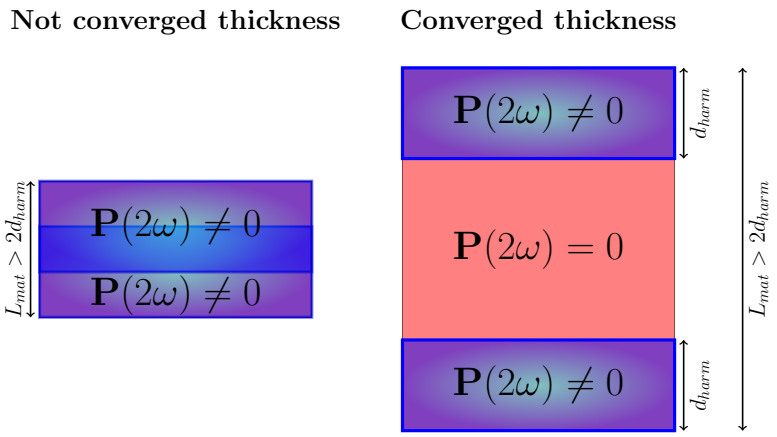

Figure 8.2: Second order polarisation induced in a slab of centrosymmetric material. Left: non-converged thickness, right: converged thickness.

A point of particular importance, when one tries to model the response of a surface using a slab, is that the slab must be thick enough in order to avoid interaction between its two faces. In fact it is true, as we have previously explained, that SHG from silicon is a purely surface phenomenon, in the sense that the second order polarisation $\mathbf{P}(2\omega)$ is confined in a harmonically active layer near to the interface between matter and vacuum. By the way, if the slab is not thick enough (i.e. smaller than two times the size of the harmonically active layer, see Fig. (8.2)), the two faces of the slab cannot be considered truly isolated, and the spectra will be affected by the spurious interaction between the two surfaces. In order to establish how thick must be the slab in order to isolate its two surfaces, we performed several calculations of the $\chi_M^{(2),S}$, increasing each time the thickness of the slab. As prototypical system, we have chosen the silicon slab functionalised with Thymine, assuming that the thickness of the harmonically active layer will be roughly the same for the surfaces functionalised with the other molecules. Indeed, these molecules are very similar, and both experimental [41] and theoretical [47],[45],[46] have suggested that they may have similar adsorption geometry.

Five different slabs have been used in this study (see Fig. (8.3)), containing respectively 8 silicon layers (corresponding to $\sim$ 20 Bohr), 16 silicon layers ($\sim$ 40 Bohr) , 24 silicon layers ($\sim$ 60 Bohr), 32 silicon layers ($\sim$ 80 Bohr) and 40 silicon layers ($\sim$ 100 Bohr). Due to the increasing computational cost, the relaxation of atomic positions has been performed just for the smallest of these slabs. The other fours has been obtained opening the first one and adding in the middle blocks of silicon in their unrelaxed bulk positions.

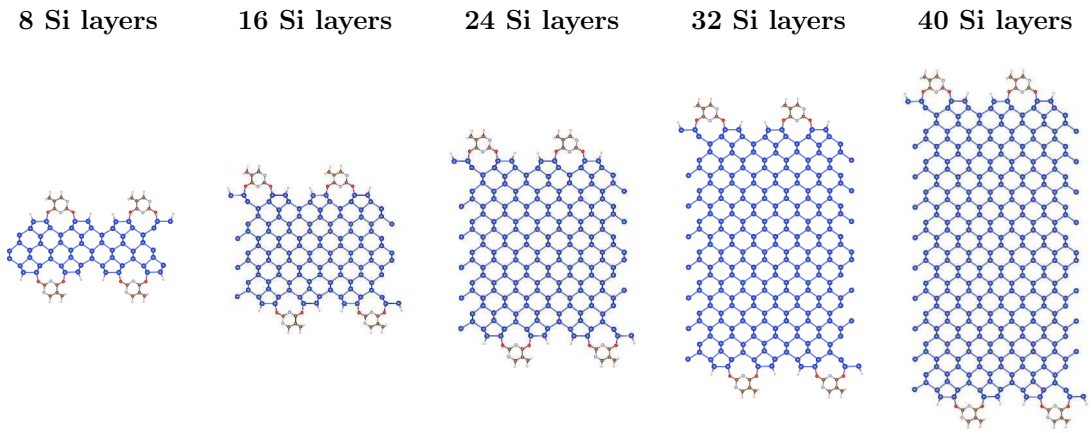

Figure 8.3: Silicon+Thymine slabs used to study the dependence of spectra on the thickness.

In Fig. (8.4), I report the zzz component of the $\chi^{(2),S}_M$, calculated in Independent Particle Approximation for each of the five aforementioned slabs. We found that, increasing the thickness of the silicon, produces a shift of the main peak at lower energies. As we can see in Fig.(8.4) in fact, the main structure of the spectrum is located at ~ 3 eV for the thinnest of the studied structures. When we increase number of Silicon layers, the spectrum is gradually red-shifted, and its main peak moves towards a energy of 2 eV, where it stops in correspondence of a thickness of 24 Silicon layers. If we further increase the thickness of the slab, we see that the shape of the spectrum is converged, but the amplitude of the peaks start to decrease. However, this should not be surprising, since the IPA spectrum is nothing but the macroscopic average of the second order independent particle response function. This quantity expresses the second order polarisation averaged on the supercell:

$$\begin{aligned}\chi^{(2)}_{0,\alpha\beta\gamma} &= \\ &= \frac{i}{2\Omega\omega^3}\sum_{n,n',n''}\sum_{\mathbf{k}}^{BZ}\frac{\langle n\mathbf{k}|\mathcal{P}^{\alpha}|n'\mathbf{k}\rangle\big(\langle n'\mathbf{k}|p^{\beta}|n''\mathbf{k}\rangle\langle n''\mathbf{k}|p^{\gamma}|n\mathbf{k}\rangle+\langle n'\mathbf{k}|p^{\gamma}|n''\mathbf{k}\rangle\langle n''\mathbf{k}|p^{\beta}|n\mathbf{k}\rangle\big)}{E_{n\mathbf{k}}-E_{n'\mathbf{k}}+2\omega+2i\eta} \\ &\times\left[\frac{f_{nn''}}{E_{n\mathbf{k}}-E_{n''\mathbf{k}}+\omega+i\eta}+\frac{f_{n'n''}}{E_{n''\mathbf{k}}-E_{n'\mathbf{k}}+\omega+i\eta}\right]\end{aligned} \tag{8.1}$$

In the case of a slab of centrosymmetric material, as we already have explained, the contribution to the second order polarisation can come just from the harmonically active layer in proximity of the surface. Once the thickness of the slab is large enough to isolate the two surfaces (i.e. the slab thickness is larger than twice the extension of the harmonically active

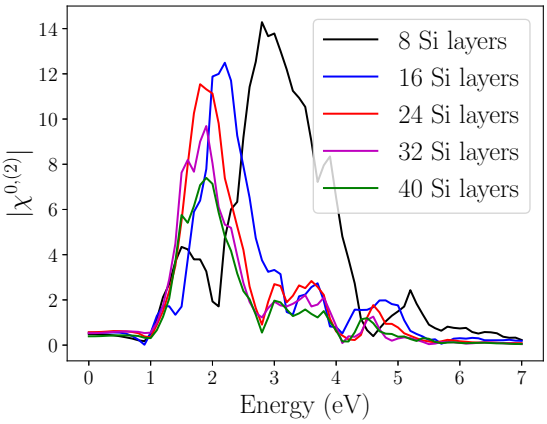

Figure 8.4: Convergence of the IPA second order susceptibility as a function of silicon thickness.

layer), adding new blocks of silicon in the middle of the slab will not change the integral of the second order polarisation, and therefore the shape of the spectrum will be unchanged. However, increasing the thickness of the slab will lead to an augmentation of the size of the supercell, and this, due to the prefactor $1/V$ in Eq. (8.1), will result in the application of a scaling factor to the spectrum. So, in a sense, the fact that the spectrum changes of a scale factor when the thickness of the slab is increased, is a clue that the convergence in the slab's thickness has been reached, and that the two surfaces are isolated. In order to conclude, we judge that 24 Silicon layers represent the best compromise between feasibility of the calculations and convergence of the spectra in the thickness of the slab. A similar conclusion has been reached by Tancogne-Dejean [20], (which in its thesis studied SHG from bare and hydrogen covered silicon surfaces).

8.2.2 The thickness of the SSHG active layer

In the previous section, we presented the IPA spectra of slabs functionalised with thymine, each of them having a different thickness. As we have explained, the spectra converge when the thickness of the slab is ~ 2 times larger than the depth of the harmonically active layer (see Fig. (8.2)) As shown in Fig. (8.4), the shape of the second harmonic spectrum is converged at $L_{Si} \sim 60$ Bohr, which seems to suggest that the size of the harmonically active layer is $d_{harm} \sim 30$ Bohr. By the way, this estimation is somehow indirect, since it has been obtained via the analysis of a quantity (the $\chi_M^{0(2)S}$) which comes from a macroscopic average procedure. Estimate the extension of the harmonically active layer is a very important task, since the extension of such layer gives a direct measurement of how surface sensitive are the second harmonic spectra. In this section, we will give an estimation of d_{harm} based on the analysis of the microscopic second order induced density $\delta\rho^{(2)}(\mathbf{r})$ (a quantity which is

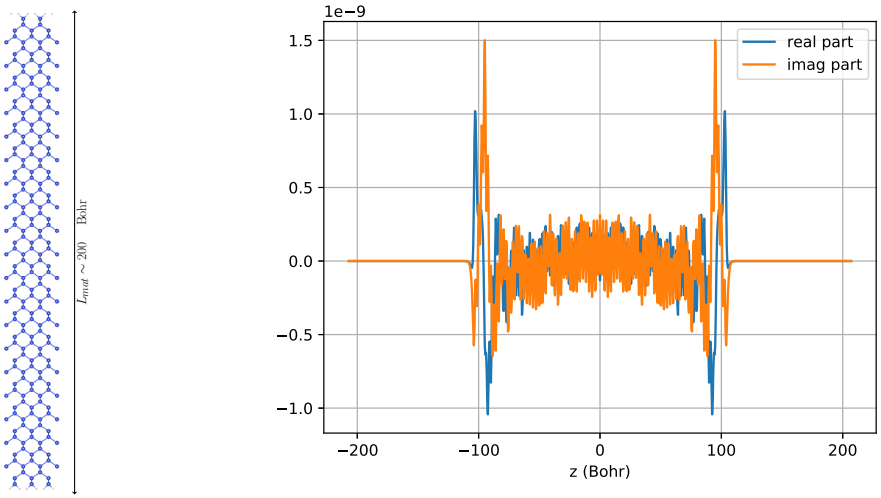

(a) (b)

Figure 8.5: Panel (a): Silicon di-hydrogenated surface used to calculate the second order induced density. Panel (b): second order density induced in the slab by an external longitudinal perturbation orthogonal to the surface.

directly linked with the second order polarisation). The extension of the region where the second order density variation is non zero will constitute a measurement of the thickness of the harmonically active layer. In order to perform such an extimation, we need a very thick slab (very thick in the sense that we want to be in the limit $L_{mat} \gg d_{harm}$, so that we can judge with relative confidence when $\delta\rho^{(2)}$ goes to zero). This cannot be obtained with the thymine functionalised slabs studied in the previous section. Those slabs in fact, have 4x1 reconstruction, which means that for each atomic layer of silicon we add we are adding four more atoms to the system, quickly leading to an unsustainable computational cost. As case study, therefore, I have chosen the di-hydrogenated silicon surface . This slab has 1x1 reconstruction, and this allows us to increase the thickness of the slab at a relatively contained computational cost. The slab used for the calculations is reported in Fig. (8.5a). This slab has a thickness of 80 silicon atomic layers, roughly equivalent to ~ 200 Bohr. In order to obtain the second order density variation, we followed a procedure somewhat similar to the one we have outlined in Chapter 5 for the linear response. First of all, we obtained the independent particle response function $\chi^{0,(2)}_{\mathbf{G}\mathbf{G_1}\mathbf{G_2}}(\mathbf{2q}, \mathbf{q}, \mathbf{q}, 2\omega, \omega)$, for $\mathbf{q} \propto \hat{\mathbf{z}}$, within the optical limit. In the reciprocal space, the Fourier coefficients of the

density induced by an external macroscopic potential will be given by[1]:

$$\delta\rho^{ind}_{\mathbf{G}}(\mathbf{2q}, 2\omega) = \chi^{0,(2)}_{\mathbf{G00}}(\mathbf{2q}, \mathbf{q}, \mathbf{q}, 2\omega, \omega) \tag{8.2}$$

In order to obtain the profile of the induced density in the real space, we performed a Fourier transform using these coefficents:

$$\delta\rho^{ind}(z, 2\omega) = \sum_{\mathbf{G}} \chi^{0,(2)}_{\mathbf{G00}}(\mathbf{2q}, \mathbf{q}, \mathbf{q}, 2\omega, \omega) e^{i(\mathbf{q_z}+\mathbf{G_z})z} \tag{8.3}$$

Result of this calculation is reported in Fig. (8.5b). As we can see, coherently with the estimation of previous section, the second order induced density is mainly concentrated in a range of $\sim 40 \div 50$ bohr within the surface.

8.3 Chemical selectivity

In this section, we will compare the second harmonic generation from surfaces functionalised with different nucleobases (Fig. (8.6)). In left part of Fig.(8.7) we report the macroscopic second order susceptibility calculated in independent particle approximation. As we can see, at independent particle level of the theory, the second order spectra of the three surfaces look very similar, regardless of the adsorbed specimen. Moreover, the three calculated components also have the same shape, all of them featuring a main peak at ~ 2 eV, and two smaller structures respectively at ~ 3.7 eV and ~ 4.6 eV. A small peak at ~ 1 eV appears for yyz and zyy for the surfaces functionalised with Cytosine and Uracil. In right part of Fig. (8.7) we report the spectrum of the three surfaces calculated with the inclusion of local field effects. As pointed out by Tancogne-Dejean for the bare silicon surfaces [20], local field effects are more important for those component of the χ^2_M tensor which contribute to the out-of-plane polarisation (here the zzz and the zyy component, reported in Fig. (8.7b) and (8.7f)). The zzz components present two main structures respectively located at 3.5 eV and 5.6 eV. Concerning the zyy component, inclusion of local field effects produces a shift of the main peak from ~ 2 eV to ~ 4 eV. On the other hand, for the yyz component of the χ^2_M, which contributes to the in-plane polarisation P_y, inclusion of local field effects results just in a slight increase of the spectral width (the main peak is still located at ~ 2 eV). We can see that the zzz component is the one for which the spectra of the three surfaces exhibit the largest differences. The two peak constituting the main features of the spectrum, change their relative amplitudes according the adsorbed molecule. This fact induces us to think that the displacement of the spectrum at higher energies occurring with the inclusion of local field effects, can be interpreted as an increase of the spectral

[1]To be precise, this is the density which would be induced in the Kohn-Sham system by an external macroscopic perturbation, and not the density that such a perturbation would induce in the real system. However, the extension of the harmonic layer should depend just on the symmetry of the system, and it should be similar in both cases.

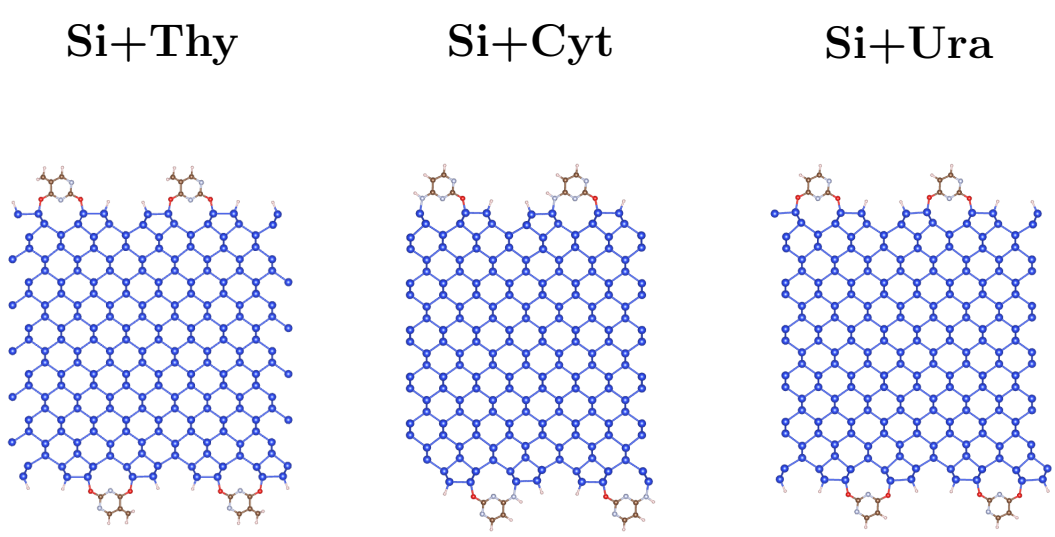

Figure 8.6: Slab used to study functionalised surfaces. From left to right: thymine, cytosine, uracil. Thickness of silicon: ~ 60 Bohr. The intermolecular vacuum occurs in the x direction.

weight of the molecular transitions. As we have seen in Chapter 5, the quenching of the spectrum occurring at linear order for the Si+Thy slab can be interpreted as a sort of effective medium theory between silicon and thymine. Since the molecule's spectrum is located at higher energies and it is much less intense than silicon one, the resulting effective medium spectrum will be given by the average of the two spectra, with the silicon contribution becoming more and more important as the thickness of the slab is increased. As we have discussed, this effective dielectric function gives a good approximation of the properties of functionalised slab, but it cannot be considered a reasonable description of a semi-infinite surface of silicon covered with a molecular monolayer of thymine. When light impinges on the surface, it penetrates for a length which is usually much greater than the thickness of our slab, and as a consequence, the contribution of substrate to the optical response is much more important than we can estimate with our modest slabs. This problem actually occurs only for the linear order. On the other hand, second harmonic generation from centrosymmetric materials is a phenomenon which occurs in a region of space much thinner ($\sim 30 \div 40$ Bohr, according the estimation of previous section). Second order polarisation is concentrated in the neighbourhood of surface (see Fig. (8.5b)). The quenching of the zzz component of the χ^2, therefore, cannot be anymore interpreted as a consequence of having chosen an inadequate slab thickness, but it's a truly physical effect due to the presence of the adsorbed layer. Due to the fact that the active layer is much smaller for SSHG than for linear response, the presence of adsorbed molecules has a much more important effect on nonlinear optical properties than on linear ones.

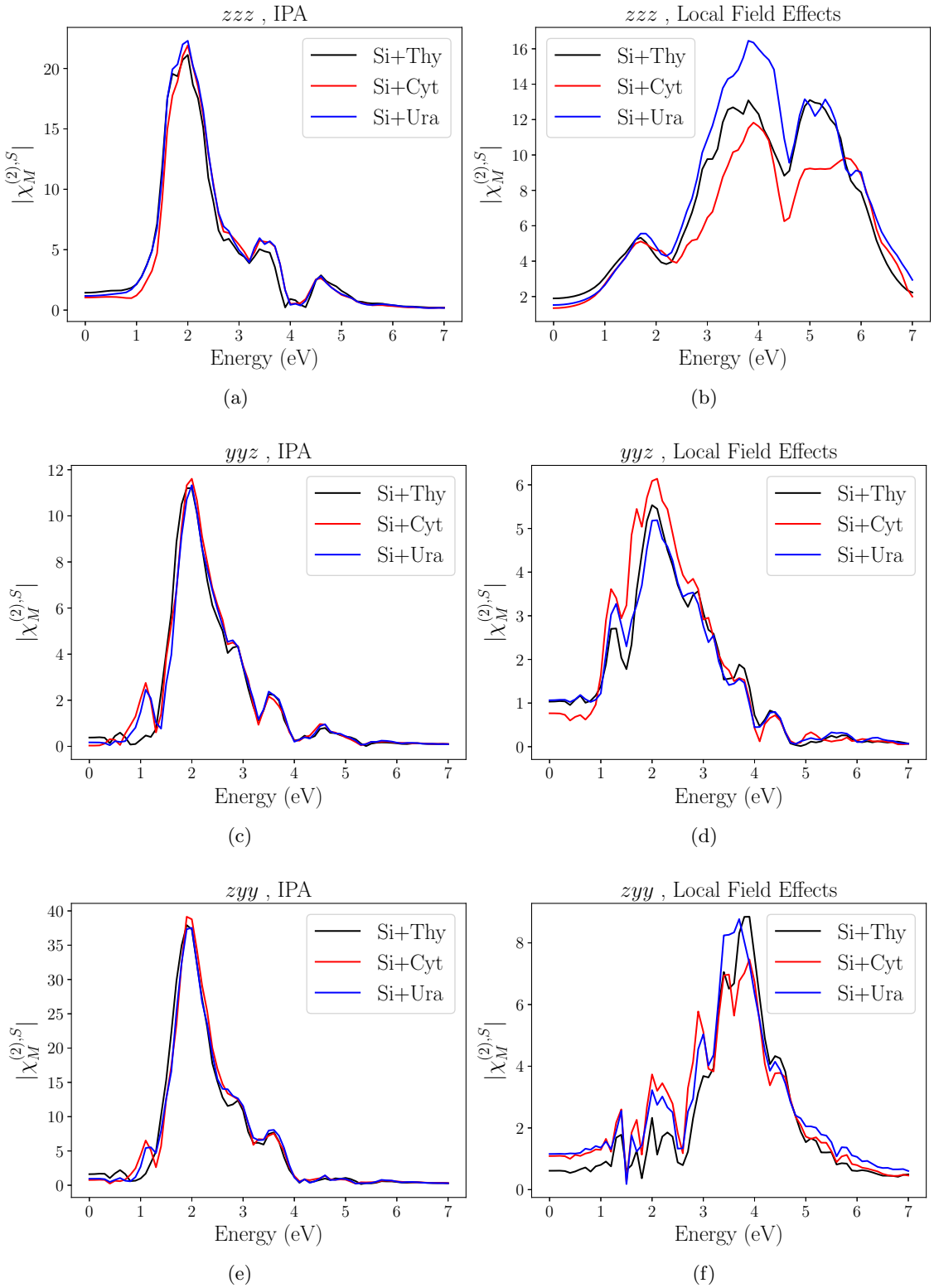

Figure 8.7: Second order susceptibility for Silicon surfaces functionalised with nucleobases. Black: thymine, red: cytosine, blue: uracil. Left: IPA, right: LFE.

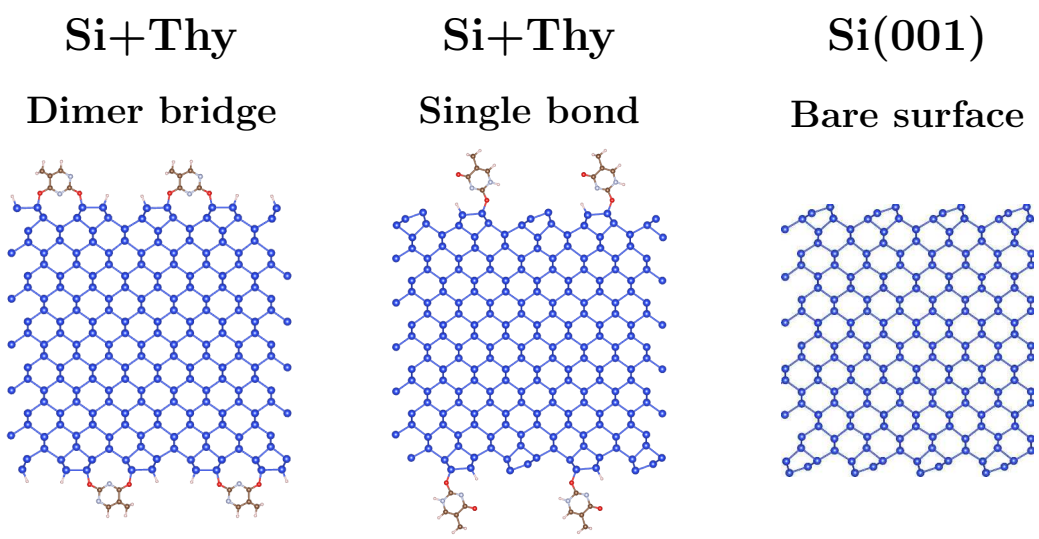

Figure 8.8: Slabs used to study the dependence of SHG upon the adsorption configuration.

8.4 Sensitivity adsorption configuration

In this section we compare the second order spectra of two different Si+Thy surfaces. The first one (reported in left panel of Fig. (8.8)) is the one in which the thymine molecule is adsorbed in the dimer bridge configuration, while in the second one (central panel of Fig. (8.8)), the molecule is attached to the silicon substrate with just one Si-O bond. In order to better understand the role played by the adsorbed molecule, we also studied the bare silicon surface (right panel of Fig. (8.8)) The SHG spectra for the three surfaces are reported in Fig. (8.9), respectively depicted in black, magenta, and red. The first step has been the calculation of the spectra in the independent particle approximation (Fig.s (8.9a),(8.9c),(8.9e)). Both the dimer bridge and the singly bonded surface present, for each of the three studied components, a main peak at around $\sim 2eV$, but in the case of the single bond adsorption geometry this peak presents a blueshift of ~ 0.2 eV (magenta line). In addition, the spectra of the singly bonded surface also present some sharp features in the low energy region ($0 \div 1$ eV), while at the same energies the spectrum of the dimer bridge configuration appears smooth and suppressed. This feature is probably due to transitions involving dangling electrons at the silicon dimers. As we can see in central panel of Fig. (8.8), in the singly bonded configuration, just one of the silicon dimers at the surface passivated, while the other one remain as it would be in the bare surface. Therefore, we can expect that the SHG of this surface will be a sort of hybrid between the bare silicon surface and the dimer bridge functionalised one.

This is confirmed by the analysis of the spectra of the bare silicon surface (red lines in Fig.s (8.9a),(8.9c),(8.9e)), which exhibit sharp structures in the low energy part of the

spectrum, exactly as the Silicon+Thymine surface in the singly-bonded adsorption configuration. In Fig.s (8.9b),(8.9d),(8.9f) we report the spectra with the inclusion of local field effects. Again, we see that local field effects impact in a more important way the components relative to the out-of-plane polarisation (i.e. yyz in Fig. (8.9b) and zyy in Fig. (8.9f)). Concerning the zzz component, the spectrum of the singly-bonded surface is blue-shifted of ~ 0.3 eV and slightly more quenched compared to the spectrum of the surface in the dimer bridge configuration. Concerning the zyy component, we see that in region between 0 and 3 eV the spectrum of the singly bonded surface (magenta) is significantly larger than the spectrum of the dimer-bridge surface (black), while at higher energies the spectra overlap. Concerning the yyz component, just minor differences between the two adsorption configuration are found. Indeed, considered also the discussion of previous section, it seems that surface second harmonic generation is more sensitive to the adsorption configuration (probably due to the presence of remaining dangling bonds) than to the adsorbed specimen (at least when relatively similar adsorbed molecules are considered, as in the present case). Quite interestingly we remark that, for all the three studied components of the susceptibility, the adsorption of the molecule tends to suppress the spectrum, as we can from comparison with the spectrum of the bare surface. This seems to suggest that second harmonic generation could be effectively be used in order to monitoring of nucleobases adsorption on silicon, at least for applications where an high sensitivity to the adsorbed specimen is not needed.

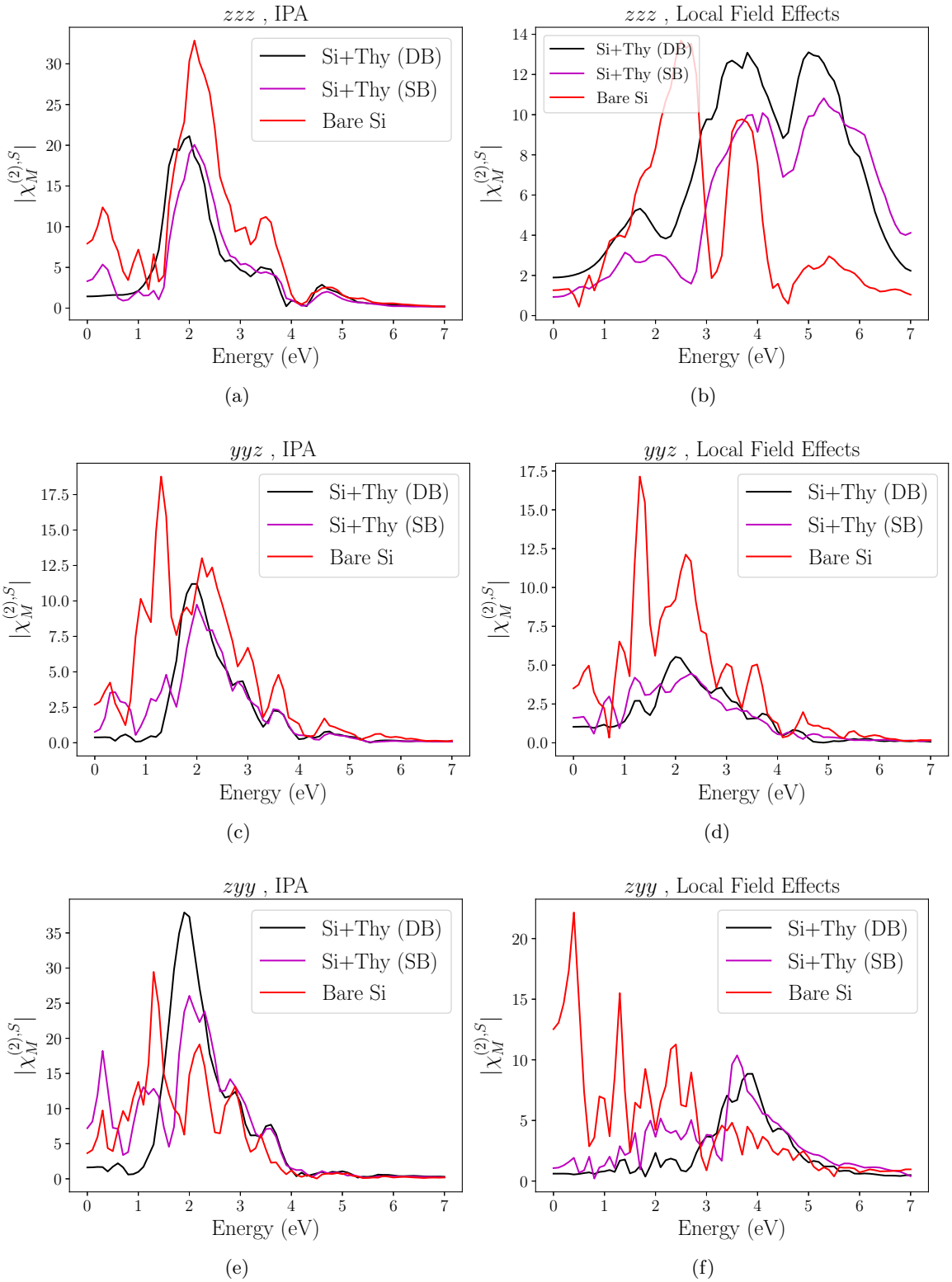

Figure 8.9: Second order susceptibility for Si+Thy in different adsorption configurations. Black: dimer bridge (DB), magenta:singly bonded (SB) configuration, red: bare surface. Left: IPA, right: LFE.

8.5 Conclusions

In this chapter I presented the calculations that I performed on the surfaces functionalised with nucleobases. According our results, the thickness of the harmonically active region has an extension of $40 \div 50$ Bohr, resulting in a great sensitivity to the surface properties. The SHG spectra (that we calculated with inclusion of local field effects) confirmed these findings: the adsorption of a molecular monolayer revealed to be enough to drastically change the second order optical response, which turns out to be very different from the one of the bare surface, confirming that SSHG could be used to monitor nucleobases adsorption on silicon. Nevertheless, the chemical selectivity between these three nucleobases is less remarkable since the SHG spectra did not exhibit radical difference upon change of the adsorbed molecule. On the contrary, they turn out to be very sensitive to the change of adsorption configuration when dangling bonds are preserved at the surface.

Conclusions

The goal of this thesis was to calculate linear and non-linear optical properties of silicon surfaces functionalised with nucleobases. The first results showed an extreme reduction of the spectra as soon as local field effects are included. The reduction of spectra, after inclusion of local field effects in the supercell framework, had already been observed and interpreted as a spurious effect of vacuum inside the cell. The selected-G method had been introduced in order to cure this problem. However, the spectra of functionalised slabs still appeared quenched despite being calculated within this framework.

Since the most stable geometry for functionalised surfaces contains line of molecules separated by empty space, I wondered if this intermolecular vacuum could be at the origin of this quenching. In order to tackle this problem I decided to follow two different paths.

One direction consisted in studying two toy-systems: the fully covered surface (which does not contain vacuum between molecules), and the silicon stepped surface (in which the place of molecules has been taken by silicon steps, and which contains the same amount of vacuum as the original functionalised surface). The stepped surface exhibit the same spectrum as the bare flat silicon slab apart from a scaling factor. No shift at higher energy is observed. On the other hand, the fully covered surface resulted having the same quenched spectrum as the original functionalised surface, demonstrating that this effect of the spectrum is really due to the functionalisation. Indeed, the absorption of the molecule is extremely low in the considered range of energy, and the spectrum results in an effective medium theory between the eight atomic planes of silicon and the adsorbed molecules.

The other direction consisted in approaching the problem of optical response of functionalised slabs in the mixed space. In this approach, the directions parallel to the surface are treated in reciprocal space (since periodicity is maintained), while the direction perpendicular to the slab (where the periodicity is broken) is treated in real space. This allows one to study the dependence along z of the microscopic response functions. Moreover, this technique allowed me to obtain the response of a single slab isolated from its replicas, making possible to exclude the effects coming from this spurious interaction. I have evidenced that the thickness of the slab was ambiguously defined, leading to a not univocally defined macroscopic dielectric function. This effect is similar to the effective medium theory with vacuum previously evidenced in the supercell formalism, but in this case it concerns the more subtle problem to establish where the matter finishes and the vacuum starts.

Mixed-space calculations also evidenced a puzzling difference in the response of the slab according to the direction of the perturbation. This brought me to investigate the fundamental differences between 2D and 3D objects. In order to eliminate unnecessary complexity, I decided to inquire the response of a slab to an external longitudinal perturbation in the different directions using a simple Lorentz oscillators model. This allowed me to establish that, for an in-plane perturbation, the induced electric field is (in the limit of very thin slab) extremely reduced, resulting in a suppression of the screening and in a redshift of the plasma oscillations. On the contrary, when the slab is perturbed in the out-of-plane direction, the induced electric field recover the bulk value, and is strictly equal to zero outside of the slab, leading to an absence of interaction between replicas in that direction. It results from this model that the density-density response function contains one peak at the resonant frequency of the dielectric function (usually associated with the absorption) for the in-plane component, and one peak at the resonant frequency of the inverse dielectric function (usually associated with the plasmon). These findings are consistent with the results obtained within my *ab initio* mixed-space approach (based on the longitudinal formalism of TD-DFT).

Since I was interested in optical response, I also inquired the link between macroscopic dielectric functions calculated within mixed space approach with the quantities measured in a spectroscopic experiment, namely reflectance, transmittance and absorbance. For this, I used the Fresnel and Airy formulas, which are well established in the framework of classical electromagnetism. Surprisingly (and happily) we found that despite the ambiguity in the definition of the thickness of the matter (which results in the impossibility to define a unique macroscopic dielectric function for a 2D object), the spectroscopic observables are unaffected by this ambiguity. Moreover, the reflectance, transmittance, and absorbance spectra exhibit two main features, one at the resonant frequency of the dielectric function, and the other one at the plasma frequency, coming from the presence of the second interface. This pushed us to investigate the thin film limit of the slab reflection coefficients. We found that they can be expressed as a linear combination of term of the form $(\varepsilon - 1)$ and $(\varepsilon^{-1} - 1)$, explaining the shape of the spectra as well as their angular dependence. These spectra reproduce the feature of the density-density response function, allowing us to calculate the optical absorption from the longitudinal formalism of TD-DFT for a 2D object. This result was unexpected since, due to the presence of surface charges, one expects a transverse component in the polarisation, even when the perturbation is purely longitudinal.

These clarifications of the different properties between 2D and 3D objects brought me to the conclusion that to describe a surface, one should define the thickness of the matter with the extension of the atomic positions, since it allows to recover the induced electric field of the (semi-)infinite material and to preserve the surface states. The selected-G method has been used to simulate SSHG for silicon surfaces functionalised with three nucleobases (Thymine, Cytosine, Uracil) adsorbed in the dimer-bridge configuration. To inquire the sensitivity of SSHG to adsorption configuration, we also studied the SSHG from a surface with Thymine adsorbed in a singly bonded-configuration. The thickness of the harmoni-

cally active layer has been estimated to some tenth of Bohr. Even if the sensitivity on the adsorbed specimen that we have studied is quite low, the SHG signal results to be strongly influenced by the adsorption of nucleobases, suggesting that SSHG may be a possible tool to monitor adsorption of nucleobases on silicon. It also appears to be very sensitive to the adsorption configuration, in particular when saturation of dangling bonds occurs.
Currently, as a result of the present work, one article has been submitted, and two others are in preparation.

Appendix A

Fourier transform of the Coulomb potential operator

Let's consider the potential:

$$v(\mathbf{q}_{||}, z, z') = 2\pi \frac{e^{-|q_{||}||z-z'|}}{|\mathbf{q}_{||}|} \tag{A.1}$$

The Fourier transform of this potential will be given by:

$$\mathcal{F}\big[v(\mathbf{q}_{||}, z, z')\big] = \int dz \int dz' e^{-iq_z z} 2\pi \frac{e^{-|q_{||}||z-z'|}}{|\mathbf{q}_{||}|} e^{iq'_z z'} \tag{A.2}$$

I perform the following change of variables:

$$Z_{CM} = \frac{z+z'}{2} \qquad\qquad \Delta z = z - z' \tag{A.3}$$

so that:

$$z = Z_{CM} + \frac{\Delta z}{2} \qquad\qquad z' = Z_{CM} - \frac{\Delta z}{2} \tag{A.4}$$

Our Fourier integral becomes:

$$
\begin{aligned}
\mathcal{F}\big[v(\mathbf{q}_{||},z,z')\big] &= \\
&= \int dZ_{CM} e^{-iq_z Z_{CM}} e^{iq'_z Z_{CM}} \times \\
&\times \int (d\Delta z) \frac{2\pi}{|\mathbf{q}_{||}|} e^{-|q_{||}||\Delta z|} e^{-iq_z \Delta z/2} e^{-iq'_z \Delta z/2} \\
&= \frac{2\pi}{|\mathbf{q}_{||}|}\delta(q_z - q'_z) \int (d\Delta z) e^{-|q_{||}||\Delta z|} e^{-iq_z \Delta z/2} e^{-iq'_z \Delta z/2} \\
&= \frac{2\pi}{|\mathbf{q}_{||}|}\delta(q_z - q'_z) \times \Big\{ \int_{-\infty}^{0} d(\Delta z) e^{(|q_{||}| - i(q_z+q'_z)/2)\Delta z} + \\
&+ \int_{0}^{\infty} d(\Delta z) e^{-(|q_{||}| + i(q_z+q'_z)/2)\Delta z} \Big\} \\
&= \frac{2\pi}{|\mathbf{q}_{||}|}\delta(q_z - q'_z) \times \Big\{ \frac{1}{|q_{||}| - i(q_z+q'_z)/2} \times \Big[e^{(|q_{||}| - i(q_z+q'_z)/2)\Delta z} \Big]_{-\infty}^{0} + \\
&+ \frac{(-)}{|q_{||}| + i(q_z+q'_z)/2} \times \Big[e^{-(|q_{||}| + i(q_z+q'_z)/2)\Delta z} \Big]_{0}^{\infty} \Big\} \\
&= \frac{2\pi}{|\mathbf{q}_{||}|}\delta(q_z - q'_z) \times \frac{|q_{||}| + i(q_z+q'_z)/2 + |q_{||}| - i(q_z+q'_z)/2}{\Big(|q_{||}| - i(q_z+q'_z)/2\Big)\Big(|q_{||}| + i(q_z+q'_z)/2\Big)} \\
&= 4\pi \frac{\delta(q_z - q'_z)}{|q_{||}|^2 + \big((q_z+q'_z)/2\big)^2} \\
&= \frac{4\pi}{q_{||}^2 + q_z^2}
\end{aligned}
\tag{A.5}
$$

Appendix B

Lorentz model

B.1 Slab: Electrostatic potential induced by an in-plane perturbation

In Section 6.2, we have given the expression of the electrostatic potential induced inside the slab by an external perturbation parallel to the surface. In this appendix, we report the derivation of this quantity. We recall that the displacement of the oscillators has the form:

$$\mathbf{\Delta}(\mathbf{r},t) = \Theta(z+\frac{L}{2})\Theta(-z+\frac{L}{2})\mathbf{\Delta}_0 e^{i\mathbf{q}_{||}\cdot\mathbf{r}-i\omega t} \tag{B.1}$$

with $\mathbf{\Delta}_0 || \mathbf{q}_{||}$. As a consequence, we can write the polarization as:

$$\mathbf{P}(\mathbf{r},t) = en_e\Theta(z+\frac{L}{2})\Theta(-z+\frac{L}{2})\mathbf{\Delta}_0 e^{i\mathbf{q}_{||}\cdot\mathbf{r}-i\omega t} \tag{B.2}$$

and the induced density of charge as:

$$\begin{aligned}\rho^{ind}(\mathbf{r},t) &= -\nabla\cdot\mathbf{P}(\mathbf{r},t) \\ &= -iq_{||}en_e\Theta(z+\frac{L}{2})\Theta(-z+\frac{L}{2})\mathbf{\Delta}_0 e^{i\mathbf{q}_{||}\cdot\mathbf{r}-i\omega t}\end{aligned} \tag{B.3}$$

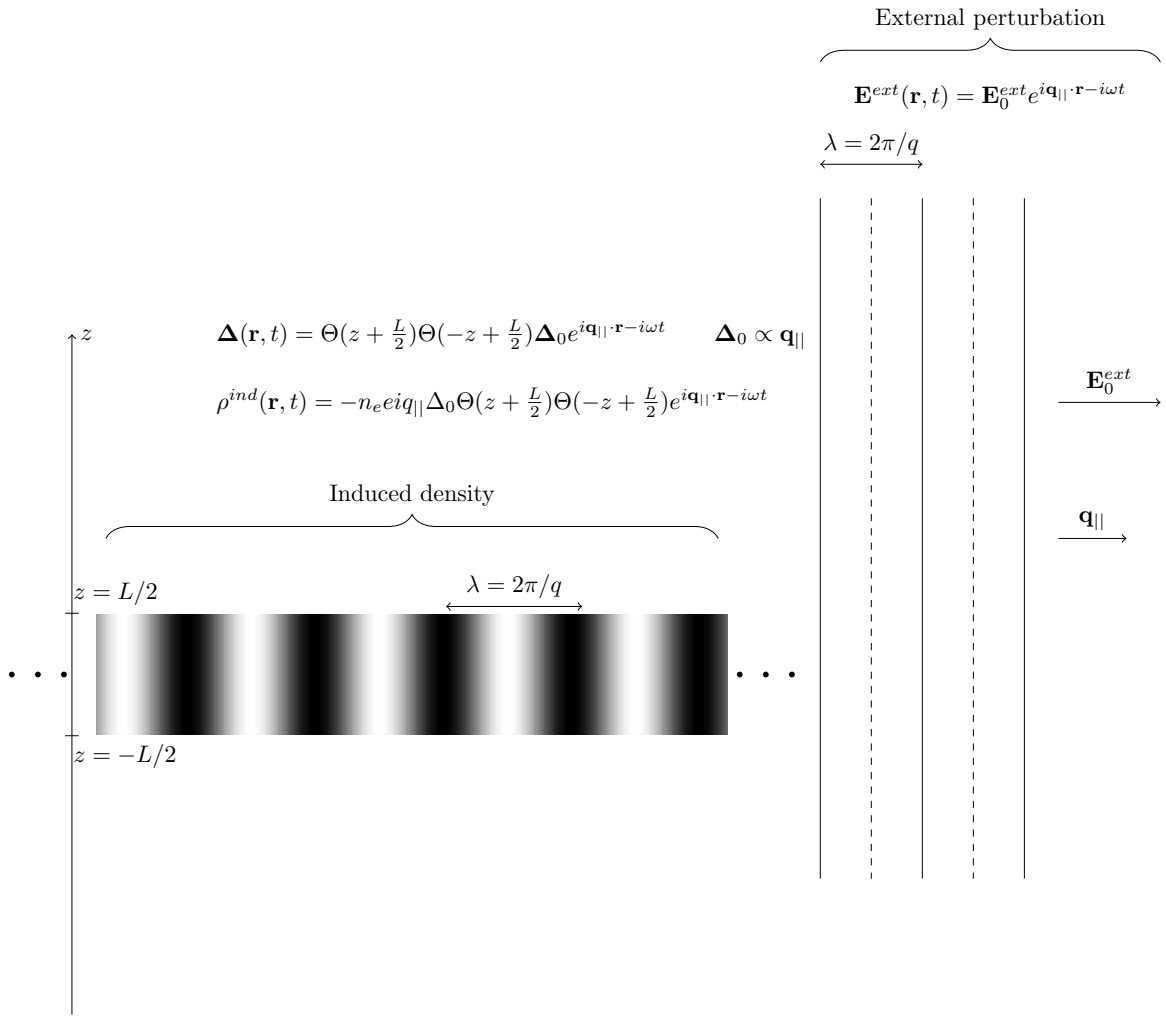

Let's focus on the form of this induced density. This density, can be seen as a distribution of planes orthogonal to the z axis, each of them containing a surface distribution of charge oscillating in time and spatially modulated by a wave-vector $\mathbf{q}_{||}$. Now, we know the potential induced by a planar distribution of charge of the form $e^{iq_{||}r_{||}}$ located in z': it is given by

$$v(\mathbf{q}_{||}, z, z') = \frac{2\pi}{|\mathbf{q}_{||}|} e^{-|\mathbf{q}_{||}||z-z'|} \tag{B.4}$$

The induced density of charge could be written as:

$$\rho^{ind}(\mathbf{r},t) = -i n_e e q_{||} \Delta_0 \int_{-L/2}^{L/2} dz' \delta(z-z') e^{iq_{||}r_{||} - i\omega t} \tag{B.5}$$

The potential induced by such a density of charge will be therefore given by:

$$\begin{aligned}
\phi^{ind} &= \int dz' v(\mathbf{q}_{||}, z, z') \rho^{ind}(\mathbf{r}', t) \\
&= (-) ie n_e q_{||} \Delta_0 \int dz' v(\mathbf{q}_{||}, z, z') \int dz'' \delta(z' - z'') e^{iq_{||} r_{||} - i\omega t} \\
&= \frac{2\pi}{|q_{||}|} (-) ie n_e q_{||} \Delta_0 \int dz' e^{-|q_{||}||z-z'|} \int_{-L/2}^{L/2} dz'' \delta(z' - z'') e^{iq_{||} r_{||} - i\omega t} \\
&= \frac{2\pi}{|q_{||}|} (-) ie n_e q_{||} \Delta_0 e^{iq_{||} r_{||} - i\omega t} \int dz' e^{-|q_{||}||z-z'|} \int_{-L/2}^{L/2} dz'' \delta(z' - z'') \\
&= \frac{2\pi}{|q_{||}|} (-) ie n_e q_{||} \Delta_0 e^{iq_{||} r_{||} - i\omega t} \int_{-L/2}^{L/2} dz' e^{-|q_{||}||z-z'|}
\end{aligned} \tag{B.6}$$

Let's focus for a moment on the integral appearing to the last member, $\int_{-L/2}^{L/2} dz' e^{-|q_{||}||z-z'|}$. The variable z' assumes value in the interval $-L/2 < z' < L/2$. We have therefore three possible cases:

$$\begin{aligned}
z &> \frac{L}{2} \\
-\frac{L}{2} < z &< \frac{L}{2} \\
z &< -\frac{L}{2}
\end{aligned}$$

for $z > L/2$, we have $z > z'$, since by definition $-L/2 < z' < L/2$. Therefore, for $z > L/2$, the integral become:

$$\begin{aligned}
\int_{-L/2}^{L/2} dz' e^{-|q_{||}||z-z'|} &= \int_{-L/2}^{L/2} dz' e^{-|q_{||}|(z-z')} \\
&= \frac{e^{-|q_{||}|z}}{|q_{||}|} \left[e^{|q_{||}|z'} \right]_{-L/2}^{L/2} \\
&= \frac{2}{|q_{||}|} e^{-|q_{||}|z} \sinh(|q_{||}|L/2)
\end{aligned} \tag{B.7}$$

For $z < -L/2$, instead, we always have $z < z'$, and so the integral will be equal to:

$$\begin{aligned}
\int_{-L/2}^{L/2} dz' e^{-|q_{||}||z-z'|} &= \int_{-L/2}^{L/2} dz' e^{|q_{||}|(z-z')} \\
&= -\frac{e^{|q_{||}|z}}{|q_{||}|} \left[e^{-|q_{||}|z'} \right]_{-L/2}^{L/2} \\
&= \frac{2}{|q_{||}|} e^{|q_{||}|z} \sinh(|q_{||}|L/2)
\end{aligned} \tag{B.8}$$

For $-L/2 < z < L/2$, z can be greater or lesser than z', so we have to split the integral in order to account correctly both case. For $-L/2 < z < L/2$ we have:

$$\begin{aligned}
\int_{-L/2}^{L/2} dz' e^{-|q_{||}||z-z'|} &= \int_{-L/2}^{z} dz' e^{-|q_{||}||z-z'|} + \int_{z}^{L/2} dz' e^{-|q_{||}||z-z'|} \\
&= \int_{-L/2}^{z} dz' e^{-|q_{||}|(z-z')} + \int_{z}^{L/2} dz' e^{|q_{||}|(z-z')} \\
&= \frac{1}{|q_{||}|} e^{-|q_{||}|z} \left[e^{|q_{||}|z'} \right]_{-L/2}^{z} + \frac{(-)}{|q_{||}|} e^{|q_{||}|z} \left[e^{-|q_{||}|z'} \right]_{z}^{L/2} \\
&= \frac{1}{|q_{||}|} e^{-|q_{||}|z} \left[e^{|q_{||}|z} - e^{-|q_{||}|\frac{L}{2}} \right] + \frac{(-)}{|q_{||}|} e^{|q_{||}|z} \left[e^{-|q_{||}|\frac{L}{2}} - e^{-|q_{||}|z} \right] \\
&= \frac{1}{|q_{||}|} \left[1 - e^{-|q_{||}|(z+\frac{L}{2})} - e^{|q_{||}|(z-\frac{L}{2})} + 1 \right] \\
&= \frac{1}{|q_{||}|} \left[2 - 2e^{-|q_{||}|\frac{L}{2}} \cosh(|q_{||}|z) \right]
\end{aligned} \tag{B.9}$$

So the induced potential will be given by:

$$\begin{aligned}
\phi^{ind} = \frac{2\pi}{|q_{||}|}(-)ien_e q_{||} \Delta_0 e^{iq_{||}r_{||} - i\omega t} \times \\
\times \begin{cases} \frac{2}{|q_{||}|} e^{-|q_{||}|z} \sinh(|q_{||}|L/2) & \text{for} \quad z > L/2 \\ \frac{1}{|q_{||}|} \left[2 - 2e^{-|q_{||}|\frac{L}{2}} \cosh(|q_{||}|z) \right] & \text{for} - L/2 < z < L/2 \\ \frac{2}{|q_{||}|} e^{|q_{||}|z} \sinh(|q_{||}|L/2) & \text{for} \quad z < -L/2 \end{cases}
\end{aligned} \tag{B.10}$$

For sake of clarity, we define the function $F(z)$:

$$F(z) = \begin{cases} e^{-|q_{||}|z} \sinh(|q_{||}|L/2) & \text{for} \quad z > L/2 \\ \left[1 - e^{-|q_{||}|\frac{L}{2}} \cosh(|q_{||}|z) \right] & \text{for} - L/2 < z < L/2 \\ e^{|q_{||}|z} \sinh(|q_{||}|L/2) & \text{for} \quad z < -L/2 \end{cases} \tag{B.11}$$

so that the induced potential can be easily rewritten as:

$$\phi^{ind} = \frac{4\pi}{|q_{||}|^2}(-)ien_e q_{||} F(z) \Delta_0 e^{iq_{||}r_{||} - i\omega t} \tag{B.12}$$

B.2 EELS within the Lorentz model

B.2.1 EELS in the case of bulk

In section 6.1 , we studied the response of an infinite material, constituted of n_e oscillators per unit of volume (of mass m_e, charge e, and frequency ω_0) to an external longitudinal perturbation of the form:

$$\mathbf{E}^{ext}(\mathbf{r},t) = \mathbf{E}_0^{ext} e^{i\mathbf{q}\cdot\mathbf{r}-i\omega t} \tag{B.13}$$

We have seen, solving the equation of motion of our oscillator system, that this external perturbation induces a reconfiguration of the charges inside of the material, i.e. an induced density of charges. This induced density of charge can be expressed as a function of the vector field describing the displacement of the oscillators from their equilibrium position:

$$\mathbf{\Delta}(\mathbf{r},t) = \frac{e}{m_e}\frac{1}{-\omega^2+\omega_0^2-i\frac{\omega}{\tau}+\omega_{pl}^2}\mathbf{E}^{ext}(\mathbf{r},t) \tag{B.14}$$

$$\mathbf{\Delta}(\mathbf{r},t) = \frac{e}{m_e}\frac{1}{-\omega^2+\omega_0^2-i\frac{\omega}{\tau}}\mathbf{E}^{tot}(\mathbf{r},t) \tag{B.15}$$

This reconfiguration of charges is responsible for the creation of an induced electric field

$$\mathbf{E}^{ind}(\mathbf{r},t) = (-)4\pi n_e e\mathbf{\Delta}(\mathbf{r},t) \tag{B.16}$$

Now: the external perturbation, being longitudinal, may be seen as the electric field of an electron beam travelling in the $\mathbf{q}$ direction. We ask therefore: does it make sense to calculate the work done from the induced electric field on the external electron beam? Of course it does, and I expect to recover a quantity linked with the energy loss function. The external electric field will be related to the external density of charge $\rho^{ext}(\mathbf{r},t)$ via the relationship:

$$\nabla\cdot\mathbf{E}^{ext}(\mathbf{r},t) = 4\pi\rho^{ext}(\mathbf{r},t) \tag{B.17}$$

and the external density of charge is related to the external density of current via the continuity equation:

$$\frac{\partial}{\partial t}\rho^{ext}(\mathbf{r},t) = -\nabla\cdot\mathbf{J}^{ext}(\mathbf{r},t) \tag{B.18}$$

Putting together these two relationships, we have:

$$\nabla\cdot\mathbf{E}^{ext}(\mathbf{r},t) = 4\pi\frac{-i}{\omega}\nabla\cdot\mathbf{J}^{ext}(\mathbf{r},t) \tag{B.19}$$

and therefore:

$$\mathbf{J}^{ext}(\mathbf{r},t) = \frac{i\omega}{4\pi}\mathbf{E}^{ext}(\mathbf{r},t) \tag{B.20}$$

The power dissipated from the electric field on the external current will be given by [83]:

$$W = \int d\mathbf{r} \mathrm{Re}\mathbf{J}^{ext}(\mathbf{r},t) \cdot \mathrm{Re}\mathbf{E}(\mathbf{r},t) \tag{B.21}$$

we define the density of dissipated power per unit of volume:

$$\begin{aligned}
\mathcal{W} &= \mathrm{Re}\mathbf{J}^{ext}(\mathbf{r},t) \cdot \mathrm{Re}\mathbf{E}(\mathbf{r},t) \\
&= \mathrm{Re}\mathbf{J}^{ext}(\mathbf{r},t) \cdot \mathrm{Re}\mathbf{E}^{ext}(\mathbf{r},t) + \mathrm{Re}\mathbf{J}^{ext}(\mathbf{r},t) \cdot \mathrm{Re}\mathbf{E}^{ind}(\mathbf{r},t) \\
&= \mathrm{Re}\left(\frac{i\omega}{4\pi}\mathbf{E}^{ext}(\mathbf{r},t)\right) \cdot \mathrm{Re}\mathbf{E}^{ext}(\mathbf{r},t) + \mathrm{Re}\left(\frac{i\omega}{4\pi}\mathbf{E}^{ext}(\mathbf{r},t)\right) \cdot \mathrm{Re}\mathbf{E}^{ind}(\mathbf{r},t) \\
&= -\frac{\omega}{4\pi}\mathrm{Im}\mathbf{E}^{ext}(\mathbf{r},t) \cdot \mathrm{Re}\mathbf{E}^{ext}(\mathbf{r},t) + -\frac{\omega}{4\pi}\mathrm{Im}\mathbf{E}^{ext}(\mathbf{r},t) \cdot \mathrm{Re}\mathbf{E}^{ind}(\mathbf{r},t)
\end{aligned} \tag{B.22}$$

Where we used relation Eq. (B.20) to link the external current with the external field, and we noticed that:

$$\mathrm{Re}\mathbf{J}^{ext}(\mathbf{r},t) = \mathrm{Re}\left(\frac{i\omega}{4\pi}\mathbf{E}^{ext}(\mathbf{r},t)\right) = -\frac{\omega}{4\pi}\mathrm{Im}\mathbf{E}^{ext}(\mathbf{r},t) \tag{B.23}$$

In order to evaluate (B.22), we write explicitly the real part of $\mathbf{E}^{ind}(\mathbf{r},t)$:

$$\begin{aligned}
&\mathrm{Re}\mathbf{E}^{ind}(\mathbf{r},t) = \\
&= -\mathrm{Re}\left[\frac{\omega_{pl}^2}{(\omega_0^2+\omega_{pl}^2)-\omega^2-i(\omega/\tau)}\mathbf{E}^{ext}(\mathbf{r},t)\right] \\
&= -\mathrm{Re}\left[\frac{\omega_{pl}^2}{(\omega_0^2+\omega_{pl}^2)-\omega^2-i(\omega/\tau)}\right]\mathrm{Re}[\mathbf{E}^{ext}(\mathbf{r},t)] + \mathrm{Im}\left[\frac{\omega_{pl}^2}{(\omega_0^2+\omega_{pl}^2)-\omega^2-i(\omega/\tau)}\right]\mathrm{Im}[\mathbf{E}^{ext}(\mathbf{r},t)] \\
&= -\left[\frac{\omega_{pl}^2[(\omega_0^2+\omega_{pl}^2)-\omega^2]}{[(\omega_0^2+\omega_{pl}^2)-\omega^2]^2+[(\omega/\tau)]^2}\right]\mathrm{Re}[\mathbf{E}^{ext}(\mathbf{r},t)] + \left[\frac{\omega_{pl}^2(\omega/\tau)}{[(\omega_0^2+\omega_{pl}^2)-\omega^2]^2+[(\omega/\tau)]^2}\right]\mathrm{Im}[\mathbf{E}^{ext}(\mathbf{r},t)]
\end{aligned}$$

Moreover, using the definition of $\mathbf{E}^{ext}(\mathbf{r})$, we have:

$$\begin{aligned}
\mathbf{E}^{ext}(\mathbf{r},t) &= \mathbf{E}_0^{ext}\ [\cos(\mathbf{q}\cdot\mathbf{r}-\omega t) + i\sin(\mathbf{q}\cdot\mathbf{r}-\omega t)] \\
&= \mathbf{E}_0^{ext}\ \Big[[\cos(\mathbf{q}\cdot\mathbf{r})\cos(\omega t) + \sin(\mathbf{q}\cdot\mathbf{r})\sin(\omega t)] + i[\sin(\mathbf{q}\cdot\mathbf{r})\cos(\omega t) - \cos(\mathbf{q}\cdot\mathbf{r})\sin(\omega t)]\Big]
\end{aligned}$$

In Eq. (B.22), therefore, there will be terms of two types:

$$\begin{aligned}
&\mathrm{Im}[\mathbf{E}^{ext}(\mathbf{r},t)]\cdot\mathrm{Re}[\mathbf{E}^{ext}(\mathbf{r},t)]=\\
=&\mathbf{E}_0^{ext\ 2}\Big[[\sin(\mathbf{q}\cdot\mathbf{r})\cos(\omega t)-\cos(\mathbf{q}\cdot\mathbf{r})\sin(\omega t)]\times\\
&\times[\cos(\mathbf{q}\cdot\mathbf{r})\cos(\omega t)+\sin(\mathbf{q}\cdot\mathbf{r})\sin(\omega t)]\Big]\\
=&\mathbf{E}_0^{ext\ 2}\Big[\sin(\mathbf{q}\cdot\mathbf{r})\cos(\mathbf{q}\cdot\mathbf{r})\cos^2(\omega t)-\cos^2(\mathbf{q}\cdot\mathbf{r})\sin(\omega t)\cos(\omega t)]\\
&+\sin^2(\mathbf{q}\cdot\mathbf{r})\cos(\omega t)\sin(\omega t)-\cos(\mathbf{q}\cdot\mathbf{r})\sin(\mathbf{q}\cdot\mathbf{r})\sin^2(\omega t)\Big]\\
=&\mathbf{E}_0^{ext\ 2}\Big[\sin(\mathbf{q}\cdot\mathbf{r})\cos(\mathbf{q}\cdot\mathbf{r})[\cos^2(\omega t)-\sin^2(\omega t)]\\
&-[\cos^2(\mathbf{q}\cdot\mathbf{r})-\sin^2(\mathbf{q}\cdot\mathbf{r})]\cos(\omega t)\sin(\omega t)\Big]\\
=&\mathbf{E}_0^{ext\ 2}\Big[\sin(\mathbf{q}\cdot\mathbf{r})\cos(\mathbf{q}\cdot\mathbf{r})\cos(2\omega t)-1/2[\cos^2(\mathbf{q}\cdot\mathbf{r})-\sin^2(\mathbf{q}\cdot\mathbf{r})]\sin(2\omega t)\Big]
\end{aligned}\tag{B.24}$$

and:

$$\begin{aligned}
&\mathrm{Im}[\mathbf{E}^{ext}(\mathbf{r},t)]\cdot\mathrm{Im}[\mathbf{E}^{ext}(\mathbf{r},t)]=\\
=&\mathbf{E}_0^{ext\ 2}\Big[\sin(\mathbf{q}\cdot\mathbf{r})\cos(\omega t)-\cos(\mathbf{q}\cdot\mathbf{r})\sin(\omega t)\Big]^2\\
=&\mathbf{E}_0^{ext\ 2}\Big[\sin^2(\mathbf{q}\cdot\mathbf{r})\cos^2(\omega t)+\\
&+\cos^2(\mathbf{q}\cdot\mathbf{r})\sin^2(\omega t)-2\sin(\mathbf{q}\cdot\mathbf{r})\cos(\mathbf{q}\cdot\mathbf{r})\cos(\omega t)\sin(\omega t)\Big]\\
=&\mathbf{E}_0^{ext\ 2}\Big[\sin^2(\mathbf{q}\cdot\mathbf{r})\frac{1+\cos(2\omega t)}{2}+\cos^2(\mathbf{q}\cdot\mathbf{r})\frac{1-\cos(2\omega t)}{2}\\
&-\sin(\mathbf{q}\cdot\mathbf{r})\cos(\mathbf{q}\cdot\mathbf{r})\sin(2\omega t)\Big]\\
=&\frac{1}{2}\mathbf{E}_0^{ext\ 2}\Big[1+\cos(2\omega t)[\sin^2(\mathbf{q}\cdot\mathbf{r})-\cos^2(\mathbf{q}\cdot\mathbf{r})]-2\sin(\mathbf{q}\cdot\mathbf{r})\cos(\mathbf{q}\cdot\mathbf{r})\sin(2\omega t)\Big]
\end{aligned}\tag{B.25}$$

The time average of term in Eq. (B.24) is equal to zero over an oscillation period. Therefore, just the term in Eq. (B.25) contribute to the dissipated power, giving:

$$\begin{aligned}
\langle\mathcal{W}\rangle&=-\frac{\omega}{4\pi}\frac{1}{2}|\mathbf{E}_0^{ext}|^2\left[\frac{\omega_{pl}^2(\omega/\tau)}{[(\omega_0^2+\omega_{pl}^2)-\omega^2]^2+[(\omega/\tau)]^2}\right]\\
&=\frac{\omega}{8\pi}\mathrm{Im}\left(\frac{1}{\varepsilon(\omega)}\right)|E_0^{ext}|^2
\end{aligned}\tag{B.26}$$

where $\varepsilon(\omega)$, as it results from the calculation for the bulk case, is the well-known Lorentz dielectric function:

$$\varepsilon(\omega) = 1 - \frac{\omega_{pl}^2}{\omega^2 - \omega_0^2 + i\frac{\omega}{\tau}}$$

B.2.2 EELS in slab (in-plane)

In this section, I will derive the expression of the energy loss for electrons travelling parallel to the slab Even in the case of the slab, the external electric field:

$$\mathbf{E}^{ext}(\mathbf{r}, t) = \mathbf{E}_0^{ext} e^{i\mathbf{q}_{||}\cdot\mathbf{r} - i\omega t}$$

can be seen as the field given by an external electron current:

$$\mathbf{J}^{ext}(\mathbf{r}, t) = \frac{i\omega}{4\pi}\mathbf{E}^{ext}(\mathbf{r}, t)$$

As we have seen in the previous section, this external current of electrons travelling in the $\mathbf{q}_{||}$ direction (i.e. in the $\hat{\mathbf{x}}$ direction) perturbs the slab, producing a rearrangement of the charge carriers. This rearrangement of charges, produces an induced electric field having x component given by:

$$\begin{aligned} E_x^{ind}(\mathbf{r}, t) &= (-)4\pi e n_e \Delta_0 e^{iq_{||}r_{||} - i\omega t} \times \\ &\times \begin{cases} e^{-|q_{||}|z}\sinh(|q_{||}|L/2) & \text{for} \quad z > L/2 \\ \left[1 - e^{-|q_{||}|\frac{L}{2}}\cosh(|q_{||}|z)\right] & \text{for} -L/2 < z < L/2 \\ e^{|q_{||}|z}\sinh(|q_{||}|L/2) & \text{for} \quad z < -L/2 \end{cases} \\ &= (-)4\pi e n_e F(z) \Delta_0 e^{iq_{||}r_{||} - i\omega t} \end{aligned}$$

It makes sense to ask the following question: what is the work done by the induced field on the external electric current? The density of power per unit of volume dissipated by the induced field on the external current will be given by:

$$\begin{aligned} \mathcal{W} &= \mathrm{Re}\mathbf{J}^{ext} \cdot \mathrm{Re}\mathbf{E}^{ind} \\ &= \mathrm{Re}J_x^{ext}\mathrm{Re}E_x^{ind} \end{aligned} \tag{B.27}$$

In the limit of thin slab, for the induced field we have:

$$\begin{aligned} \mathrm{Re}[E_x^{ind}(\mathbf{r}, t)] = -\mathrm{Re}[\frac{\omega_{pl}^2 F(z)}{\omega_0^2 + \omega_{pl}^2 \ |\mathbf{q}_{||}| \ \frac{L}{2} - \omega^2 - i(\omega/\tau)}]\mathrm{Re}[E^{ext}(\mathbf{r}, t)] + \\ + \mathrm{Im}[\frac{\omega_{pl}^2 F(z)}{\omega_0^2 + \omega_{pl}^2 \ |\mathbf{q}_{||}| \ \frac{L}{2} - \omega^2 - i(\omega/\tau)}]\mathrm{Im}[E^{ext}(\mathbf{r}, t)] \end{aligned} \tag{B.28}$$

Of the latter expression, just the second term will contribute to the power dissipated in average over an oscillation period, and therefore we will have:

$$\begin{aligned}\langle \mathcal{W} \rangle &= -\frac{\omega}{4\pi} \frac{\omega_{pl}^2 F(z)(\omega/\tau)}{[\omega_0^2 + \omega_{pl}^2 \ |\mathbf{q}_{||}| \ \frac{L}{2} - \omega^2]^2 + [(\omega/\tau)]^2} \langle \mathrm{Im}[E^{ext}(\mathbf{r},t)] \mathrm{Im}[E^{ext}(\mathbf{r},t)] \rangle \\ &= -\frac{\omega}{4\pi} \frac{\omega_{pl}^2 F(z)(\omega/\tau)}{[\omega_0^2 + \omega_{pl}^2 \ |\mathbf{q}_{||}| \ \frac{L}{2} - \omega^2]^2 + [(\omega/\tau)]^2} \frac{1}{2} |E_0^{ext}|^2\end{aligned} \tag{B.29}$$

In the case of a thin film, $|\mathbf{q}_{||}|L \ll 1$, and therefore one has:

$$\begin{aligned}\langle \mathcal{W} \rangle &= -\frac{\omega}{4\pi} \frac{\omega_{pl}^2 F(z)(\omega/\tau)}{[\omega_0^2 - \omega^2]^2 + [(\omega/\tau)]^2} \frac{1}{2} |E_0^{ext}|^2 \\ &= -\frac{\omega}{8\pi} F(z) \mathrm{Im}\big(\varepsilon(\omega)\big) |E_0^{ext}|^2\end{aligned} \tag{B.30}$$

In conclusion, we have that, in the case of a thin slab, the density of power (averaged over a period of oscillation) per unit of volume, dissipated by the induced field over the external electron current, is proportional to the imaginary part of the dielectric function. In order to make easier the comparison between the bulk and the slab, we report here the expression of dissipated power for both the systems:

$$\langle \mathcal{W} \rangle = \begin{cases} \dfrac{\omega}{8\pi} \mathrm{Im}\left(\dfrac{1}{\varepsilon(\omega)}\right) |E_0^{ext}|^2 & \text{(Bulk)} \\ -\dfrac{\omega}{8\pi} F(z) \mathrm{Im}\big(\varepsilon(\omega)\big) |E_0^{ext}|^2 & \text{(Slab)} \end{cases} \tag{B.31}$$

As we can see, there are two main differences between these two expressions. First of all, the density of dissipated power, in the case of bulk is proportional to $\mathrm{Im}\big(1/\varepsilon(\omega)\big)$, while in the case of the (thin) slab is proportional to $\mathrm{Im}\big(\varepsilon(\omega)\big)$. The second difference to be noticed is that, contrarily to what happens in the bulk, the density of dissipated power in the case of the slab depend on z. This is due to the fact that the infinite bulk is translationally invariant in the z direction, while the slab is not. The electric field induced by the slab, in particular, is not invariant along z, but decreases exponentially with the distance from the surface. It makes sense to integrate the density of power in z: in this way, I will obtain the power dissipated by the induced field per unit of surface.

$$\langle \mathcal{W} \rangle_S^{slab} = -\frac{\omega}{8\pi} \mathrm{Im}\big(\varepsilon(\omega)\big) |E_0^{ext}|^2 \times \int_{-\infty}^{\infty} dz F(z) \tag{B.32}$$

After a bit of algebra, we obtain that:

$$\int_{-\infty}^{\infty} dz F(z) = L \tag{B.33}$$

and therefore:

$$\langle \mathcal{W} \rangle_S^{slab} = -\frac{\omega}{8\pi} L \mathrm{Im}\big(\varepsilon(\omega)\big) |E_0^{ext}|^2 \tag{B.34}$$

An interesting observation

It is interesting to notice that we could have obtained the latter result with another approach. In the previous section, we have found that the density of power per unit of surface dissipated *by the induced field* on the *external current* is given by:

$$\langle \mathcal{W} \rangle_S^{slab} = -\frac{\omega}{8\pi} L \mathrm{Im}\big(\varepsilon(\omega)\big) |E_0^{ext}|^2$$

We could have obtained this same result, calculating instead the density of power dissipated *by the external field* on the *induced current*. The induced density of current can be related t the induced density via the continuity equation:

$$\nabla \cdot \mathbf{J}^{ind} = -\partial_t \rho^{ind} \tag{B.35}$$

At the same time, the induced density of charge can be expressed via the density response function:

$$\rho^{ind} = \chi_{\rho\rho} \phi^{ext} \tag{B.36}$$

where the $\chi_{\rho\rho}$ is the one of Eq. (6.41):

$$\chi_{\rho\rho} = \frac{|\mathbf{q}|^2}{4\pi} \frac{\omega_{pl}^2}{\omega^2 - \omega_0^2 + i\frac{\omega}{\tau} - \frac{|\mathbf{q}|^2 L}{2}\omega_{pl}^2} \tag{B.37}$$

and the external potential is related to the external field via:

$$\mathbf{E}^{ext} = -\nabla \phi^{ext} \tag{B.38}$$

Putting together Eq.s (B.35),(B.36),(B.37), and (B.38), we obtain the following expression for the current as a function of the external field:

$$\mathbf{J}^{ind} = i\frac{\omega}{q^2} \chi_{\rho\rho} \mathbf{E}^{ext} \tag{B.39}$$

At this point, we have all that we need to calculate the work done by the external field on the induced current: averaging over an oscillation period, we have:

$$\langle \mathrm{Re}\mathbf{E}^{ext} \cdot \mathrm{Re}\mathbf{J}^{ind} \rangle = -\frac{1}{2}\frac{\omega}{q^2} \mathrm{Im}(\chi_{\rho\rho}) |E_0^{ext}|^2 \tag{B.40}$$

and, with some simple algebraic manipulations (see Eq. (6.44)):

$$\langle \mathrm{Re}\mathbf{E}^{ext} \cdot \mathrm{Re}\mathbf{J}^{ind} \rangle = \frac{\omega}{8\pi} \Theta(z + \frac{L}{2}) \Theta(-z + \frac{L}{2}) \mathrm{Im}\big(\varepsilon(\omega)\big) |E_0^{ext}|^2 \tag{B.41}$$

And, integrating in z, we obtain:

$$\langle \mathrm{Re}\mathbf{E}^{ext} \cdot \mathrm{Re}\mathbf{J}^{ind} \rangle_S = \frac{\omega}{8\pi} L \mathrm{Im}\big(\varepsilon(\omega)\big) |E_0^{ext}|^2 \tag{B.42}$$

which is the same result reported in Eq. (B.34) (up to a minus sign). Because of the energy conservation, the work done by the external field on the induced current must be equal in modulus (and opposite in sign) to the work done by the induced field on the external current. In other words, the energy loss by the external electron beam must be equal to the energy spent to excite the density oscillation inside the slab. The interesting point, is that in the case of a bulk, this equality is already clear when looking at the density of power *per unit of volume*. In the case of the infinite material, in fact, it is immediate to verify that:

$$\langle \mathrm{Re}\mathbf{E}^{ext} \cdot \mathrm{Re}\mathbf{J}^{ind} \rangle = -\langle \mathrm{Re}\mathbf{E}^{ind} \cdot \mathrm{Re}\mathbf{J}^{ext} \rangle \qquad \text{(Bulk)} \tag{B.43}$$

In the case of the slab, the last equality does not hold anymore!

$$\langle \mathrm{Re}\mathbf{E}^{ext} \cdot \mathrm{Re}\mathbf{J}^{ind} \rangle \neq -\langle \mathrm{Re}\mathbf{E}^{ind} \cdot \mathrm{Re}\mathbf{J}^{ext} \rangle \qquad \text{(Slab)} \tag{B.44}$$

This is due to the fact that the induced electric field and the induced current, in a slab, have a totally different dependence in z. In order to see the conservation of energy in the case of a slab we have to compare the integral in z of these two quantities, i.e. the density of power *per unit of surface*:

$$\begin{aligned} \langle \mathrm{Re}\mathbf{E}^{ext} \cdot \mathrm{Re}\mathbf{J}^{ind} \rangle_S &= \int_{-\infty}^{\infty} dz \langle \mathrm{Re}\mathbf{E}^{ext} \cdot \mathrm{Re}\mathbf{J}^{ind} \rangle \\ &= -\int_{-\infty}^{\infty} dz \langle \mathrm{Re}\mathbf{E}^{ind} \cdot \mathrm{Re}\mathbf{J}^{ext} \rangle = -\langle \mathrm{Re}\mathbf{E}^{ind} \cdot \mathrm{Re}\mathbf{J}^{ext} \rangle_S \end{aligned} \tag{B.45}$$

B.2.3 EELS in slab (out-of-plane)

In this section I will derive the expression of the energy loss for electrons travelling orthogonally to the slab. As we have seen in section 6.3, the displacement of oscillators undergoing an external perturbation orthogonal to the surface will be given by:

$$\mathbf{\Delta}(\mathbf{r}, t) = \frac{e}{m_e} \frac{\Theta(z + \frac{L}{2})\Theta(-z + \frac{L}{2})}{-\omega^2 + \omega_0^2 - i\frac{\omega}{\tau} + \omega_{pl}^2} \mathbf{E}^{ext}(\mathbf{r}, t) \tag{B.46}$$

While the induced electric field can be written as:

$$\mathbf{E}^{ind}(\mathbf{r}, t) = \begin{cases} -\dfrac{m_e}{e}\omega_{pl}^2 \mathbf{\Delta}(\mathbf{r}, t) & \text{for} \quad |z| < \dfrac{L}{2} \\ 0 \quad \text{for} \quad |z| \geq \dfrac{L}{2} \end{cases} \tag{B.47}$$

The current of external electrons will be linked with the external electric field via the relationship

$$\mathbf{J}^{ext} = \frac{i\omega}{4\pi} \mathbf{E}^{ext} \tag{B.48}$$

The induced field, on the other hand, will be written:

$$\mathbf{E}^{ind} = \Theta(z+\frac{L}{2})\Theta(-z+\frac{L}{2})\frac{\omega_{pl}^2}{-\omega^2+\omega_0^2-i\frac{\omega}{\tau}+\omega_{pl}^2}\mathbf{E}^{ext}(\mathbf{r},t) \tag{B.49}$$

Therefore, the density of dissipated power (averaged over an oscillation period) will be given by:

$$\begin{aligned}\mathcal{W} &= \mathrm{Re}\mathbf{J}^{ext}\cdot\mathrm{Re}\mathbf{E}^{ind} \\ &= \frac{\omega}{8\pi}\mathrm{Im}\frac{1}{\varepsilon(\omega)}\Theta(z+\frac{L}{2})\Theta(-z+\frac{L}{2})|E_0^{ext}|^2\end{aligned} \tag{B.50}$$

B.2.4 EELS: conclusion

In this section we derived, within the Lorentz model, the expression for the energy loss of an electron beam crosssing the matter, and we compared the case of an infinite bulk with the case of a very thin slab (limit $\mathbf{q}L/2 \ll 1$). For the bulk, we found again the well known result $EELS \propto \mathrm{Im}\frac{1}{\varepsilon(\omega)}$. For the slab, we found that the expression for the energy loss depends on the direction of the external beam. In the case of electrons propagating parallel to the slab, the induced field is strongly suppressed, and as a consequence, the density of dissipated power is nomore proportional to $\mathrm{Im}\frac{1}{\varepsilon(\omega)}$, but to $\mathrm{Im}\varepsilon(\omega)$. When the external electron beam is travelling orthogonally to the slab, we recover the bulk result $EELS \propto \mathrm{Im}\frac{1}{\varepsilon(\omega)}$.

Appendix C

Transfer matrix formalism

C.1 Schubert's transfer matrix

In this section we briefly illustrate the formalism of the Schubert's transfer matrix. As we have mentioned in Chapter 7, this method allows one to calculate the reflection coefficients of an arbitrarily big stack of arbitrarily anisotropic films. Even if during this thesis we limited ourselves to study the case of a single anisotropic film (for which the expression of reflection coefficients has already been reported in Chapter 7), in the code that we have written for the calculation of reflectance spectra we implemented the expression for the reflection coefficients in their most general form. We will not give here the proof of these formulas (for which we refer to Ref. [68]), but we will limit ourselves to report the most important results. Let's suppose to have a stack of N films, having thickness d_i and dielectric tensor $\overset{\leftrightarrow}{\varepsilon}^{(i)}$ (with $i = 1, \ldots, N$), sandwiched between two infinite and homogeneous halfspaces , called respectively *ambient medium* and *exit medium*, and having dielectric function ε_a and ε_f[1]. Let's suppose that an electromagnetic wave is impinging from the ambient medium to the sample. The amplitude of the s and p component of the incident wave will be respectively denoted as A_s and A_p, while the amplitude of the s and p component of the reflected and transmitted wave will be respectively B_s,B_p and C_s,C_p. We will make also the assumption, physically meaningful, that no wave is backpropagating in the exit medium. The transfer matrix of the system is defined as the matrix which relates the amplitude of propagating fields in the ambient medium with the amplitude of

[1] In the following, we will make the assumption that the ambient medium and the exit medium are both isotropic. Actually, in Ref. [68], it is also considered the more general case in which ε_f is not a scalar, in order to allow the description of anisotropic substrate. We will make moreover the assumption that the crystal axis of the films lay parallel to the cartesian axis, i.e. two axis parallel to the interface and the third one orthogonal.

the fields in the exit medium:

$$\begin{pmatrix} A_s \\ B_s \\ A_p \\ B_p \end{pmatrix} = \mathbf{T} \begin{pmatrix} C_s \\ 0 \\ C_p \\ 0 \end{pmatrix} \tag{C.1}$$

From Eq. (C.1), one can trivially obtain the expressions of the reflection coefficients of the system as function of the matrix elements of T:

$$r_{ss} = \frac{T_{21}T_{33} - T_{23}T_{31}}{T_{11}T_{33} - T_{13}T_{31}} \tag{C.2}$$

$$t_{ss} = \frac{T_{33}}{T_{11}T_{33} - T_{13}T_{31}} \tag{C.3}$$

$$r_{pp} = \frac{T_{43}T_{11} - T_{13}T_{41}}{T_{33}T_{11} - T_{31}T_{13}} \tag{C.4}$$

$$t_{pp} = \frac{T_{11}}{T_{33}T_{11} - T_{31}T_{13}} \tag{C.5}$$

As reported in Ref. [68], the transfer matrix of the system can be expressed as product of several partial transfer matrices, each of them describing the reflection and the transmission of the fields at one of the interfaces of the system:

$$\begin{aligned} \mathbf{T} &= \mathbf{L}_a^{-1} \prod_{i=1}^{N} [\mathbf{T}_p^i(d_i)]^{-1} \mathbf{L}_f \\ &= \mathbf{L}_a^{-1} \prod_{i=1}^{N} [\mathbf{T}_p^i(-d_i)] \mathbf{L}_f \end{aligned} \tag{C.6}$$

Here $\mathbf{L}_a^{-1}$ is called the *inverse incident matrix*, and it just depends on the properties of the ambient medium. The $\mathbf{T}_p^i(d_i)$ are the *partial transfer matrices*, each of them associated to one of the films which compose the sample, while the $\mathbf{L}_f$ is called *exit matrix*, which just depend on the properties of the exit material (typically the substrate). If we make the assumption that the ambient medium is homogenous, non magnetic, and isotropic, the inverse incident matrix can be written as:

$$\mathbf{L}_a^{-1} = \frac{1}{2} \begin{pmatrix} 0 & 1 & -1/(\sqrt{\varepsilon_a}\cos\theta_i) & 0 \\ 0 & 1 & 1/(\sqrt{\varepsilon_a}\cos\theta_i) & 0 \\ 1/\cos\theta_i & 0 & 0 & 1/\sqrt{\varepsilon_a} \\ -1/\cos\theta_i & 0 & 0 & 1/\sqrt{\varepsilon_a} \end{pmatrix} \tag{C.7}$$

Let's suppose that the exit medium is isotropic. Assuming that θ_i is the incidence angle in the ambient medium, the exit angle will be given by:

$$\cos\theta_f = \sqrt{1 - \frac{\varepsilon_a}{\varepsilon_f}\sin^2\theta_i} \tag{C.8}$$

and the exit matrix will be given by:

$$\mathbf{L_f} = \begin{pmatrix} 0 & 0 & \cos\theta_f & 0 \\ 1 & 0 & 0 & 0 \\ -\sqrt{\varepsilon_f}\cos\theta_f & 0 & 0 & 0 \\ 0 & 0 & \sqrt{\varepsilon_f} & 0 \end{pmatrix} \tag{C.9}$$

Let's now suppose to have a layer of anisotropic material of thickness d, having optical axes laying parallel with the cartesian axis (i.e. $\varepsilon_{xx} \neq \varepsilon_{yy} \neq \varepsilon_{zz}$ and $\varepsilon_{ij} = 0 \forall i \neq j$). We introduce the following auxiliary quantities:

$$N_{ij} = \varepsilon_{ii}\sqrt{1 - (\varepsilon_a/\varepsilon_{jj})\sin^2\theta_i} \tag{C.10}$$

$$\begin{aligned} \kappa_p &= k_0 d N_{xz} \\ \kappa_s &= k_0 d N_{yy} \end{aligned} \tag{C.11}$$

The partial transfer matrix for such a film will be :

$$\mathbf{T}_p(d) = \begin{pmatrix} \cos\kappa_p & 0 & 0 & i(N_{xz}/\varepsilon_{xx})\sin\kappa_p \\ 0 & \cos\kappa_s & -i(1/N_{yy})\sin\kappa_s & 0 \\ 0 & -iN_{yy}\sin\kappa_s & \cos\kappa_s & 0 \\ i(\varepsilon_{xx}/N_{xz})\sin\kappa_p & 0 & 0 & \cos\kappa_p \end{pmatrix} \tag{C.12}$$

C.2 True film vs effective film

In chapter 7, we calculated the reflectance of a thin film and the reflectance of an effective slab obtained combining with the original film an additional layer of vacuum. As we have shown in Fig. (7.10), in the limit of very thin material , the reflectance of the two systems results to be the same, despite the fact that the dielectric function of the two systems are very different. In this section, we want to proof analytically this result. In order to do that, we recall briefly here the properties of the two systems. The first (which we informally called "the true film") is a slab of thickness d and dielectric function

$$\varepsilon(\omega) = 1 - \frac{\omega_{pl}^2}{\omega^2 - \omega_0^2 + i\omega/\tau} \tag{C.13}$$

and it is sandwiched between two infinite half-spaces having dielectric function $\varepsilon_{vac} = 1$. The reflection coefficient of this slab will be given by:

$$r_{slab}^{true} = \frac{r(1 - e^{2i\beta})}{1 - r^2 e^{-2i\beta}} \tag{C.14}$$

with

$$\beta = k_0 d\sqrt{\varepsilon - \varepsilon_{vac}\sin^2\theta_i} \tag{C.15}$$

Here k_0 stands for the wave-vector of light in vacuum, while, according the usual notation, θ_i is the incidence angle. Instead, r represent the Fresnel coefficient at the vacuum-matter interface, and it will be given by:

$$r = \frac{\varepsilon\cos\theta_i - \varepsilon_{vac}^{\frac{1}{2}}\sqrt{\varepsilon - \varepsilon_{vac}\sin^2\theta_i}}{\varepsilon\cos\theta_i + \varepsilon_{vac}^{\frac{1}{2}}\sqrt{\varepsilon - \varepsilon_{vac}\sin^2\theta_i}} \tag{C.16}$$

The effective slab instead, will have thickness $d^{eff} = d + d_{vac}$, and dielectric tensor

$$\overleftrightarrow{\varepsilon}^{eff}(\omega) = \begin{pmatrix} \varepsilon_{||}^{eff}(\omega) & 0 & 0 \\ 0 & \varepsilon_{||}^{eff}(\omega) & 0 \\ 0 & 0 & \varepsilon_{\perp}^{eff}(\omega) \end{pmatrix} \tag{C.17}$$

with:

$$\begin{aligned} \varepsilon_{||}^{eff}(\omega) &= \frac{d_{vac}\varepsilon_{vac} + d\varepsilon}{d + d_{vac}} \\ \varepsilon_{\perp}^{eff}(\omega) &= \frac{\varepsilon\varepsilon_{vac}}{d\varepsilon_{vac} + d_{vac}\varepsilon}(d + d_{vac}) \end{aligned} \tag{C.18}$$

The reflection coefficient will be given by:

$$r_{010}^{eff} = r^{eff}\frac{1 - e^{2i\beta^{eff}}}{1 - (r^{eff})^2 e^{2i\beta^{eff}}} \tag{C.19}$$

where:

$$\beta^{eff} = k_0 d^{eff} \left(\frac{\varepsilon_{||}^{eff}}{\varepsilon_{\perp}^{eff}} \right)^{\frac{1}{2}} \sqrt{\varepsilon_{\perp}^{eff} - \varepsilon_{vac} \sin^2 \theta_i} \tag{C.20}$$

and r^{eff} is the Fresnel coefficient of the interface between the vacuum and the semi-infinite material having dielectric function (C.18):

$$r^{eff} = \frac{(\varepsilon_{\perp}^{eff} \varepsilon_{||}^{eff})^{\frac{1}{2}} \cos\theta_i - \varepsilon_{vac}^{\frac{1}{2}} \sqrt{\varepsilon_{\perp}^{eff} - \varepsilon_{vac} \sin^2 \theta_i}}{(\varepsilon_{\perp}^{eff} \varepsilon_{||}^{eff})^{\frac{1}{2}} \cos\theta_i + \varepsilon_{vac}^{\frac{1}{2}} \sqrt{\varepsilon_{\perp}^{eff} - \varepsilon_{vac} \sin^2 \theta_i}} \tag{C.21}$$

In the limit $|\beta| \sim |(d/\lambda_0)\sqrt{\varepsilon}| \ll 1$ the exponential appearing in Eq. (C.14) can be expanded as:

$$e^{-2i\beta} \approx 1 - 2ik_0 d \sqrt{\varepsilon - \varepsilon_{vac} \sin^2 \theta_i} \tag{C.22}$$

Analogously, the exponential appearing in Eq. (C.19), may be approximated as:

$$e^{-2i\beta^{eff}} \approx 1 - 2ik_0 d^{eff} \left(\frac{\varepsilon_{||}^{eff}}{\varepsilon_{\perp}^{eff}} \right)^{\frac{1}{2}} \sqrt{\varepsilon_{\perp}^{eff} - \varepsilon_{vac} \sin^2 \theta_i} \tag{C.23}$$

Substituting expressions (C.22) and (C.23) respectively in Eq.s (C.14) and (C.19), one obtain the following expression for the reflection coefficients, valid in the limit $(d/\lambda_0 \ll 1)$:

$$r \approx -2ik_0 d \frac{\varepsilon^2 \cos^2 \theta_i - \varepsilon_{vac}(\varepsilon - \varepsilon_{vac} \sin^2 \theta_i)}{4\varepsilon \varepsilon_{vac}^{\frac{1}{2}} \cos\theta_i - 2ik_0 d \big(\varepsilon \cos\theta_i - \varepsilon_{vac}^{\frac{1}{2}} \sqrt{\varepsilon - \varepsilon_{vac} \sin^2 \theta_i}\big)^2} \tag{C.24}$$

$$r^{eff} \approx -2ik_0 d \frac{\varepsilon^2 \cos^2 \theta_i - \varepsilon_{vac}(\varepsilon - \varepsilon_{vac} \sin^2 \theta_i)}{4\varepsilon \varepsilon_{vac}^{\frac{1}{2}} \cos\theta_i - 2ik_0 d^{eff} \left(\big(\varepsilon \varepsilon_{||}^{eff}\big)^{\frac{1}{2}} \cos\theta_i - \big(\varepsilon \varepsilon_{vac} / \varepsilon_{\perp}^{eff}\big)^{\frac{1}{2}} \sqrt{\varepsilon_{\perp}^{eff} - \varepsilon_{vac} \sin^2 \theta_i} \right)^2} \tag{C.25}$$

As we can see, the two expression just differ in the denominators. The denominator of the Eq. (C.24) can be written:

$$\begin{aligned} D_1 = & \\ & = 4\varepsilon\varepsilon_{vac}^{\frac{1}{2}}\cos\theta_i - 2ik_0d\big(\varepsilon\cos\theta_i - \varepsilon_{vac}^{\frac{1}{2}}\sqrt{\varepsilon-\varepsilon_{vac}\sin^2\theta_i}\big)^2 \\ & = 4\varepsilon\varepsilon_{vac}^{\frac{1}{2}}\cos\theta_i - 2ik_0d\Big[\varepsilon^2\cos^2\theta_i + \varepsilon_{vac}(\varepsilon-\varepsilon_{vac}\sin^2\theta_i) + \\ & - 2\varepsilon\varepsilon_{vac}^{\frac{1}{2}}\cos\theta_i\sqrt{\varepsilon-\varepsilon_{vac}\sin^2\theta_i}\Big] \\ & = 4\varepsilon\varepsilon_{vac}^{\frac{1}{2}}\cos\theta_i - 2ik_0d\varepsilon^2\cos^2\theta_i - 2ik_0d\varepsilon_{vac}\varepsilon + 2ik_0d\varepsilon_{vac}^2\sin^2\theta_i \\ & + 4ik_0d\varepsilon\varepsilon_{vac}^{\frac{1}{2}}\cos\theta_i\sqrt{\varepsilon-\varepsilon_{vac}\sin^2\theta_i} \end{aligned} \tag{C.26}$$

The denominator of Eq. (C.25), substituting $\varepsilon_{||}^{eff}$ and $\varepsilon_{\perp}^{eff}$ with expressions (C.18), and making the further assumption that $d_{vac} = d$ (implying $d^{eff} = 2d$), can be rewritten as:

$$\begin{aligned} D_2 = & \\ & = 4\varepsilon\varepsilon_{vac}^{\frac{1}{2}}\cos\theta_i + \\ & - 2ik_0d^{eff}\left(\big(\varepsilon\varepsilon_{||}^{eff}\big)^{\frac{1}{2}}\cos\theta_i - \big(\varepsilon\varepsilon_{vac}/\varepsilon_{\perp}^{eff}\big)^{\frac{1}{2}}\sqrt{\varepsilon_{\perp}^{eff}-\varepsilon_{vac}\sin^2\theta_i}\right)^2 \\ & = 4\varepsilon\varepsilon_{vac}^{\frac{1}{2}}\cos\theta_i + \\ & - 2ik_0d\Big[\varepsilon^2\cos^2\theta_i + \varepsilon\varepsilon_{vac}\cos^2\theta_i + 2\varepsilon\varepsilon_{vac} - \varepsilon\varepsilon_{vac}\sin^2\theta_i - \varepsilon_{vac}^2\sin^2\theta_i + \\ & - 2\varepsilon^{\frac{1}{2}}(\varepsilon+\varepsilon_{vac})\cos\theta_i\sqrt{2\varepsilon\varepsilon_{vac}/(\varepsilon+\varepsilon_{vac}) - \varepsilon_{vac}\sin^2\theta}\Big] \\ & = 4\varepsilon\varepsilon_{vac}^{\frac{1}{2}}\cos\theta_i - 2ik_0d\varepsilon^2\cos^2\theta_i - 2ik_0d\varepsilon\varepsilon_{vac} + 2ik_0d\varepsilon_{vac}^2\sin^2\theta_i + \\ & - 4ik_0d\varepsilon\varepsilon_{vac}\cos^2\theta_i - 4ik_0d\varepsilon^{\frac{1}{2}}(\varepsilon+\varepsilon_{vac})\cos\theta_i\sqrt{2\varepsilon\varepsilon_{vac}/(\varepsilon+\varepsilon_{vac}) - \varepsilon_{vac}\sin^2\theta} \end{aligned} \tag{C.27}$$

As we can see from direct comparison of Eq.s (C.26) and (C.27), D_1 and D_2 just differ for terms which are $\sim (d/\lambda_0)\sqrt{\varepsilon}\varepsilon$ or smaller.

Appendix D

Convergence of SHG spectra

In this Appendix we present the convergence test that we have performed for the silicon slab (made of 24 silicon layers) functionalised with Thymine. The convergence test for the surfaces functionalised with the other nucleobases have been performed in analogous way. Chosing the parameters for which the calculation can be considered converged is a less trivial task than it could appear. In fact, if on one side we want to perform the calculation with the maximum of the accuracy, on the other side we have to chose them carefully, in order to keep under control the computational cost of the calculation. The spectra have been converged in the following way: first of all, we calculated the Kohn-Sham wave-functions on a relatively small k-points grid (1x4x1 with double shift). After that, we gradually increased the number of bands included in the calculation. The result of this test is reported, for all the calculated components, in Fig. (D.1). As we can see in the figure, the spectrum requires at least 400 bands in order to be considered converged in the energy region between 0 and 4 eV. If we further increase the number of bands, we see that a new feature appears in the spectrum in the energy region between 4 and 5 eV. We consider therefore the spectrum converged for `nbands`=600. The number of bands included in the spectra depends also on the parameter `lomo`, which allows one to set the lowest valence band to be included in the calculation. This parameter allows one to greatly optimise the calculation of the second order response: the valence bands which lay at low energy in fact are expected to give a modest contribution to the spectrum, and therefore they can be eliminated from the calculation. In Fig. (D.2), we report the calculation of the IPA spectrum for several value of the `lomo` parameter, while in Fig. (D.3) we report the number of transitions per **k**-point (which is proportional to the computational time) as a function of the `lomo` parameter. As we can see in Fig. (D.2), eliminating from the calculation the 50 lowest valence bands does not produce almost any change in the spectra, and as we can see in Fig. (D.2) reduces of the 30% the number of transitions to be evaluated. In Fig. (D.4), the convergence test in the number of plane waves is reported. As shown in figure, `npwwfn`=3000 is enough to converge all the components of the spectrum. Finally,

we performed the convergence in the number of k-points. Using the converged values for the parameters `nbands`,`lomo`,and `npwwfn`, we calculated several times the IPA spectrum, increasing each time the number of k-points included in the calculation. The result of this series of calculations is reported in Fig. (D.5)

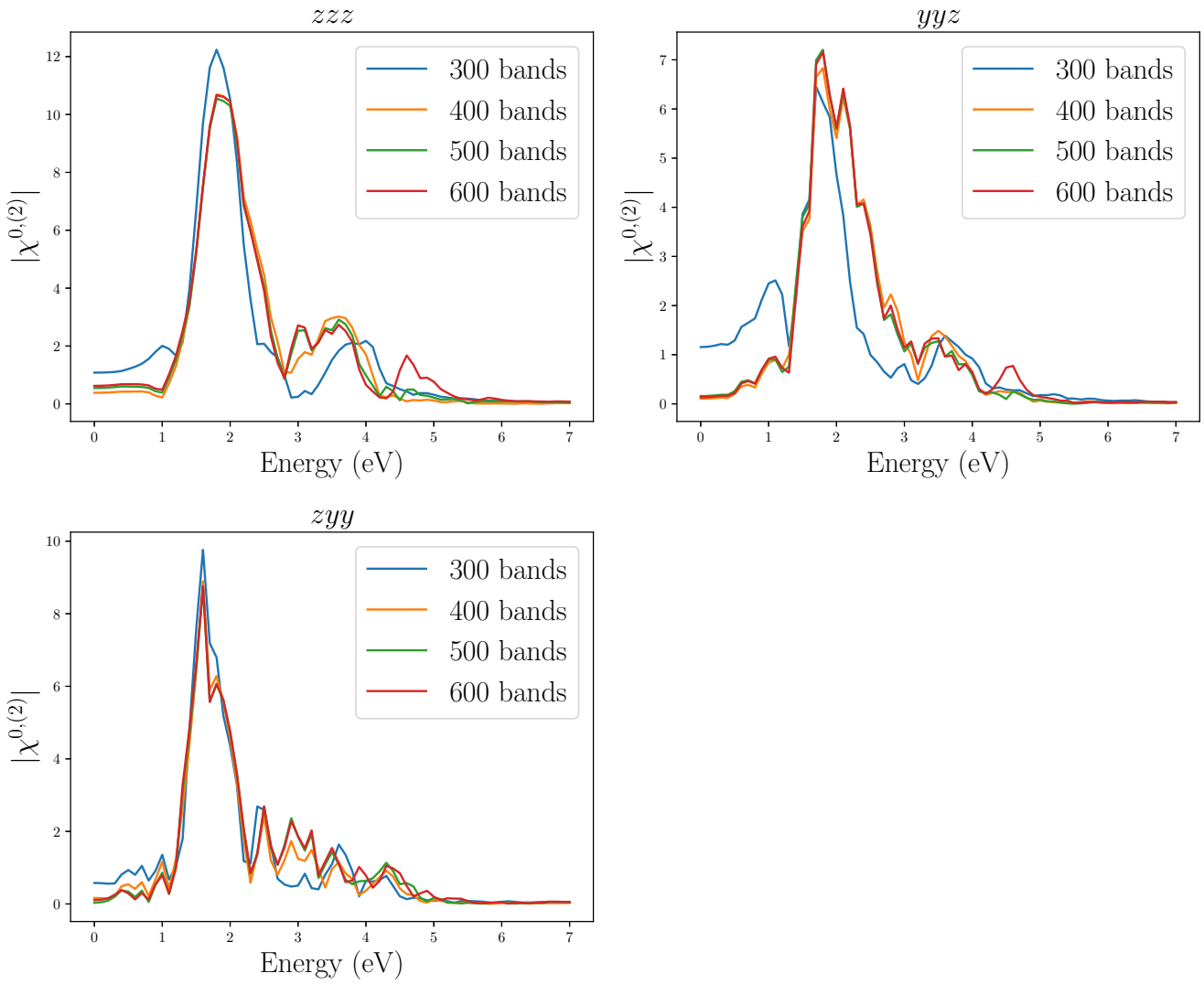
zzz
yyz
zyy
300 bands
400 bands
500 bands
600 bands
$|\chi^{0,(2)}|$
Energy (eV)

Figure D.1

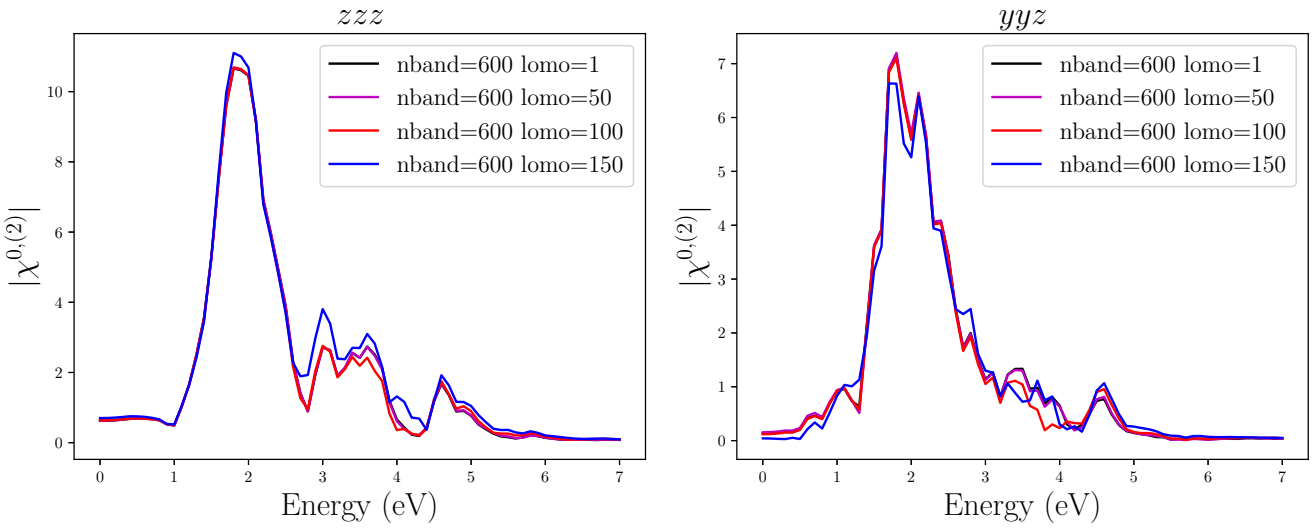

Figure D.2

Figure D.3

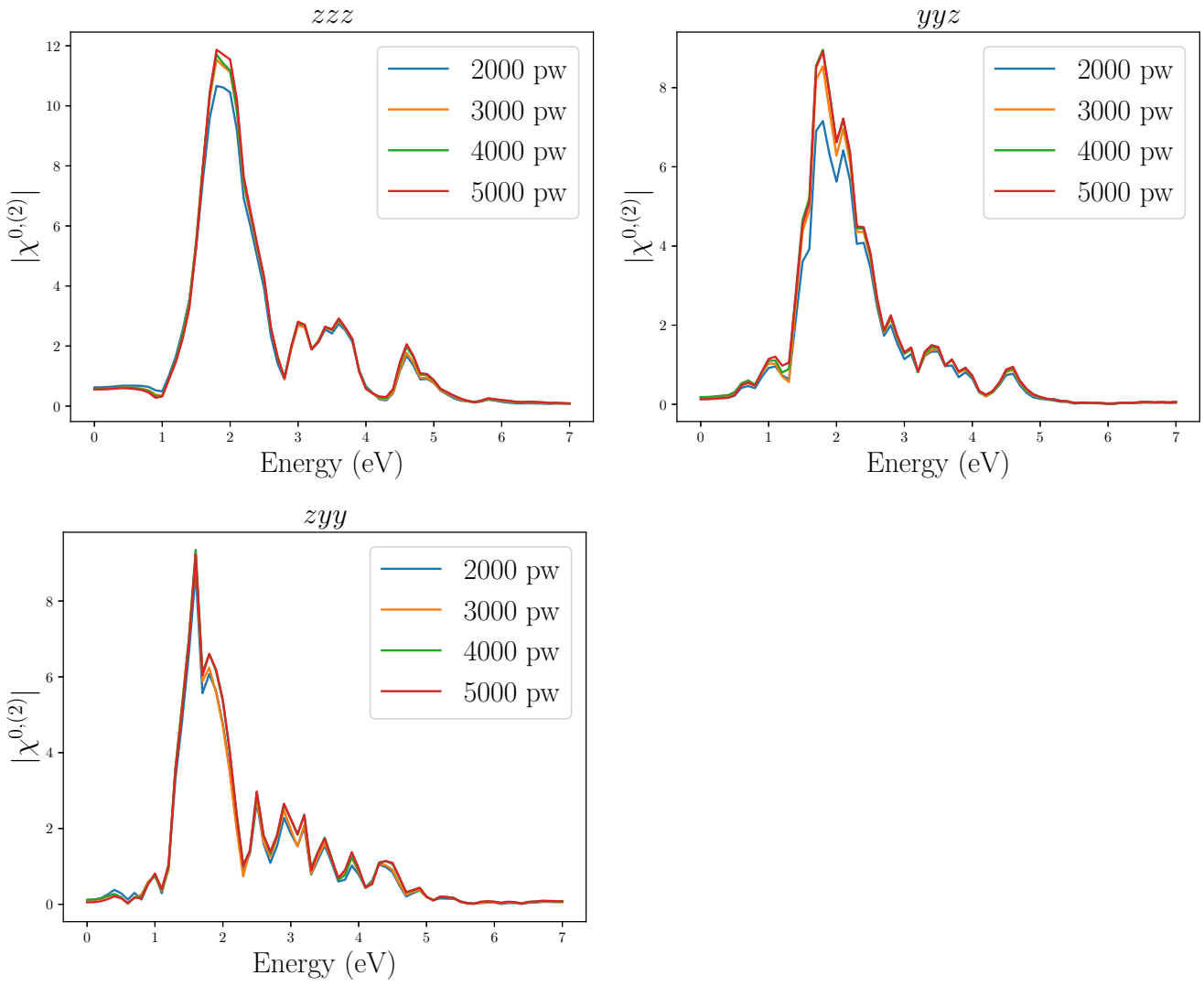

Figure D.4

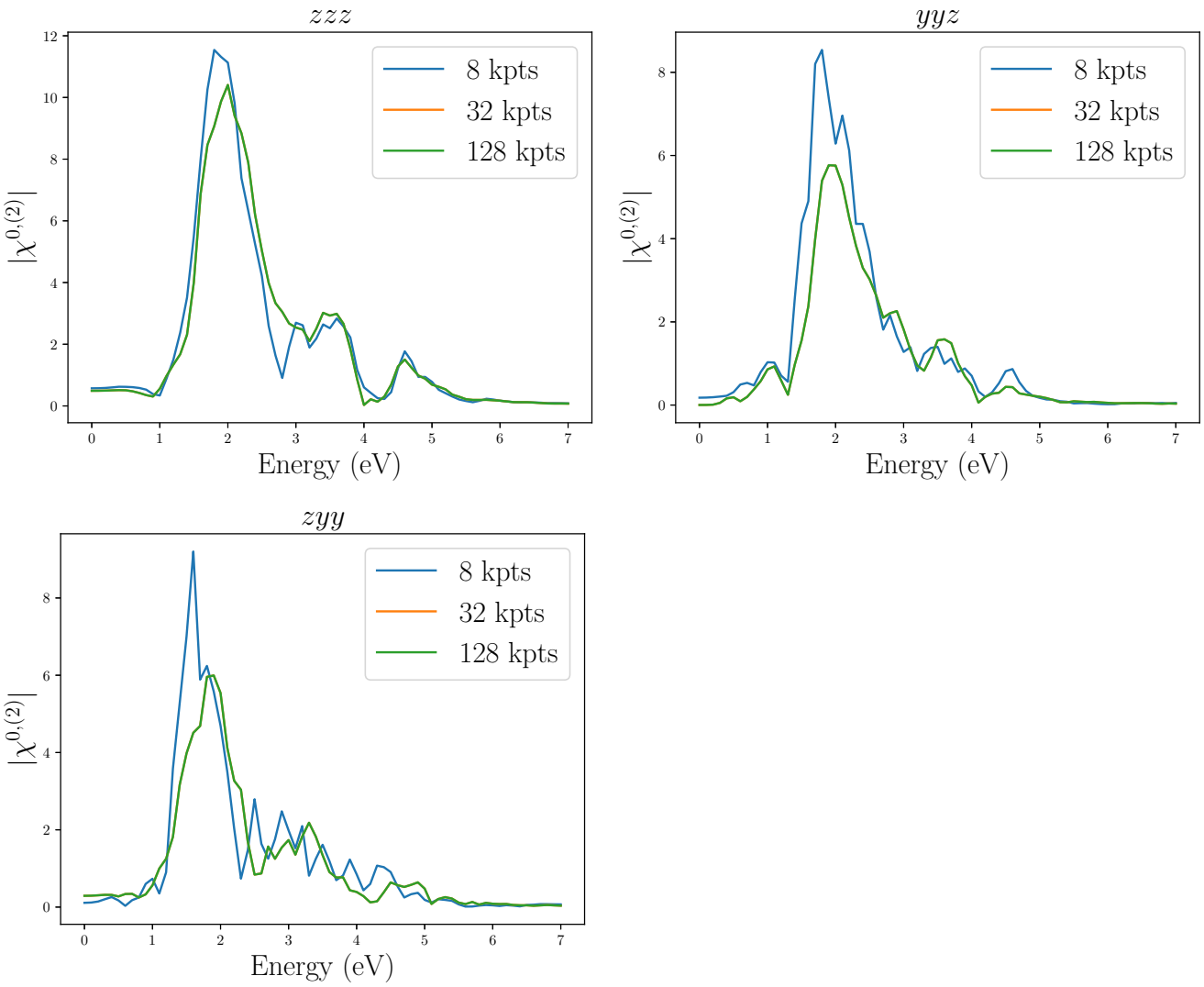

Figure D.5

Abstract

Understanding the mechanism of interaction between amino acids and peptides with surfaces opens new perspectives. Adsorption of DNA molecules on semiconducting surfaces is regularly evoked for the design of biosensors or the production of bio-materials. The possibility to functionalize surfaces with bio-molecules, to create organized structures up to nanometers' distances depends on our capability to understand precisely the mechanisms which govern the deposition of molecular films onto different kinds of surfaces.

Non-linear optics and more precisely Second Harmonic Generation (SHG) is particularly adapted to study surfaces. In this spectroscopy, two photons of the same energy are absorbed and a photon of double energy is emitted. Describing this physical phenomenon requires the calculation of the second order susceptibility: since it is zero for centrosymmetric material, the response can only comes from the surface, which is at the origin of the symmetry breaking.

Through this thesis, functionalised surfaces have been modelled as slabs introduced in a the supercell, within a reciprocal space formalism. Beyond the elimination of spurious vacuum effects, that we perform within the selected-G method, we also investigated optical properties of 2D systems.

A mixed-space formalism - which allows us to treat the direction orthogonal to the surface in real space, and to decouple the slab from its replicas- has been developed, and the differences between the in-plane and out-of-plane response of an isolated slab of silicon have been investigated in detail. The link with experimentally measured quantities has also be done. More specifically, while the macroscopic dielectric function of a thin film is intrinsically hard to be defined, experimental quantities such as reflectance and transmittance are not affected by this ambiguity. The conditions in which the calculation must be performed in order to model a surface, i.e. a semi-infinite object, have been clarified.

SHG spectra of a silicon surface (4x1) functionalised with molecules of thymine, uracil, and cytosine have been calculated in presence of local field effects. The differences between spectra have been studied, and the possibility to use SHG as a tool to characterise the chemical nature of the adsorbate has been analysed. The sensitivity of SHG to the adsorption configuration has been also investigated, by comparison of SHG spectra generated by surfaces functionalised with thymine in different adsorption geometries.

Résumé

Comprendre les mécanismes d'interaction entre des acides aminés ou des peptides avec les surfaces ouvre de nouvelles perspectives. L'adsorption de molécules d'ADN sur des surfaces semiconductrices est régulièrement évoquée pour la conception de biosenseurs ou la production de bio-matériaux. La possibilité de fonctionaliser des surfaces à l'aide de bio-molécules, de créer des structures ordonnées sur des distances de quelques nanomètres dépend de notre capacité à comprendre les phénomènes gouvernant la déposition de films moléculaires sur différents types de surfaces.

L'optique non-linéaire et plus précisément la génération de seconde harmonique (SHG) est particulièrement adaptée à l'étude des surfaces. Dans cette spectrocopie, deux photons de même énergie sont absorbés et un photon d'énergie double est émis. La description de ce phénomène physique passe par le calcul de susceptibilité d'ordre 2 : celle-ci étant nulle pour les matériaux centrosymmétriques, la réponse ne peut provenir que de la surface, qui est à l'origine de la brisure de symétrie .

Pendant cette thèse, les surfaces fonctionnalisées ont été représentées par des couches introduites dans une supercellule, dans un formalisme en espace réciproque. Au delà de la suppression du vide introduit dans la supercellule, que nous traitons par la méthode Selected-G, nous avons également été amenés à nous interroger sur les propriétés optiques des systèmes 2D. Un formalisme en espace mixte - qui permet de traiter la direction orthogonale à la surface dans l'espace réel, et d'isoler la couche de ses répliques - a été mis au point, et les différences entre les réponses hors-plan et dans le plan d'une couche de silicium isolée ont été investiguées en détail. Le lien avec les grandeurs expérimentalement mesurées a également été fait. En particulier, alors que la fonction diélectrique macroscopique d'une couche mince est intrinsèquement difficile à définir, les quantités expérimentales telles que la réflectance et la transmittance ne sont pas affectées par cette ambiguïté. Les conditions du calcul pour modéliser une surface, c'est-à-dire un espace semi-infini ont été clarifiées.

Les spectres de SHG d'une surface de silicium (4x1) fonctionnalisées avec des molécules de thymine, uracil et cytosine ont été calculés avec les champs locaux. Les différences entre les spectres ont été étudiées, et les potentialités de la SHG comme outil pour reconnaître la nature chimique de l'adsorbat ont été analysées. La sensibilité de la SHG à la configuration d'adsorption a également été évaluée, en comparant les spectres au second ordre générés par des surfaces fonctionnalisées à la thymine dans différentes géométries d'adsorption.

Bibliography

[1] Keiichi Itakura, Tadaaki Hirose, Roberto Crea, Arthur D. Riggs, Herbert L. Heyneker, Francisco Bolivar, and Herbert W. Boyer. Expression in Escherichia coli of a Chemically Synthesized Gene for the Hormone Somatostatin. *Science*, 198(4321):1056–1063, December 1977.

[2] B. Doris, Meikei Ieong, T. Kanarsky, Ying Zhang, R.A. Roy, O. Dokumaci, Zhibin Ren, Fen-Fen Jamin, Leathen Shi, W. Natzle, Hsiang-Jen Huang, J. Mezzapelle, A. Mocuta, S. Womack, M. Gribelyuk, E.C. Jones, R.J. Miller, H.-S.P. Wong, and W. Haensch. Extreme scaling with ultra-thin si channel mosfets. In *Digest. International Electron Devices Meeting,*, pages 267–270, 2002.

[3] H. Wakabayashi, S. Yamagami, N. Ikezawa, A. Ogura, M. Narihiro, K. Arai, Y. Ochiai, K. Takeuchi, T. Yamamoto, and T. Mogami. Sub-10-nm planar-bulk-cmos devices using lateral junction control. In *IEEE International Electron Devices Meeting 2003*, pages 20.7.1–20.7.3, 2003.

[4] Giuseppe Iannaccone, Francesco Bonaccorso, Luigi Colombo, and Gianluca Fiori. Quantum engineering of transistors based on 2d materials heterostructures. *Nature Nanotechnology*, 13(3):183–191, 2018.

[5] Manish Chhowalla, Debdeep Jena, and Hua Zhang. Two-dimensional semiconductors for transistors. *Nature Reviews Materials*, 1(11):16052, 2016.

[6] Hirotaka Miyachi. *Nucleic Acid Arrays*, chapter 53. American Cancer Society, 2008.

[7] M. Schienle, C. Paulus, A. Frey, F. Hofmann, B. Holzapfl, P. Schindler-Bauer, and R. Thewes. A fully electronic dna sensor with 128 positions and in-pixel a/d conversion. *IEEE Journal of Solid-State Circuits*, 39(12):2438–2445, 2004.

[8] Victor Zhirnov, Reza M. Zadegan, Gurtej S. Sandhu, George M. Church, and William L. Hughes. Nucleic acid memory. *Nature Materials*, 15(4):366–370, 2016.

[9] P. A. Franken, A. E. Hill, C. W. Peters, and G. Weinreich. Generation of optical harmonics. *Phys. Rev. Lett.*, 7:118–119, Aug 1961.

[10] G. H. C. New and J. F. Ward. Optical third-harmonic generation in gases. *Phys. Rev. Lett.*, 19:556–559, Sep 1967.

[11] C. H. Lee, R. K. Chang, and N. Bloembergen. Nonlinear electroreflectance in silicon and silver. *Phys. Rev. Lett.*, 18:167–170, Jan 1967.

[12] Thomas Brabec and Ferenc Krausz. Intense few-cycle laser fields: Frontiers of nonlinear optics. *Rev. Mod. Phys.*, 72:545–591, Apr 2000.

[13] Shen Y.R. *The principles of nonlinear optics*. John Wiley & Sons, 1984.

[14] Hongping Wu, Hongwei Yu, Zhihua Yang, Xueling Hou, Xin Su, Shilie Pan, Kenneth R. Poeppelmeier, and James M. Rondinelli. Designing a deep-ultraviolet nonlinear optical material with a large second harmonic generation response. *Journal of the American Chemical Society*, 135(11):4215–4218, 03 2013.

[15] Theodossis A. Theodossiou, Christopher Thrasivoulou, Chidi Ekwobi, and David L. Becker. Second harmonic generation confocal microscopy of collagen type i from rat tendon cryosections. *Biophysical Journal*, 91(12):4665–4677, 2006.

[16] Mutsuo Nuriya, Jiang Jiang, Boaz Nemet, Kenneth B. Eisenthal, and Rafael Yuste. Imaging membrane potential in dendritic spines. *Proceedings of the National Academy of Sciences*, 103(3):786–790, 2006.

[17] Xiaobo Yin, Ziliang Ye, Daniel A. Chenet, Yu Ye, Kevin O'Brien, James C. Hone, and Xiang Zhang. Edge nonlinear optics on a mos2 atomic monolayer. *Science*, 344(6183):488–490, 2014.

[18] Nicolas Tancogne-Dejean, Christine Giorgetti, and Valérie Véniard. Optical properties of surfaces with supercell ab initio calculations: Local-field effects. *Phys. Rev. B*, 92:245308, Dec 2015.

[19] Nicolas Tancogne-Dejean, Christine Giorgetti, and Valérie Véniard. Ab initio description of second-harmonic generation from crystal surfaces. *Phys. Rev. B*, 94:125301, Sep 2016.

[20] Nicolas Tancogne-Dejean. *Ab initio description of second-harmonic generation from crystal surfaces*. Theses, Ecole polytechnique, September 2015.

[21] Attila Szabo and Neil S. Ostlund. *Modern Quantum Chemistry: Introduction to Advanced Electronic Structure Theory*. Dover Publications, Inc., Mineola, first edition, 1996.

[22] P. Hohenberg and W. Kohn. Inhomogeneous electron gas. *Phys. Rev.*, 136:B864–B871, Nov 1964.

[23] W. Kohn and L. J. Sham. Self-consistent equations including exchange and correlation effects. *Phys. Rev.*, 140:A1133–A1138, Nov 1965.

[24] S. Goedecker, M. Teter, and J. Hutter. Separable dual-space gaussian pseudopotentials. *Phys. Rev. B*, 54:1703–1710, Jul 1996.

[25] N. Troullier. Efficient pseudopotentials for plane-wave calculations. *Physical Review B*, 43(3):1993–2006, 1991.

[26] Erich Runge and E. K. U. Gross. Density-functional theory for time-dependent systems. *Phys. Rev. Lett.*, 52:997–1000, Mar 1984.

[27] Robert van Leeuwen. Mapping from densities to potentials in time-dependent density-functional theory. *Phys. Rev. Lett.*, 82:3863–3866, May 1999.

[28] H. Ehrenreich. Electromagnetic transport in solids: optical properties and plasma effects. In J. Tauc, editor, *The Optical Properties of Solids*, page 106, 1966.

[29] Eleonora Luppi, Hannes Hübener, and Valérie Véniard. Ab initio second-order nonlinear optics in solids: Second-harmonic generation spectroscopy from time-dependent density-functional theory. *Phys. Rev. B*, 82:235201, Dec 2010.

[30] Hannes Hübener, Eleonora Luppi, and Valérie Véniard. Ab initio calculation of second harmonic generation in solids. *physica status solidi (b)*, 247(8):1984–1991, 2010.

[31] Hannes Hübener. *Second Harmonic Generation in Solids: Theory and Simulation*. Theses, Ecole polytechnique, September 2010.

[32] R. Del Sole and E. Fiorino. Macroscopic dielectric tensor at crystal surfaces. *Phys. Rev. B*, 29:4631–4645, Apr 1984.

[33] D. J. Moss, E. Ghahramani, J. E. Sipe, and H. M. van Driel. Band-structure calculation of dispersion and anisotropy in $\chi \rightarrow^{(3)}$ for third-harmonic generation in si, ge, and gaas. *Phys. Rev. B*, 41:1542–1560, Jan 1990.

[34] Lucia Reining, R. Del Sole, M. Cini, and Jiang Guo Ping. Microscopic calculation of second-harmonic generation at semiconductor surfaces: As/si(111) as a test case. *Phys. Rev. B*, 50:8411–8422, Sep 1994.

[35] Maurizia Palummo, Giovanni Onida, Rodolfo Del Sole, and Bernardo S. Mendoza. Ab initio optical properties of si(100). *Phys. Rev. B*, 60:2522–2527, Jul 1999.

[36] D. J. Chadi. Atomic and electronic structures of reconstructed si(100) surfaces. *Phys. Rev. Lett.*, 43:43–47, Jul 1979.

[37] Michael Rohlfing, Peter Krüger, and Johannes Pollmann. Metallic nature of the symmetric dimer model of si(001). *Phys. Rev. B*, 52:13753–13756, Nov 1995.

[38] Friedhelm Bechstedt. *Principles of surface physics*. Springer Science & Business Media, 2012.

[39] D. Badt, H. Wengelnik, and H. Neddermeyer. Scanning tunneling microscopy at low temperatures on the c(4x2)/(2x1) phase transition of si(100). *Journal of Vacuum Science & Technology B: Microelectronics and Nanometer Structures Processing, Measurement, and Phenomena*, 12(3):2015–2017, 1994.

[40] James D. Watson and Francis H. Crick. A structure for deoxyribose nucleic acid. *Nature*, 171:737–738, April 1953.

[41] Alberto Lopez, Qiao Chen, and Neville V. Richardson. Combined stm, hreels and ab initio study of the adsorption of uracil on si(100)-2 x 1. *Surface and Interface Analysis*, 33(5):441–446, 2002.

[42] K. Seino, W. G. Schmidt, M. Preuss, and F. Bechstedt. Uracil adsorbed on si(001): structure and energetics. *J. Phys. Chem. B*, 107(21):5031–5035, May 2003.

[43] K. Seino, W. G. Schmidt, and F. Bechstedt. Organic modification of surface electronic properties: A first-principles study of uracil on si(001). *Phys. Rev. B*, 69:245309, Jun 2004.

[44] K Seino and WG Schmidt. Reflectance anisotropy of uracil covered si(001) surfaces: Ab initio predictions. *Surface science*, 548(1-3):183–186, 2004.

[45] Elena Molteni, Giovanni Onida, and Giancarlo Cappellini. Electronic structure of uracil-like nucleobases adsorbed on si(001): uracil, thymine and 5-fluorouracil. *The European Physical Journal B*, 89(4):98–, 2016.

[46] Elena Molteni, Giancarlo Cappellini, Giovanni Onida, and Guido Fratesi. Optical properties of organically functionalized silicon surfaces: Uracil-like nucleobases on si(001). *Phys. Rev. B*, 95:075437, Feb 2017.

[47] Hyun-Kyung Kim and Do Hwan Kim. Density functional theory calculations of the adsorption of cytosine on si(100). *Bulletin of the Korean Chemical Society*, 41(11):1060–1067, 2020.

[48] Valerio Olevano, Lucia Reining and Francesco Sottile. Dielectric properties. `http://www.dp-code.org`, 2021.

[49] V. M. Silkin, E. V. Chulkov, and P. M. Echenique. Band structure versus dynamical exchange-correlation effects in surface plasmon energy and damping: A first-principles calculation. *Phys. Rev. Lett.*, 93:176801, Oct 2004.

[50] X. Gonze, F. Jollet, F. Abreu Araujo, D. Adams, B. Amadon, T. Applencourt, C. Audouze, J.-M. Beuken, J. Bieder, A. Bokhanchuk, E. Bousquet, F. Bruneval, D. Caliste, M. Côté, F. Dahm, F. Da Pieve, M. Delaveau, M. Di Gennaro, B. Dorado, C. Espejo, G. Geneste, L. Genovese, A. Gerossier, M. Giantomassi, Y. Gillet, D.R. Hamann, L. He, G. Jomard, J. Laflamme Janssen, S. Le Roux, A. Levitt, A. Lherbier, F. Liu, I. Lukacevic, A. Martin, C. Martins, M.J.T. Oliveira, S. Poncé, Y. Pouillon, T. Rangel, G.-M. Rignanese, A.H. Romero, B. Rousseau, O. Rubel, A.A. Shukri, M. Stankovski, M. Torrent, M.J. Van Setten, B. Van troeye, M.J. Verstraete, D. Waroquier, J. Wiktor, B. Xue, A. Zhou, and J.W. Zwanziger. Recent developments in the ABINIT software package. *Computer Physics Communications*, 205:106, 2016.

[51] John P. Perdew, Kieron Burke, and Matthias Ernzerhof. Generalized gradient approximation made simple. *Phys. Rev. Lett.*, 77:3865–3868, Oct 1996.

[52] V.E. Kenner, R.E. Allen, and W.M. Saslow. Screening of external fields and distribution of excess charge near a metal surface. *Physics Letters A*, 38(4):255–256, 1972.

[53] N. D. Lang and W. Kohn. Theory of metal surfaces: Charge density and surface energy. *Phys. Rev. B*, 1:4555–4568, Jun 1970.

[54] E. K. Yu, D. A. Stewart, and S. Tiwari. Ab initio study of polarizability and induced charge densities in multilayer graphene films. *Phys. Rev. B*, 77:195406, May 2008.

[55] Yanmin Yang, Kehua Zhong, Guigui Xu, Jian-Min Zhang, and Zhigao Huang. Electronic structure and its external electric field modulation of pbpdo2 ultrathin slabs with (002) and (211) preferred orientations. *Scientific Reports*, 7(1):6898, 2017.

[56] T. Eberlein, U. Bangert, R. R. Nair, R. Jones, M. Gass, A. L. Bleloch, K. S. Novoselov, A. Geim, and P. R. Briddon. Plasmon spectroscopy of free-standing graphene films. *Phys. Rev. B*, 77:233406, Jun 2008.

[57] Falco Hüser, Thomas Olsen, and Kristian S. Thygesen. How dielectric screening in two-dimensional crystals affects the convergence of excited-state calculations: Monolayer mos_2. *Phys. Rev. B*, 88:245309, Dec 2013.

[58] Carlo A. Rozzi, Daniele Varsano, Andrea Marini, Eberhard K. U. Gross, and Angel Rubio. Exact coulomb cutoff technique for supercell calculations. *Phys. Rev. B*, 73:205119, May 2006.

[59] Filip A. Rasmussen, Per S. Schmidt, Kirsten T. Winther, and Kristian S. Thygesen. Efficient many-body calculations for two-dimensional materials using exact limits for the screened potential: Band gaps of $\mathbf{mos}_2$, h-bn, and phosphorene. *Phys. Rev. B*, 94:155406, Oct 2016.

[60] Kristian Sommer Thygesen. Calculating excitons, plasmons, and quasiparticles in 2d materials and van der waals heterostructures. 4(2):022004, jun 2017.

[61] . Yambo forum. `http://www.yambo-code.org/wiki/index.php?title=How_to_treat_low_dimensional_systems`, 2021.

[62] Alejandro Molina-Sánchez, Gonçalo Catarina, Davide Sangalli, and Joaquín Fernández-Rossier. Magneto-optical response of chromium trihalide monolayers: chemical trends. *Journal of Materials Chemistry C*, 8(26):8856–8863, 2020.

[63] J.D. Jackson. *Classical Electrodynamics*. Wiley, 2012.

[64] M. Born and E. Wolf. *Principles of Optics*. Cambridge University Press, 2019.

[65] G.B. Airy. Vi. on the phænomena of newton's rings when formed between two transparent substances of different refractive powers. *The London, Edinburgh, and Dublin Philosophical Magazine and Journal of Science*, 2(7):20–30, 1833.

[66] Abelès, Florin. Recherches sur la propagation des ondes électromagnétiques sinusoïdales dans les milieux stratifiés - application aux couches minces. *Ann. Phys.*, 12(5):596–640, 1950.

[67] P. Yeh. *Optical Waves in Layered Media*. Wiley Series in Pure and Applied Optics. Wiley, 2005.

[68] Mathias Schubert. Polarization-dependent optical parameters of arbitrarily anisotropic homogeneous layered systems. *Phys. Rev. B*, 53:4265–4274, Feb 1996.

[69] E. N. Economou. Surface plasmons in thin films. *Phys. Rev.*, 182:539–554, Jun 1969.

[70] Klaus-Jochen Eichhorn Karsten Hinrichs, editor. *Ellipsometry of Functional Organic Surfaces and Films*. Springer, 2018.

[71] Oscar Baseggio, Martina De Vetta, Giovanna Fronzoni, Mauro Stener, Luca Sementa, Alessandro Fortunelli, and Arrigo Calzolari. Photoabsorption of icosahedral noble metal clusters: An efficient tddft approach to large-scale systems. *The Journal of Physical Chemistry C*, 120(23):12773–12782, 06 2016.

[72] W. Ekardt. Dynamical polarizability of small metal particles: Self-consistent spherical jellium background model. *Phys. Rev. Lett.*, 52:1925–1928, May 1984.

[73] W. Ekardt. Size-dependent photoabsorption and photoemission of small metal particles. *Phys. Rev. B*, 31:6360–6370, May 1985.

[74] Igor Vasiliev, Serdar Öğüt, and James R. Chelikowsky. Ab initio absorption spectra and optical gaps in nanocrystalline silicon. *Phys. Rev. Lett.*, 86:1813–1816, Feb 2001.

[75] P.V. Kelly, J.D. O'Mahony, J.F. McGilp, and Th. Rasing. Study of surface electronic structure of si(111)-ga by resonant optical second harmonic generation. *Surface Science*, 269-270:849–853, 1992.

[76] P.V. Kelly, J.D. O'Mahony, J.F. McGilp, and Th. Rasing. Optical second harmonic generation from the si(111)-ga interface. *Applied Surface Science*, 56-58:453–456, 1992.

[77] U. Höfer. Nonlinear optical investigations of the dynamics of hydrogen interaction with silicon surfaces. *Applied Physics A*, 63(6):533–547, 1996.

[78] JD O'Mahony, PV Kelly, and JF McGilp. Optical second harmonic generation from ordered si (111)-au interfaces. *Applied surface science*, 56:449–452, 1992.

[79] D. Lim, M. C. Downer, J. G. Ekerdt, N. Arzate, Bernardo S. Mendoza, V. I. Gavrilenko, and R. Q. Wu. Optical second harmonic spectroscopy of boron-reconstructed si(001). *Phys. Rev. Lett.*, 84:3406–3409, Apr 2000.

[80] Bernardo S. Mendoza, Andrea Gaggiotti, and Rodolfo Del Sole. Microscopic theory of second harmonic generation at si(100) surfaces. *Phys. Rev. Lett.*, 81:3781–3784, Oct 1998.

[81] Bernardo S. Mendoza, Maurizia Palummo, Giovanni Onida, and Rodolfo Del Sole. Ab initio calculation of second-harmonic-generation at the Si(100) surface. *Phys. Rev. B*, 63:205406, Apr 2001.

[82] Hendrik J. Monkhorst and James D. Pack. Special points for brillouin-zone integrations. *Phys. Rev. B*, 13:5188–5192, Jun 1976.

[83] G. Grosso and G.P. Parravicini. *Solid State Physics*. Elsevier Science, 2000.

ECOLE DOCTORALE

Titre : Génération de seconde harmonique de surfaces de silicium fonctionnalisées par des bases d'ADN : une description ab initio

Mots clés : DFT, TD-DFT, SHG, Couche minces, nucléobases

Résumé : Comprendre les mécanismes d'interaction entre des acides aminés ou des peptides avec les surfaces ouvre de nouvelles perspectives. L'adsorption de molécules d'ADN sur des surfaces semiconductrices est régulièrement évoquée pour la conception de biosenseurs ou la production de bio-matériaux. La possibilité de fonctionaliser des surfaces à l'aide de bio-molécules, de créer des structures ordonnées sur des distances de quelques nanomètres dépend de notre capacité à comprendre les phénomènes gouvernant la déposition de films moléculaires sur différents types de surfaces.
L'optique non-linéaire et plus précisément la génération de seconde harmonique (SHG) est particulièrement adaptée à l'étude des surfaces. Dans cette spectrocopie, deux photons de même énergie sont absorbés et un photon d'énergie double est émis. La description de ce phénomène physique passe par le calcul de susceptibilité d'ordre 2 : celle-ci étant nulle pour les matériaux centrosymmétriques, la réponse ne peut provenir que de la surface, qui est à l'origine de la brisure de symétrie .
Pendant cette thèse, les surfaces fonctionnalisées ont été représentées par des couches introduites dans une supercellule, dans un formalisme en espace réciproque. Au delà de la suppression du vide introduit dans la supercellule, que nous traitons par la méthode Selected-G, nous avons également été amenés à nous interroger sur les propriétés optiques des systèmes 2D. Un formalisme en espace mixte - qui permet de traiter la direction orthogonale à la surface dans l'espace réel, et d'isoler la couche de ses répliques - a été mis au point, et les différences entre les réponses hors-plan et dans le plan d'une couche de silicium isolée ont été investiguées en détail. Le lien avec les grandeurs expérimentalement mesurées a également été fait. En particulier, alors que la fonction diélectrique macroscopique d'une couche mince est intrinsèquement difficile à définir, les quantités expérimentales telles que la réflectance et la transmittance ne sont pas affectées par cette ambiguïté. Les conditions du calcul pour modéliser une surface, c'est-à-dire un espace semi-infini ont été clarifiées.
Les spectres de SHG d'une surface de silicium (4x1) fonctionnalisées avec des molécules de thymine, uracil et cytosine ont été calculés en présence des champs locaux. Les différences entre les spectres ont été étudiées, et les potentialités de la SHG comme outil pour reconnaître la nature chimique de l'adsorbat ont été analysées. La sensibilité de la SHG à la configuration d'adsorption a également été évaluée, en comparant les spectres au second ordre générés par des surfaces fonctionnalisées à la thymine dans différentes géométries d'adsorption.

Title : Second Harmonic Generation from silicon surfaces functionalized with DNA nucleobases: an ab initio description

Keywords : DFT, TD-DFT, 2D systems, SHG, nucleobases

Abstract : Understanding the mechanism of interaction between amino acids and peptides with surfaces opens new perspectives. Adsorption of DNA molecules on semiconducting surfaces is regularly evoked for the design of biosensors or the production of bio-materials. The possibility to functionalize surfaces with bio-molecules, to create organized structures up to nanometers' distances depends on our capability to understand precisely the mechanisms which govern the deposition of molecular films onto different kinds of surfaces.
Non-linear optics and more precisely Second Harmonic Generation (SHG) is particularly adapted to study surfaces. In this spectroscopy, two photons of the same energy are absorbed and a photon of double energy is emitted. Describing this physical phenomenon requires the calculation of the second order susceptibility: since it is zero for centrosymmetric material, the response can only comes from the surface, which is at the origin of the symmetry breaking.
Through this thesis, functionalised surfaces have been modelled as slabs introduced in a the supercell, within a reciprocal space formalism. Beyond the elimination of spurious vacuum effects, that we perform within the selected-G method, we also investigated optical properties of 2D systems. A mixed-space formalism - which allows us to treat the direction orthogonal to the surface in real space, and to decouple the slab from its replicas- has been developed, and the differences between the in-plane and out-of-plane response of an isolated slab of silicon have been investigated in detail. The link with experimentally measured quantities has also be done. More specifically, while the macroscopic dielectric function of a thin film is intrinsically hard to be defined, experimental quantities such as reflectance and transmittance are not affected by this ambiguity. The conditions in which the calculation must be performed in order to model a surface, i.e. a semi-infinite object, have been clarified.
SHG spectra of a silicon surface (4x1) functionalised with molecules of thymine, uracil, and cytosine have been calculated in presence of local field effects. The differences between spectra have been studied, and the possibility to use SHG as a tool to characterise the chemical nature of the adsorbate has been analysed. The sensitivity of SHG to the adsorption configuration has been also investigated, by comparison of SHG spectra generated by surfaces functionalised with thymine in different adsorption geometries.

Institut Polytechnique de Paris
91120 Palaiseau, France